CHEMICAL BIOLOGY AND GENETIC STUDIES TARGETING THE MYCOBACTERIAL CELL ENVELOPE

By

John Tison Williams

A DISSERTATION

Submitted to
Michigan State University
in partial fulfillment of the requirements
for the degree of

Microbiology & Molecular Genetics – Doctor of Philosophy

2021

ABSTRACT

CHEMICAL BIOLOGY AND GENETIC STUDIES TARGETING THE MYCOBACTERIAL CELL ENVELOPE

By

John Tison Williams

Mycobacterium tuberculosis is one of the leading causes of death due to a single infectious pathogen. The evolution and spread of drug resistant strains requires new antibiotics to control the TB pandemic. Over the last decade, the lipid flippase MmpL3 has been identified as a potential drug candidate based on its essential nature for cell viability and repeated identification as the lead target of small molecule inhibitors of Mtb growth. Using a combined untargeted and targeted whole cell phenotypic screen I identified novel inhibitors of this valued target. A combination of lipid profiling and an innovative competitive binding assay supported MmpL3 as the target of these inhibitors. Cross resistance profiling of MmpL3 inhibitors against twenty-four unique *mmpL3* Mtb mutants demonstrated that the level of resistance is associated with the proximity of resistant mutants to essential residues for protein function. Further, these resistance profiles suggested that MmpL3 inhibitors fall into separate clades depending on their chemical scaffolds.

The results of this screen led to the development of novel potent analogs for one of the identified MmpL3 inhibitors, HC2099. These analogs were active against clinically relevant drug resistant Mtb strains that cause treatment failure in patients. Active analogs were able to kill Mtb inside of infected macrophages, an infectious niche of Mtb, without inducing cytotoxicity against these important immune cells. One of these analogs, MSU-43085, was orally bioavailable and successfully inhibited Mtb growth in infected mice, supporting further development and highlighting the therapeutic potential of this series.

High throughput screens are often used to identify new inhibitors of Mtb growth. However, prioritized hits form these screens often identify similar targets such as MmpL3, lipid synthesis

enzymes, redox cyclers, as well as inhibitors of the electron transport chain. Follow up studies of these inhibitors are often time consuming, costly and result in the rediscovery of previously identified targets. While this is not necessarily detrimental to Mtb drug discovery, as these reoccurring targets have therapeutic potential. The continued prioritization of inhibitors for these common metabolic pathways potentially limits the identification of inhibitors for novel targets. Therefore, additional steps that identify inhibitors of these common pathways could reshape how high throughput screen hits are prioritized. By applying the targeted mutant screen used to identify MmpL3 inhibitors to a non-prioritized library of hits from a high throughput screen, we identified more than fifty new potential MmpL3 inhibitors. Using an iterative strategy of applying additional mutants of commonly identified targets, this strategy promises to lead to parallel follow-up studies of inhibitors with known and unknown mechanisms of action.

The ability of Mtb to enter into quiescent states in response to host stresses is one of the leading causes for the extended time to cure and evolution of drug resistance. These states can be induced by several environmental stresses including acidic pH, hypoxia, and others. In an effort to study this adaptation in the rapidly growing mycobacterial species *M. smegmatis*, we identified a lethal sodium citrate phenotype. Transcriptional profiling and genetic screening of mutants tolerant to sodium citrate indicated that this phenotype was due to the combined action of both chelation and osmotic stresses. Cell viability could be reduced from sodium citrate killing by cation and osmoprotectant supplementation. From these experiments we propose a model that can be applied to study carbon source uptake and probe the role of genes identified from the forward genetic screen with unknown function.

This dissertation is dedicated to Alaina Covert.
Thank you for standing by me.

ACKNOWLEDGEMENTS

I would like to thank my advisor Dr. Robert B. Abramovitch for supporting me and introducing me to Tuberculosis research and members of the TB field. Thank you for your guidance in lab and your genuine enthusiasm and encouragement for the experiments I proposed. I have enjoyed my time in your lab and learning about the academic career path. You are a great mentor and person. I look forward to seeing you at conferences and watching your lab grow.

To Dr. Edmund Ellsworth, thank you for serving not only as a committee member but as a collaborator. Our talks really put into perspective how much I did not know and how to think about the chemical matter and what I need to think about for drug development.

To Dr. Neal Hammer and Dr. Chris Waters, thank you both for the opportunity to rotate through your labs. Although I decided to go in a different direction meeting each of you and the people in your labs made my PhD experience a pleasant one.

To Dr. Vic DiRita thank you for repeatedly asking one of the simplest yet hardest questions to answer, “What’s the point?”. I have kept this question in mind since my first committee meeting as I have thought about my current research and future interests.

Thank you all for helping me become a better scientist.

TABLE OF CONTENTS

LIST OF TABLES

LIST OF FIGURES

KEY TO ABBREVIATIONS

MmpL3 – mycobacteria membrane protein large 3

Mtb – *Mycobacterium tuberculosis*

TB – tuberculosis

RIF – rifampicin

INH – isoniazid

EMB – ethambutol

PZA – pyrazinamide

MDR – multi-drug resistant

XDR – extremely drug resistant

NTM – non-tuberculosis mycobacteria

MAC – *Mycobacterium avium* complex

MAB – *Mycobacterium abscessus* complex

HTS – high throughput screen

RND – resistance nodulation and division

CM – cytoplasmic membrane

TMD – transmembrane domain

BACTH - bacterial adenylate cyclase-based two hybrid

TMM – trehalose monomycolate

MmpS – mycobacteria membrane protein small

FA – fatty acid

acTMM – acylated trehalose monomycolate

MS – mass spectrometry

PMF – proton motive force

CCCP - carbonyl cyanide m-chlorophenyl hydrazone

MM – mycomembrane

TDM – trehalose dimycolate

SPR – surface plasmon resonance

SAR – structure activity relationship study

NRP – non-replicating persistent

MOA – mechanism of action

FoR – frequency of resistance

RFI – relative fluorescence intensity

Δψ – membrane potential

ICA – indolcarboxamide

MorPHEUS – morphological evaluation and understanding of stress

OD600 – optical density at 600 nm

WT – wild type

AG – arabinogalactan

PG – peptidoglycan

TM – transmembrane

L – loop

SNV – single nucleotide variations

BMMΦ – bone marrow derived macrophages

OADC – oleic acid, albumin, dextrose, catalase

DMSO – dimethyl sulfoxide

TLC – thin layer chromatography

BDQ – bedaquiline

CFZ – clofazimine

PAS – para-amino salicylic acid

EC_{50} – half maximal effective concentration

CC50 – cytotoxicity

H2O2 – hydrogen peroxide

ATP – adenosine triphosphate

AUC – area under the curve

DiaMOND – diagonal measurement of *n*-way drug interactions

FIC_2 – fractional inhibitory concentration for pairwise interactions

RMSD – root mean square deviation

DiOC2 – 3,3′-Diethyloxacarbocyanine, iodide

CYP – cytochrome P450

FFLuc – firefly luciferase

MOX – moxifloxacin

PRT – pretamonid

OFX – ofloxacin

PBS – phosphate buffer solution

ICCB – Institute of Chemistry and Cell Biology at Harvard Medical School

MLSMR – Molecular Libraries Small Molecule Repository

%GI – percent growth inhibition

%FI – percent fluorescence inhibition

GFP – green fluorescent protein

(W)TA – wall teichoic acids

LPS – lipopolysaccharides

PIMs – phosphatidylinositol mannosides

Msm – *Mycobacterium smegmatis*

SC – sodium citrate

FACL – fatty acyl-CoA ligase

TAG – triacylglycerol

A.U. – arbitrary units

Ex – excitation

Em – emission

ANOVA – analysis of variance

CHAPTER 1: Molecular Insights of MmpL3: Cellular Function, Localization, Regulation, and Inhibition

Abstract:

Mycobacteria spp. include a large number of pathogenic organisms such as *M. tuberculosis*, *M. leprae*, and various non-tuberculosis mycobacteria. Mycobacteria membrane protein large 3 (MmpL3) is an essential mycolic acid and lipid transporter required for growth and cell viability. In the last decade numerous studies have further characterized MmpL3 with respect to protein function, localization, regulation, and substrate/inhibitor interactions. This review summarizes these findings and seeks to bring up additional areas of research yet to be addressed in the literature.

Body of Review:

Introduction

Mycobacterium tuberculosis (Mtb) is the bacterium that causes Tuberculosis (TB) in humans. In 2019, the WHO estimated that 10 million people became sick with TB and 1.4 million people died from the disease[1]. Currently no vaccine protects against pulmonary TB[1]. In the absence of an effective vaccine, antibiotic therapy requires patients to take a daily combination of four drugs including rifampin (RIF), isoniazid (INH), ethambutol (EMB), and pyrazinamide (PZA) for six months. However, the long course of treatment and incomplete therapy has led to the selection and evolution of multi- (MDR-) and extensively- (XDR-) drug resistant Mtb strains which are currently spreading person to person[2]. In the case of MDR- and XDR-TB strains, antibiotic therapy increases to as many as six drugs taken daily for two or more years[1]. Therefore, additional therapeutic targets and strategies need to be identified. Additionally, other pathogenic non-tuberculous mycobacteria (NTM), such as *M. avium* (MAC) and *M. abscessus* (MAB), are emerging as common causes of infections, particularly in the immunocompromised, the elderly and those with predisposing conditions, such as cystic fibrosis. These NTMs are resistant to most Mtb drugs[3,4] and therefore new drugs are also needed to control NTM-mediated diseases[5].

Over the last few decades, high throughput screens (HTS) have been conducted to identify the next Mtb drug. Subsequent studies into the mechanism of action of hits identified from these screens have identified QcrB[6-14], DprE1[15-20], and **M**ycobacteria **m**embrane **p**rotein **L**arge **3** (MmpL3)[20-37] as re-occurring "promiscuous" targets. Of these three targets, the essential mycolic acid flippase MmpL3[20-37] is the most commonly identified with 17 reports identifying over 30 chemical scaffolds targeting MmpL3[20-37]. While several of the MmpL3 inhibitors have overlapping chemical groups (discussed further below), the specific structural differences between them make predicting MmpL3 inhibitors within a chemical library difficult. However, the essential nature of MmpL3 makes it a highly sought-after therapeutic target for Mtb[38]. Additionally, naturally occurring point mutations in MAB and MAC clinical strains render them resistant to QcrB and DprE1

inhibitors[20,39-41]. In contrast to this, many MmpL3 inhibitors remain highly active against clinical strains of both MAB and MAC[42] making MmpL3 the most viable of the three targets for these two NTMs. Owing to the high therapeutic potential of MmpL3, several studies over the last decade have increased our understanding of MmpL3 in terms of function, regulation, and protein-substrate/inhibitor interactions. In this introduction, I will discuss the function of MmpL3 in mycobacteria as well as the molecular insights gained from studying MmpL3 and the inhibitors proposed to target this essential flippase.

MmpL3 Protein Structure and Function

MmpL3 is one of several MmpL proteins found in mycobacteria[43] and is a member of the resistance nodulation and division (RND) family of proteins[44-52]. Like other RND proteins, MmpL3 protein function is driven by proton translocation through a central vestibule that spans the cytoplasmic membrane (CM)[45,53]. The central vestibule of MmpL3 is made up of twelve transmembrane α-helix domains (TMD)[45,47,48,51,52,54]. Proton translocation is guided by conserved Asp/Tyr pairs on TMD 4 and 10[45,46,48,50-52,54]. The structural architecture of MmpL3 is similar to the other twelve MmpL proteins in Mtb[47], however, there are several distinct and unique domains that separate MmpL3 from the other MmpL proteins as well as from most other RND proteins[44,47]. For example, MmpL3 has a large cytoplasmic C-terminal tail domain[45,47] involved in protein localization[55], protein interactions[55,56], and post-translational phospho-regulation[57,58]. This C-terminal tail is non-essential[45] and is not found in other canonical RND proteins[47]. The tertiary structure of MmpL3 from *M. smegmatis* ($MmpL3_{Msm}$) has been resolved and crystal structures have suggested that MmpL3 is a monomer[51,52,54]. However, these structures were from truncated forms of MmpL3 lacking the C-terminal tail[51,52,54]. Recently, a bacterial adenylate cyclase-based two hybrid (BACTH) system study suggested that full-length MmpL3 forms a trimer[55]. A complexed MmpL3 is consistent with previous modeling predictions[45] and observations for canonical RND proteins such as AcrB of *E. coli*[53]. MmpL3 is further characterized by two large

periplasmic porter domains located between TMD 1+2 and 5+6[44,45,51,52,54]. These porter domains bind to trehalose monomycolate (TMM)[51], the primary substrate of MmpL3 flipping[48,51] as well as other lipids including phosphatidylethanolamine, cardiolipin, diacylglycerol, phosphatidylglycerol, and phosphatidylinositol[51]. However, it is unclear if MmpL3 directly transports these additional lipids like TMM. The porter domains of MmpL3 were also shown to interact with heme[59], but it is unclear what role MmpL3 may play in iron metabolism.

MmpL3 is one of several MmpL proteins found in mycobacteria with the number of encoded *mmpL* genes varying between species. For example, *M. leprae* encodes five *mmpL* genes, Mtb encodes thirteen *mmpL* genes, and *M. immunogenum*, of the MAB complex, encodes twenty-nine *mmpL* genes[47]. However, only *mmpL3* and *mmpL11* are conserved in all species of mycobacteria[47] and only MmpL3 is essential for growth and viability both *in vitro* and *in vivo* in most mycobacteria[29,45,60-70]. Comparative protein structure prediction studies show that Mtb MmpL proteins fall into two distinct clusters[44]. MmpL3 is a member of the Cluster II MmpL proteins, along with MmpL11 and MmpL13, with the remaining ten Mtb MmpL proteins falling into Cluster I. Cluster II MmpL proteins are distinguished from Cluster I MmpL proteins by the inclusion of the cytosolic C-terminal tail domain and the lack of a docking domain in the second porter loop[44]. It should be noted that some MmpL proteins have associated mycobacteria membrane protein small (MmpS) proteins that help power MmpL function and are typically encoded adjacent to their cognate *mmpL* genes[43]. However, not all MmpL proteins have associated MmpS proteins, including MmpL3[71]. While the exact function of all MmpL proteins in mycobacteria are not yet clearly defined, it is largely believed that they serve as substrate exporters including xenobiotic efflux[72]. A thorough review for the MmpL proteins in Mtb has recently been published[50], and the functions of the other twelve MmpL proteins will not be discussed in detail here.

Synthesis and Transport of TMM and TDM

MmpL3 is the flippase and the sole transporter for the essential long chain (C_{60-90}) glycolipid TMM synthesized in the cytoplasm. The full synthetic pathway of TMM is still not fully understood and some differences occur between species of mycobacteria. An overview of the TMM synthetic pathway is outlined in Figure 1.1 and a description is as follows. Acetyl-CoA (C_2) and Malonyl-CoA (C_3) generated from catabolic pathways serve as primers for the synthesis of short chain (C_{24-26} or C_{16-18}) fatty acids (FAs**)** by the prokaryotic like FAS-I enzyme Fas (Rv2524c)[73,74]. From here, mycolic acid synthesis diverges along two paths to form the α-branch and the meromycolate chain. The α-branch consists of carboxyacyl-CoA (C_{24-26}) and is formed by the ACC complex consisting of AccA3 and AccD4[75]. Along the other branch, C_{16-18} short chain FAs are shuttled as co-enzyme As (CoA) from Fas to the eukaryotic-like multi-enzyme FAS-II complex via mtFabH (Rv0533)[76-78]. FAs entering the FAS-II complex undergo additional elongation steps to form long chain FAs through the incorporation of malonyl-CoA carried by mtFabD (Rv2243)[79-81]. The FAS-II complex is composed of several enzymes including MabA (Rv1483)[82-85], HadAB/HadBC (Rv0635-0637)[86,87], InhA (Rv1484)[88-90], and KasA/KasB (Rv2245/Rv2246)[91,92]. It is hypothesized that to form the fully mature long chain FAs, up to three unique FAS-II complexes exist and are composed of specific combinations of the FAS-II enzymes[93,94]. From here long chain FAs undergo several reactions independent of the FAS-II complex including modifications, such as desaturation and cyclopropanation[95-102], to form the meromycolate chain (C_{48-62}). FadD32 (Rv3801c) then activates the meromycolate chain[75,103-105] to undergo a multistep reaction carried out by Pks13 (Rv3800c). Pks13 induces a condensation reaction between the meromycolate chain and the α-branch to form mycolic β-ketoesters[103,106]. Pks13 then carries out an additional reaction to add the disaccharide trehalose to the β-ketoester to form the α-alkyl β-ketoacyl trehalose glycolipid[107]. In the final synthesis step CmrA (Rv2509) reduces α-alkyl β-ketoacyl trehalose to form TMM[108].

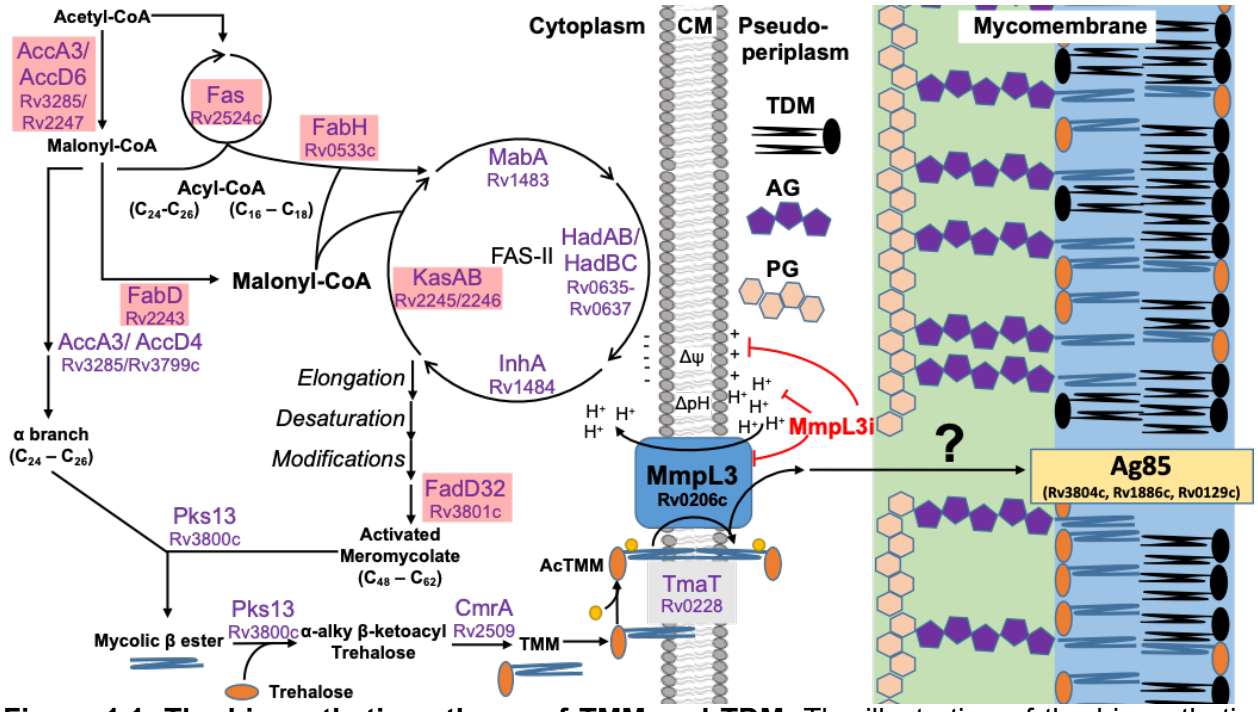

Figure 1.1. The biosynthetic pathway of TMM and TDM. The illustration of the biosynthetic route of trehalose monomycolate (TMM) and trehalose dimycolate (TDM) in mycobacteria. Gene names of each step include corresponding gene numbers from M. tuberculosis H37Rv. Enzymes highlighted in red are genes that are downregulated following MmpL3 disruption. Δψ – membrane potential, AG – arabinogalactan, PG – peptidoglycan, CM – cytoplasmic membrane, MmpL3i – unspecified MmpL3 inhibitor, yellow sphere attached to TMM is an acyl group. ? – an unknown transport system that shuttles TMM to the mycomembrane.

Several steps in the synthesis of TMM are still not understood including double bond formation in MAs. In this review we illustrate MA modifications such as cyclopropanation occurring after exiting the FAS-II complex; however, when exactly these steps occur is unknown and may occur after TMM is transported into the CM. Additionally, not all TMM synthetic pathways are the same and can result in different chain lengths and structural modifications[109,110]. For example, TMM of Mtb includes clycloproyl, keto-, methoxy, and hydroxyl groups while TMM of *M. smegmatis* contain *cis*-, *trans*-, or epoxy groups[110]. Also, chain length regulation is not fully understood but is likely regulated by higher order protein-protein and protein-cofactor interactions[73,111,112]. TMM is essential for mycobacteria cell viability, and therefore many proteins involved in the synthesis of TMM are also essential[60,62,66,68,70]. Consistent with a model of essentiality, enzymes involve in MA synthesis are often identified as targets of anti-tuberculosis

inhibitors. Notable targets include InhA and HadAB which are inhibited by the TB drugs INH[89]/ethionamide[113,114] and isoxyl[115]/thiacetazone[115] respectively.

While the synthesis of TMM has been fairly well described, the transport of TMM, and other mycolic acids and cell wall components, across the CM is less well characterized and gaps still exist in this pathway. However, one essential step required prior to MmpL3 transport is that TMM must first be acylated (acTMM) by TmaT (Rv0228) [45,116]. TmaT is an essential integral membrane protein[45,60,62,66] and it is hypothesized that TmaT plays a role in intercalation of (ac)TMM into the inner leaflet of the CM[116]. However, how this occurs is unclear and additional enzymes may be involved in this step. Once acylated, acTMM is transported across the CM from the inner leaflet to the outer leaflet in what is hypothesized to be a two-step flipping mechanism carried out by MmpL3 (Rv0206c) (Figure 1.1). The two steps consist of guided acTMM flipping from the CM inner leaflet to the outer leaflet followed by acTMM transport from the outer leaflet to the porter domain of MmpL3 powered by the PMF[48,51,52]. This two-step mechanism is based on three observations. The first observation is that TMM accumulates in the outer leaflet of the CM in *M. smegmatis* spheroplasts[48]. TMM accumulation in *M. smegmatis* spheroplasts suggests that following TMM flipping from the inner leaflet of the CM, TMM is first deposited in the outer leaflet before being transported. TMM accumulation in spheroplasts can be decreased in *M. smegmatis* spheroplasts treated with MmpL3 inhibitors AU1235 and BM212[48], suggesting MmpL3 inhibitors prevent TMM flipping. In the second step, TMM is removed from the outer leaflet and associated with the porter domains of MmpL3 that extend in the pseudo-periplasm. This model is based on crystal structures and mass spectrometry (MS) data that demonstrates TMM interacts with the MmpL3 porter domains[51]. This process is powered by proton translocation generated by the proton motive force (PMF)[117]; however, *M. smegmatis* spheroplasts treated with PMF uncouplers, such as CCCP, still accumulate TMM in the outer leaflet[48]. This suggests that rather than TMM flipping, proton translocation powers removal of TMM from the outer leaflet of the CM to the porter domains. While this two-step model has been proposed by several groups[48,51,52], direct

observation of MmpL3-TMM flipping has not been observed. Additionally, it is possible that MmpL3 only transports acTMM as a complex with other proteins. For example, TtfA (Rv0383c), a protein of unknown function, is part of the MmpL3 interactome and is required for TMM transport[56]. Also, it still remains unclear how MmpL3 recognizes and binds to (ac)TMM in the inner leaflet of the CM. To date binding of MmpL3 has only been visualized in the MmpL3 porter domains[51,52]. A recent photoactivatable probe was created by Kavunja and colleagues that structurally resembles TMM[118]. Upon photoactivation, this probe is covalently linked to interacting proteins and allows for enrichment of proteins that associate with the probe. This probe enriched several proteins in *M. smegmatis* cells previously demonstrated to interact with TMM including MmpL3. The authors identified the enriched proteins through peptide-based MS; however, which residues the probe specifically linked to were either not identified or not reported. Additional experiments using these probes with pre-enriched MmpL3 expressing cells or inverted membrane vesicles may identify which MmpL3 residues TMM interacts with in the inner leaflet of the CM.

Once transported across the CM and associated with the porter domain of MmpL3, it is hypothesized that acTMM is shuttled by a yet identified chaperone system across the peptidoglycan and arabinogalactan layers to the mycomembrane (MM) (Figure 1.1). Once in the MM, TMM can either accumulate or undergo two different acyltransferase reactions carried out by the Ag85 complex (FbpA, FbpB, and FbpC2)[119-123]. The first acyltransferase reaction removes the trehalose moiety and covalently links the mycolic acid to terminus of the arabinogalactan layer[121]. This acyltransferase reaction is essential for cell viability[121,122], and is the reason why MmpL3, as the sole transporter of TMM, is essential. The second possible acyltransferase reaction moves the mycolic acid moiety of one TMM molecule to the C6' of a second TMM molecule to form trehalose dimycolate (TDM)[121]. TDM is also known as "Cord Factor" due its role in the formation of mycobacterial cords[124], a multicellular aggregate characteristic of mycobacteria[125]. TDM is primarily found in the outer leaflet of the MM and plays roles in barrier

protection[102,122,126], biofilm formation[127], granuloma formation[128-133], and macrophage stimulation[131-134].

Preceding the acyltransferase reactions in the MM, several questions revolving around the fate of acTMM following transport across the CM still remain. For one, it is still unclear when TMM undergoes de-acylation (acTMM to TMM) and whether or not this is an essential step. Secondly, one of the main pressing questions concerning the fate of (ac)TMM is how it is transported across the peptidoglycan and arabinogalactan layers. Surface plasmon resonance (SPR) data from Belardinelli and colleagues demonstrated that MmpL3 does not directly interact with proteins from the Ag85 complex[55]. This is consistent with distance measurements that the 35 Å porter domains protruding from the CM would not reach across the 100 nM gap between the CM and the MM[55]. Two studies have attempted to find periplasmic interacting partners of MmpL3 using the BACTH system and protein co-precipitation methods but neither identified any periplasmic or cell wall localized candidates[55,56]. Further studies into (ac)TMM transport may identify additional drug targets as well as further our understanding of the physiology and cell wall biogenesis of mycobacteria.

MmpL3 Localization and Interactome

Following biosynthesis and transport, TMM is incorporated into the cell wall during cell division. Mycobacteria undergo asymmetric cell division and extend from the old pole[135]. Therefore, it stands to reason that proteins involved in cell wall synthesis, including MmpL3, would localize to the same area. Indeed, fluorescently labeled MmpL3 has been demonstrated to localize at the dividing pole during cell division[33,49,55,56,136,137]. Localization of MmpL3 to the dividing pole is guided, in part, by the C-terminal tail, as mycobacteria expressing truncated MmpL3 lacking the C-terminal tail show decreased protein localization during cell division[55]. In addition to the C-terminal tail, the DivIVA homolog Wag31 (Rv2145c) may also play a role in MmpL3 localization[138]. While it is not clear if Wag31 directly interacts with MmpL3[138], Wag31 does

coordinate cell division machinery to the pole during cell division, including enzymes involved in peptidoglycan synthesis[139,140] and mycolic acid biosynthesis including AccA3[138]. Recent reports have identified additional proteins that directly interact with MmpL3, including additional proteins involved in mycolic acid transport, as well as proteins involved in peptidoglycan and arabinogalactan substrate transport[55,56]. MmpL3 interacting proteins involved in TMM transport included the TMM acylation protein TmaT[55], as well as TtfA (Rv0383c) and Msmeg_5308 (Rv1057)[56]. The function of TtfA is not fully defined but is essential in mycobacteria and is required for the transport of TMM[56] while MSMEG_5308 is not required for TMM transport and dispensable for cell viability[141], but may stabilize TtfA-MmpL3 interactions during cell stress[56]. MmpL3 was also demonstrated to interact with MmpL11 (Rv0202c)[55] which is involved in the transport of mycolic acid containing lipids, monomeromycolic diacylglycerol, and mycolate wax ester[142]. Additional proteins of unknown or ill-defined function were also demonstrated to interact with MmpL3 including Rv0204c, Rv0207c, Rv0625c, Rv1275 (LprC), Rv1337, Rv1457c, Rv1799 (LppT), Rv2169c, Rv3064c, Rv3271c, Rv3483c, Rv3909, and MT2653[55] and suggests a large cell wall transport complex exists. Notably MmpL3 does not interacts with the Ag85 complex or enzymes involved in mycolic acid synthesis enzymes such as FAS-II enzymes or Pks13[55,56]. While a lack of interaction between the Ag85 complex and MmpL3 could be predicted based on distance measurements[55]. The lack of interaction between mycolic acid synthesis enzymes and MmpL3 was surprising given they are co-coordinated by Wag31[138] to localize to the dividing pole[137] and are co-regulated by PknAB/PstP[57,58,139].

Current studies of MmpL3 localization and co-localization have focused on dividing cells to gain better insights into cell wall biogenesis and the mycobacterial divisome[33,49,55,56,136,137]. However, questions remain for where MmpL3, and other divisome proteins, localize during states of non-replication when MmpL3 is dispensable for cell viability[45,64] and some MmpL3 inhibitors do not kill non-replicating mycobacteria[22,117]. Using scanning electron microscopy, Lun and colleagues observed that Mtb treated with an MmpL3 inhibitor developed dimples at the dividing

pole where MmpL3 localizes[143]. They hypothesized that these dimples were actually holes forming at the site of MmpL3 localization leading to cell death[143]. If MmpL3 does not localize to the dividing pole during states of non-replication, then these holes may not develop which could explain why MmpL3 inhibitors do not kill non-replicating cells. Future studies may seek to address where proteins involved in cell wall synthesis and division, including MmpL3, localize during states of non-replication.

Regulation of MmpL3

mmpL3 is encoded in a monocystronic operon in mycobacteria[63]. To date, the transcriptional regulation of *mmpL3* is not fully understood. However, ChIP-Seq and EMSA assays identified Rv1816 and Rv3249c as repressors of *mmpL3* as well as all other *mmpS/mmpL* genes with the exception of *mmpL6*[144,145]. The observation that so many *mmpS/mmpL* genes share transcriptional regulators with *mmpL3* suggests that a coordinated regulatory pathway is needed for Mtb to adapt to new environments. Additionally, Rv1816 also regulates *kasA* of the FAS-II pathway[144]. This finding suggests that *mmpL3* regulation is co-coordinated with mycolic acid synthesis despite no direct protein-protein interaction[55]. This finding is consistent with the observation that FAS-I/FAS-II genes are downregulated following *mmpL3* knockdown or MmpL3 inhibition[22,65,146]. Repression by Rv1816 and Rv3249c is relieved upon binding to either palmitic acid or isopropyl laurate[144]. The identification of palmitic acid as an inducer was serendipitous[144] but is consistent with model that links mycolic acid synthesis with transport regulation as Mtb Fas is biased to stearic acid (C_{18})[73,74]. One model that may link Fas with MmpL3, is that as Fas begins to generate short chain FAs, *mmpL3,* as well as other genes regulated by Rv1816/Rv3249c, is induced to ready the cell for replication. However, additional experiments would be needed to test this model.

In addition to transcriptional regulation, MmpL3 activity is post-translationally phospho-regulated by PknA, PknB, and PstP at the C-terminal tail[57,58]. In two separate studies, the authors

demonstrated that over expression of PknB led to increased phosphorylation of $MmpL3_{Msm}$ at T920 and T984[57], while depletion of *pknA* resulted in decreased phosphorylation of the $MmpL3_{Mtb}$ residues T893 and T910[58]. Consistent with a repressive model, overexpression of PknB is lethal and mirrored MmpL3 perturbation lipid profiles resulting in increased TMM as MmpL3 transport was lost and decreased TDM due to lower TMM substrate[57]. In accordance with this model, both genetic depletion of *pknA* and *pknB* or small molecule inhibition of PknA and PknB, resulted in increased TMM but no alterations in TDM levels[58,147]. The lipid profiles of the PknA/B disruption studies are consistent with a model of unregulated MmpL3 activity in which TMM is synthesized and exported at increased rates but without TDM conversion due to lower Ag85B expression following PknA/B disruption[58,147]. These studies were conducted in two mycobacterial species, Msm and Mtb[57,58,147], suggesting MmpL3 phospho-regulation is conserved in other mycobacteria. Phosphorylation based inhibition of MmpL3 activity is relieved by the serine/threonine phosphatase PstP[57]. Repression of *pstP* resulted in loss of viability and a decrease in TMM abundance consistent with loss of MmpL3 activity through phosphorylation[57]. That phosphorylation of the MmpL3 C-terminal inhibits protein activity is consistent with observations that the C-terminal tail is not essential for MmpL3 activity or cell viability[45]. Regulation by PknAB/PstP is not limited to MmpL3, and includes other lipid/mycolic acid synthesis enzymes including Fas, FabG, HadA, AccD5, FadD32, AccA3, and Pks13[57], as well as Wag31[139,140] further linking MmpL3 activity with cell wall synthesis and division. PknAB/PstP also regulates peptidoglycan synthesis[148] linking mycolic acid transport regulation with peptidoglycan biosynthesis.

Interestingly, while depletion of *pknA* led to decreased phosphorylation of MmpL3, depletion of *pknB* did not[58]. This may suggest differential regulatory roles of PknA and PknB despite *pknB* being encoded immediately downstream of *pknA* in the same operon[58]. Consistent with this model, the threonine residues phosphorylated by PknB in $MmpL3_{Msm}$ and PknA in $MmpL3_{Mtb}$ are non-orthologous when aligned (Supplemental Data). PknB localizes at the dividing

pole during cell division[149]; however, PknB was not identified as a part of the MmpL3 interactome[55,56], suggesting a transient association with MmpL3. Interestingly, depletion of both *pknA* and *pknB* in a double knockdown strain led to increased phosphorylation of $MmpL3_{Mtb}$ at residues S823, T840, S868, T872, T893, and T910[58]. As only Ser/Thr residues were phosphorylated in the *pknA/B* double knockdown strain, this suggests that other Ser/Thr kinases are involved in MmpL3 phosphoregulation. Mtb has eleven Ser/Thr kinases[43], including PknA and PknB, suggesting that the other nine Ser/Thr kinases may play a role in phosphoregulating MmpL3. A study by Prisic and colleagues identified Thr residues as the preferred phosphorylation sites for PknA, PknB, PknD, PknE, PknF, and PknH[150]. This would suggest that the Ser residues identified to by phosphorylated by Zeng and colleagues in the *pknA/B* double knockdown strain may be phosphorylated by PknG, PknI, PknJ, PknK, or PknL.

Additional studies are required to understand the transcriptional and post translational regulation of MmpL3. While MmpL3 is post-translationally regulated through phosphorylation of the C-terminal tail[57,58], the residues identified are not conserved in all mycobacteria (Supplemental Data). These differences may result in differential post-translation regulation of MmpL3 between species. Additionally, how phosphorylation of the C-terminal tail results in decreased MmpL3 activity is not clear but may result in 1) dissociation of predicted MmpL3 homotrimers[45,55], 2) dissociation of MmpL3 from other interacting proteins such as TmaT[55] and TtfA[56] or 3) delocalization from the dividing pole.

The Therapeutic Potential of MmpL3

MmpL3 is conserved in all mycobacteria as well as the closely related *Corynebacterium* spp. (CmpL1)[45,63]. MmpL3 was initially demonstrated to be essential in two studies by Lamichhane and colleagues in a transposon screen[151] and by Domenech and colleagues who could not generate an *mmpL3* knock out[72]. Since then, several additional lines of genetic evidence have validated this finding, including the observation that mycobacteria rapidly lose viability upon

following *mmpL3* knockdown or MmpL3 protein depletion[64,65,69]. Additionally, saturating transposon mutagenesis studies have failed to identify null mutants in Mtb, *M. bovis* (BCG) or *M. paratuberculosis*[60-62,66,68,70]. However, recently Xiong and colleagues reported an *mmpL3* knockout in *M. neoaurum* (ATCC 25795)[67]. The method used to create this knockout strain failed to generate knockouts in Mtb[72] and *M. smegmatis*[29]. So, why Xiong and colleagues were able to knockout *mmpL3* in *M. neoaurum* is unclear. Some possibilities include 1) the presence of an additional (ac)TMM transporter or 2) a lowered dependency on TMM for MM anchoring in *M. neoaurum*. Precedent for either scenario exists for closely related Corynebacterium species, which are viable without the TMM equivalent trehalose corynemycolate (TMCM)[63,116]. To date the effects of MmpL3 inhibitors have not been tested in *M. neoaurum,* which may give some insights into the essentiality of MmpL3 and TMM transport in this mycobacterial species. However, in most species of mycobacteria, including clinically relevant Mtb, MAC, and MAB, *mmpL3* remains classified as an essential gene in replicating cells.

The essentiality of MmpL3 *in vitro* translates to both *ex vivo* and *in vivo* infection models. Genetic knockdown and protein depletion models have demonstrated that Mtb rapidly loses cell viability in both infected macrophages[65] and mice (C57Bl/6)[64] following MmpL3 depletion. These observations make MmpL3 an attractive target for TB chemotherapy and efforts to identify MmpL3 inhibitors have been remarkably successful through both untargeted[20-35,37] and targeted[25,36] screening approaches. To date, at least thirty parental chemical scaffolds have been proposed as MmpL3 inhibitors[20-37]. Treatment of Mtb and other mycobacteria result in bactericidal effects *in vitro*[20-37] as well as growth inhibitory effects in *ex vivo* models[21,22,25,26,35,152-154]. Follow up structure activity relationship (SAR) studies have resulted in the development of hundreds of active analogs[22,31,35,37,153-156] with some demonstrating activity against Mtb and MAB *in vivo*[27,28,35,143,152,155-162]. Adding to the success of MmpL3 inhibitors in preclinical models, SQ109 has had success in clinical trials[163,164] and recently passed a Phase IIb clinical trial[165]. In humans, SQ109 is well tolerated[163-165] and leads to decreases in viable Mtb in sputum samples when taken

in combination with RIF over 14 days[164]. While SQ109 is active against MDR-TB in patients[165], SQ109 has a short half-life due to host drug metabolism[166,167] which is exacerbated when taken in combination with RIF[163]. However, the success of SQ109 thus far validates MmpL3 as a clinical target for Mtb therapy. Moving forward, clinical trials involving other MmpL3 inhibitors with altered pharmacokinetic profiles may find additional success.

The success of SQ109 as an active MmpL3 inhibitor in human TB patients shows promise for other MmpL3 inhibitors being studied and developed elsewhere. However, MmpL3 as a target is not without its limitations. Despite being a commonly identified target for inhibitors active against Mtb, these same inhibitors are not pan-active in all mycobacterial species. Using a wide selection of previously described MmpL3 inhibitors, Li and colleagues demonstrated that some MmpL3 inhibitors, including SQ109, have low activity against MAB and MAC species[42]. The low activity in NTM species was scaffold specific, and some MmpL3 inhibitors such as the indolecarboxamides NITD-304 and NITD-349 demonstrating high activity against NTMs[42]. Another limitation of MmpL3 as a target is the non-essential nature of MmpL3 in non-replicating mycobacteria[45,64]. In the granuloma, the growth rate of Mtb exists along a spectrum of actively replicating to non-replicating due to factors including nutrient starvation, host derived stresses, and hypoxia[168]. Using an inducible MmpL3 depletion strain, Li and colleagues demonstrated that during states of non-replication, depletion of MmpL3 did not significantly reduce the viability of Mtb[64]. This observation is consistent with observations that treatment of non-replicating Mtb with indocarboxamides, AU1235, and HC2091 did not lead to significant losses in viability[22,117]; however, others do kill non-replicating bacteria (discussed further below). Taken together, these observations indicate that strategies must be developed to overcome therapeutic limitations of targeting MmpL3.

While MmpL3, as a target, has limitations for non-replicating mycobacteria. Similar “lack of activity” observations for non-replicating bacteria have been made for the first line drug INH[22,117,169-172], which has been used clinically for nearly 70 years[173]. Additionally, some MmpL3

inhibitors including SQ109, BM212, C215, TBL-140, E11, HC2032, HC2134, HC2138, HC2149, HC2178, and HC2184 have additional effects, including PMF uncoupling[25,31,117,153], and are active against non-replicating persistent (NRP-) Mtb[22,31,117,153]. While these off-target effects, do not add to the therapeutic potential of MmpL3, they do suggest that limitations in MmpL3 inhibition can be overcome through secondary mechanisms of action (MOA). Additionally, mycobacteria are treated using drug combinations, and inclusion of drugs active against non-replicating mycobacteria such as BDQ[174], RIF and others[175] could overcome therapeutic limitations of MmpL3. MmpL3 inhibitors have also demonstrated high activity against clinical mono-drug resistant, MDR-, and XDR- Mtb strains[26,27,29,32,35,153,159]. Additionally, there have been no reports of resistant mutants isolated from patients who received SQ109 during clinical trials, suggesting clinical strains resistant to MmpL3 inhibitors might not (yet) exist. Furthering the therapeutic potential of MmpL3 inhibitors, are the observation that *mmpL3* mutants resistant to MmpL3 inhibitors are hyper susceptible to RIF[25,176], suggesting a co-therapy of RIF and an MmpL3 inhibitor could reduce the frequency of resistance (FoR) to MmpL3 inhibitors. Taken together, while MmpL3 does have limitations as a target, strategies are available to overcome them and MmpL3 remains a viable therapeutic target.

Approaches to Identifying MmpL3 Inhibitors

MmpL3 remains a common target, owing to its continued identification as the target of a broad number of compounds with varying chemical scaffolds (Figure 1.4a-f). However, most MmpL3 inhibitors have been identified through two methods; 1) the isolation and whole genome sequencing of *mmpL3* mutants resistant to the selected to an inhibitor[20-37,152-157,159,160,176,177] and 2) the observation that treatment of mycobacteria with MmpL3 inhibitors leads to the accumulation of TMM and a decrease in TDM in whole cell lipid extracts[21,22,25,27,29,31-33,35,152,154]. While these two methods have served as early indicators for the MOA of these compounds, they are confounded by the additional observations that 1) MmpL3 inhibitors can have multiple MOA and can kill Mtb

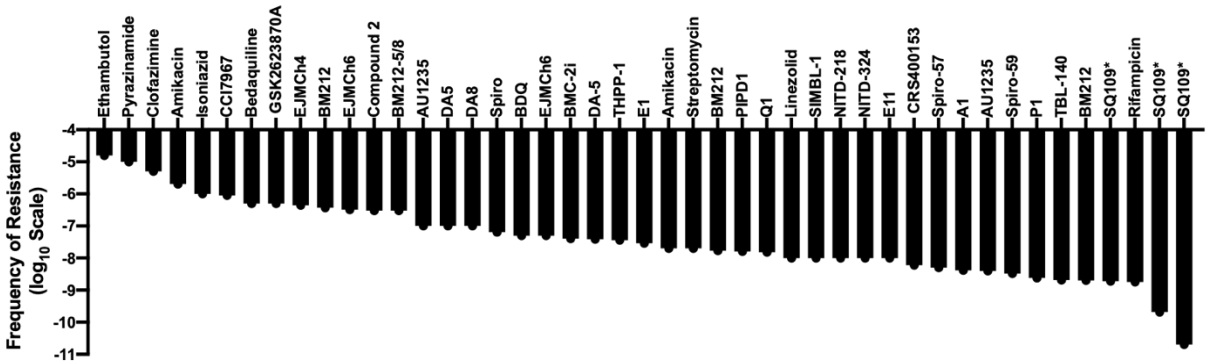

Figure 1.2. Mycobacteria have a moderate frequency of resistance to MmpL3 Inhibitors. Frequency of resistance plot for MmpL3 inhibitors as well as other TB drugs against mycobacteria[21,23,26-31,33-36,152,153,155,157,178-187]. * indicates FoR for SQ109 measured in *H. pylori*.

in non-replicating states[31,117,153], and 2) disruption of the PMF can lead to similar lipid abundance profiles as cells treated with proposed MmpL3 inhibitors[117]. These two observations previously brought into question the true target of proposed MmpL3 inhibitors.

The isolation and whole genome sequencing of mutants resistant to novel inhibitors can act as an early indicator of the cellular target. Mutants resistant to MmpL3 inhibitors have been isolated in multiple species including Mtb, *M. smegmatis*, *M. bovis* (BCG), and *M. abscessus*[20-37,152-157,159,160,176,177] (Figure 1.3). The FoR to MmpL3 inhibitors generally ranges from 10^{-7} to 10^{-9} (Figure 1.2)[20-37,152-157,159,160,176,177], but can vary between species[30]. Mutations to MmpL3 inhibitors primarily occur in regions encoding TMD surrounding the central vestibule[52] (Figure 1.3) where inhibitors bind to MmpL3[52,54]. While the isolation of *mmpL3* mutants against proposed MmpL3 inhibitors has a good track record as an early indicator that a compound targets MmpL3, it is not proof that MmpL3 is the target. For example, resistant mutants isolated against THPP-based MmpL3 inhibitors by both Ioerger as well as Remuinan and their respective colleagues, indicated that THPP inhibits MmpL3[24,35]. However, a protein pull-down study conducted by Cox and colleagues using chiral enantiomers of THPP, GSK729 (active) and GSK730 (inactive), identified EchA6, but not MmpL3, as a strong binder of THPP (GSK729)[188]. Targeted mutagenesis of *echA6* conferred resistance to THPP both *in vitro* and *in vivo* (murine) indicating that EchA6 was, at least, an additional target of THPP[188]. These observations led Cox and colleagues to hypothesize that

MmpL3 acted as a drug importer, and that mutations in *mmpL3* blocked this function[188]. However, *mmpL3* mutants resistant to AU1235 and BM212 demonstrated no differences in cellular accumulation of these inhibitors indicating MmpL3 is not an importer for these inhibitors[29,30]. Later studies would also validate MmpL3 as a target of THPP based on protein-inhibitor interaction studies including biolayer interferometry and surface plasmon resonance[49]. In addition to THPP, SQ109 also has multiple proposed targets including MmpL3[34], PMF uncoupling[117], and menaquinone biosynthesis by targeting MenA[189]. As an additional limitation to this primary method, no Mtb resistant mutants have been identified against SQ109 either *in vitro* or reported from clinical trials. FoR studies in *H. pylori* have indicated that the FoR for SQ109 is 10^{-9} to 10^{-11} (Figure 1.2) which is likely due to the multi-target nature of SQ109[182]. Due to this limitation, resistance studies for SQ109 have utilized *mmpL3* mutants isolated against other inhibitors that are cross-resistant to SQ109[34]. However, taken together observations for THPP and SQ109 suggest that isolation of *mmpL3* mutants is not enough to validate MmpL3 as a target, nor does it rule out the possibility of additional MOAs.

The other common method for validating MmpL3 as a target is to perform lipid profiling of mycobacteria treated with an MmpL3 inhibitor. This method relies on the comparison of relative lipid abundance of TMM and TDM in MmpL3 inhibitor treated vs untreated control cells. Following MmpL3 disruption, mycobacteria accumulate TMM as it can no longer be transported across the CM. This leads to a decrease in TDM due to a lack of TMM substrate in the MM. These lipids profiles are consistent between mycobacteria treated with MmpL3 inhibitors[117] and inducible MmpL3 depletion strains[45,49,64]. However, MmpL3 is powered by proton translocation and PMF uncoupling can lead to MmpL3 perturbation. Studies by Li and colleagues generated similar lipid profiles from *M. smegmatis* cells treated with MmpL3 inhibitors or PMF uncouplers such as CCCP and nigericin[117]. Further studies conducted by multiple groups have indicated that MmpL3 inhibitors such as SQ109, BM212, C215, TBL-140, E11, HC2032, HC2134, HC2138, HC2149, HC2178, HC2184, and SIMBL-2 can disrupt one or more components of the PMF [25,31,33,48,117,153].

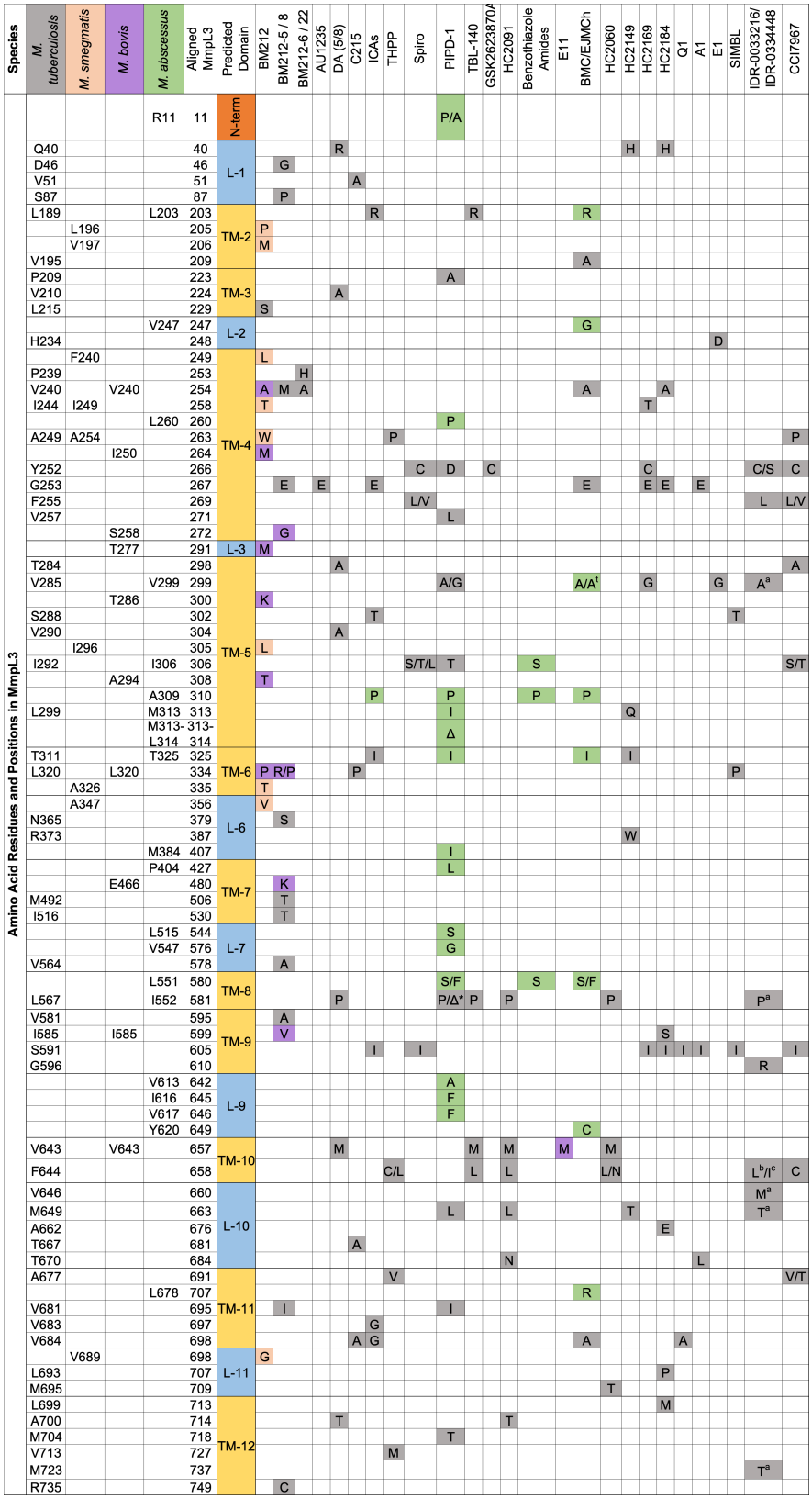

Figure 1.3. Mutation localization for MmpL3 inhibitor resistant mutants.

Figure 1.3. (cont'd) A mutation matrix that demonstrates the amino acid position and substitution for non-synonymous mutations found in MmpL3 inhibitor resistant mutants. The matrix includes inhibitors for which resistant mutants have been identified in four species including *M. tuberculosis* (grey), *M smegmatis* (orange), *M. bovis* BCG (purple), and *M. abscessus* (green). MmpL3 protein sequences were aligned and indicate orthologous positions between species. * - Substitutions in position 581 of the aligned protein for PIPD-1 were discovered in either the *M. tuberculosis* (P) or *M. abscessus* (Δ), A† indicates substitution in *M. tuberculosis* background at the 299 position of the aligned sequence (*M. tuberculosis* - V285). [a] - indicates secondary mutations made in the *M. tuberculosis* F255L background isolated from IDR-0033216, [b] and [c] - indicate tertiary mutations sequenced from AU1235 resistant mutants in *M. tuberculosis* F255L/L567P and F255L/V646M backgrounds respectively. TM – transmembrane, L – loop.

These observations brought into question whether proposed inhibitors inhibit MmpL3 through direct protein binding or indirectly through PMF uncoupling. More recently, several protein binding methods have indicated that MmpL3 inhibitors bind to MmpL3 directly[49,52,54], and that PMF uncoupling is likely a secondary effect independent of MmpL3 inhibition (discussed further below). Taken together, while the isolation of *mmpL3* mutants coupled with lipid profiling can act as an early indicator that a compound is an MmpL3 inhibitor, additional studies are required to validate MmpL3 as the primary target. Some methods that have been used to test for on target specificity (discussed further below) include transcriptional profiling[22,65,146], sensitivity testing in *mmpL3* knockdown strains [36], fluorophore displacement [49], and metabolic profiling [23].

MmpL3 Protein-Inhibitor Interactions

Despite the limitations of the two primary methods used to identify MmpL3 inhibitors listed in the previous section, a competitive binding assay developed by Li and colleagues has demonstrated direct interaction for many of the MmpL3 inhibitors with MmpL3[49]. This binding assay uses a fluorescent probe composed of MmpL3 inhibitors linked to a TAMRA fluorophore. These NORTH series probes directly bind to MmpL3 but can be displaced by competing MmpL3 inhibitors. Leveraging this displacement property, these probes can be used to determine direct MmpL3 interaction in live cell mycobacteria through competitive binding using flow cytometry by measuring the relative fluorescent intensity (RFI). Unlike the TMM/TDM abundance assays, this method is insensitive to PMF uncoupling as CCCP does not lead to probe displacement.

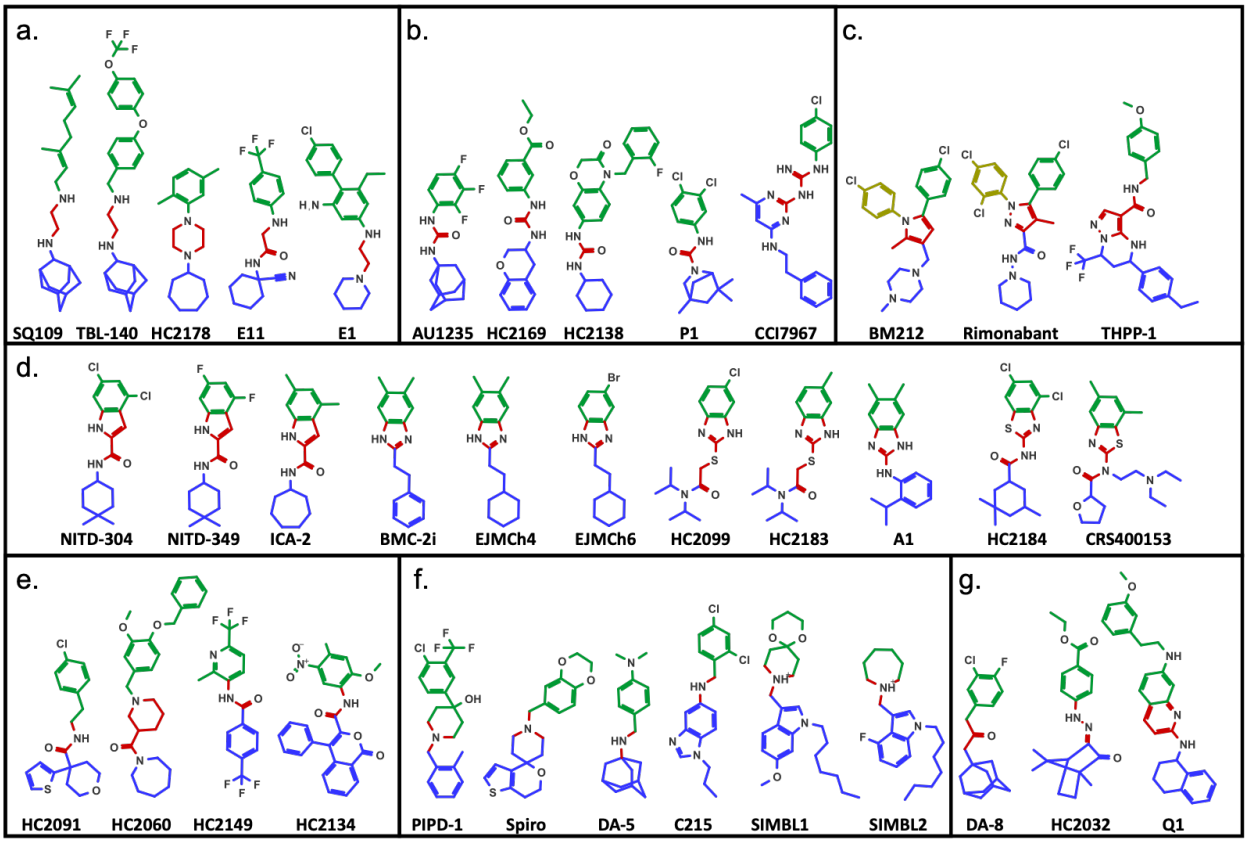

Figure 1.4. MmpL3 inhibitors share distinguishing and overlapping features. MmpL3 inhibitors fall into five distinct classes of inhibitors based on shared Central core chemical groups including diamines / acetamides (a), ureas / guanidines (b), pyrole / pyrazoles (c), indoles / imidazoles / thiazoles (d), amides (e), amines (f), and a seventh class of unshared core chemical groups (g). Colored circles indicate shared chemical groups found between all MmpL3 inhibitors including the Northern lipophilic groups (Green), the Central electrophilic / basic core group (Red), and the Southern hydrophobic group (Blue). Noted exception are the additional North Western chemical groups (Yellow) found in BM212 and Rimonabant. North, Central, and South chemical nomenclature is based on work done by Guardia and colleagues[158].

This system has already been used in three separate studies to demonstrate direct interaction of MmpL3 with inhibitors SQ109, NITD-304, NITD-349, BM212, AU1235, THPP1, HC2032, HC2060, HC2091, HC2099, HC2134, HC2138, HC2149, HC2169, HC2178, HC2184, C215, SIMBL-1 and SIMBL-2[25,33,49]. The results for SQ109, NITD-304, NITD-349, AU1235, and THPP1 have been backed by protein binding data including biolayer interferometry and surface plasmon resonance[49]. However, while this competitive binding assay does allow for the simple measurement of direct interaction between MmpL3 and an inhibitor in live cells, this competitive binding assay does not rule out the possibility of additional effects. Inhibitors like SQ109, BM212,

C215, TBL-140, E11, and many of the listed HC2 compounds have the additional property of PMF disruption[25,31,117,153]. Compounds like BM212 and SQ109 have both demonstrated bactericidal properties against Mtb in non-replicating states[117] when MmpL3 is dispensable for viability[64]. Additionally, evidence does support secondary protein targets for both THPP[188] and SQ109[189].

While the specific chemical structures varies between proposed MmpL3 inhibitors, the compounds can be broadly classified into a seven primary categories based on shared core structures (Figure 1.4a-g). Broadly, the six classes consists of diamine/acetamides, ureas/guanidines, pyrole/pyrazoles, benz-amides/indoles/imidazole/thiazoles, amides, amines, and a seventh class of scaffolds that do not share a common core structure (Figure 1.4a-g). For simplicity of description, we borrow nomenclature from Guardia and colleagues[158] and described the shared core structures as the Central chemical groups (Figure 1.4a-e, Red). The Central cores are typically composed of nucleophilic/basic residues, and even in the seventh chemical class, which lack a shared core structure, the inhibitors share a Central core with similar chemical properties (Figure 1.4g). Again, borrowing nomenclature from Guardia and colleagues, the Central cores are flanked by Northern lipophilic groups, typically in the form of a substituted benzene (Figure 1.4a-g, Green), and Southern hydrophobic groups, typically in the form of cyclic alkyl groups (Figure 1.4a-g, Blue). While the shared chemical cores exist for nearly all MmpL3 inhibitors, additional groups have been identified for the BM212 and Rimonabant which each have additional substituted benzene rings classified here as North-Western groups (Figure 1.4c, Yellow). A review of the modeled and co-crystal structures indicates that the chemical domains align to specific MmpL3 binding subdomains (SD1-5) identified by Zhang and colleagues[52]. The northern groups are typically found in SD-3 towards the periplasmic side of the Asp-Tyr residues[52]. Exceptions to this are noted for BM212 and Rimonabant, where the Northern groups bind to SD-2 and the North-Western groups bind to SD-1[52]. The electrophilic/basic Central groups interact with the essential Tyr groups in SD-4. The Central groups typically bind to the Tyr residues through H-bonding or non-covalent interactions[52]. This binding disrupts Asp-Tyr pairing

preventing H^+ translocation that powers MmpL3 function[52]. The Southern group of MmpL3 inhibitors are typically located in SD-5 and act as stabilizers through hydrophobic interactions[52]. Based on these binding patterns, while specific protein-inhibitor interactions exist, as exemplified through different inhibitory concentrations for structurally similar series identified in SAR studies [22,31,37,153-156,158,190,191], MmpL3-inhibitor interactions are characterized by a limited number of general protein inhibitor binding motifs.

mmpL3 Mutations Affect MmpL3 Structure Function and Mycobacterial Growth

Forward genetic screening for *mmpL3* mutants resistant to MmpL3 inhibitors has been one of the primary methods used to identify MmpL3 inhibitors. Some researchers have noted that these mutant strains have *in vitro* growth defects[25,49,176]. Mutations in *mmpL3* are primarily located in codons encoding residues located in the central vestibule[20-35,37,152-157,159,160,176,177,192]. Protein gels of trypsin digested WT and mutant MmpL3 demonstrated altered folding motifs in MmpL3[49] and modeled substitutions in the MmpL3 protein structure suggests that substitutions lead to changes in the protein folding around the central vestibule[52]. A recent study by McNeil and colleagues demonstrated that *mmpL3* mutants isolated against MmpL3 inhibitors have altered membrane potential ($\Delta\psi$)[176]. The altered $\Delta\psi$ had global effects on *M. smegmatis* cells including lowered efflux, increased cell permeability, RIF hyper susceptibility, and altered TMM/TDM profiles similar to MmpL3 inhibition. These altered physiologies suggested that mutations in *mmpL3* lowered MmpL3 function resulting in lower growth rates[176]. Additional studies by McNeil and colleagues demonstrated that passaging these mutants in the presence or absence of an MmpL3 inhibitor led to the selection of compensatory mutations in the form of secondary, as well as tertiary, mutations in *mmpL3*[176,177]. These additional mutations often arose in the central vestibule in TMD adjacent to the primary mutation[176]. The passaged mutants demonstrated a reversion to WT levels of growth, suggesting a return to normal protein function, while maintaining inhibitor resistance[176,177]. While this allowed for insights into the biology and structure-function

relationship of MmpL3 it also supports the potential selection of *mmpL3* mutants resistant to MmpL3 inhibitors in the clinic. Passaging the mutants in the presence of ever increasing MmpL3 inhibitor only led to additional mutations and increased resistance without a growth defect[177]. The isolated tertiary *mmpL3* mutants were also cross resistant between IDR-0033216, IDR-0334448, AU1235, and SQ109[177]. Based on this observation, it is possible to speculate that that swapping between future clinically used MmpL3 inhibitors may only select for additional mutations and higher resistance. The compensatory mutants also did not have increased susceptibility to RIF like primary *mmpL3* mutants[177]. How these findings translate to the clinic will only be answered with time, but underscore the need for vigilant antibiotic resistance monitoring.

Physiological Impacts of MmpL3 Disruption

Because MmpL3 is involved in MM synthesis, it would be expected that perturbation of MmpL3 would put mycobacteria into a state of cell wall stress. Mycobacterial reporter strains for cell wall stress were generated through -*gfp* and -*lacZ* fusions to *iniB* which, along with downstream genes *iniAC*, are highly upregulated following INH and EMB treatment[193,194]. These reporter systems are largely insensitive to non-cell wall inhibitors[193,194]. The *iniB* reporter system was used in screens that identified MmpL3 inhibitors DA-5, DA-8, and E11[31,34]. These observations are consistent with transcriptional profiles of Mtb treated with SQ109, HC2091 and *mmpL3* knockdown which resulted in increased *iniBAC* expression[22,65,146]. These findings support a cell wall stress model for MmpL3 inhibitor treatment even in the case of E11 which has the added effect of PMF disruption[31]. As described earlier, the inhibition of MmpL3 leads to a decrease in TMM transport resulting in TMM accumulation in the CM. This was most clearly demonstrated by Xu and colleagues using *M. smegmatis* spheroplasts and dual TMM fluorescent metabolic probes and TMM lysozyme assays[48]. They demonstrated that treatment of *M. smegmatis* spheroplasts with MmpL3 inhibitors BM212 and AU1235 resulted in decreased TMM flipping to the outer leaflet of the CM. These results were later confirmed for BM212 in separate

studies by Shetty and colleagues as well as Dupont and colleagues[31,32]. Interestingly, while MmpL3 inhibitors BM212 and AU1235, as well as PIPD1 and the SIMBL based inhibitors, resulted in decreased TMM flipping in treated spheroplasts, SQ109 and E11 did not[31,32,48]. The interpretations of these studies were that SQ109 and E11 indirectly inhibit MmpL3 through PMF disruption; however, Zhang and colleagues as well as Li and colleagues clearly demonstrated direct binding of MmpL3 by SQ109 in co-crystal and SPR studies respectively[49,52]. A reinterpretation of these findings may be that PMF disrupting MmpL3 inhibitors block the second step in TMM transport in which TMM leaves the CM to associate with the periplasmic loop domains. How exactly differences in the exact MOA between MmpL3 inhibitors would occur is unclear as co-crystal structures and 3D modeling indicate that MmpL3 inhibitors have similar protein binding[52].

Whatever differences may exist in the exact nature of each inhibitors MOA, it remains clear that MmpL3 inhibition leads to the accumulation of TMM and a decrease in TDM. As discussed above, TMM covalently anchors the MM to the rest of the cell wall, and TDM, the metabolic product of Ag85 and TMM, acts as a major penetration barrier in mycobacteria[122]. Mycobacteria treated with MmpL3 inhibitors have increased cell permeability similar to strains with lower MmpL3 function[36,195]. Aligned with this idea, scanning electron micrographs of Mtb treated with an ICA based MmpL3 inhibitor revealed the formation of dimples at the dividing pole where MmpL3 localizes during cell division[143]. The authors hypothesized that these dimples were holes that formed across the cell envelope following MmpL3 inhibition. This model would suggest that MmpL3 inhibition leads to cell death through destabilization of the cell envelope and is consistent with a cell wall stress phenotype.

The Transcriptional and Metabolic Response to MmpL3 Disruption

Treatment of bacteria can lead to whole cell responses in the form of differential transcriptional and metabolomic profiles. Early studies into the MOA of SQ109 included a large

transcriptional profiling experiment conducted by Boshoff and colleagues that conducted over 400 microarray experiments of Mtb cultured and treated under different conditions[146]. The resulting profiles placed SQ109 (then diamine 109) with EMB. However, the gene expression profiles of SQ109 included the downregulation of genes involved in mycolic acid biosynthesis including *fas, fadA2, pks16,* and the *fabD-acpM-kasA-kasB-accD6* operon (Figure 1.1, Red highlight). While these genes were downregulated in the SQ109 profiles, they were upregulated in the EMB and INH profiles, suggesting SQ109 had a unique MOA[146]. Later, similar patterns for down regulated genes were observed in our lab from RNAseq profiles of Mtb treated with SQ109 or HC2091[22]. Similarly, the RNAseq profile from an Mtb *mmpL3* knockdown strain also identified the downregulation of mycolic acid biosynthesis genes[65]. The profiles generated in these three studies were highly similar and generated in the presence of SQ109 which decreases the $\Delta\psi$[117], HC2091 which does not affect the $\Delta\psi$[22], and following *mmpL3* depletion which, presumably, leads to an increased $\Delta\psi$ as observed by Li and colleagues[49]. This suggests that the transcriptional responses identified were highly specific to MmpL3 disruption and independent of secondary membrane energetic effects.

The consistent differential profiles generated by MmpL3 disruption not shared by other cell wall inhibitors, suggests that mycobacteria can sense when MmpL3 specifically is inhibited. As a consequence of these expression changes, the associated metabolites should also decrease in abundance. Consistent with this model, metabolomic profiles generated by Zampieri and colleagues of *M. smegmatis* treated with GSK2623870A identified a decrease in trehalose 6-phosphate[23], the activated form of trehalose that serves as a substrate to make TMM[107]. Additionally, Zampieri and colleagues identified that fatty acid synthesis proteins, such as Fas, were primarily affected in a proteomic analysis[23].

Of the three profiles generated to date, the *mmpL3* knockdown profile was the most robust, with several regulatory pathways identified as differentially expressed in addition to mycolic acid biosynthesis[65]. The regulatory pathways may be involved in the sensing of changes to the cell

envelope following MmpL3 perturbation. However, it is also possible that this profile includes genes responding to the increase in the Δψ following *mmpL3* knockdown[49]. Based on the transcriptional profiles, we know that Mtb represses genes involved in both the FAS-I and FAS-II pathways. Mtb also upregulates expression of the cell wall stress operon *iniBAC* in response to MmpL3 disruption[22,65,146]. How Mtb specifically senses MmpL3 disruption, and differentially regulates its genes from other cell wall inhibitors such as EMB and INH, is not clear. One model may suggest that Mtb senses changes in CM fluidity following TMM accumulation[48]. Such changes would not occur in INH treated cells, as FAS-II disruption from INH would not directly affect CM fluidity as CM lipids are generated through FAS-I[196]. If so then this may be through either the alternative sigma factor, SigE (Rv1221), or the two-component system regulator MprAB (Rv0981 and Rv0982), which respond to cell wall stress[197,198] and whose regulons were upregulated in the *mmpL3* knockdown profile[65].

Of note, the transcriptional effects of MmpL3 disruption are primarily repressive, and few genes are observed to be upregulated in response to MmpL3 inhibition[22,65,146]. One response was the induction of osmotic stress genes, *oprA* (*Rv0516c*) in the *mmpL3* knockdown profile[65] , suggesting that the bacteria are experiencing osmotic stress. Other genes upregulated in these profiles include SigE and MprAB regulated genes in the *mmpL3* knockdown profile, and the *iniBAC* cell wall stress signature genes in all three profiles[22,65,146]. However, these transcriptional signatures are not specific to MmpL3 disruption and are upregulated in Mtb in other stresses[146]. Several reporter strains for have been built around specific genes being upregulated following specific stresses[193,194]. However, the non-specific transcriptional response following MmpL3 disruption in Mtb does not lend itself for the use of building a reporter strain. While the gene repression signature following MmpL3 disruption is unique compared to FAS-II or arabinogalactan synthesis inhibition[146], disentangling this gene repression signature from cell death or transcriptional repression from RNA polymerase and DNA gyrase inhibitors is difficult.

Screening for MmpL3 Inhibitors

MmpL3 inhibitors continue to be the most diverse class of inhibitors that share a single target for Mtb. Because of the slow growth of Mtb and *M. bovis*, untargeted screening approaches for MmpL3 inhibitors through the isolation and sequencing of resistant mutants is largely ineffective and time consuming. An alternative approach of using the rapidly growing mycobacteria *M. smegmatis* or *M. abscessus* is limited by observations that not all MmpL3 inhibitors are active in these two species[25,42]. Because MmpL3 is such a common target with high therapeutic potential, screening platforms to identify these inhibitors are highly sought. This is not only to identify potential early drug candidates for the treatment of infectious mycobacteria, but also to set aside such inhibitors in favor of novel targets. While reporter strains such as the *iniB* reporter system have identified some MmpL3 inhibitors[31,34], the low specificity for MmpL3 limits the use of this reporter system to its original intended purpose of identifying cell wall inhibitors. Additionally, while reporter systems have been built around genes highly expressed following target inhibition, MmpL3 inhibition largely leads to gene downregulation signature genes[146]. Alternatively, whole cell morphological changes were recently described to differentiate the inhibitors by their specific MOA using a system called Morphological Evaluation and Understanding of Stress (MorphEUS)[199]. While this system is unique in its ability to identify both primary and secondary MOAs, it is limited by specificity, and places inhibitors in broad stressor categories like cell wall stress. Recently, however; four potential screening methods have been proposed as screening platforms for MmpL3 inhibitors. These include 1) a high-throughput metabolic screening platform[23], 2) a whole cell targeted mutant screen that uses *mmpL3* mutants[25], 3) a two-way *mmpL3* regulatory phenotypic reporter system[36], and 4) a competitive binding assay that uses MmpL3 binding fluorophore[49].

The MOA of inhibitors can lead to differential responses in bacteria that can be measured in a number of ways. One of these measurements is the metabolomic response bacteria develop following the inhibition of specific metabolic pathways. Using a high-throughput metabolic analysis

platform Zimpieri and colleagues identified several MmpL3 inhibitors through differential metabolic profiles[23]. They observed that six inhibitors from a library of 212 compounds led to repeated decreases in the metabolite α,α-trehalose-6-phosphate and neighboring lipids, precursors to TMM. Two of the inhibitors, GSK1829729A and GSK1829728A, were reported to be chemically similar to THPP and isolation of resistant mutants to a third compound, GSK2623870A, resulted in *mmpL3* mutants. While not specifically designed to identify MmpL3 inhibitors, this system was fast and accurate at identifying the MOA of mycobacterial growth inhibitors. This system is not specifically limited to mycobacteria and could feasibly be applied to other bacterial and pathogenic species. Though this system can be applied to larger libraries, the technological and computational requirements to perform this assay are still somewhat limiting and requires specific expertise.

The second MmpL3 inhibitor screening platform was developed in our lab and was built on the observation that *mmpL3* mutants have broad cross-resistance to MmpL3 inhibitors[22,25,28,32,34,36,49,153,156,177] but low cross-resistance to non-MmpL3 inhibitors[25,27,28,32,34,35,37,49,152,156,176]. Another observation previously made was that the amount cross-resistance depended on the specific combination of *mmpL3* mutant and MmpL3 inhibitor tested[49]. To overcome potential limitations, we generated a pool of twenty-four unique *mmpL3* mutants isolate against five structurally unique MmpL3 inhibitors[22,25]. We hypothesized that MmpL3 inhibitors would select for the mutant(s) with the highest resistance, while non-MmpL3 inhibitors would equally affect all the mutants. The resulting *Targeted Mutant Screening* assay compared the effects inhibitors have on the growth (OD_{600}) of wild type (WT) vs the *mmpL3* mutant pool, in which the mutants would be less effected by an MmpL3 inhibitor. Using this mutant assay, we screened a small library of 174 Mtb growth inhibitors including, previously described MmpL3 inhibitors SQ109, C215, and HC2091[20,22,25,34]. The results of our assay identified controls SQ109 and C215, as well as HC2060, HC2091, HC149, HC2169, and HC2184 which were used to generate the *mmpL3* mutants used in the assay[25]. In addition to these seven compounds, we also

identified six other inhibitors HC2032, HC2099, HC2134, HC2138, HC2178, and HC2183[25]. Overall, the screen was highly successful and confirmed hits induced lipid profiles consistent with MmpL3 inhibition and were positive for the competitive binding assay described above[25,49]. However, this system has limitations. For one, we did not observe differences in the inhibitory effects for Rimonabant between the WT and *mmpL3* mutant pool[25]. Rimonabant is highly similar to BM212 which demonstrates cross resistance to a very small number of *mmpL3* mutants[49] which were not included in our pool. Future versions of this screen may seek to include *mmpL3* mutants isolated against BM212 or Rimonabant to broaden the screening potential of this system.

The third screening platform uses strains that differentially express *mmpL3.* An early version of this screen was originally proposed by Li and colleagues who observed inducible knockdown of *mmpL3* to sub-inhibitory levels rendered Mtb sensitive to MmpL3 inhibitors[64]. While promising, this system was limited by synthetically lethal combinations with other TB drugs such as RIF[64]. Alternatively, Zhang as well as Kozikowski, and their respective colleagues, demonstrated that *mmpL3* overexpression mycobacterial strains, expressing either WT or a resistant mutant *mmpL3* alleles, conferred high resistance to MmpL3 inhibitors[52,154]. The overexpression strain created by Zhang and colleagues did not confer cross resistance to INH[52], but further investigation into the screening potential of overexpression strains like these were not conducted. However, recently Grover and colleagues demonstrated that a combined dual regulatory strain of Mtb that either repressed or overexpressed *mmpL3* was highly accurate at identifying MmpL3 inhibitors from a library of 220 Mtb growth inhibitors[36]. The authors of this study demonstrated that *mmpL3* knockdown sensitized bacteria to MmpL3 inhibitors as previously described. However, this knockdown also made Mtb hypersensitive to non-MmpL3 inhibitors such as RIF, clarithromycin, erythromycin, fidaxomicin, fusidic acid, as well as β-lactams[36]. Conversely, overexpression of *mmpL3* resulted in decreased activity of MmpL3 inhibitors but did not lead to differential inhibitory effects for non-MmpL3 inhibitors[36]. The recognition of a bidirectional shift that only occurred for MmpL3 inhibitors indicated that this system could be used to screen for MmpL3

inhibitors, which was applied to a library of 220 Mtb growth inhibitors. The results of this screen identified several previously described MmpL3 inhibitor scaffolds including THPP-, Spiro-, Urea-, Pyrole-, PIPD-, Oxadiazole-like compounds, as well as a novel guanidine-based MmpL3 inhibitor CCI7967[36]. The identification of CCI7967 was backed by the isolation of *mmpL3* mutants resistant to CCI7967. This screening platform overcomes the limitations of the Targeted Mutant Screening platform by identifying Pyrole-based MmpL3 inhibitors such as BM212[25]. However, this screen, along with the Targeted Mutant Screen, share a common limitation of requiring compounds to be tested against both the WT reference strain as well as the experimental *mmpL3* strain(s). While these screens are not burdensome for larger pharmaceutical companies or smaller compound libraries for academic institutes, such as the ones conducted in either screen, the doubling of resources required to run these screens would become costly for larger libraries. This limitation renders both screening platforms to be used as mechanisms to identify MmpL3 inhibitors from hits from larger HTS. This limitation could be overcome in the fourth potential screening platform described next.

Finally, the fourth potential screening platform proposed uses the competitive binding assay mentioned above using the NORTH series of MmpL3 binding probes[49]. This competitive binding assay utilizes MmpL3 inhibitor scaffolds such as ICAs, AU125, or the SIMBL covalently linked to the commercially available fluorophore TAMRA through click chemistry[49]. These MmpL3-fluorophores co-localize with MmpL3 in dividing *M. smegmatis* cells and are demonstrated to interact with MmpL3 based on SPR and biolayer interferometry[49]. Using flowcytometry, researchers can measure the relative fluorescence intensity of cells treated with the NORTH probes which decreases in the presence of a competing MmpL3 inhibitor. This competitive binding assay is insensitive to non-MmpL3 inhibitors such as RIF and INH as well as PMF uncouplers such as CCCP[49]. This screen works in both whole cell mycobacteria as well as isolated MmpL3 protein adding diversity not available to the previously described Targeted Mutant and Two-Way Regulation screens described above Additionally, both the whole cell and biochemical assays can

measure MmpL3 binding within hours, overcoming the slower times required for the other two screen platforms which take place over days due to the slow growth of mycobacteria[25,36]. This screen also has the potential to be used to conduct SAR campaigns directly against MmpL3 rather than whole cell bacteria. As mentioned above, SAR campaigns can result in either gain or loss in activity through the modification of parental structures. It has never been clear if modifications of parental compounds lead to loss of activity due to the inability to bind to MmpL3 or due to the inability to permeate the cell wall. While this system has yet to be tested in a screen, the rapid nature of this assay coupled with the direct measurement of MmpL3 binding without the requirement for comparative strains suggests that this assay will likely make for an efficient platform to screen for MmpL3 inhibitors in a large library. However, this screen is limited and could identify non-inhibitory MmpL3 interacting substrates that could also lead to probe displacement. Further, biochemical screens have previously identified metabolic inhibitors devoid of whole cell activity due to factors such as cell impermeability[200]. Therefore, this screening platform will still require secondary assays to demonstrate whole cell activity.

It is clear that MmpL3 inhibitors will continue to be identified through the traditional untargeted approaches of isolating *mmpL3* mutants, but with the invention of the novel screening systems listed here, the rate of identification will likely increase dramatically. While SQ109 has demonstrated great drug potential so far, if SQ109 were to fail in clinical trials, then it is likely that another MmpL3 inhibitor from the ones identified in the last decade could take its place.

Concluding Remarks

MmpL3 continues to be an attractive target for TB therapy. The essential nature of the protein both *in vitro* and *in vivo* and the clinical success of SQ109 so far support further development of MmpL3 inhibitors. Protein localization and interactome studies have demonstrated that MmpL3 complexes with other cell wall synthesis metabolic pathways as part of the mycobacterial divisome. While some questions still remain including how MmpL3

complexes with TMM in the CM, live cell microscopy and biochemical evidence demonstrates that MmpL3 plays a direct role in TMM transport across the CM. Additionally, biochemical studies have clearly demonstrated that MmpL3 directly binds to many of the proposed inhibitors described in the literature. These direct protein-inhibitor interactions support the isolation of resistant *mmpL3* mutants and lipid profiling as good early indicators of the MOA of identified inhibitors. Further, the similar chemical properties and protein localization of these inhibitors indicate a general threshold of what makes an MmpL3 inhibitor and how they bind to MmpL3. While additional questions still remain for MmpL3 regarding regulation, protein-protein interaction, and function remain, the insights gained in the last decade have advanced our understanding of the role MmpL3 plays in cell biology of mycobacteria.

CHAPTER 2: Identification of New MmpL3 Inhibitors by Untargeted and Targeted Mutant Screens Defines MmpL3 Domains with Differential Resistance

Work presented in this chapter has been published as John T. Williams[1], Elizabeth R. Haiderer[1], Garry B. Coulson[1], Kayla N. Conner[1], Edmund Ellsworth[2], Chao Chen[3], Nadine Alvarez-Cabrera[3], Wei Li[4], Mary Jackson[4], Thomas Dick[3], and Robert B. Abramovitch[1]*. Identification of new MmpL3 inhibitors by untargeted and targeted mutant screens defines MmpL3 domains with differential resistance. Antimicrobial Agents and Chemother 63:e00547-19.

[1]Department of Microbiology and Molecular Genetics, and [2]Department of Pharmacology and Toxicology, Michigan State University, East Lansing, Michigan, 48824, United States. [3]Center for Discovery and Innovation, Hackensack Meridian Health, Nutley, New Jersey, 07110; [4]Mycobacteria Research Laboratories, Department of Microbiology, Immunology and Pathology, Colorado State University, Fort Collins, Colorado, 80523, United States.

Abstract:

The *Mycobacterium tuberculosis* (Mtb) mycolate flippase MmpL3 has been the proposed target for multiple inhibitors with diverse chemical scaffolds. This diversity in chemical scaffolds has made it difficult to predict compounds that inhibit MmpL3 without whole genome sequencing of isolated resistant mutants. Here we describe the identification of four new inhibitors that select for resistance mutations in *mmpL3.* Using these resistant mutants, we conducted a targeted whole-cell phenotypic screen of 163 novel Mtb growth inhibitors for differential growth inhibition of wild type Mtb as compared to a pool of twenty-four unique *mmpL3* mutants. The screen successfully identified six additional putative MmpL3 inhibitors. The compounds were bactericidal both *in vitro* and against intracellular Mtb. Mtb cells treated with these compounds were shown to accumulate trehalose monomycolates, have reduced levels of trehalose dimycolate, and displace a MmpL3 specific probe, supporting MmpL3 as the target. The inhibitors were mycobacteria specific with several also showing activity against the non-tuberculous mycobacterial species *M. abscessus.* Cluster analysis of cross resistance profiles generated by dose response experiments for each combination of 13 MmpL3 inhibitors against each of the 24 *mmpL3* mutants defined two clades of inhibitors and two clades of *mmpL3* mutants. Pairwise combination studies of the inhibitors revealed interactions that were specific to the clades identified in the cross-resistance profiling. Additionally, modeling of resistance substitutions to the MmpL3 crystal structure revealed clade specific localization of the residues to specific domains of MmpL3, with the clades showing differential resistance. Several compounds exhibited high solubility and stability in microsomes and low cytotoxicity in macrophages, supporting their further development. The combined study of multiple mutants and novel compounds provides new insights into structure-function interactions of MmpL3 and small molecule inhibitors.

Introduction:

In efforts to identify new tuberculosis (TB) antibiotics, whole cell-based phenotypic screens have been conducted against the pathogen *Mycobacterium tuberculosis* (Mtb). Over the last decade, several of these screens have identified MmpL3 as the proposed target for diverse small molecule inhibitors including AU1235, BM212, C215, DA-5, E11, indolecarboxamides, HC2091, NITD-349, PIPD1, Rimonabant, Spiro, TBL-140, THPP and SQ109[20,27-31,34,35,52,152,153,201]. MmpL3 is an essential flippase responsible for transporting trehalose monomycolate (TMM) or acylated-trehalose monomycolate synthesized in the cytoplasm to the pseudo-periplasmic space[44,45,64,116,202]. These TMMs are then converted into trehalose dimycolate (TDM) by the Ag85 complex in the cell envelope[63]. Additionally, MmpL3 has recently been proposed to transport phosphatidylethanolamine[51], expanding the function of MmpL3 lipid transport. MmpL3 is essential as evidenced by a pre-existing rescue allele being required to generate an *mmpL3* knockout[29,42,45,64,65,203], lack of mutants in high-throughput transposon mutagenesis screens[62,151], and studies that show rapid killing *in vitro* and *in vivo* in acute infection models when *mmpL3* expression is conditionally inhibited[64,65]. This makes MmpL3 an attractive target for drug development, with one of its inhibitors, SQ109, currently in clinical trials[204].

MmpL3 inhibitors fall into diverse classes of chemical scaffolds[117,205,206], making it hard to computationally predict potential MmpL3 inhibitors based on chemical scaffolds. However, given the frequent finding of MmpL3 as a target, it is reasonable to expect that many new hits in a high throughput screen (HTS) may be acting against MmpL3. MmpL3 inhibitors have been identified by the isolation and sequencing of resistant mutants with single nucleotide variations (SNVs) mapping to the coding region of *mmpL3,* which is time-consuming and costly. Efforts to discover MmpL3 inhibitors using targeted approaches include generating hypomorphs, where an *mmpL3* knock down strain showed enhanced sensitivity to MmpL3 inhibitors, including AU1235[64]. However, this strain was also shown to be sensitive to isoniazid (INH) an inhibitor of InhA of the FAS-II pathway involved in mycolic acid synthesis, suggesting that while a *mmpL3* knockdown

strain has robust screening potential for inhibitors of mycolic acid synthesis, maturation, and transport, such strains are not specific enough to identify inhibitors that selectively target MmpL3.

An alternative approach, employed in this study, is to use a pool of *mmpL3* resistant mutants to discover potential MmpL3 inhibitors. MmpL3 is a member of the resistance nodulation and division (RND) family of proteins, normally associated with efflux pumps in gram-negative bacteria[29,44,45]. However, evidence suggests MmpL3 does not act as a general efflux pump in resistant backgrounds as resistant mutants do not differ in the amount of inhibitor isolated from cell fractions compared to WT Mtb[29]. In further support that MmpL3 does not act as an efflux pump, the low level of cross resistance to compounds not associated with MmpL3 inhibition, including INH, suggests that MmpL3 does not act as a general efflux pump[203]. This suggests that MmpL3 inhibitor resistant mutants could be used to screen for other potential MmpL3 inhibitors. The goal of this study was to discover MmpL3 inhibitors from a collection of 163 newly discovered, uncharacterized inhibitors of Mtb growth[207]. Herein we describe the identification of four novel MmpL3 inhibitors by isolation of resistant Mtb mutants with mutations mapping to *mmpL3.* These twenty-four unique Mtb *mmpL3* mutant strains were then pooled into a single batch culture to conduct a targeted whole-cell phenotypic screen to identify six new scaffolds with reduced activity in the mixed mutant population as compared to the wild type. Cross resistance and compound interactions studies demonstrate specific structure function interactions between the molecules and MmpL3 and defined domains of MmpL3 associated with differential resistance to MmpL3 inhibitors.

Results:

Identification of Four New MmpL3 Inhibitors by Isolation of Resistant Mutants

Previously, two HTS were conducted, targeting the two component regulatory systems, DosRST and PhoPR[207-209]. In addition to inhibitors targeting these pathways, a series of compounds was identified that inhibited Mtb growth independent of the targeted pathways[201,207,209]. A series of high throughput assays were then conducted to prioritize these compounds (Figure A.2.1) including confirming hits, testing for eukaryotic cytotoxicity in primary murine bone marrow-derived macrophages (BMMΦ, ≤10% cytotoxicity), and testing for the ability of the compounds to inhibit Mtb growth inside BMMΦ (≥25% growth inhibition). Results of these screens identified 216 compounds of which 163 commercially available compounds were purchased as fresh powders. In order to identify the mechanism of action of these Mtb growth inhibitors our lab selected several compounds with potent Mtb growth inhibition, both *in vitro* and in macrophages, as well as low murine macrophage cytotoxicity.

Four compounds of interest HC2060, HC2149, HC2169, and HC2184 (1-({1-[4-(Benzyloxy)-3-methoxybenzyl]piperidin-3-yl)carbonyl}azepane, N-[2-Methyl-6-(trifluoromethyl)pyridin-3-yl]-4-(trifluoromethyl)benzamide, Ethyl 3-{[(3,4-dihydro-2H-chromen-3-ylamino)carbonyl]amino}benzoate, and N-(2-Diethylaminoethyl)-N-(5,7-dimethyl-1,3-benzothiazol-2-yl)furan-2-carboxamide, respectively) (Figure 2.1a) had half maximal effective concentrations (EC_{50}) ranging from 1.8 μM to 16.9 μM *in vitro* (Figure 2.1b, Table 2.1). All four compounds had bactericidal activity when measured at 20 μM (2x the initial screening concentration) (Figure 2.1c). To our knowledge, the structures of these compounds are unique from previously described inhibitors of Mtb growth.

To understand the mechanism of action of these four compounds, resistant mutants were isolated using solid agar plates (7H10 OADC) amended with 20 or 40 μM of each compound inoculated with 10^9 CFU of Mtb (Erdman). Isolated mutants were tested for resistance via dose response curves. Confirmed resistant clones were isolated as single colonies and retested to

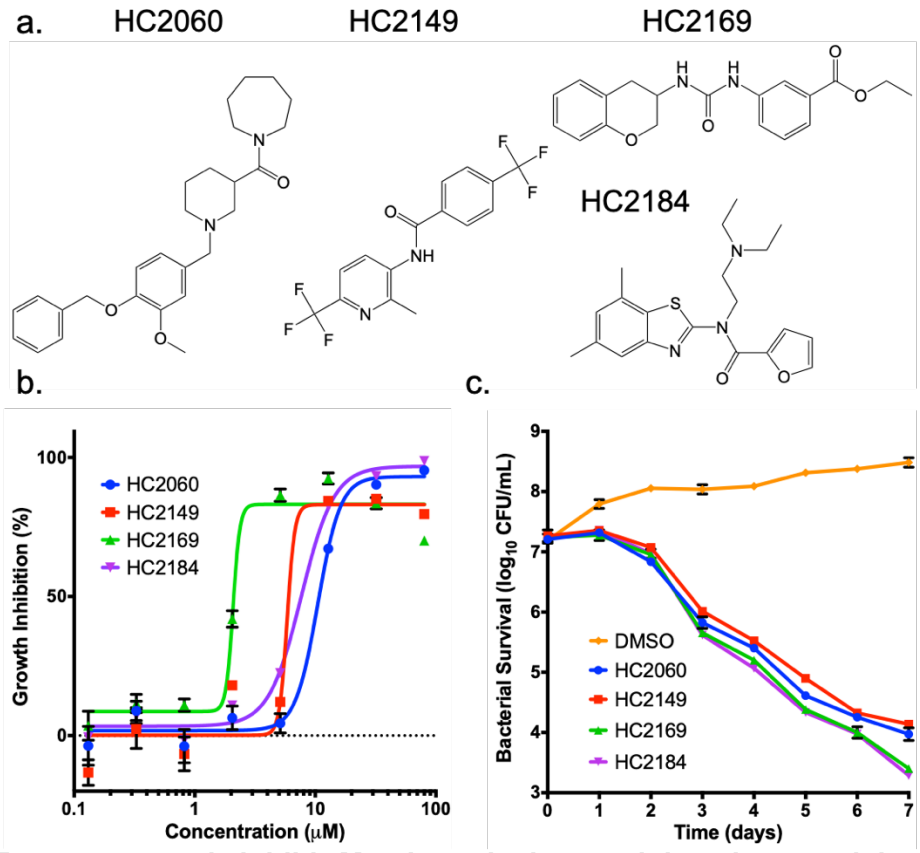

Figure 2.1. Four compounds inhibit *M. tuberculosis* growth in a dose- and time-dependent manner. (a) Structures of HC2060, HC2149, HC2169, and HC2184. (b) Inhibition of *M. tuberculosis* growth in a dose-dependent manner. (c) Killing of *M. tuberculosis* in a time-dependent manner when treated with the inhibitors at 20 μM. Error bars indicate the standard deviations from the mean values. Experiments were conducted in biological triplicates.

confirm resistance (Figure A.2.2a-d). Genomic DNA was extracted from confirmed resistant mutant strains and the genomes were sequenced. Analysis of the genome sequences identified single nucleotide variants (SNVs) in all of the genomes in the coding region of *mmpL3* (Rv0206c, Table A.2.1). These mutations encoded for nonsynonymous mutations located throughout the gene (Table A.2.1, Figure A.2.2e). These findings suggest these compounds may be functioning as MmpL3 inhibitors.

Table 2.1. Characterization of MmpL3 inhibitors

Compound	Clade	WT EC_{50} (μM)	*mmpL3* Mutant Pool EC_{50} (μM)	Differential EC_{50}	MΦ EC_{50}	Δψ Disruption	Cytotoxicity (CC_{50}) (μM)	Solubility (μM)	Microsome Stability (% remain 30 min)
HC2032	B	2.2	>80	>36	0.8	Yes	>100	18	102
HC2060	B	16.9	>80	>5	4.1	No	>100	>300	44
HC2091	B	6.2	>80	>13	2.2	No	>100	>300	45
HC2099	B	1.7	38.9	23	<0.3	No	>100	178	71
HC2134	A	1.4	>80	>57	7.3	Yes	>100	116	N.D.
HC2138	A	4.0	>80	>20	<0.3	Yes	>100	66	122
HC2149	A	6.6	>80	>12	3.6	Yes	>100	131	138
HC2169	A	1.8	>80	>44	<0.3	No	>100	17	168
HC2178	B	3.8	>80	>24	2.0	Yes	>100	>200	4
HC2183	B	3.2	59.9	19	3.0	No	>100	>200	25
HC2184	B	7.6	>80	>11	0.7	Yes	>100	>300	30
C215	B	11.2	57.5	5	4.0	Yes	14.3	87	62
SQ109	B	2.4	6.9	2	<0.3	Yes	N.D.	N.D.	N.D.

N.D. – Not determined
Relative EC_{50} is fold difference between WT vs. *mmpL3* mutant pool.

Modulation of TMM and TDM Accumulation

MmpL3 is responsible for the transport of TMM across the inner membrane[63,64,116,202]. To determine if these compounds inhibited the activity of MmpL3, cultures of Mtb were grown in the presence of ^{14}C-acetate and treated for 24 h with 20 μM of HC2060, HC2149, HC2169, HC2184, SQ109 or equal volumes of dimethylsulfoxide (DMSO). Radiolabeled lipids were isolated and analyzed by thin layer chromatography (TLC) (Figure 2.2a, Figure A.2.3a). The results of the lipid assay show that TMM accumulates in Mtb samples treated with the proposed MmpL3 inhibitors as well as the SQ109 treated samples. Additionally, TDM significantly decreased in cultures treated with HC2169 and HC2184 as well as the positive control SQ109 (Figure 2.2a and Figure A.2.3a). These results are consistent with previously described MmpL3 inhibitors[20,28-31,34,117,153,201] and support that these four compounds inhibit MmpL3 activity.

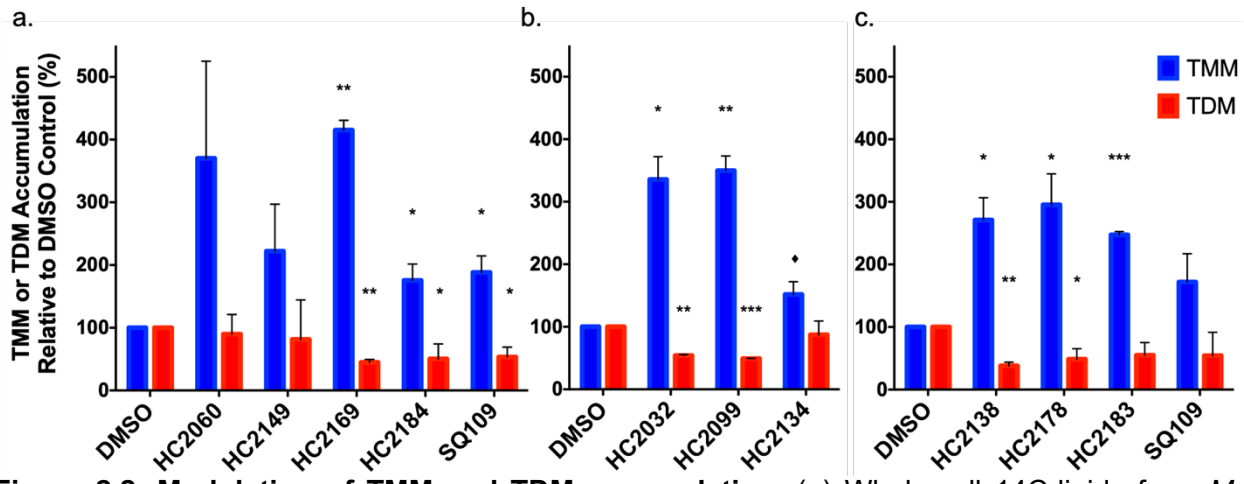

Figure 2.2. Modulation of TMM and TDM accumulation. (a) Whole-cell 14C-lipids from *M. tuberculosis* cells treated with 20 μM HC2060, HC2149, HC2169, and HC2184 show increased levels of TMM and decreased levels of TDM. (b and c) Whole-cell 14C-lipids from *M. tuberculosis* cells treated with a concentration of 20 μM of the six inhibitors identified by the targeted phenotypic screen show increased levels of TMM and decreased levels of TDM. Experiments were conducted in biological duplicates. In both experiments, *M. tuberculosis* samples were treated with DMSO or 20 μM SQ109 as controls. Error bars indicate the standard deviations. *, $P < 0.05$; **, <0.005; ***, <0.001; ♦, value that just missed the cut off ($P = 0.07$ compared to TMM level after HC2134 treatment). The results for HC2060 and HC2149 missed the significance cutoff, but this may be due to the high variability in replicates, as there was a >2-fold difference for HC2060 and HC2149.

Targeted Whole-Cell Phenotypic Screen for MmpL3 Inhibitors

The identification of four new MmpL3 inhibitors, as well as the previously published inhibitor HC2091[22], suggested additional MmpL3 inhibitors may exist in the prioritized 163-compound library of Mtb growth inhibitors (Figure A.2.1). Review of the known MmpL3 inhibitor scaffolds and those in our compound library identified HC2172 as the previously describedidentified HC2172 as the previously described MmpL3 inhibitor C215[20]. A recent study by McNeil *et al.,* showed that *mmpL3* mutant strains had low cross resistance against non-MmpL3 inhibitors[203], suggesting that *mmpL3* mutants could be used to screen for MmpL3 inhibitors. Additionally, this study also showed that different mutations conferred varying levels of cross resistance between MmpL3 inhibitors. We therefore, hypothesized that by pooling unique *mmpL3* mutant strains into a single mixed culture we could overcome limitations of cross resistance variability. For the targeted phenotypic screen, we directly compared percent growth inhibition

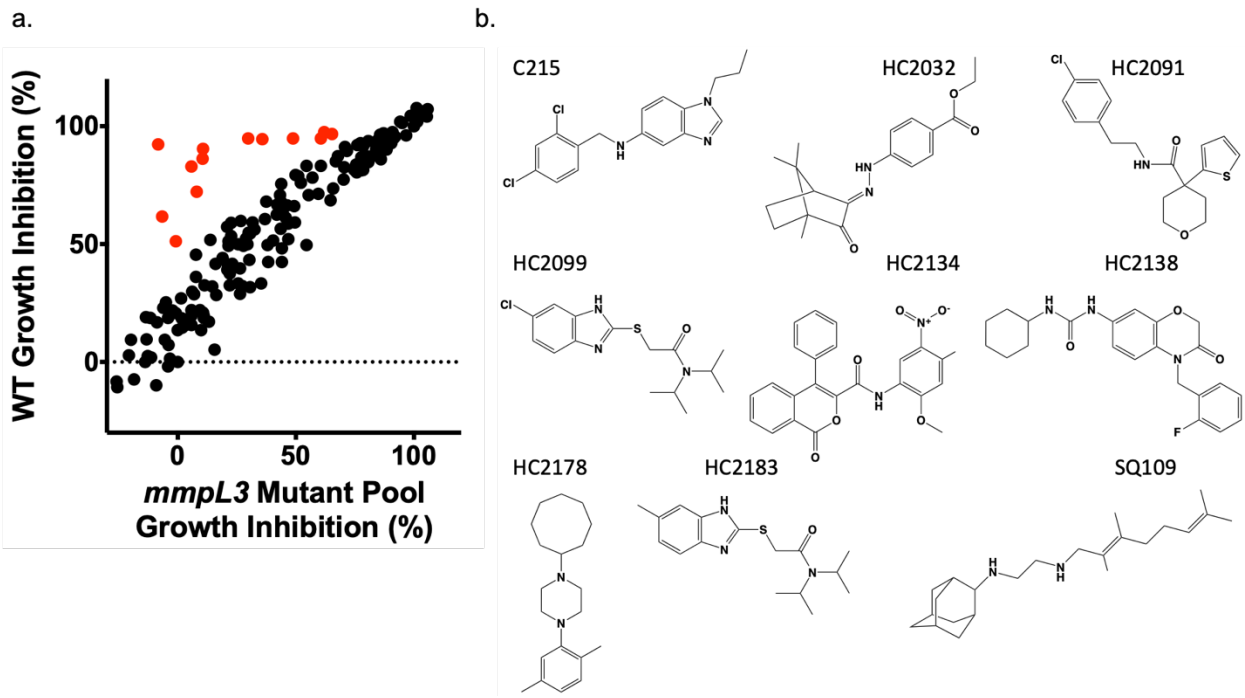

Figure 2.3. A targeted whole-cell phenotypic screen identifies six new MmpL3 inhibitors. (a) Results of a direct head-to-head comparison of percentages of growth inhibition of WT M. tuberculosis and a pooled mmpL3 mutant population treated with 163 compounds at 20 μM. Additional treatments included 0.5 μM BDQ, CFZ, INH, PAS, or SQ109 or 0.03% H_2O_2. Examples of hit compounds with reduced activity in the MmpL3 mutant pool are shown in red. (b) Structures of the confirmed hit compounds from the screen, including six new compounds, HC2032, HC2099, HC2134, HC2138, HC2178, and HC2183. Previously described compounds include C215, HC2091, and SQ109.

(%GI) of either WT or a mixed *mmpL3* mutant pool consisting of twenty-four unique *mmpL3* mutant strains, including three strains previously described as resistant to HC2091[201] (see Table A.2.2). We tested for differences in growth between WT and the twenty-four unique *mmpL3* strains and did not observe major growth differences following nine days of incubation. Given that mutant abundance is normalized at the beginning of the assay, and growth is similar by Day 6 when the assay is completed, the relative abundance of each strain is not anticipated to bias the screen (Figure A.2.4). The cultures were treated with 20μM of each of the 163-Mtb growth inhibitors as well as DMSO (negative control), Rifampin (RIF, positive control), Bedaquiline (BDQ), Clofazimine (CFZ), INH, para-amino salicylic acid (PAS), H_2O_2, or SQ109 for a total of 171 different treatments (Figure A.2.5a and A.2.5b). The results of this screen identified thirty-two compounds with 15% GI in the WT background and 1.5x reduced activity in the mixed *mmpL3*

mutant background relative to the WT background (examples of positive hits are illustrated in red in Figure 2.3a). These hits were tested by dose response experiments conducted in both the WT and mixed *mmpL3* mutant background. In total, we identified thirteen compounds with reduced activity in the mixed *mmpL3* mutant background (Table 2.1, Figure A.2.6). Included in our confirmed hits were each of the five inhibitors used to generate the *mmpL3* mutant strains (HC2060, HC2091, HC2149, HC2169, and HC2184) and the two control compounds C215 and SQ109. The targeted screen also identified six novel inhibitors including HC2032, HC2099, HC2134, HC2138, HC2178, and HC2183 (ethyl 4-[(2E)-2-(4,7,7-trimethyl-3-oxo-2-bicyclo[2.2.1]heptanylidene)hydrazinyl]benzoate, 2-[(6-chloro-1H-benzimidazol-2-yl)sulfanyl]-N,N-di(propan-2-yl)acetamide, N-(2-methoxy-5-nitrophenyl)-1-oxo-4-phenylisochromene-3-carboxamide, 1-cyclohexyl-3-[4-[(2-fluorophenyl)methyl]-3-oxo-1,4-benzoxazin-7-yl]urea, 1-cyclooctyl-4-(2,5-dimethylphenyl)piperazine, and 2-[(6-methyl-1H-benzimidazol-2-yl)sulfanyl]-N,N-di(propan-2-yl)acetamide, respectively) (Figure 2.3b), which have not been previously described as MmpL3 inhibitors. The amount of resistance conferred by the mixed *mmpL3* mutant strains against each compound varied, with some compounds, like HC2032, HC2138, and HC2169 losing nearly all activity in the mutant background (Figure A.2.6) as indicated by the high differential EC_{50} (fold difference between *mmpL3* mutant pool and WT) values of >36, >20, and >44 (Table 2.1). Despite the high activity of SQ109 in the WT background, the relative EC_{50} was only 2 (Table 2.1); however, this observation is consistent with previous studies which only report marginal increases in MIC values in *mmpL3* mutant backgrounds[34,117,201,203]. Included in our hits were two urea-based compounds HC2138 and HC2169 (Figure 2.1 and Figure 2.3b). These urea-based compounds have structures reminiscent of the adamantyl-urea MmpL3 inhibitor AU1235[29]. Additionally, two of the compounds identified in the screen HC2099 and HC2183 had high structure similarity. We also tested our mixed mutant population against Rimonabant, an analogue of BM212, previously shown to bind to MmpL3[52]; however, we did not identify any difference between the WT or the mixed mutant population (Figure A.2.7). This finding is consistent with the

mutant pool not containing mutations known to provide resistance to BM212 or rimonabant[30] and demonstrates the current mutant pool does not comprehensively identify all known MmpL3 inhibitors.

The compounds were also tested for murine macrophage cytotoxicity, solubility and stability in mouse microsomes, and the structures were confirmed by mass spectrometry (Table 2.1). The compounds exhibited low cytotoxicity (CC_{50} >100 μM), consistent with our secondary assay screening (Figure A.2.1). Compounds exhibited varying levels of solubility with HC2169 and HC2138 showing lower solubility (66 μM and 17 μM respectively) but high microsome stability (122% and 168% respectively), and compounds like HC2183 showing high solubility (>200 μM) but low microsome stability (25%). Interestingly HC2099, which has high structure similarity to HC2183 showed higher solubility (178 μM) and higher microsome stability (71%). Several of the compounds (e.g. HC2091, HC2099, HC2138 and HC2149), exhibited favorable solubility and microsome stability, with no observed macrophage cytotoxicity, supporting their potential for further development.

The phenotypic screen was selective as it did not identify any of the control treatments known to not target MmpL3 including BDQ, INH, PAS, H_2O_2, or HC2051, a proposed Pks13 inhibitor (given its similarity to the TAM16[24]). To confirm the specificity of our screen, we conducted dose response studies in both the WT and mixed *mmpL3* mutant background for each of the aforementioned inhibitors, as well as RIF. Results of the dose response studies did not identify any significant levels of resistance to these compounds in the mixed *mmpL3* mixed mutant background (Table A.2.3 and Figure A.2.8). This was true for both inhibitors of mycolic acid synthesis and maturation (INH and HC2051), suggesting our screen was specific for inhibitors of MmpL3. Consistent with previous results, we identified increased susceptibility to RIF treatment in the mixed *mmpL3* mutant background[203] (Table A.2.3, Figure A.2.8). The dose response profiles for BDQ, CFZ, and PAS did not show any differences in susceptibility, further supporting that *mmpL3* mutations do not confer resistance through general efflux.

Modulation of TDM, Membrane Potential and Viability

To determine if the six compounds identified in the screen can inhibit MmpL3 activity, we examined accumulation of TMM and TDM as described above. The inhibitors modulated mycolic acid accumulation in whole cell extracts, with lipids for all treatments showing a significant accumulation in TMM (except for HC2134) and treatment with HC2032, HC2099, HC2138, and HC2178 showing a significant decrease in TDM relative to the DMSO control samples (Figure 2.2b and 2.2c, Figure A.2.3b). A recent report has shown that because MmpL3 activity is dependent on the proton motive force (PMF), disruptors of PMF, such as the protonophore carbonyl cyanide m-chlorophenyl hydrazine (CCCP) can also modulate MmpL3 activity [117]. Studies have suggested that some proposed MmpL3 inhibitors such as SQ109 and E11 may indirectly target MmpL3 through disruption of the membrane potential[31,117,202], although direct interactions of MmpL3 and SQ109 have been recently reported[49,52]. To determine if the newly identified inhibitors disrupt membrane potential (Δψ) we conducted dose response studies using a $DiOC_2$-based assay. Some compounds, including HC2060, HC2169, and HC2183 did not disrupt membrane potential (Table 2.1, Figure A.2.9), while others, such as HC2032, HC2099, HC2134, HC2138, HC2149, HC2178, HC2184 and C215 did disrupt membrane potential (Table 2.1, Figure A.2.9). Consistent with previous observations HC2091 did not disrupt membrane potential, while SQ109 did disrupt membrane potential (Table 2.1, Figure A.2.9)[117,201,202]. Surprisingly, there were differences in outcome for the two urea containing compounds HC2169 and HC2138 as well as between HC2099 and HC2183 which only differ by a chloro and methyl substitution, respectively. The results for HC2138 and HC2169 is also interesting because the previously described urea-based MmpL3 inhibitor, AU1235, does not disrupt the membrane potential[117,202]. These results suggest that the ability to disrupt membrane potential is highly structure specific.

Inhibition of MmpL3 has been shown to have bactericidal effects[65,117], therefore we tested these compounds for bactericidal activity using a firefly luciferase reporter strain of Mtb in

conjunction with a luciferase assay[210,211]. This assay relies on active luciferase generated by the reporter Mtb strain, and the presence of ATP which is generated in living cells, but rapidly hydrolyzed in lysed cells. All of these compounds showed bactericidal activity (Figure A.2.10). These results suggest that the growth inhibition is due to compounds killing Mtb in a dose dependent manner. The bactericidal activity of these inhibitors is consistent with these compounds targeting MmpL3 which is essential for cell viability[64,65], although other potential mechanisms, such as modulation of PMF or membrane integrity, are also consistent with bacterial killing.

Direct Binding of Inhibitors to MmpL3

To determine if the inhibitors directly interact with MmpL3, we used a recently described fluorescence-based competitive binding assay in whole cell *M. smegmatis mmpL3* mutant expressing Mtb *mmpL3* (*MsmgΔmmpL3/*pMVGH1-*mmpL3tb*)[49]. This assay utilizes a fluorophore probe (North 114) consisting of an analogue of the NITD series of MmpL3 inhibitors covalently linked to the fluorophore TAMRA. North 114 has previously been shown to directly bind to MmpL3 and addition of MmpL3 inhibitors displaces North 114 allowing for a competitive binding assay[49]. We tested all of the new MmpL3 inhibitors in this assay, along with NITD-349 as a positive control and INH and RIF as negative controls. The results of the assay showed that the inhibitors lead to displacement of North 114 similar to the positive control NITD-349[27] (Figure 2.4). Each of the inhibitors lead to displacement of North 114 at concentrations starting at 2 μM, with the exception of HC2178 and C215, which had modest activity at the highest tested concentration of 8 μM (Figure 2.4). SQ109 has previously been shown to displace North 114[49] and was not tested for this study. The results of the competitive binding assays, coupled with the lipid assay and decreased activity in the *mmpL3* mixed mutant background, support MmpL3 as a direct target for the compounds identified in our screening approach. However, these findings do not rule out that

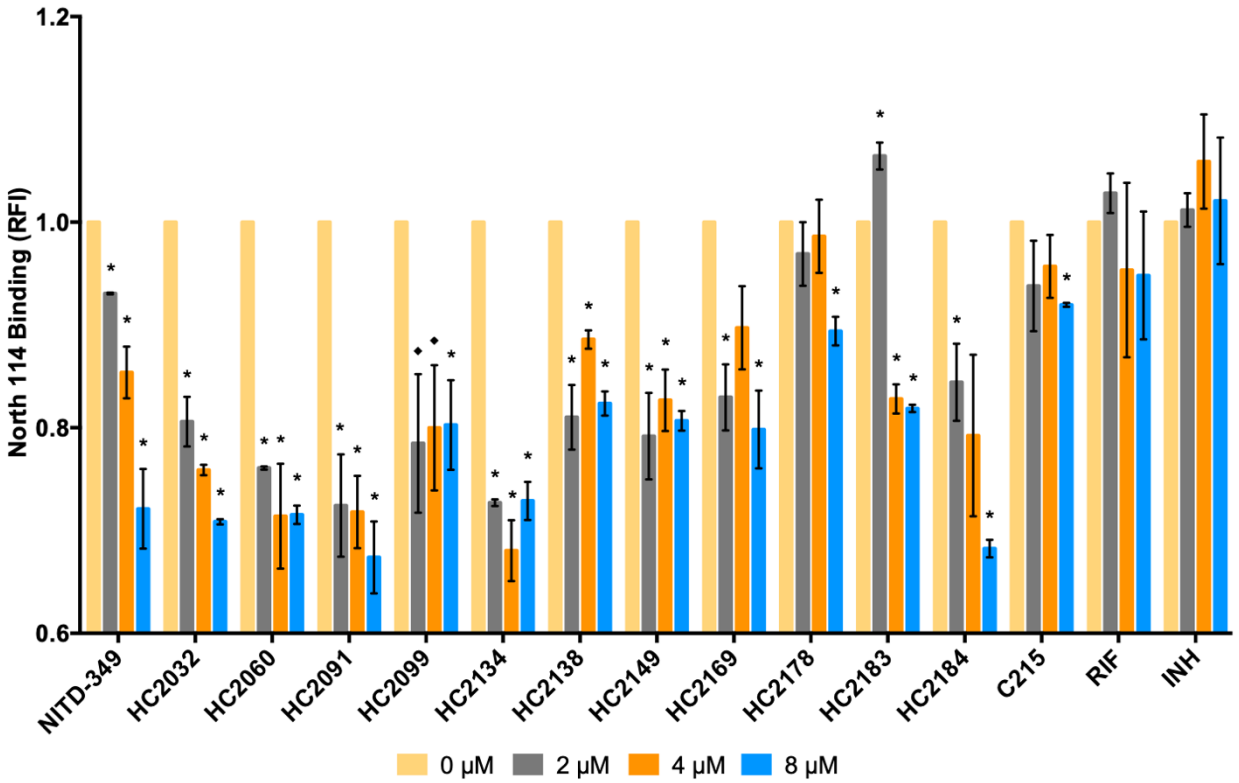

Figure 2.4. Flow cytometry-based competition binding assay using intact *M. smegmatis* cells expressing *M. tuberculosis* MmpL3 (MmpL3tb). The assay was performed in an *M. smegmatis* mmpL3 deletion mutant expressing the wild-type mmpL3tb gene (*M. smegmatis* MsmgΔ*mmpL3*/pMVGH1-*mmpL3*tb). Cells were labeled with 4 mM North 114 and subsequently treated with increasing concentrations of the inhibitors. Shown on the y axis are the mean fluorescence intensities (MFI) of the bacilli from each treatment group expressed relative to the MFI of bacilli not treated with any inhibitor (relative fluorescence intensity [RFI] arbitrarily set to 1). MFIs were determined by analyzing 10,000 bacilli under each condition. The data reported are mean values ± standard deviations of technical duplicates. Replicate samples were analyzed by t test. *, $P \leq 0.05$; ♦, $P \leq 0.1$.

secondary activity independent of MmpL3 may contribute to whole cell activity, particularly for the compounds shown to modulate membrane potential.

Spectrum of Activity

While MmpL3 is conserved in mycobacteria, functional orthologs are not found in other bacteria and fungi. Despite this, several proposed MmpL3 inhibitors including BM212, THPP, and SQ109 have been shown to inhibit multiple bacterial and eukaryotic species[34,212-214] while other MmpL3 inhibitors including HC2091, AU1235, and indolecarboxamides are specific to

Table 2.2. EC_{50} values for spectrum of activity of MmpL3 inhibitors*

	HC2032	HC2060	HC2091	HC2099	HC2134	HC2138	HC2149	HC2169	HC2178	HC2184	C215
Mtb – Erdman	3.0	14.8	7.0	5.3	2.1	2.3	11	2.4	3.7	8.9	16.2
Mtb – CDC1551	2.4	12.8	6.3	4.8	1.5	2.0	10.5	2.2	2.3	7.6	14.3
Mab	34.5[a]	13.6[a]	96.5[a]	81.8[a]	81.9[a]	8.2[a]	-28[a]	-36[a]	13.5[a]	7.0[a]	2.3[a]
Msm	2.2	80	20[9]	0.9	1.8	N.D.	>200	13.2	4.5	85.7	>200
S. aureus (1)	>200	>200	>200[9]	>200	51.0	N.D.	>200	>200	>200	>200	15.1
S. aureus (2)	>200	>200	>200[9]	>200	51.8	N.D.	>200	>200	>200	>200	22.8
E. coli	>200	>200	>200[9]	>200	>200	N.D.	>200	>200	>200	>200	>200
P. vulgaris	>200	>200	>200[9]	>200	35.1	N.D.	>200	>200	>100	>200	>200
E. faecalis	>200	>200	>200[9]	>200	>200	N.D.	>200	>200	>200	>200	34
P. aeruginosa	>200	>200	>200[9]	>200	>200	N.D.	>200	>200	>200	>200	>200

*All values are EC_{50} except for *M. abscessus* data which are single concentration % inhibition data
a – Growth Inhibition (%) at 20μM
9 – Reference number of previously published data
Mab, *M. abscessus;* Msm, *M. smegmatis*
S. aureus (1) – *S. aureus* ATCC29213, *S. aureus* (2) – *S. aureus* ATCC25923
N.D. – not determined

mycobacteria. To define the spectrum of activity, the compounds were tested against several diverse species including *Staphylococcus aureus, Escherichia coli, Pseudomonas aeruginosa, Proteus vulgaris,* and *Enterococcus faecalis* (Table 2.2). For HC2032, HC2060, HC2099, HC2149, HC2169, HC2178, and HC2184, even at high concentrations (200μM), no inhibition was observed against non-mycobacteria. However, these inhibitors were positive for activity against other mycobacteria, including the pathogenic non-tuberculous mycobacterial species *M. abscessus* and the saprophytic species *M. smegmatis* (Table 2.2). For example, HC2091, HC2099, and HC2134 exhibited MIC_{50} of 6.25 μM, 25 μM and 12.5 μM against *M. abscessus,* respectively. Additionally, all of the MmpL3 inhibitors tested, except for HC2149 and C215, were active against *M. smegmatis*. This suggests that most of the inhibitors are specific for mycobacteria and may be effective against diverse mycobacterial species. The specificity may be

driven by the conservation of MmpL3 in mycobacteria or, should the killing be dependent on a secondary activity independent of MmpL3, by the Mycobacterium-specificity of the secondary target(s), differences in cell envelope composition that limit compound permeability or differences in metabolism of the compounds. The observation that HC2134 and C215 are active against non-mycobacterial species has been observed with other MmpL3 inhibitors[204,213,214] and may be due to non-specific activities such as PMF disruption.

Activity against Intracellular Mtb

The compounds were tested against Mtb growing in BMMΦ using the luciferase expressing Mtb strain described above. BMMΦ were infected with Mtb and treated with the inhibitors for six days across a range of concentrations (200 – 0.3μM). The BMMΦ EC_{50} values are summarized in Table 2.1 and Figure A.2.11. The results of the assay show that many of the inhibitors have bactericidal activity in MΦ several magnitudes lower than the eukaryotic cytotoxicity CC_{50}, supporting a high selectivity index. The identification of bactericidal effects against Mtb in BMMΦ is consistent with genetic knockdown studies that show *mmpL3* is essential for actively replicating bacteria[64,65].

Cross-Resistance Profiles Indicate Specific MmpL3 Protein-Inhibitor Interactions

While the results of the screen showed potential for rapid identification of MmpL3 inhibitors, the screen relied on the use of a mixed mutant population. To resolve this issue, we conducted dose response studies for each combination of the twenty-four unique *mmpL3* mutants against each MmpL3 inhibitor identified from the screen (with WT Mtb Erdman or CDC1551 as a control). Because there was a complete lack of activity for compounds like HC2169 against HC2169-specific resistant mutants (Figure A.2.2c), units of measure such as EC_{50} and MIC cannot be calculated or are not a good measure for comparing responses. Instead, we used the

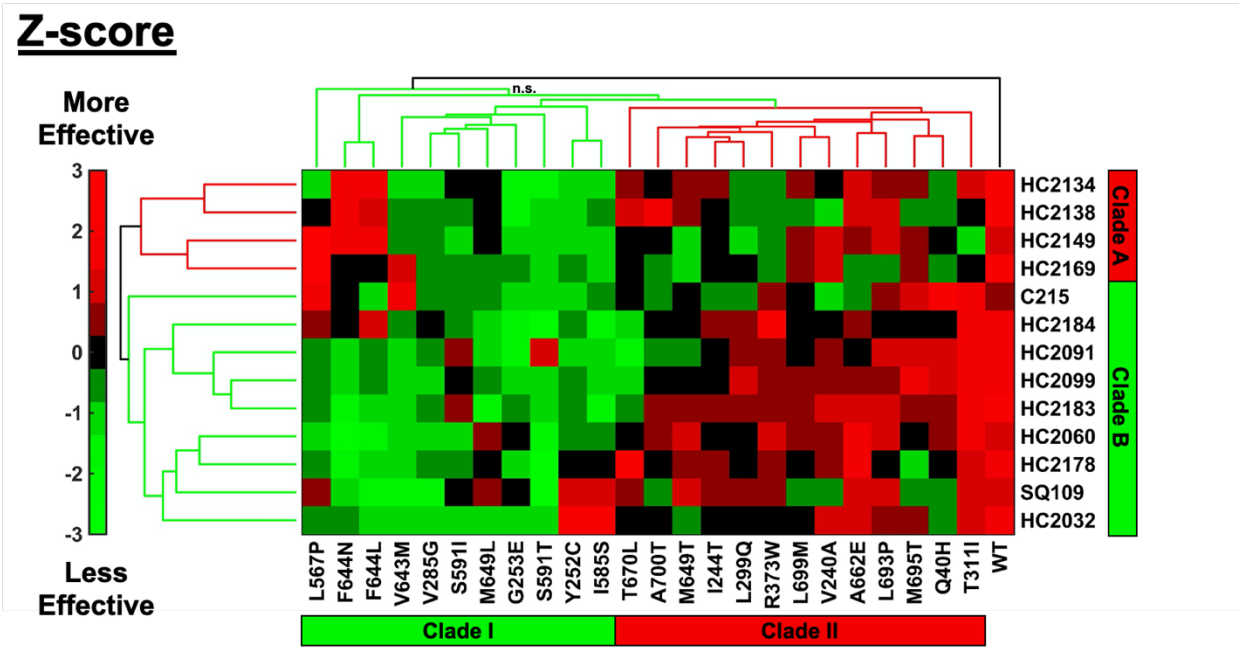

Figure 2.5. Cross-resistance profiling identifies clustering of compounds and mutations. Cluster analysis of cross-resistance profiling of 24 *mmpL3* strains treated with each of the 13 MmpL3 inhibitors normalized by Z-scoring by treatment. Compounds clustered into two clades: clade A and clade B. Mutant strains, denoted by amino acid substitution, clustered into two clades: clade I and clade II. Colors are based on Z-score normalization of treatment; green indicates when treatments were less effective than the average, and red indicates when treatments were more effective than the average. Black (n.s., not significant) indicates a branch where the approximate unbiased (AU) value was <75. All other branches were significant based on bootstrap AU values of >75.

area under the curve (AUC) for each dose response in the *mmpL3* mutant backgrounds relative to the AUC for the WT response for a given treatment (Table A.2.4). Because the compounds have differences in potency, the AUC for the WT for each treatment differs and to account for this issue we normalized our values by Z-score for each treatment[215]. Cluster analysis grouped the data based on both treatment effectiveness and resistance conferred by each *mmpL3* mutant. The resulting cluster-gram (Figure 2.5) shows that both compounds and *mmpL3* mutant strains, denoted by the amino acid substitutions, fall into distinct clades. The compounds fall into two distinct clades, Clade A (Red), which contains HC2134, HC2138, HC2149, HC2169, and Clade B (Green) which contains HC2032, HC2060, HC2091, HC2099, HC2178, HC2183, HC2184, C215, and SQ109. The identification of two distinct clades of compounds, suggested that the

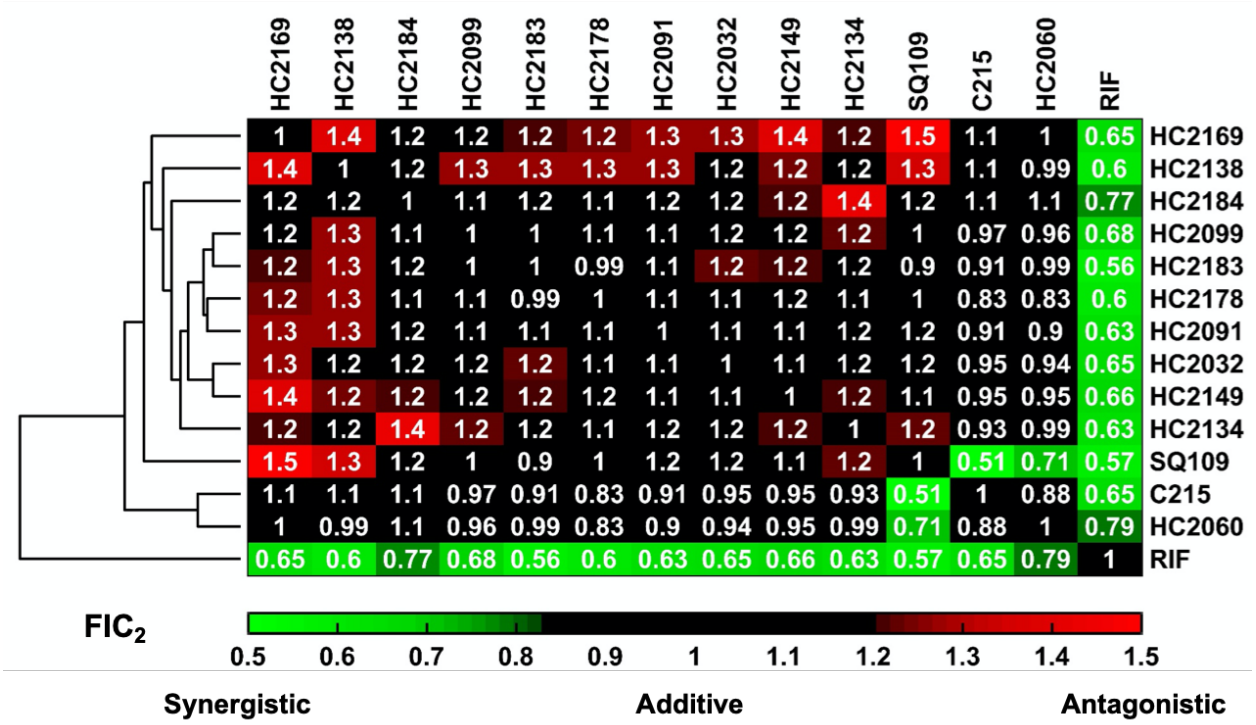

Figure 2.6. DiaMOND analysis identifies additive, synergistic, and antagonistic inhibitor interactions. Hierarchical cluster analysis of DiaMOND-based pairwise inhibitor interactions of all combinations of MmpL3 inhibitors and RIF identifies additive (FIC_2 of 0.82 to 1.18), antagonistic (FIC_2 > 1.18), and synergistic (FIC_2 < 0.82) interactions.

compounds may be interacting with the MmpL3 protein in distinct ways. The resistance mutations also showed specific clustering. Cluster analysis of the strains showed that WT clustered on its own and the mutants formed a large complex cluster (Figure 2.5). Within this large cluster, the *mmpL3* mutant strains formed into two sub-clades; Clade I (Green) which conferred relatively high resistance (lower inhibitor effectiveness) and Clade II (Red) which conferred relatively low resistance (higher inhibitor effectiveness). Clade I, which contained eleven *mmpL3* mutant strains denoted as Y252C, V285G, G253E, L567P, I585S, S591I, S591T, V643M, F644N, F644L, and M649L. Clade II consisted of the remaining thirteen *mmpL3* mutant strains denoted as Q40H, V240A, I244T, L299Q, T311I, R373W, M649T, A662E, T670L, L693P, M695T, L699M, and A700T. Surprisingly M649T fell into Clade II mutations, this was striking as the *mmpL3* mutant denoted as M649L was clustered with the Clade I *mmpL3* strains.

Pairwise Combination Studies using DiaMOND

We hypothesized that the clustering of compounds into two clades was due to their having distinct interactions with MmpL3; therefore, combination treatments may reveal antagonistic, additive or synergistic interactions. In order to test this hypothesis in whole cell Mtb, we used the recently described diagonal measurement of *n*-way drug interactions (DiaMOND) approach[216]. RIF was included as a control for these assays, as this drug has been shown to be synergistic when tested with other MmpL3 inhibitors such as AU1235 and SQ109[217,218]. The results of DiaMOND, shown in Figure 2.6, identified synergistic interactions (FIC_2 < 0.82) between all combinations of MmpL3 inhibitors and RIF. Additionally, the results identified mostly additive interactions (FIC_2 = 0.82 – 1.18) consistent with the compounds sharing a single target. Interestingly, most combinations between MmpL3 inhibitors and the compounds HC2134, HC2138, HC2149, and HC2169 showed antagonistic interactions (FIC_2 > 1.18). These four compounds were clustered together in Clade A in the cross-resistance profiles described above (Figure 2.5). This antagonistic relationship further supports that the Clade A compounds are distinct from the Clade B compounds. Another observation from the DiaMOND assay is that pairwise combinations of compounds HC2060, C215, and SQ109 all had synergistic interactions (Figure 2.5). The reason for this observation is not clear as the compounds did not have differential cross resistance profiles (Figure 2.4). Interestingly, combinations of HC2060 and C215, but not SQ109, with the Clade A compounds HC2138 and HC2169 did not reveal antagonist interactions, but instead additive interactions (Figure 2.6). This finding supports that HC2060 and C215 compounds interact with MmpL3 in a manner distinct from the other compounds.

3D Modeling of MmpL3 Clade I and Clade II Substitutions

The cross-resistance profiles showed that the *mmpL3* mutant strains clustered separately into two clades, Clade I and Clade II, with WT clustering on its own as an outgroup (Figure 2.5).

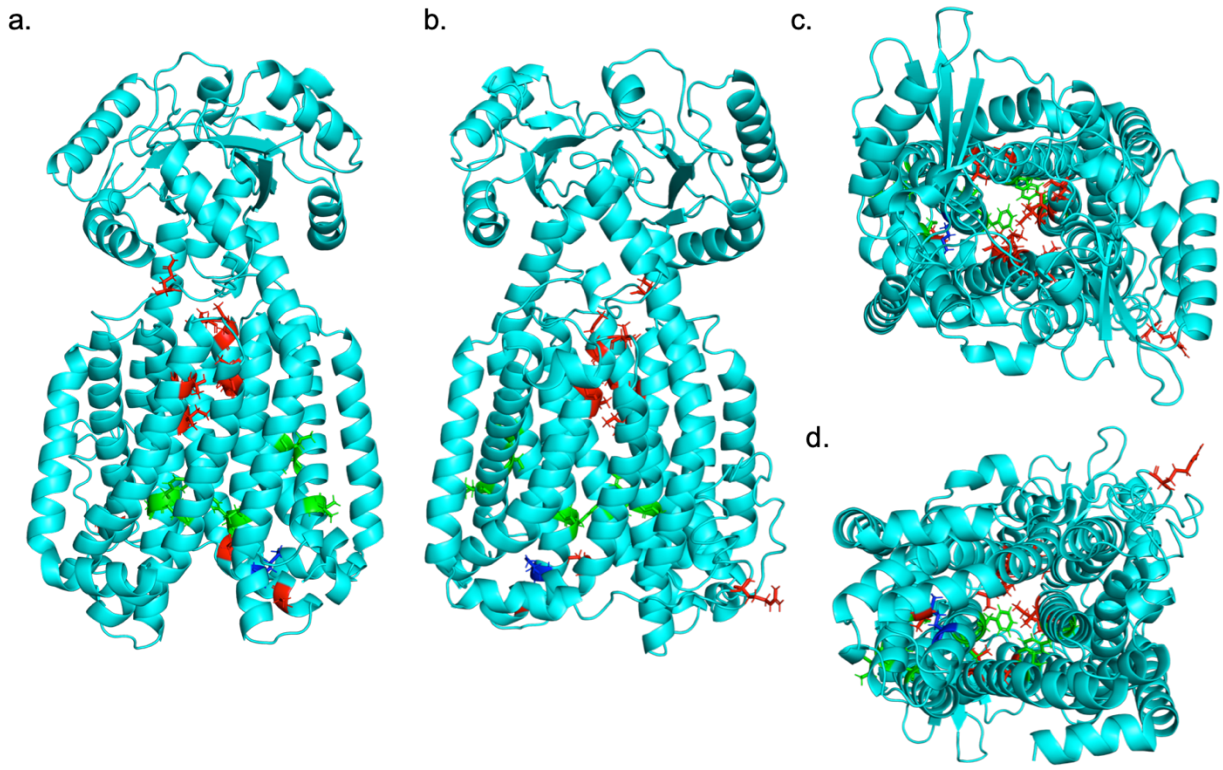

Figure 2.7. Mutation substitutions cluster according to cross-resistance clades. (a to d) Front, back, top, and bottom views, respectively, of an I-TASSER-predicted structure of *M. tuberculosis* MmpL3 based on *M. smegmatis* MmpL3 structure (PDB code 6AJH). Substitutions conferred by mutations in mmpL3 are indicated. Substitutions are colored based on clade from cross-resistance profiling as follows: green, clade I substitutions; red, clade II substitutions; blue, M649, which fell into both clades depending on the substitution. The model shows a truncated version (732/944 aa) of the MmpL3 protein lacking the C-terminal tail.

In order to understand this observation, we generated a 3D model of the Mtb MmpL3 protein aligned to the recently described crystal structure of MmpL3 from *M. smegmatis* [52] (C-score 0.17, RMSD 8.4 ±4.5Å). Substitutions from the *mmpL3* mutant strains used in the cross-resistance profiles are highlighted in the model (red, green, and blue) (Figure 2.7). Consistent with previously described resistant strains of Mtb, the majority of the substitutions, localized along the central vestibule with the exception of T670, R373, and A662 which did not align along the central vestibule of the model (Figure 2.7)[45]. This vestibule is conserved amongst the RND family of proteins and is responsible for the proton translocation that drives protein activity[45,117]. To understand the clustering pattern of the cross-resistance profiling we highlighted the mutations based on their clade, revealing that the two distinct clades separated spatially in the model. The

substitutions of Clade I (Green), that conferred higher resistance, localized towards the cytoplasmic face of the protein. While substitutions of Clade II (Red), which generated lower resistance, localized into two separate locations: i) towards the pseudo-periplasmic face of the protein; and, ii) another region which does not line the central vestibule (Figure 2.7). Interestingly, substitutions for M649 (Blue) separated into either Clade I or Clade II depending on the substitution. Structure function profiling by Bellardinelli and colleagues[45] had previously described seven essential residues for MmpL3 function (D251, S288, G543, D640, Y641, D710, and R715) that clustered in a single domain[45]. This study also modeled substitutions commonly identified from resistant mutants to multiple inhibitors to this same region. To determine if the two clades separated based on their approximation to this essential region, we highlighted these seven residues in the model (Figure 2.12). Notably, the two clades separate based on their proximity to these residues, with Clade I substitutions localizing in the same region as the essential residues and Clade II substitutions localizing distally from the essential residues. This finding suggests that the strength of resistance conferred by a mutation may be dependent on the proximity of the substitution to residues essential for protein function.

Discussion:

Over the last decade MmpL3 has been identified as the proposed target of nearly a dozen small molecule inhibitors of Mtb by the whole genome sequencing of spontaneous resistant mutants. This process, while successful for identifying inhibitors of MmpL3, is time consuming due to the slow growth of Mtb, and costly due to the expense of whole genome sequencing. Here we described a simple growth-based assay to rapidly identify small molecule inhibitors of Mtb growth that target MmpL3 using a pool of *mmpL3* mutants. This process is specific to small molecules that inhibit MmpL3 activity with no observable cross resistance to non-MmpL3 inhibitors. Using a competitive binding assay and lipid accumulation assays, the compounds were found to directly inhibit MmpL3 activity. Cross resistance profiling of MmpL3 inhibitors against each *mmpL3* mutant indicated that both the inhibitors and mutants fell into separate clades. These clades indicated that the compounds interacted differently with MmpL3 and that the mutations conferred different levels of resistance based on the proximity of substitutions to essential residues for MmpL3 function.

The screening approach described here is fast and accurate in identifying MmpL3 inhibitors; however, this screening approach relies on the potential for cross resistance between inhibitors and *mmpL3* mutant strains present in the mixed mutant population. While our approach was successful at identifying a total of thirteen MmpL3 inhibitors, including SQ109, this screening platform could not identify Rimonabant, an analogue of BM212[52,219]. Rimonabant has been shown to have low cross resistance with *mmpL3* mutants isolated from other MmpL3 inhibitors, including SQ109 and AU1235[52]. Additionally, Rimonabant has been shown to bind differently with MmpL3 compared to other MmpL3 inhibitors including SQ109, AU125 and an indolecarboxamide (ICA38) when co-crystalized with MmpL3[52]. While the current version of our screen could not identify Rimonabant, future versions of our mixed mutant screening approach could include BM212 or Rimonabant specific *mmpL3* mutants in the mixed mutant population, allowing for a more robust screening platform. Genome sequences of the isolated resistant mutants identified a total of 21

unique mutations in *mmpL3*. These mutations translated to substitutions that were a mix of ones previously described and novel to this study. Included in this list were substitutions that had previously been described including G253E, Y252C, T311I, L567P, S591I, V643M, F644L, L699M[24,27,29,31,34,35,153,201,203]. Mutations that were unique to this study included ones in positions in V240, I244, V285, L299, R373, I585, A662, and L693. We also isolated mutations that had previously been described to occur in positions Q40, Y252, G253, L567, S591, F644, M649, and L699[24,29,31,34,35,153,201,203]; however, the exact substitutions in several of these strains' positions including Q40H, S591T, F644N, and M649T were unique to this study. Our cross-resistance profiling found that G253E, V285G, S591I, S591T, L699M, and A700T, conferred pan resistance including against SQ109. The number of compounds proposed to target MmpL3 and the large number of substitutions that confer resistance highlights the importance of identifying combinations of drugs that would reduce the frequency of resistance.

Cross resistance profiling for each combination of *mmpL3* mutant and MmpL3 inhibitor identified two clades of mutants, Clade I with higher resistance and Clade II with lower resistance. Our findings suggest that the strength of the resistance conferred by a substitution is related to the proximity of the substitution to essential residues for MmpL3 function. While we found that the substituted residues of the same location fell into the same clade for F644 and S591, both falling into Clade I; substitutions for M649 fell into two separate clades (M649L – Clade I, and M649T – Clade II). Similar findings have recently been described by Li *et al.* who found similar results when comparing resistance to different substitutions of the same residue[49]. These studies showed that resistance is dependent on the chemical properties of the amino acid substitutions and conformational changes to the protein. However, this does not fully explain our findings as both the F644 and S591 substitutions fall into the same clades despite the substitutions having different chemical properties. Another possible explanation is the location of the substituted residues. Both the F644 and the S591 residues are located more centrally within the folded protein, while M649 is located near the cytoplasmic face of the protein potentially allowing for more flexibility in terms

of orientation of the specific residue. It therefore may be possible that the orientation of the substituted residue may change, conferring different amounts of resistance to each compound tested. Recent efforts have successfully crystalized MmpL3 from *M. smegmatis*[51,52] , and efforts to co-crystallize MmpL3 and MmpL3 inhibitors have indicated how different MmpL3 inhibitors disrupt the conformation of MmpL3[52]. Because substitutions in MmpL3 have combined effects of conferring resistance to MmpL3 inhibitors and costs to fitness that are highly dependent on the specific substitution, future efforts to crystallize MmpL3 variants containing substitutions may shed light on how these resistance effects are conferred.

The favorable properties of many of these compounds, including low cytotoxicity, high solubility and microsome stability, and activity in macrophages, suggests that these compounds warrant further development as new therapeutics. It is also possible that combinations of these scaffolds may be developed in a single molecule that can function to reduce the frequency of resistance. Three of the compounds used to isolate resistant mutants in this study, HC2149, HC2169 and HC2184, had a frequency of resistance (FoR) of 3×10^{-7}, which is similar to the FoR of other MmpL3 inhibitors that have a FoR ranging from 10^{-7} to 10^{-8} [28-31,35,203]. That the FoR for HC2184 was the same as the FoR for HC2149 and HC2169 is interesting as the cross-resistance profiles suggested that these compounds interact differently with MmpL3. While the antagonistic interactions identified by DiaMOND suggest that scaffold combinations may lower the activity of a single inhibitor, antagonistic drug combinations have been proposed to decrease the rate of resistance [220,221]. It therefore may be possible to design a single inhibitor that fuses more than one scaffold to decrease the rate of resistance. This hypothesis could initially be tested by conducting pairwise combination studies examining for synergistic reductions in the FoR. Given the relative ease of resistance occurring to MmpL3 inhibitors, a reduced FoR could be a valuable new property for this class of inhibitors.

Many MmpL3 inhibitors with distinct chemical scaffolds have been described. The proposed target of these inhibitors has been driven by the mapping of resistance mutations to

mmpL3. The screening platform we describe here greatly accelerates target identification of such inhibitors. The use of a diverse pool of unique *mmpL3* mutants, rapidly identified inhibitors of MmpL3 activity, as demonstrated by their ability to modulate TDM and TMM accumulation and direct interaction with MmpL3 by displacement of a probe. A subset of these inhibitors was shown to disrupt membrane potential, and potentially the PMF which energizes MmpL3 activity. Two recent studies have suggested that two MmpL3 inhibitors, SQ109 and E11, indirectly inhibit MmpL3 by targeting the PMF despite the isolation of *mmpL3* resistant mutants[31,202] and co-crystallization of SQ109 to MmpL3[52]. Notably, genetic inhibition of *mmpL3* results in an increase in membrane potential, in contrast to inhibitors such BM212, AU1235 and SQ109 which dissipate membrane potential[49]. Given that not all MmpL3 inhibitors modulate PMF and that genetic and chemical inhibition of MmpL3 have different outcomes, this suggests that dissipation of membrane potential is not due to a direct activity on MmpL3, but rather a secondary mechanism. It is therefore possible that some of these new compounds inhibit MmpL3 and also independently dissipate PMF. It is also possible that these inhibitors are killing Mtb by a secondary mechanism that is independent of MmpL3. Indeed, the inhibitor THPP selects for resistance mutants in *mmpL3*, consistent with its ability to directly bind to the transporter[49], but has been proposed to also function by an alternative target, EchA6[188]. Continued studies of these inhibitors will further define if the mechanism of killing is due to direct inhibition of MmpL3, a secondary mechanism or a combination of multiple mechanisms.

Methods:

Media and Growth Conditions

Unless otherwise specified, streptomycin resistant strains of Mtb Erdman or CDC1551 were cultured in 7H9 media supplemented with 10% OADC (v/v) with 0.05% Tween-80 (v/v) in standing T25, T75 or T150 flasks at 37 ºC with 5% CO_2. Spectrum of activity studies in different bacterial species (Table 2.2) were conducted as described by Coulson et al.[209], with the exception of the *M. abscessus* studies which are described in the supplemental methods.

Dose Response Curves

Mtb was grown in rich medium to an OD_{600} of 0.5-1.0. Cultures were diluted to an OD_{600} of 0.1 in 7H9 medium and aliquoted into black walled clear bottom 96 well assay plates. Compounds were tested between 80-0.13 µM with 2.5-fold dilutions, controls included DMSO and 3 µM RIF. Plates were placed in zip lock bags with moistened paper towels and incubated at 37ºC for 6 days. Plates were read on a PerkinElmer Enspire plate reader. %GI was calculated using DMSO and RIF as 0% and 100% inhibition, respectively and EC_{50} values were calculated using Prism 6 Software. Dose responses were conducted in biological triplicate and repeated at least once. Significant differences of EC_{50} were compared using 95% confidence intervals. EC_{90} values were calculated based on the EC_{50} values and the Hillslope.

To examine the spectrum of activity of the MmpL3 inhibitors, the EC_{50} of each compound was also determined for *M. smegmatis* and other nonmycobacteria, including *S. aureus, E. coli, P. aeruginosa, P. vulgaris,* and *E. faecalis*. Tests were performed in 96-well plates in LB broth with shaking at 37°C, with the exception of *E. faecalis*, which was grown in brain heart infusion medium in standing flasks at 37°C, and *M. smegmatis*, which was also grown standing at 37°C in LB broth with 0.05% Tween-80. Culture was diluted to a starting OD_{600} of 0.05. Bacteria were incubated in the presence of an 8-point (2-fold) dilution series of each inhibitor ranging from 200 µM to 1.5 µM for 6 h, except for *M. smegmatis*, which was incubated for 72 h. Growth was

monitored by measuring optical density and normalized based on kanamycin (100% growth inhibition) and DMSO (0% growth inhibition) controls, with the exception of *P. aeruginosa*, for which 10 µg/mL tobramycin was used as the control for 100% growth inhibition. The experiments were performed with three technical replicates per plate. EC_{50}s were calculated based on a variable-slope four-parameter nonlinear least-squares regression model in the GraphPad Prism software package (version 8).

Kinetic Kill Curves

Mtb was cultured in 7H9 medium to an OD_{600} of 0.5-1.0 and diluted to an OD_{600} of 0.1. In triplicate, diluted samples were aliquoted into 96 well plates and inoculated with 20 µM concentrations of each compound with DMSO as a negative control. Plates were placed in zip lock bags with moistened paper towels and incubated at 37 ºC. Daily samples were taken and serial diluted in 96 well plates using 1x PBS + 0.05% Tween-80 (v/v) and plated on 7H10 quadrant plates supplemented with OADC (10% v/v). Plates were incubated at 37ºC and colonies were counted to calculate CFU/mL. Experiments were conducted in biological triplicate and repeated at least twice.

Isolation of Resistant Mutants

Mtb was grown to an OD_{600} of 0.6-1.0 and samples were resuspended in fresh media for a final cell count of 2×10^9 cells/ml. Cell pellets were resuspended in 0.5 ml of 7H9 medium and plated on 7H10 OADC plates supplemented with 20 µM or 40 µM concentrations of HC2060, HC2149, HC2169, and HC2184. Plates were incubated at 37 ºC until isolated colonies appeared. Colonies were picked and inoculated into 5 ml of 7H9 medium in T25 standing flasks and grown to an OD_{600} 0.5-1.0. Samples were taken and tested for resistance using dose response curves described above along with WT grown to an OD_{600} of 0.6-1.0 and 3 µM RIF and DMSO were used as controls. Samples were also serial diluted as described above and plated for colony purified

single colony isolates on X-plates containing 7H10 OADC. Single colony isolates were picked and inoculated into 5 ml of 7H9 OADC in T25 flasks. Resistance was re-confirmed using the same methods described above. Differences in EC_{50} values were deemed significant based on the 95% confidence intervals.

Whole Genome Sequencing and Analysis

Whole genome sequencing was performed as previously described[222]. Briefly cultures of single colony isolates were grown to an OD_{600} ~1.0 and pelleted. Genomic DNA was extracted and sequenced by Illumina-based whole genome sequencing at 250 bp reads. Sequencing results were analyzed using the GATK workflow for the identification of single nucleotide variations[223].

TMM and TDM Accumulation Assay

The lipid assay was carried out as previously described(6). Briefly, 30 ml cultures of Mtb was cultured to an OD_{600} of 0.6. Samples were diluted to an OD_{600} of 0.1 in 8 ml cultures in T25 flasks. Cultures were inoculated with 8 µCi of ^{14}C-acetate. Cultures were co-inoculated with 20 µM samples of MmpL3 inhibitors and then incubated for 24 hours before performing lipid extraction as previously described[201]. Total extractable lipid ^{14}C-incorporation was determined by scintillation counting, and 5,000 cpm of lipids of each sample were spotted and separated on TLC plates with a 24:1:0.5 Chloroform:Methanol:H_2O solvent system. TLCs plates were imaged using a Typhoon FLA 7000 and images were quantified using IQ image quantifying software. Experiments were conducted in biological duplicate. Comparison to the DMSO controls was conducted using the T-test.

Growth Curves

Each *mmpL3* Mtb mutant or WT Mtb (Erdman or CDC1551) were cultured independently in 8 ml of 7H9 medium in T25 standing flasks to an OD_{600} of ~0.6. Cultures were then resuspended in 8 ml of 7H9 medium in T25 standing flasks at a starting OD_{600} of 0.1 in biological triplicate. Cultures were incubated at 37°C in 5% CO_2 and 500 µl samples were taken for optical density reading every three days.

Targeted Whole Cell Phenotypic Screening

Each *mmpL3* mutant was cultured independently in 8 ml of 7H9 medium in T25 standing flasks to an OD_{600} of 0.6 – 1.0. Mutant cultures were separately back diluted to an OD_{600} of 0.6 in 1.5 ml of 7H9 medium in 2 ml screw cap tubes. The contents of each tube were mixed into a single batch culture in a T75 culture flask. The mixed mutant culture was allowed to recover overnight (~8 hours) at 37°C. Samples of Mtb Erdman (WT, OD_{600} = 0.6) and the mixed mutant population were back diluted to an OD_{600} of 0.1 in 7H9 medium. WT and mutant pools were aliquoted, in technical duplicate, into separate clear bottom black walled 96 well plates. Samples of WT and mixed mutant cultures were inoculated with 20 µM of each of the 163 compounds from the small molecule library. Additional treatments included 0.5 µM samples of *para*-amino salicylic acid (PAS), SQ109, bedaquiline (BDQ), isoniazid (INH), clofazimine (CFZ), as well as DMSO and 0.3 µM RIF. Percent growth inhibition (%GI) of WT and mutant mix population were calculated for each treatment and hits were defined as 1) compounds with at least 15% GI in the WT background and 2) 1.5 fold decreased inhibition in the mutant pool relative to the WT background. The hit compounds were confirmed by conducting dose responses curves of screen hits as described above against WT and *mmpL3* mutant pools. Dose response curves were conducted in technical duplicate and differences between the WT and *mmpL3* mutant pool was deemed significant based on 95% confidence interval. Confirmed hits were reassessed with similar results.

Cross resistance studies were conducted by generating dose response curves for every combination of MmpL3 inhibitor and each *mmpL3* mutant, and WT Mtb strain, CDC1551 or Erdman depending on the background of the *mmpL3* strain (for a total of 338 dose response curves). Cross resistance dose responses were conducted singly, unless the dose response identified increased sensitivity in the *mmpL3* mutant background, in which case the responses were re-examined using dose responses carried out in biological duplicate. The dose responses were then used to calculate the area under the curve (AUC) using Prism 8 software using the default setting. AUCs were compare to the respective WT strains by dividing the AUC of the *mmpL3* strain by the respective WT parent strain. AUC fractions were then standardized by treatment by Z-scoring[65]. Z-score standardized data was then clustered in MatLab by hierarchical agglomerative clustering using the *clustergram* function with default settings (Euclidean distance model, Average linkage clustering). Hierarchical agglomerative clustering using bootstrapped data was conducted in R using *pvclust* (nboot = 1000) using the Euclidean distance model and average linkage clustering[224].

Membrane Potential Assays

The $DiOC_2$ membrane potential assay was carried out as previously described[153,201]. Briefly, Mtb Erdman cells were labeled with 30 μM DiOC2 (Thermo Scientific) in 1 ml of 1X phosphate-buffered saline (PBS) (pH 7.4), supplemented with 50 mM KCl, and incubated at 37°C for 15 min. Cells were washed twice and suspended in 1X PBS at a final concentration of an OD_{600} of 0.2, and 200 μL of labeled cells were aliquoted to 96-well plates and treated with each of the MmpL3 inhibitors at 80 μM, 20 μM, or 5 μM concentrations. Samples were also treated with DMSO (negative control) or 25 μM CCCP (Sigma-Aldrich) (positive control). Each treatment included three technical replicates per plate. The kinetics of fluorescence (excitation, 485 nm; emission, 610 nm/515 nm) was measured every 2 min for 60 min. The red/green (610 nm/515 nm) fluorescence intensity ratio was calculated and used to quantify membrane potential. The

experiment was repeated at least twice with similar results. The error bars represent the standard deviation of the geometric mean.

Competition Binding Assays using Intact *M. smegmatis* Cells

Competition binding assays in intact *MsmgΔmmpL3/*pMVGH1-*mmpL3tb* bacilli were conducted by treating the cells with 4 mM of probe North 114 for one hour at 37°C, prior to washing the cells twice with 7H9-ADC + 0.05% Tween-80 and resuspending them with different concentrations of the test compounds for another hour at 37°C[49]. Treated cells washed with 7H9-ADC +0.05% Tween-80 and fixed with 2% paraformaldehyde were finally resuspended in PBS + 0.05% Tween-80 and subjected to flow cytometry analysis on a Cytek Aurora Spectral cytometer. Flow Cytometry Standard (FCS) file data were analyzed using Flowjo® software (Treestar Inc., Ashland, OR).

Bactericidal Activity *in vitro* and in Macrophages

An Mtb CDC1551 strain with a chromosomally encoded firefly luciferase expressed from the *hsp60* promoter (CDC1551 pMV306:hsp60:FFLuc[210]) was grown to an OD_{600} of 0.6 – 1.0 in rich medium. For *in vitro* experiments cultures were diluted to an OD_{600} of 0.1 and aliquoted at 100µL in white walled 96 well plates and inoculated with compounds with each inhibitor, along with DMSO or RIF controls. The luciferase assay was carried out as previously described and plates were read on a PerkinElmer Enspire plate reader.

For studies in macrophages, primary bone marrow derived macrophages were harvested and infected as previously described [211]. Briefly, BMMΦ from C57Bl/6 mice were distributed into 96 well white plates and infected for 1 hour with a CDC1551 luciferase reporter strain[210]. Following 1 hour of infection, cells were treated with inhibitors ranging from 200 – 0.2 µM of MmpL3 inhibitors. 20 µM PAS, 3 µM RIF, and DMSO were used as controls. Samples were incubated in the 96 wells plates at 37ºC + 5% CO_2 for 6 days before carrying monitoring bacterial survival by

measuring luciferase activity. Experiments were conducted in biological triplicate and repeated at least once with similar results.

Protein Modeling

The 3D structure for MmpL3 was generated using the I-TASSER server[225]. The MmpL3 protein sequence of H37Rv from Mycobrowser (Rv0206c)[226] was aligned to the MmpL3 crystal structure of Msm (PDB: 6AJF) with a resulting C-score of 0.17 (TM-score 0.74 ± 0.11, RMSD 8.4 ± 4.5Å). The resulting structure was modified to remove the C-terminal tail (732/944AA) in PyMol 2.2.3[227].

DiaMOND

DiaMOND analysis was carried as described by Cokol *et al.,* with modifications as described[216]. Briefly concentration ranges were linearized using the equation

$$\Delta D = \frac{M - m}{N - 1}$$

$$\Delta D = D_N - D_{N-1}$$

Where *ΔD* is the difference between concentrations of each dose, *M* is the lowest concentration to inhibit Mtb growth 100%, and *m* is the highest concentration estimated to confer 0% growth inhibition based on the EC_{50} dose response curves. *N* is the number of doses to be used in DiaMOND. Mtb was then treated with each concentration range for each compound by itself (Null treatment) at a [X_N] or in combination with another inhibitor at a [½X_N]. Dose responses were used to generate a dose response curve for each treatment which was used to interpolate the IC_{50} which was set for the observed, "*o*" to calculate the FIC_2 ($FIC_2 = \frac{o}{e}$) as previously described[216]. Dose responses were conducted in biological duplicate and reported FIC_2 values are representative of the geometric mean of two reps. Experiments were repeated with similar results.

Eukaryotic Cytotoxicity

Primary BMMΦ were isolated and distributed into white wall 96 well plates as described above. Cells were treated with inhibitors ranging in concentration from 200 – 0.26 μM. Cells were incubated at 37C for 3 or 6 days with 5% CO_2. Cytotoxicity was tested using the Cell Titer Glow assay kit using the methods from the provider. For a negative control cells were treated with 4% of TritonX-100 and DMSO as a positive control[207].

Kinetic Solubility and Microsomal Stability Assays

The kinetic solubility assay was conducted as described by Bevan *et al.*[228] Briefly, the assay was performed with 7-point (2-fold) dilutions from 200 μM - 3.125 μM for the compounds. Mebendazole, benxarotene and aspirin were also included as controls. The drug dilutions were added to PBS, pH 7.4, with the final DMSO concentration of 1%, and incubated at 37 °C for 2 h. The absorbance at 620 nm was measured for each drug dilution to estimate of the compound solubility. Three replicates were examined for each dilution. Mouse microsomal stability was conducted as described by Obach[229] and presented as % remaining following 30 minutes. Values greater than 100% are likely due to changes in the solubility of the compounds over the course of the assay and represent high stability in microsomes.

Acknowledgements:

We thank Bree Aldridge for assistance in designing the DiaMOND studies. Christopher Colvin and Benjamin Johnson provided technical assistance in the initial prioritization of compounds. Additional technical assistance was provided by Bilal Alewei and Tom Dexheimer, in the MSU medicinal chemistry and screening cores, to conduct the solubility and microsomal stability studies. Research in the Abramovitch lab was supported by start-up funding from Michigan State University and AgBioResearch, and grants from the NIH-NIAID (U54AI057153, R21AI1170181 and R01AI116605), the Bill and Melinda Gates Foundation (OPP1059227), a strategic partnership grant from the MSU Foundation (14-SPG-Full-2966), and the Jean P. Schultz Endowed Biomedical Research Fund at the MSU College of Human Medicine. This study was also supported by NIH grants to Thomas Dick (R01AI132374) and Mary Jackson (R01AI116525).

Author Contributions

JW and RBA designed the experiments and wrote the manuscript; GC conducted prioritization assays; JW, EH, KC conducted the Mtb and spectrum of activity experiments; CC, NAC and TD designed and conducted the *M. abscessus* experiments; WL and MJ designed and conducted the MmpL3 competitive binding experiments; and, EE directed the solubility and microsomal stability studies. All authors reviewed the manuscript.

Disclosures

RBA is the founder and owner of Tarn Biosciences, Inc., a company that is working to develop new TB drugs.

CHAPTER 3: Proof-of-concept Studies Showing the MmpL3 Inhibitor MSU-43085 as an Active, Orally Bioavailable Inhibitor of *Mycobacterium tuberculosis, M. abscessus* and *M. avium* Infection

The following scientists contributed to this chapter: John T. Williams[1], Matthew Giletto[2], Elizabeth R. Haiderer[1], Bilal Aleiwi[2], Richard Slayden[3], Edmund Ellsworth[2], and Robert B. Abramovitch.

[1]Department of Microbiology and Molecular Genetics, and [2]Department of Pharmacology and Toxicology, Michigan State University, East Lansing, Michigan, 48824, United States. [3] Antimycobacterial Testing Service at Colorado State University.

The compounds synthesized in this chapter were conceptualized and synthesized by EE and MG. *in* vitro and *ex vivo* testing experiments were conducted by JTW and RS. PK studies were conducted by JTW, ERH, BA, and EE. Mouse experiments were conducted by JTW and ERH. The manuscript was prepared by JTW and RBA.

Abstract:

Addressing drug resistance in *M. tuberculosis* (Mtb) requires the development of new drugs with new targets. We previously identified thirteen MmpL3 inhibitors from a screen of a small library of Mtb growth inhibitors. In this report, we describe structure-activity relationship (SAR) studies to optimize potent analogs of the MmpL3 inhibitor HC2099 that are active *in vivo* when delivered orally. These analogs are active against Mtb *in vitro* and against intracellular Mtb as well as against *M. abscessus* and *M. avium*. Early pharmacokinetic testing identified MSU-43085, MSU-43165, and MSU-43170 as orally bioavailable in the plasma and lungs of treated mice. The results of an *in vivo* efficacy study found that MSU-43085 was active against Mtb in an acute murine TB infection model, but lacked activity in a chronic murine TB infection model. The results of this study serve as a proof of concept for this series and support further optimizations of this series of MmpL3 inhibitors.

Introduction:

M. tuberculosis (Mtb) is the primary causative agent of Tuberculosis (TB). In 2019, 1.4 million people died from TB, making it the leading cause of death due to single infectious bacterium in the world[230]. Current TB therapy requires a 6-month long regimen of four drugs: rifampin (RIF), isoniazid (INH), ethambutol (EMB), and pyrazinamide (PZA). The evolution of multi-drug resistance (MDR-) and extensively drug resistance (XDR-) strains of Mtb, that can still spread person-to-person[231], demands the development of new drugs with novel mechanisms of action (MOA). In the last decade the essential mycolic acid flippase[48] MmpL3 has been identified as a potential target for TB therapy[20-37]. In total there have been more than twenty different chemical scaffolds proposed to inhibit MmpL3[20-37]. To date SQ109 is the most clinically advanced MmpL3 inhibitor, completing Phase IIb clinical trials in 2018[232]. Though SQ109 has favorable properties for a TB drug candidate, including actively killing both replicating and non-replicating Mtb *in vitro*[117], SQ109 has several metabolic and spectrum of activity shortcomings. For one, SQ109 has a short half-life owing to degradation by cytochrome P450 (CYP) enzymes CYPD6 and CYP2C19[166,167,233], the latter of which is induced by RIF limiting combinatorial therapy[164]. Additionally, SQ109 does not work well against non-tuberculosis mycobacteria (NTM) complexes such as *M. abscessus* (MAB) or *M. avium* (MAC)[42]. Due to these short comings, there is room for additional MmpL3 inhibitors to be developed for clinical therapy.

We previously reported a targeted mutant screening approach for the identification of MmpL3 inhibitors[25]. This screen identified thirteen MmpL3 inhibitors including the previously identified SQ109[34], C215[20], and HC2091[22] that inhibited Mtb both *in vitro* and in infected macrophages. Included in this group of inhibitors, were two highly similar compounds, HC2099 and HC2183. These inhibitors had modest activity against Mtb *in vitro* (EC_{50} of 1.7 μM and 3.2 μM for HC2099 and HC2183 respectively) and no detectable cytotoxicity in macrophages. Additionally, these compounds demonstrated potent activity against intracellular Mtb (EC_{50} of < 0.3 μM and 3.0 μM for HC2099 and HC2183 respectively), especially HC2099 which

demonstrated 5-fold enhanced *ex vivo* activity compared to *in vitro* activity. These compounds also had favorable pharmacokinetic (PK) properties, including high solubility and microsome stability[25], making them prime candidates for early-preclinical drug development.

Several MmpL3 inhibitors of similar chemical structure to HC2099 have been described in the literature. The 1H-benzimidazole MmpL3 inhibitors EJMCh4 and EJMCh6 are potent inhibitors against both Mtb and NTMs[21,156]. This series of MmpL3 inhibitors was active against intracellular Mtb in infected macrophages[21]. These compounds were also able to kill *M. abscessus* in a zebrafish infection model[156]. Similarly, the NITD series of MmpL3 inhibitors, namely NITD-304 and NITD-349, are highly potent MmpL3 inhibitors with MICs reported as 20 and 30 nM respectively[27]. This series was demonstrated to kill Mtb in both acute and chronic murine infection models[27]. Based on the similarity between these compounds and parental HC2099 we sought to further optimize HC2099 through a structure activity relationship (SAR) study that would translate to *in vivo* efficacy.

In this study, we describe the results of a SAR campaign that identified multiple HC2099 analogs that are highly active against Mtb both *in vitro* and *ex vivo*. Using a mixed *mmpL3* mutant population and an *mmpR5* efflux strain, we demonstrate that active compounds target MmpL3 and are not susceptible to MmpR5 regulated efflux. Three of these compounds MSU-43085, MSU-43165, and MSU-43170 demonstrated drug-like properties including high solubility, high microsome stability, and low cytotoxicity. The compounds were also active against MAB and MAC *in vitro* and in macrophages, with activity comparable to standard of care drugs amikacin and clarithromycin. *In vivo* studies showed the optimized analogs were orally bioavailable and well tolerated in mice treated at a high dose. Using an acute infection model, we demonstrated that MSU-43085 was able to prevent Mtb growth in C57Bl/6 mice similar to INH in an acute infection model. However, the compounds were not effective in a study using the chronic TB infection model. These results provide proof-of-concept for a new, orally bioavailable series of MmpL3 inhibitors and supports further pre-clinical studies.

Results:

HC2099 Analogs are Potent Mtb Inhibitors

In a previous report, we identified thirteen MmpL3 inhibitors using a combined untargeted and targeted whole cell phenotypic mutant screen[25]. Of these thirteen compounds, three (SQ109, C215, and HC2091) were previously identified as MmpL3 inhibitors[20,22,34], while the remaining ten (HC2032, HC2060, HC2099, HC2134, HC2138, HC2149, HC2169, HC2178, and HC2184) were novel or new versions of previously described chemical scaffolds[25]. Of the thirteen compounds, HC2099 and HC2183 were structural analogs of each other and only differed by a single substitution on the benzimidazole ring (-Cl vs -CH_3 substitution) (Table A.3.1). These two compounds were active against Mtb both *in vitro* and *ex vivo*, and had favorable kinetic solubility and microsome stability[25]. We sought to functionally characterize and improve on the properties of the HC2099 series in a SAR study involving the synthesis of > 50 analogs. The whole cell Mtb activity (growth inhibition half maximal effective concentration, EC_{50}) of these analogs ranged between 116 nM to > 80 μM (upper limit of detection) (Table A.3.1). The SAR of HC2099 provided new insights into groups required for the function of the series. A general outline for the modification and optimization of the series is outlined in Figure A.3.1a with resulting effects (EC_{50}) illustrated in Figure A.3.1b and specific structures and *in vitro* activities are described in Table A.3.1. First, modification of the hydrophobic isopropyl groups (R1) led to either a decrease or loss of activity in this series (Figure A.3.1 and Table A.3.1). Second substitutions of the 1H position (R2) of the imidazole with a methyl (MSU-42830) led to complete loss of activity, suggesting that this H^+ may play a role in hydrogen bonding (Table A.3.1). Initial gain of activity occurred through modification of the benzene ring substitution (R3) (Figure A.3.1 and Table A.3.1). These substitutions were required for activity as analogs lacking these substitutions were devoid of activity (Table A.3.1, MSU-42765, MSU-42767 – MSU-42769, and MSU-43249). The series was optimized to have two chloro substitutions at the R2 group consistent with previously described 1H-benzimidazole MmpL3 inhibitors[234]. Finally, the sulfur (S) atom was replaced due to concerns

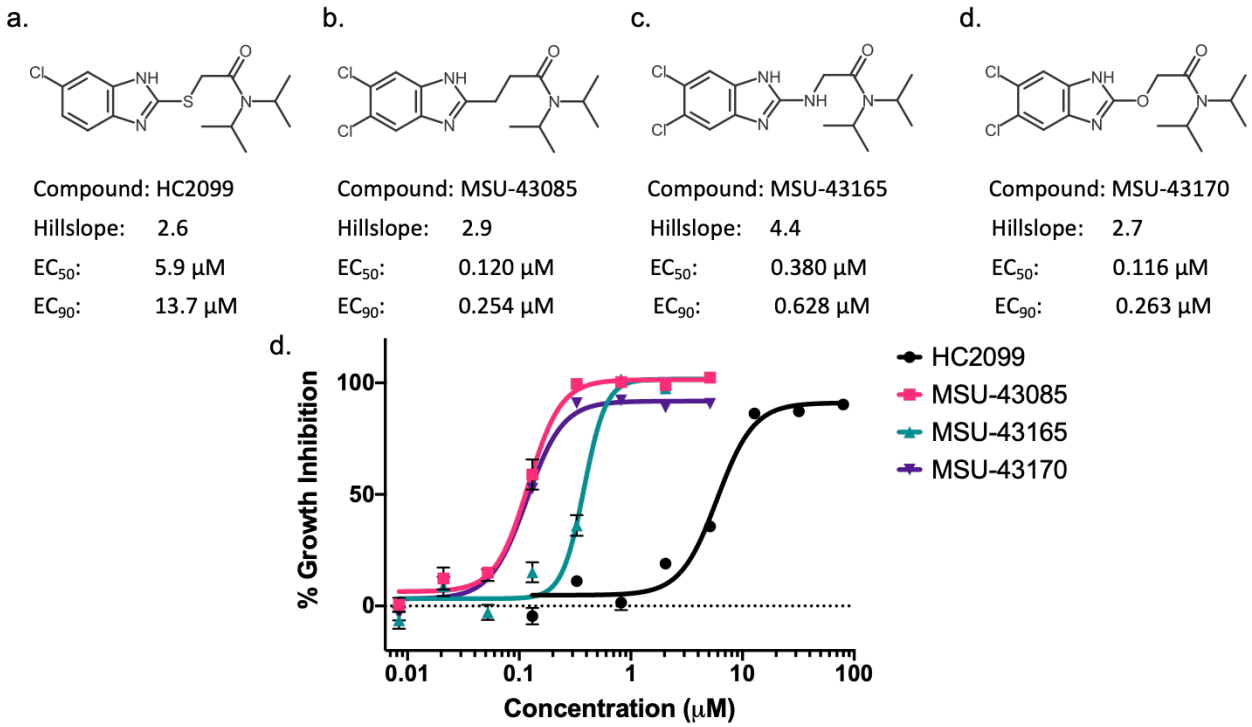

Figure 3.1. Structure activity relationship studies enhances potency of several HC2099 analogs. a-d) Structures and activity of HC2099 (a) analogs MSU-43085 (b), MSU-43165 (c), and MSU-43170 (d). Corresponding inhibitor descriptors for dose response curves (e) are included as the hillslope, EC50, and EC90. The dose response curves for each inhibitor (e) are compared to parental HC2099 (black). Dose response curves were run in triplicate, error bars indicate the S.D. of the mean.

of metabolic instability as host drug metabolism by cytochrome P450 enzymes (CYP) can oxidize sulfur groups rendering them inactive[235]. Consistent with this hypothesis, substitution of the S with a SO_2 group led to complete loss of activity in this series (Table A.3.1, MSU-43066). Substitution of the S atom for other hetero atoms (X, Figure A.3.1a) such as carbon (C), nitrogen (N) or oxygen (O) led to 10-50x enhanced activity compared to parental HC2099 and HC2183 depending on the R3 substitution (Table A.3.1, Figure A.3.1, Figure 3.1a-e). Additional attempts to modify the R1 groups were made (Figure A.3.1a); however, this was deleterious for activity (Figure A.3.1b) leaving the di-isopropyl group as the optimized substitution group for this series. The highest gain in activity (MSU43170, 116 nM) was ~10-fold higher than the leading MmpL3 inhibitor SQ109, but ~3- to 5- fold lower than similar NITD-304 and NITD-349 (Figure A.3.1b). We prioritized active compounds from the initial screen for follow up studies described below. While additional active

Table 3.1. *ex vivo* and cytotoxicity of HC2099 analogs

Compound	*ex vivo* EC_{50} (μM)	CC_{50} (μM)	S.I. (CC_{50}/EC_{50})
MSU-43085	0.13	> 80	> 595.7
MSU-43165	0.13	> 80	> 596.6
MSU-43170	0.035	> 80	>2285

S.I.- selective index

analogs will be referred to in the text and presented in supplemental data, three compounds MSU-43085, MSU-43165, and MSU-43170 that were highly active *in vitro* with EC_{50}s of 130 nM, 320 nM, and 116 nM respectively (Figure 3.1b-e), will be specifically focused on in this report.

HC2099 Analogs Kill Intracellular Mtb with a High Selective Index

Mtb is a facultative intracellular bacterium that actively replicates in immune phagocytes such as macrophages[236]. Genetic knockdown studies demonstrated that MmpL3 is essential for Mtb growth inside of macrophages[64]. Consistent with this phenotype, we previously showed that the parental HC2099 and HC2183 compounds had potent *ex vivo* activity against Mtb[25]. Using a firefly luciferase (FFLuc) reporter strain of Mtb CDC1551[236], we screened select active analogs for *ex vivo* activity against Mtb in infected primary bone marrow derived macrophages (BMMΦ) via dose response (Table A.3.2, Table 3.1). Our findings show that the prioritized analogs were potent inhibitors of intracellular Mtb with MSU-43085, MSU-43165 and MSU-4170 exhibiting *ex vivo* EC_{50}s of 134 nM, 134 nM, and 35 nM respectively (Table 3.1). The results for MSU-43170 demonstrated 3.3-fold enhanced activity compared to *in vitro* activity. Similarly, HC2099 demonstrated > 10-fold enhanced activity in the same model[25]. This *ex vivo* enhanced activity was not observed for C substituted heteroatom analogs (Table A.3.2, Table 3.1). This indicates that both O and S based analogs potentially have enhanced penetration into the macrophages leading to increased intracellular Mtb killing.

To ensure that the active analogs were specifically killing Mtb and not the macrophages, we tested active analogs for cytotoxicity using the Cell Titer Glow assay(Promega). The analogs

Table 3.2. *in vitro* and *ex vivo* activity of HC2099 analogs against NTMs

	***in vitro* MIC (μg/mL)**		***ex vivo* (> 90% inhibition (μg/mL)**	
Compound	*M. abscessus* ATCC 19977	*M. avium* ATC 700891 (MAC 101)	*M. abscessus* ATCC 19977	*M. avium* ATC 700891 (MAC 101)
Clarithromycin	1	0.06	64	128
Amikacin	4	N.D.	N.D.	N.D.
Rifampicin	N.D.	0.06	N.D.	N.D.
MSU-42766	4	> 64	128	> 128
MSU-43065	2	16	> 128	> 128
MSU-43085	1	8	64	16

N.D. – not determined

demonstrated little to no cytotoxicity (CC_{50} > 80 μM), with a selective index (CC_{50}/EC_{50}) range of 34.3 to > 644.6 (Table A.3.2, Table 3.1). MSU-43085, MSU-43165, and MSU-43170 specifically demonstrated selective indexes of >645, >210, and >2200 in BMMΦ respectively (Table 3.1). As an additional study, we also tested MSU-43085, as well as MSU-42766 and MSU-43065 for cytotoxicity against THP-1, HepG2, and HeLa cell lines and found similarly low cytotoxicity in these cell lines (Table A.3.3). These results indicate that our compounds are highly active against intracellular Mtb without mammalian cell cytotoxicity.

HC2099 Analogs are Active against NTMs

In addition to Mtb, NTMs are another class of pathogenic mycobacteria with high levels of drug resistance. We previously demonstrated that parental HC2099 could inhibit MAB growth *in vitro* (96.5% at 20μM)[25]. To determine if the new analogs retain or improve NTM growth inhibition, we tested select analogs against NTM species MAB and MAC. For these assays we selected analogs MSU-42766, MSU-43065, and MSU-43085 which ranged in activity from low to high activity against Mtb with 1.3 μM, 463 nM, and 130 nM *in vitro* EC_{50}s respectively (Table A.3.1, Figure 3.1b). The activity (MICs) against both MAB and MAC *in vitro* followed similar trends as activity against Mtb (Table A.3.1). Specifically, MSU43085 was the most potent with MICs of 1 and 8 μg/mL against MAB and MAC respectively (Table 3.2). Comparatively, MSU-43065 demonstrated lower activity with MICs of 2 and 16 μg/mL respectively, and MSU-42766

Table 3.3. Cross resistance of HC2099 analogs against a mixed Mtb *mmpL3* mutant pool

Compound	WT AUC	*mmpL3* AUC	Fold Resistance (WT / *mmpL3*)
MSU-43085	231.7	165.2	1.4x
MSU-43165	214.5	147.2	2.0x
MSU-43170	247.5	160.3	1.5x

AUC – area under the curve

demonstrated the lowest activity at 4 µg/mL against MAB and no detectable activity against MAC at > 64 µg/mL (Table 3.2). While the compounds were not as potent against MAB and MAC as they were against Mtb, the activity of MSU-43085 was still higher than standard of care drugs clarithromycin (1 µg/mL) and amikacin (4 µg/mL) for MAB (Table 3.2). Similarly, MSU-43065 had higher activity than amikacin against MAB while MSU-42766 had similar activity as amikacin (Table 3.2).

Based on these results we next tested the activity of these compounds against intracellular MAB and MAC in infected macrophages. While MSU-42766 and MSU-43065 demonstrated low activity in the *ex vivo* model with MICs ≥ 128 µg/mL, MSU-43085 demonstrated equal or higher activity against both MAB (64 µg/mL) and MAC (16 µg/mL) than clarithromycin (64 µg/mL and 128 µg/mL respectively) (Table 3.2). These results demonstrate that MSU43085 out competes standard of care drugs clarithromycin and amikacin in both *in vitro* and *ex vivo* models.

mmpL3 Mutants are Resistant to Active HC2099 Analogs

The SAR studies identified analogs with enhanced activity against Mtb. However, such modifications can lead to a phenomenon known as *target drift*, in which the new analog targets an alternative pathway from the parental compound. One example of such a phenomenon is SQ109, which was developed in an effort to improve the therapeutic potential of EMB[237]. However, by modifying the structure of EMB to SQ109 the target changed from the arabinosyl transferase

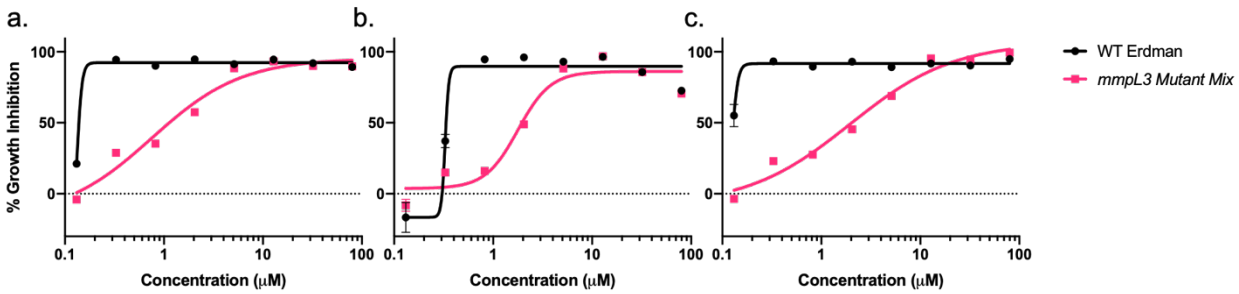

Figure 3.2. Cross resistance of a mixed *mmpL3* mutant pool against select analogs. a-c) Dose response curves for compounds MSU-43085 (a), MSU-43165 (b), and MSU-43170 (c) in either a wild type (WT) or mixed *mmpL3* mutant background. Fold differences in the effective concentration are listed as the area under the curve in Table 3.3. *mmpL3* mutant strains used are listed in Table A.3.4.

EmbABC to MmpL3[34]. While target drift is not necessarily detrimental to the therapeutic potential of a new analog, such alterations in the MOA can derail the original purpose of an SAR study and confound further optimization studies.

We previously demonstrated that a mixed mutant population of twenty-four unique Mtb *mmpL3* mutants could be used to accurately identify MmpL3 inhibitors from a small library of 163 Mtb growth inhibitors[25]. This mutant pool was demonstrated to be highly resistant to MmpL3 inhibitors while demonstrating no cross-resistance to non-MmpL3 inhibitors[25]. We monitored for target drift by screening active analogs via dose response against the mixed *mmpL3* mutant pool (see Table A.3.4 for list of mutants used). The results of this screen demonstrated that the mixed *mmpL3* mutant pool conferred 1.5-3.5x fold resistance to all active analogs when compared to WT using the relative area under the curve (AUC) (Table A.3.5, Table 3.3). MSU-43085, MSU-43165, and MSU-43170 demonstrated 1.4x, 2.0x, and 1.5x fold less activity in the *mmpL3* mixed mutant background respectively compared to WT (Table 3.3). This suggests that that active analogs continued to target MmpL3 and enhanced activity gained during SAR is not due to target drift.

Table 3.4. Activity of HC2099 against drug resistant *M. tuberculosis*

Compound	MIC (μg/mL)				EC_{50} (μM)	
	H37Rv	H37Rv (*rpoB*^{S450L})	H37Rv (*ΔkatG*)	H37Rv (*gyrA*^{D94K})	Erdman	Erdman (*mmpR5*^{E21K})
Isoniazid	0.03	0.06	> 2	0.03	N.T.	N.T.
Moxifloxacin	0.06	0.06	0.06	> 2	N.T.	N.T.
Bedaquiline	N.T.	N.T.	N.T.	N.T.	0.22	0.91
Clofazimine	N.T.	N.T.	N.T.	N.T.	0.3	1.6
MSU-42766	0.5	0.25	0.5	0.5	1.3	1.8
MSU-43065	0.25	0.25	≤ 0.125	≤ 0.125	0.54	0.39
MSU-43085	≤ 0.125	≤ 0.125	≤ 0.125	≤ 0.125	N.T.	N.T.

N.T. – not tested

HC2099 Analogs are Active against Drug Resistant Mtb Strains

Mtb drug resistance contributes to treatment failure in many individuals[230]. Therefore, new drugs that are active against these drug resistant strains are needed. To determine the therapeutic potential of our compounds, we tested prioritized analogs against clinically relevant mono-drug resistant Mtb strains including INH (*ΔkatG*), RIF (*rpoB*^{S450L}), and moxifloxacin (MOX, *gyrA*^{D94K}) resistant strains. As expected, the INH and MOX resistant strains conferred resistance to INH and MOX respectively (Table 3.4) and the drug resistant strains did not confer resistance to the tested analogs MSU-42766, MSU-43065, or MSU-43085 (Table 3.4). These results are consistent with other MmpL3 inhibitors, which also demonstrate low cross-resistance in drug resistant Mtb strains[26,27,29,35,37,153,204]. Interestingly, the activity of MSU42766 was higher against the *rpoB*^{S450L} strain (0.25 μg/mL) compared to WT (0.5 μg/mL) (Table 3.4). Additionally, the activity of MSU-43065 was higher against the *ΔkatG* and *gyrA*^{D94K} strains (≤ 0.125 μg/mL) compared to WT (0.25 μg/mL) (Table 3.4). Whether this was due to background mutations that conferred higher susceptibility to our compounds, or because Mtb strains with these specific resistance mutations are more sensitive to MmpL3 inhibitors is unknown.

In addition to drug resistance conferred through mutations in the target enzymes such as *gyrA*^{D94K} for MOX or activating enzymes such as *ΔkatG* for INH, non-specific resistance through efflux can confer resistance to some antibiotics. MmpR5 (Rv0678) is a member of the MarR family of repressors and is a regulator of the *mmpS5-mmpL5* operon involved in mycobactin export and

drug efflux[238]. Several reports have described the *in vitro* isolation of *mmpR5* mutants resistant to bedaquiline (BDQ**)** and clofazimine (CFZ)[239,240] which is mediated through increased MmpL5 efflux pump expression[240]. Several reports have already identified *mmpR5* clinical mutants including from BDQ and CFZ naïve patients in both drug sensitive and MDR-TB strain backgrounds[240-242]. Recently, Li and colleagues demonstrated that *mmpR5* mutants are resistant to the SIMBL class of MmpL3 inhibitors[243], suggesting that some MmpL3 inhibitors may be susceptible to efflux by MmpL5. To determine if *mmpR5* mutations confer resistance to our inhibitors, we tested active analogs against an *mmpR5* mutant (MmpR5-E21K) isolated against an experimental compound HC2194. The *mmpR5* mutant demonstrated resistance to both BDQ and CFZ similar to previous reports (Table 3.3)[239-242,244]. However, the *mmpR5* mutant did not confer resistance to tested HC2099 analogs, including MSU-43065, indicating that this series of MmpL3 inhibitors are not susceptible to MmpL5 mediated efflux (Table A.3.6, Table 3.4). In fact MSU-43065 was more potent in the *mmpR5* strain (EC_{50} 0.36 μM) compared to parental WT (EC_{50} 0.54 μM). These results show this series is highly active against clinically relevant mono-drug resistant and *mmpR5* efflux strains of Mtb, an activity profile consistent with future clinical use of the series.

HC2099 Analogs have a Moderate Frequency of Resistance

The evolution of resistance to new Mtb drugs occurs at different frequencies depending on the specific drug. For example, the prodrug INH has an *in vitro* frequency of resistance (FoR) of 10^{-6} [180] while RIF has a lower *in vitro* FoR of 10^{-8} [21](Table 3.5) depending on the concentration tested. The results of our cross-resistance study against a mixed pool of *mmpL3* mutants, suggested that our compounds likely target MmpL3 (Table A.3.5, Table 3.3) and should have FoR similar to other MmpL3 inhibitors[29,30]. To determine the potential for the evolution of resistance we isolated resistant mutants to the three analogs MSU-42766, MSU-43065, and MSU-43085

Table 3.5. *M. tuberculosis* frequency of resistance to HC2099 analogs

Inhibitor	MIC (μg/mL)	Frequency of Resistance		
		2x MIC	8x MIC	16x MIC
Bedaquiline	2	1.43×10^{-7}	3.57×10^{-8}	3.57×10^{-8}
Ethambutol	1	3.61×10^{-6}	8.57×10^{-7}	1.79×10^{-8}
Isoniazid	0.125	5.0×10^{-6}	3.93×10^{-6}	2.71×10^{-6}
Ofloxacin	1	5.36×10^{-7}	7.14×10^{-8}	3.57×10^{-8}
Pretomanid	0.5	1.79×10^{-6}	8.57×10^{-7}	1.43×10^{-7}
Rifampicin	0.5	5.36×10^{-7}	7.14×10^{-8}	3.57×10^{-8}
MSU-42766	0.5	1.36×10^{-6}	8.0×10^{-8}	0
MSU-43065	0.25	4.0×10^{-7}	8.0×10^{-8}	0
MSU-43085	0.125	1.8×10^{-6}	4.0×10^{-8}	0

MIC – minimum inhibitory concentration

used in the MAB/MAC and mono-drug resistance studies (Table 3.2, Table 3.4). We also isolated mutants against control drugs BDQ, EMB, INH, ofloxacin (OFX), pretomanid (PRT), and RIF using increasing concentrations that were 2x, 8x, and 16x the MIC for each inhibitor (Table 3.5). For all inhibitors tested, the FoR was relative to the concentration tested, where increasing concentrations of inhibitor led to a decrease in the FoR (Table 3.5). The FoR for each inhibitor was similar to those previously reported[21,179,180,184,245] (Table 3.5). The HC2099 analogs had similar FoR ranging from 1.36×10^{-6} at 2x the MIC to 4×10^{-8} at 8x the MIC (Table 3.5). For all three compounds, isolates confirmed for resistance were not detected at the highest concentrations (16x MIC) (Table 3.5). These data indicate that the FoR for the HC2099 analogs occurs at a moderate rate compared to other Mtb drugs.

HC2099 Analogs are Soluble, Tolerable and Orally Bioavailable in Mice

Based on the large selective index, and the potent whole cell activity of the compounds both *in vitro* and *ex vivo*, we sought to determine early PK properties of the selected analogs (Table A.3.6) including MSU-43085, MSU-43165, and MSU-43170 (Table 3.5). To gain insights into the *in vivo* use of these series, we first tested the kinetic solubility of these compounds in phosphate buffer saline (PBS) at pH 7.4 (blood relevant) and 2.0 (stomach relevant). The results of these studies suggested that MSU-43085, MSU-43165 and MSU-43170, as well as the other

Table 3.6. Early PK properties of prioritized HC2099 analogs

Compound	Kinetic Solubility (μM)		Microsome Stability (%)	Blood Plasma Concentration (1 hr, Fold EC_{50})	Lung Concentration (4 hr, Fold EC_{50})
	pH 7.4	pH 2.0			
MSU-43085	248	> 300	102	10-50x	8x
MSU-43165	32	> 300	106	1.3x	Present
MSU-43170	51	> 300	95	4x*	Present

* - 1 hour time point unavailable so 2 hour time point data is reported
Present – compounds detected but concentrations incalculable

compounds, have moderate solubility at pH 7.4 (32 to > 300 μM) and increased solubility at pH 2.0 (all >300 μM). We next tested the compounds for metabolic stability in the presence of mouse microsomes. We exposed several analogs, including MSU-43085, MSU-43165, and MSU-43170, to microsomal fractions for thirty minutes and quantified the amount remaining by mass spectrometry. Of the compounds tested, each had moderate (≤ 85%) to high (> 85%) microsome stability (Table A.3.6) including MSU-43085, MSU-43165, and MSU-43170 which had high microsome stability (> 95%) (Table 3.5).

Based on these results, we performed a “snap-shot” PK study to determine if the compounds were orally bioavailable in mice. To do this, we orally dosed female C57Bl/6 mice with 200 mg/kg of MSU-43085, MSU-43165, or MSU-43170 (formulated in corn oil). We then collected plasma at one, two, and four hours post dosing and lung tissues at four hours post dosing and compound concentrations were quantified by MS. All three compounds were detected in both the blood plasma and lung tissue samples at one, two and four hours post treatment (Table 3.5). MSU-43085 was maximally detected at one hour post treatment at concentrations 10-50x and 8x the EC_{50} in the blood plasma and lung tissue respectively (Table 3.6). MSU-43165 was detected at a relatively lower concentration than MSU-43085 (1.3x the EC_{50}) (Table 3.6). For MSU-43170, usable sample volumes were not obtained for one-hour post treatment, so instead we report for two-hours at 4x the EC_{50} (Table 3.6). MSU-43165 and MSU-43170 were both detected in the lung; however, the exact concentrations could not be determined (Table 3.6). The

results of these assays suggested that the analogs could be used to orally treat Mtb in an infected mouse.

MSU-43085 is Active *in vivo* in an Acute Murine Infection Model

Based on the high activity against Mtb, as well as favorable PK properties of the compounds, we tested MSU-43085 and MSU-43165 in an early acute infection. For this study we infected C57Bl/6 mice via low dose aerosol with 200 CFUs of Mtb Erdman. In four treatment arms, the mice were treated by oral gavage, daily for two weeks with vehicle control (corn oil), 25 mg/kg INH, 200 mg/kg MSU-43085 or 200 mg/kg MSU-43165. The results of this acute infection model demonstrated that the lungs of vehicle control mice became well infected over two weeks (median = 2.2 x 10^4 CFUs/mL) (Figure 3.3a). By contrast, no colonies were isolated from lung homogenates of INH treated mice (Figure 3.3a). In comparison to vehicle control mice, mice treated with MSU-43085 had significantly fewer colonies ($p = 0.0093$), with a median lung bacterial burden equal to the limit of detection (20 CFUs) (Figure 3.3a). While colonies could still be isolated from MSU-43085 treated mice, this was not significantly different from INH treated mice ($p > 0.99$, Figure 3.3a). In contrast to MSU-43085 treated mice, mice treated with MSU-43165 still became well infected (median = 5.7x10^3 CFUs/mL of lung). While mice from the MSU-43165 treatment cohort had lower bacterial lung burden than vehicle control mice (Absolute difference of the median = 1.6x10^4 CFUs/mL), this was not significant ($p > 0.99$).

Following infection in the lung, Mtb can disseminate to other tissues including the spleen. While colonies could be detected in the spleens of vehicle control mice, this was only possible in half of the infected mice (Figure A.3.2). By comparison to vehicle control mice, no colonies were isolated from mice treated with either INH or MSU43085 (Figure A.3.2). While significance could not be established due to high variability, the trend suggests that MSU-43085 may prevent dissemination to the spleen. Consistent with the results for lung homogenates, MSU-43165 did not appear to prevent Mtb dissemination as colonies could also be detected in the spleens of

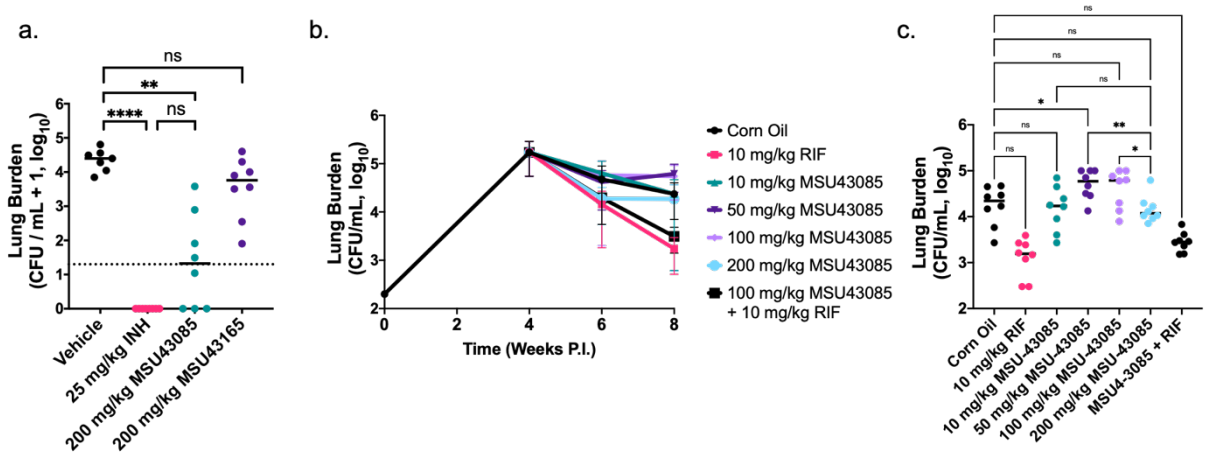

Figure 3.3. *in vivo* activity of prioritized HC2099 analogs. a) Bacterial lung burden (CFU/mL + 1) of C57Bl/6 mice following an acute (two week) infection with Mtb Erdman and treated with vehicle (corn oil), INH (25 mg/kg), MSU-43085 (200 mg/kg) or MSU-43165 (200 mg/kg). Dotted line indicates limit of detection (20 CFUs). CFU/mL data was +1 transformed to visualize 0 CFU data on a log scale. Solid black lines indicate the median bacterial infection in each group. Groups were compared using a Two-way ANOVA. ** $p < 0.005$, **** $p < 0.0001$. b) Bacterial lung burden (CFU/mL) of C57Bl/6 mice in a chronic infection model. Following four weeks of infection, mice were split into seven treatment groups and treated for two- and four- weeks via p.o. c) Bacterial lung burden (CFU/mL) of mice at week 8. Significant differences were observed between treatment groups based on a two-way ANOVA.

treated mice (Figure A.3.2).

Based on the results of the initial *in vivo* study, we tested the *in vivo* activity of MSU43085 in a chronic infection model. We infected C57Bl/6 mice via low dose (200 CFUs) aerosol and allowed the infection to establish over four weeks ($4.7x10^4$ CFUs/mL) before splitting the mice into seven treatment arms that included mice treated with MSU-43085 at 200, 100, 50, and 10 mg/kg of body weight, and control arms of vehicle (corn oil) or RIF (10 mg/kg). RIF and MmpL3 inhibitors, including parental HC2099 and HC2183, act synergistically with RIF i*n vitro*[25,218,246]. Therefore, we included a combination arm of mice co-treated with 10 mg/kg of RIF and 100 mg/kg MSU-43085. Mice treated with corn oil demonstrated a small decrease in CFUs over the four weeks of treatment but was not significantly different from week four untreated mice (Figure 3.2b). Comparatively, mice treated with RIF controls saw a significant decrease in CFUs after four weeks of treatment (Figure 3.2b). However, in all cases of mice treated with MSU-43085, no decrease in CFU compared to week four untreated mice was observed (Figure 3.2b). In addition, there was

no significant decrease of CFUs in the co-treatment arm compared to mice treated with RIF only (Figure 3.2b). While significant differences were observed between week two and four post treatment in the 200 mg/kg MSU-43085 treatment group, similar differences were observed for the vehicle control group. Therefore conclusive interpretations could not be made from these datasets. We hypothesize that the differences in response for the 200 mg/kg between the acute infection and the chronic infection study was due to drug clearance due to unoptimized formulation. While the data indicates that MSU-43085 was not active against Mtb in the model tested, MSU-43085 was well tolerated even at 200 mg/kg as indicated by the changes in body weight (Δ%) of the mice throughout the experiment (Figure A.3.3). This indicates that the compound can be safely administered over a long treatment period without signs of toxicity.

Discussion:

The SAR study identified analogs of the MmpL3 inhibitor HC2099 that ranged in activity (EC_{50}) from > 80 μM to 116 nM, with the largest gain of activity resulting from substituting the S for heteroatoms C, N, or O. Active analogs, including MSU-43085, MSU-43165, and MSU-43170, demonstrated potent activity against Mtb in an *ex vivo* infection model with a high selective index. In addition to Mtb, MSU43085 demonstrated high activity against both MAB and MAC, especially in an *ex vivo* model where MSU-43085 outcompeted standard of care drugs amikacin and clarithromycin. Selected analogs, including MSU-43085, demonstrated equal activity against both mono-drug resistant and efflux strains of Mtb. Analogs, including MSU-43085, MSU-43165, and MSU-43170, demonstrated favorable PK properties and were found to be bioavailable when dosed at a high concentration. The results of an acute infection study demonstrates that MSU-43085 was active against Mtb *in vivo*. However, the results of a chronic infection model indicate that further optimization for this series is still required. The compounds also demonstrated a moderate FoR that was dose dependent. The results of these studies demonstrate that MSU-43085 is a potent inhibitor of both Mtb, MAB and MAC with high therapeutic potential that requires additional optimization.

These early preclinical studies support continued development of the HC2099 series for treatment of Mtb and NTM infection. While additional *in vitro* PK studies are required to further characterize this series of compounds, one property of note is that the MSU-43085, as well as other analogs, had higher solubility than the leading NITD series[27]. Further, similar series of compounds including the NITD, EJMCh, and CRS series of MmpL3 inhibitors were demonstrated to be potent inhibitors of Mtb and NTMs[27,42,156,157]. The data reported here demonstrates that our series of compounds has similar spectrum of activity against other *Mycobacterium* spp. In line with this, De Groote and colleagues recently demonstrated that a benzothiazole-based MmpL3 inhibitor (CRS400359) had higher activity against MAB compared to Mtb[157]. Additional

optimization studies may seek to design an SAR study around lead optimization for MAB in addition to Mtb.

The results of the *in vivo* mouse infections described here suggests that MSU-43085 can inhibit Mtb in the mouse lung during an acute infection but activity was lost in an established chronic infection. We currently speculate that the failure in this model is driven by the delivery of the compound. For this study we used corn oil as the vehicle because MSU-43085 could melt into solution at high concentrations (50 mg/mL). However, future studies will seek to optimize formulation to further improve bioavailability. Recently Lun and colleagues demonstrated that by modifying the formulation for the indole amide series of MmpL3 inhibitors, they could increase the bioavailability and increase the anti-Mtb activity of these compounds *in vivo*[143]. In this study we performed a snap-shot PK study to establish that the compounds are bioavailable, the results demonstrated that MSU-43085 was present both in blood plasma and lung tissue and were backed by the *in vivo* activity for MSU-43085 against Mtb in an acute infection. However, we do not know the full PK parameters for this series of inhibitors including parameters such as the hall-life or if MSU-43085 accumulates in the lungs over time. Therefore, additional studies are required to understand the pharmacokinetics of this series to guide further optimizations, formulation and dosing schedules. During the *in vivo* studies, we did not observe any behavioral changes or weight loss in mice treated with MSU-43085, even when taken for four weeks at a high (200 mg/kg) dose. This demonstrates the compound is tolerable. However, additional studies into the potential side effects and toxicity of this series of inhibitors still need to be conducted. Future experiments will also seek to determine the *in vivo* activity of these compounds against MAB and MAC as an additional proof of concept.

Methods:

Culture Conditions and Strains

Mtb strains were cultured in 10 mL 7H9 OADC (10% v/v) and 0.05% Tween-80 in standing T25 flasks. Cultures were incubated at 37°C in 5.0% CO_2. Cultures were aliquoted into 2 mL screw cap tubes and mixed 1:1 with 40% glycerol. Mtb-glycerol tubes were stored in a -80C freezer. When needed, stocks were thawed at room temperature and inoculated into 30 mL or 100 mL cultured of 7H9 OADC (10% v/v) with 0.05% Tween-80 in standing T75 or T150 flasks respectively and grown to exponential phase (OD_{600} = 0.5 – 1.0).

For the mixed mutant pool of *mmpL3* mutants, twenty-four unique Mtb *mmpL3* mutants were pooled in an equal density mixture based on OD_{600} as previously described[25]. The pooled mutant culture was then aliquoted into 2 mL cryo-tubes and mixed 1:1 with 40% glycerol (20% glycerol final) and stored at -80C. For a full list of *mmpL3* mutants used see Table A.3.4. Cryo-tubes were thawed as described above and inoculated into 30 mL or 100 mL of 7H9 medium in T75 or T150 standing flasks and incubated at 37°C with 5.0% CO_2.

M. abscessus (ATCC19977) and *M. avium* (ATCC 700891 – MAC 101) were cultured on solid medium plates and CFUs were taken to inoculate 7H9 ADC with 0.05% tween-80 and supplemented with glycerol (2 mL/L) liquid cultures. Liquid cultures were incubated at 35-37°C

HC2099 Analog Synthesis

The analogs tested were synthesized by Matt Gilletto in Dr. Edmund Ellsworth's lab. The methods for synthesis are provided in supplemental methods (Appendix C). Compound structures were verified by HNMR and MS (Table A.3.8).

***in vitro* Dose Responses**

EC_{50} dose response curves were conducted as previously described[22,25]. Briefly, Mtb strains were grown to mid-log phase and seeded in 96 or 384 well plates at a starting OD_{600} of

0.1 or 0.05 for 384 well. Wells of bacteria were then treated with each compound in a range of 80 – 0.13 μM or 5.12 μM – 8.3 nM (2.5-fold dilutions, for 8 dose points) as well as DMSO (negative) and 0.3 μM RIF (positive) controls. Plates were then placed into re-sealable bags with a wet paper towel and incubated at 37°C with 5.0% CO_2 for six days. After six days, plates were removed, and bacterial wells were resuspended by pipetting. Growth (OD_{600}) was analyzed using a PerkinElmer Enspire plate reader and percent growth inhibition (%GI) was calculated relative to DMSO and RIF controls. Dose responses were log transformed and used to calculate EC_{50}s, Hillslopes, EC_{90}s, 95% confidence intervals (CI), and area under the curves (AUCs) using Graphpad Prism 9 software.

The MIC of the compounds and drugs tested were determined using the microbroth dilution method. Briefly, bacterial strains were grown to logarithmic phase and seeded into 96 wells plates at 5 x 10^5 CFU/mL. Cells were then treated with each compound (32 – 0.12 μg/mL) or control drugs RIF (1 – 0.004 μg/mL), INH and MOX (2 – 0.008 μg/mL), and Pretomanid (8 – 0.03 μg/mL). Bacterial plates were then sealed and incubated at 37°C for 7-8 days. Following OD_{600} measuring, 10 μL of Alamar blue dye was added and scanned on a flatbed color. The MIC for optical density was defined as the first concentration to decrease the OD_{600} while the MIC for the calorimetric assay was calculated as the first concentration for the observed color change form pink (active growth) to blue (no growth).

mmpL3 Cross Resistance Profiling

Dose response curves were generated as described above. Area under the curve (AUC) was calculated in Prism 9 software and compared between the mixed mutant pool and Mtb Erdman strains. Relative AUCs were calculated by dividing the AUC of the mixed *mmpL3* pool by the WT Erdman AUC. Fold resistance was calculated as the inverse of the Relative AUCs.

Isolation and Sequencing of an *mmpR5* Mtb Mutant

mmpR5 mutants were isolated, screened and sequenced as previously described[25]. Briefly, Mtb Erdman was cultured to exponential phase in 7H9 medium. 1 x 10^9 CFUs were harvested and plated on a 150 mm 7H10 OADC plate (with 10 µg/mL cycloheximide) amended with 20 µM of experimental compound HC2194. Plates were incubated at 37°C until single colonies appeared. Strains were colony purified to remove potential contaminating WT and screened for resistance by dose response. The genomes of confirmed resistant mutants were isolated and sequenced as previously described[25]. Sequenced genomes of resistant mutants were analyzed using the GATK workflow to identify single nucleotide variations[223].

Sensitivity Testing against Drug Resistant and an *mmpR5* Efflux Mutant

The MICs and EC_{50} were determined as described above. Sensitivity testing was compared between mono-drug resistant strains *rpoB*^{S450L} (RIF^R), *ΔkatG* (INH^R), and *gyrA*^{D94K} (MOX^R) strains as well as against an *mmpR5*^{E21K} efflux pump mutant. EC_{50}s were considered significantly different if the EC_{50} 95% CI did not overlap.

Intracellular EC_{50} Dose Response Curves

Intracellular dose response curves were carried out as previously described[211]. Briefly a firefly luciferase (FFluc) reporter strain of Mtb CDC1551[210] was grown to mid-log phase. Cultured resting primary bone marrow derived macrophages were isolated from C57bl/6 mice and seeded into 96 well plates as described[211]. Macrophages were then infected with the reporter strain at a MOI of 1[211]. Wells were then treated in duplicate with selected compounds in a range of either 80 µM – 8.3 nM or 5.12 µM – 8.3 nM (8 or 12 dose points, 2.5-fold dilutions). DMSO and 0.3 µM RIF were included as controls. 96 wells plates were then incubated in vented re-sealable bags with a wet paper towel at 37°C with 5.0% CO_2 for six days. After six days, the bright glow luciferase agent (Promega) was added to the 96 wells plates in a 1:1 ratio for each well. Plates were then

read using a PerkinElmer Enspire plate reader. Percent intracellular growth inhibition was calculated relative to DMSO and RIF controls. EC_{50}s, Hillslopes, and EC_{90}s were calculated as described above using Graphpad Prism 8 Software.

Cytotoxicity

Macrophage cytotoxicity for tested analogs was calculated for BMMΦ using the Cell Titer Glow (Promega) assay as previously described[211]. Briefly, BMMΦ were harvested form mice and seeded in 96 well plates at a starting inoculum of $1x10^7$ cells. Wells were treated with select compounds at a range of 80 μM to 8.3 nM in duplicate (12 dose points, with 2.5-fold dilutions). DMSO and 4.0% Triton X-100. 96 well plates were incubated at 37°C with 5.0% CO_2 in vented re-sealable bags with a wet paper towel. After six days, wells were treated 1:1 with Cell Titer Glow reagent and plates were read using a PerkinElmer Enspire plate reader. Percent cytotoxicity was calculated relative to DMSO (negative) and Triton (positive) controls. Transformed % cytotoxicity was used to calculate the CC_{50} using Graphpad Prism 8 Software.

For additional cell lines including HepG2, HeLa, and THP-1, the following protocol was used. HepG2 (ATCC HB-8065) and HeLa (ATCC CCL-2) were cultured in cEMEM supplemented with 10% v/v/ FBS and 1% v/v PenStrep. THP-1 cells were cultured in cRPMI-1640 medium (ATCC 30-2001) supplanted with 10% v/v FBS and 0.05 mM 2-mercaptoethanol (Sigma M3148). THP-1 cells were seeded in 96 well plates at $1x10^5$ cells/mL with complete medium. HepG2 and HeLa cells were seeded in 96 well plates with cEMEM at $1x10^6$ cells/mL. Cells were treated with compounds by dose response in a range of 128 – 0.48 μg/mL in triplicate or mitomycin C at a range of 128 μM to 0.0625 μM. Cells were treated for 24 hours at 37°C with 5% CO_2. Cells were then treated with either MTT or resazurin for four hours. Absorbance was then measured at 570 nm for MTT plates. Percent cytotoxicity was calculated relative to positive mitomycin C and untreated controls. Percent cytotoxicity was used to calculate the IC_{50} using Graphpad prism software using non-linear regression analysis.

In vitro and *ex vivo* Activity against NTMs

The MICs for *M. avium* (MAC 101) and *M. abscessus* (ATCC 19977) were calculated as above with minor alterations. Bacteria were suspended in cation-adjusted Mueller Hinton broth and seeded in 96 well plates at 5 x 10^5 CFUs/mL. Cells were then treated with compounds as well as clarithromycin and amikacin at concentrations ranging from 32 – 0.12 µg/mL. Plates were then sealed and incubated for 7 days at 37°C. Optical density and calorimetric readings were then taken as described above. MICs were defined as above.

THP-1 cells were infected with either *M. avium* or *M. abscessus* at an MOI of 10 for four hours prior to treatment. Following infection, cells were washed twice with PBS to remove non-phagocytosed bacteria. Fresh medium was then added, and cells were treated with concentrations ranging from 64 – 0.24 µg/mL and incubated for 24 hours at 37°C with 5% CO_2. Following twenty-four hours of treatment, cells were treated with resazurin (0.04 mg/mL) and incubated for an additional 3-5 days. Absorbance was measured for each well at 570 nm and 600 nm. The percent growth reduction was calculated relative to treated and untreated controls.

Kinetic Solubility and Microsomal Stability Assays

The kinetic solubility assay was conducted as previously described[25]. Briefly, using methods described by Bevan and Lloyd[228], the assay was performed with 7-point (2-fold) dilutions of the compounds, from 200 µM to 3.125 µM along with mebendazole, bexarotene, and aspirin as controls. The drug dilutions were added to PBS, pH 7.4, with a DMSO concentration of 1% (final), and incubated at 37°C for 2 h. The absorbance at 620 nm was measured for each drug dilution to estimate the solubility of the compound in triplicate/ dilution.

The mouse microsomal stability assay was conducted as described by Obach[229], and the results are presented as the percentages remaining after 30 min. Values greater than 100% are likely due to changes in the solubility of the compounds over the course of the assay and represent high stability in microsomes.

Frequency of Resistance

Freezer stocks of Mtb H37Rv were thawed and inoculated into 7H9 OADC and grown to stationary phase (OD_{600} of ~ 1.0) at 37°C rotating at 150 rpm. Samples were sub-cultured 1:100 in 100 mL of fresh 7H9 OADC and incubated at 37°C rotating at 150 rpm to an OD_{600} of ~1.0 (*i.e.* ~1 x 10^8 CFU/mL). 0.2 mL aliquots of sub-culture adjusted Mtb (OD_{600} of 1.00) were plated onto 7H10 ADC agar plates amended with or without (control) tested inhibitors (Table 3.6) at two-, eight, and sixteen-times the MIC. Plates were incubated at 37°C for three-four weeks to enumerate resistant mutant colonies (CFU). After incubation, colonies were inoculated into 4 mL of 7H9 containing equivalent to concentrations tested and cultured at 37°C rotating at 150 rpm for two to three weeks to confirm resistance. The FoR was calculated as the number of confirmed resistance colonies compared to the number of colonies initially plated (unamended control plate).

Mouse PK Study

All experiments were performed in compliance with Michigan State University IACUC approved protocols. Female C57Bl/6 mice were dosed with 200 mg/kg (based on the average body mass of 27 mice) of MSU-43085, MSU-43165, or MSU-43170 formulated in corn oil by oral gavage. At one, two, and four hours post treatment, blood samples were taken from three mice from each treatment group by cardiac puncture and placed in BD Lithium HeparinN Vacutainer tubes. Plasma was separated from whole blood by centrifuge and compounds were methanol extracted. Lungs were harvested from mice four hours post treatment. Lung samples were homogenized using a closed tissue grinder system (Fisherbrand – 02-542-09), and compounds were methanol extracted from lung homogenates. Methanol extracted samples were quantified by LC-MS.

Acute Mouse Infections

Forty 6- to 8-week-old female C57Bl/6 mice were infected with Mtb Erdman via low dose aerosol (200 CFUs) using a Glas-col nebulizer. One day post infection (P.I.), whole lungs from untreated mice were harvested from euthanized mice and homogenized using a Next Advance Bullet Blender in PBS with 0.1% tween-80 using 1.6 mm diameter steel beads. Samples of lung homogenates were plated in duplicate on 7H10 agar plates supplemented with 10% v/v OADC with 100 µg/mL cycloheximide, 50 µg/mL carbenicillin, 25 µg/mL polymyxin B, 20 µg/mL trimethoprim and incubated at 37°C for 40 days. Starting one day post infection, the remaining 32 mice were separated into four treatment arms of eight mice each. Mice from each arm were treated five days per week (over a total of 12 days) with either vehicle control (Corn oil), 25 mg/kg INH (in H_2O), 200 mg/kg MSU-43085, or 200 mg/kg MSU-43165 melted into corn oil. Thirteen days P.I., mice were euthanized as described above, and spleens and right lung lobes were homogenized as described above. Tissue homogenates were serial diluted in PBS (pH 7.4) + 0.05% Tween-80 and plated in duplicate onto 7H10 plates. Plates were incubated for 40 days at 37°C and CFUs enumerated. Left lung lobes were fixed in 4% paraformaldehyde.

No colonies were isolated from four out of the eight spleen samples from untreated mice; therefore, no statistical tests were performed on these samples. No colonies were detected in samples from one of the untreated control mice even in undiluted samples. A Grubb's outlier test of Log_{10} transformed CFUs of the untreated control group indicated that this mouse was an outlier ($p < 0.01$); therefore, this mouse was removed from downstream analysis. Bacterial burden was compared between treatment groups using a One-way ANOVA with Kruskal-Wallis post hoc test.

Chronic Mouse Infection

Female C57Bl/6 mice were infected by low dose aerosol (200 CFUs) with Mtb Erdman as described above. One day P.I. eight mice were euthanized and CFUs were enumerated from lung homogenates as described above. For the remaining 120 mice, Mtb infection was left to establish

for four weeks before being broken into treatment arms. Following four weeks of infection, eight mice were euthanized and lung and spleen samples were homogenized as described above to quantify infection prior to treatment. The remaining mice were broken into seven treatment arms of sixteen mice each and treated five days per week over four weeks. Treatment arms consisted of a vehicle control (100 µL corn oil), 10 mg/kg Rif (in 200 µL H_2O), 10, 50, 100, or 200 mg/kg MSU-43085 (in 100 µL corn oil), or a combined treatment of 10 mg/kg RIF (in 200 µL H_2O) and 100 mg/kg MSU-43085 (in 100 µL corn oil). At six and eight weeks P.I., eight mice form each treatment group were euthanized and spleen and right lung lobes were homogenized as described above. Lung and spleen homogenates were serial diluted in PBS (pH 7.4) with 0.05% Tween-80 and inoculated onto 7H10 antibiotic plates. Plates were incubated for up to forty days at 37°C and CFUs enumerated.

Body weights (g) of mice were measured to the nearest 0.5 g at the start of treatment and were measured once a week throughout the experiment. The changes in percent body weight were calculated for each mouse relative to body weights measured prior to treatment. A positive gain indicates a gain in weight. The average body weights measured per group were used as the basis for dosing the mice each week.

Acknowledgements:

Several of the above experiments were conducted by the In vitro Antimycobacterial Testing Service at Colorado State University, including: activity against mono-drug resistant Mtb strains, HeLa, HepG2, and THP cytotoxicity, *in vitro* and *ex vivo* MAB and MAC studies, as well as frequency of resistance studies. This NIH testing contract was directed by Prof. Richard Slayden and supported by the National Institutes of Allergy and Infectious Diseases Preclinical Service Contract 75N93019D00005. We gratefully acknowledge their contribution to this project.

CHAPTER 4: Whole Cell Phenotypic Screens to Identify MmpL3 and DosRST Inhibitors from the Molecular Libraries Small Molecule Repository

Abstract:

Hits from high throughput screens (HTS) conducted against *Mycobacterium tuberculosis* often undergo similar secondary pipeline assays of hit confirmation, testing for cytotoxicity and inhibition of intracellular Mtb. The results of such pipelines often lead to prioritization and discovery of novel inhibitors of commonly identified targets. One of the most common targets is the essential mycolic acid flippase, MmpL3. We previously conducted a HTS to identify inhibitors of the DosRST two-component system involved in the adaptation of Mtb in response to hypoxia. The result of this screen also identified > 1000 compounds that inhibit Mtb growth, independent of DosRST signaling. To rapidly identify inhibitors of MmpL3 from these hits, we utilized the MmpL3 whole cell phenotypic targeted mutant screen in parallel to standard pipeline assays. The results identified > 50 putative MmpL3 inhibitors, several belonging to new chemical classes. We also identified additional putative inhibitors of the DosRST reporter system. These compounds were further characterized for eukaryotic cytotoxicity and activity against Mtb growing in murine macrophages.

Introduction:

To address the growing problem of drug resistance in *Mycobacterium tuberculosis* (Mtb), several high throughput screens (HTS) have been performed to identify the next Mtb drug candidate. Following HTS, hits typically undergo similar secondary assay pipelines that 1) confirm activity *in vitro*, 2) test for cytotoxicity, and 3) test for intracellular Mtb growth inhibition[20,22,24-26,31]. These assays are meant to prioritize hits prior to in depth investigations into their mechanisms of action (MOA). However, following these prioritization pipelines, many research groups report the discovery of inhibitors of reoccurring targets such as QcrB[6-14], DprE1[15-20,40,41,247-253], and MmpL3[20-37,152-157,159,160,176,177]. While not necessarily detrimental to Mtb drug discovery as these are prioritized targets for Mtb therapy, the methods used to identify the target of newly discovered inhibitors can be either costly and/or time consuming. For example, the most common method resulting in the discovery of MmpL3 inhibitors is the isolation and sequencing of *mmpL3* mutants resistant to new inhibitors[20-37,152-157,159,160,176,177]. However, in the slow growing pathogen, Mtb, this can take several months. Alternative methods to identify the targeted pathway for prioritized inhibitors may include using reporter strains that are induced following the inhibition of specific metabolic pathways such as *cydA* or *iniB* reporters for electron transport chain and cell wall inhibitors respectively[193,194,254]. However, these reporters are broad in their interpretation and do not rule out secondary MOA.

We previously reported the results of a HTS using an ~220,000 chemical library available from the Institute of Chemistry and Cell Biology at Harvard Medical School (ICCB library), and the 350,478 compound NIH Molecular Libraries Small Molecule Repository (MLSMR library), that identified inhibitors of the DosRST two component system using an *hspX*-GFP reporter[207,255]. Hits from this screen included compounds that inhibited reporter fluorescence, but not growth, a property consistent with inhibition of DosRST[207,255]. Validation assays defined six new types of inhibitors, named HC101-HC106, as inhibitors of DosRST signaling. Notable example of compounds hit in the screens include the anti-malarial drug artemisinin (HC101A) and HC106A

which inhibited the ability of Mtb to sense hypoxia by targeting heme embedded in the DosS and DosT sensor kinases[207]. HC102 and HC103 inhibited sensor kinase autophosphorylation and HC104 inhibited DosR response regulator binding of promoter DNA. In addition to inhibitors of the DosRST system, we also identified compounds that inhibited Mtb growth[25]. We further prioritized 163 of the ~1000 HTS hits from the ICCB library using standard prioritization pipeline assays described above, including activity against Mtb in macrophages and low eukaryotic cytotoxicity[25]. However, investigation into the MOA of five structurally distinct prioritized compounds HC2060, HC2091, HC2149, HC2169, and HC2184 indicated that MmpL3 was the target for all five compounds[22,25]. The earliest indicator for the MOA of these compounds was the isolation and sequencing of *mmpL3* mutants resistant to these compounds[25]. We hypothesized that many other hits in the prioritized compounds were also MmpL3 inhibitors and sought a means to directly screen for this target. Towards this goal, we created a whole cell targeted mutant screen that compared the inhibitory effect of all 163 compounds against either WT or an *mmpL3* mutant pool[25]. The *mmpL3* mutant pool was highly specific for MmpL3 inhibitors and insensitive to standard Mtb drugs. The result of this screen identified a total of thirteen MmpL3 inhibitors, 7.4% of the 163-compound library. All thirteen inhibitors were validated as MmpL3 inhibitors based on lipid profiling and results of a competitive binding assay[25].

In addition to the ICCB library, we also conducted a HTS against the MLSMR compound library[207]. From this screen we identified > 1000 Mtb growth inhibitors (independent of DosRST) and several putative DosRST inhibitors. To improve on the results of prioritization pipeline we previously used, we incorporated the *mmpL3* mutant screen into the prioritization pipeline to rapidly identify MmpL3 inhibitors and allow for early assessment of MOA for prioritized hits. By screening the > 1000 compound library against both the *hspX*-GFP reporter strain (wild type (WT) and the mixed *mmpL3* mutant pool, we identified > 15 putative DosRST inhibitors and > 60 novel MmpL3 inhibitors. Inhibitors of both the *hspX*-GFP reporter and MmpL3 included previously described and novel classes of inhibitors. We further tested these compounds using standard

pipeline assays including cytotoxicity and intracellular Mtb growth inhibition testing. The results of this modified prioritization pipeline will allow for parallel lead compound selection for compounds hit in the *hspX*-GFP and MmpL3 screen and further MOA studies for compounds not hit in either screen but are potent, and active in macrophages with low cytotoxicity.

Results:

A High Throughput Screen Identifies Inhibitors of the DosRST Regulon and Mtb Growth

Mtb utilizes the DosS and DosT sensor kinases to sense hypoxia both *in vitro* and *in vivo*. In turn, these sensor kinases phosphorylate the DosR response regulator which allows Mtb to adapt to low oxygen environments, nitric oxide, and carbon monoxide[256-258]. One of the most highly induced genes in the 50 gene DosR regulon is the α-crystalline protein *hspX*[207]. We previously screened the NIH MLSMR compound library of > 300,000 compounds using an *hspX*-GFP reporter that is induced in low oxygen environments[207]. From this screen we identified > 1000 compounds that (1) inhibited *hspX* induction (percent fluorescent inhibition, %FI) > 40% or (2) inhibited Mtb growth (percent growth inhibition, %GI) > 50% relative to DMSO (negative) and rifampicin (RIF, positive) controls. The screen had a Z-score of 0.89 indicating that the screen was of high quality[207].

Cherry pick samples of ~1000 hits were provided for confirmation and follow-up studies. The cherry pick compounds were aliquoted into new plates to generate an 8-point dose response (80 - 0.13 uM, 2.5-fold for 8 concentrations). The initial screen was conducted at a concentration of ~10 μM. Using the original assay conditions, we first conducted a confirmation assay with the dose response diluted cherry picks against the Mtb *hspX*-GFP reporter strain. The results of this screen confirmed 584 out of 1116 (52.3%) compounds could inhibit Mtb growth > 50% at 12.8 μM (Figure 4.1a and 4.2a). Additionally, several compounds inhibited fluorescence induction > 25% with < 40% growth inhibition, indicating that fluorescence inhibition was likely independent of growth inhibition (Figure 4.1a). These compounds included analogs of previously described DosRST inhibitors including two HC106 analogs and artemisinin that were previously demonstrated to interact with the DosS and DosT heme domains (Figure 4.1b and 4.1c)[255]. We also identified HC103a and HC104a which prevent DosS and DosT auto-phosphorylation as well as DosR DNA binding respectively (Figure 4.1d and 4.1e)[207,255]. The identification of known

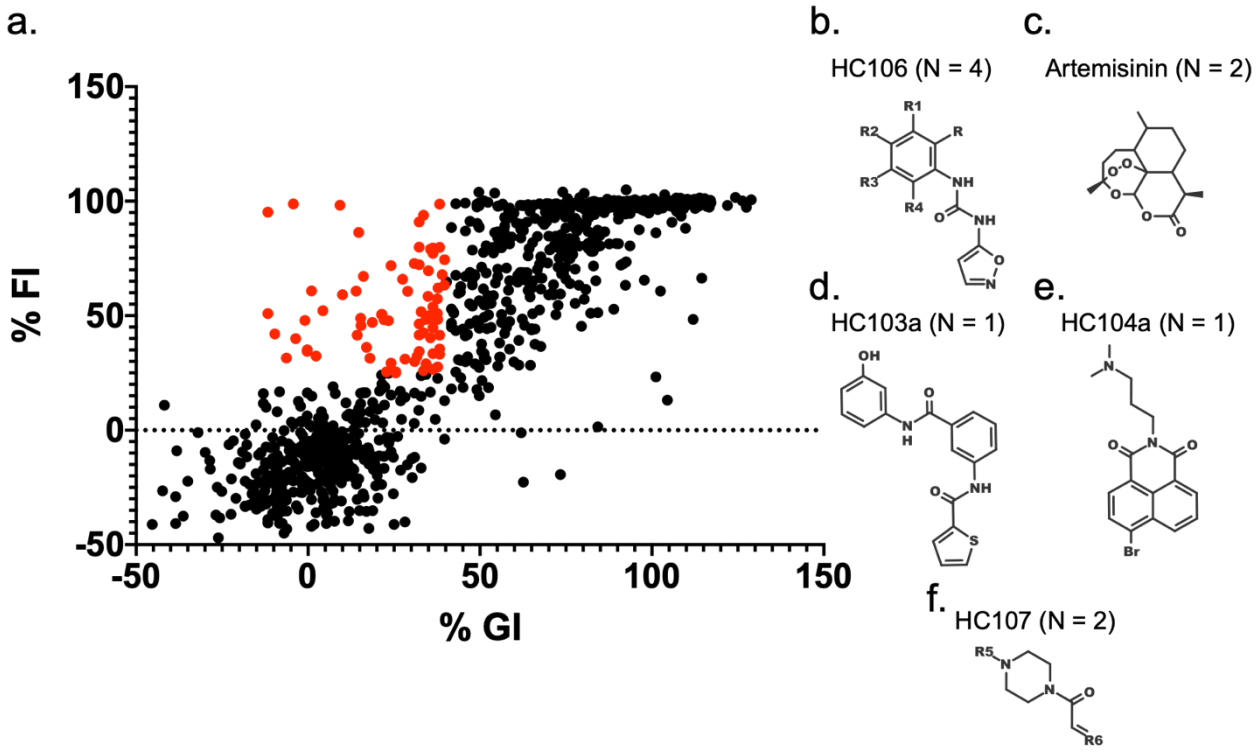

Figure 4.1. A Mtb hspX':GFP reporter strain identifies inhibitors of the DosRST two component system. a) A library of > 1000 compounds were screened against a Mtb DosRST inducible GFP reporter strains. Compounds were screened at 12.8 μM and measured for growth inhibition (OD600, % GI) and fluorescence inhibition (RFI, % FI) relative to DMSO and RIF controls. Red dots identify compounds that inhibited growth ≤ 40% and fluorescence ≥ 25%. b-e) Chemical structures of previously identified DosRST inhibitors. f) The cores structure of a novel diamine based MmpL3 inhibitor (HC107). N represents the number of compounds that share a similar structure for each series.

inhibitors of *hspX* induction suggest that other compounds identified in this assay may interfere with the DosRST signaling pathway; however, it is also possible that these compounds are quenching GFP fluorescence, and the result is an artifact of the screening. Fresh powders of all new hits will need to be purchased and tested in a GFP quenching assay[207]. In addition to these previously described DosRST inhibitors, we also identified novel diamine scaffolds, referred to here as HC107a and HC107b (Figure 4.1f). The high similarity between these two compounds and repeated pattern of higher fluorescence inhibition compared to growth inhibition support that this series warrant further study in GFP quenching assays and genetic and biochemical confirmation assays showing inhibition of DosRST signaling.

HTS Hits Inhibit Intracellular Mtb Growth with Low Cytotoxicity

During pathogenesis, Mtb colonizes and replicates in macrophages. Therefore, assessing the potential for a new inhibitor to inhibit intracellular Mtb growth is an essential test in a prioritization pipeline. However, compounds that inhibit not only Mtb, but also directly kill host macrophages can confound the results of intracellular growth inhibition assays. Therefore, compounds must also be assessed for non-specific macrophage cytotoxicity. To address these concerns, we tested the HTS hits for both cytotoxicity and the ability to inhibit intracellular growth.

To test for cytotoxicity, we treated primary bone marrow derived macrophages with each compound using the same dose range used in the *in vitro* Mtb growth inhibition screen described above. The results of the cytotoxicity screen identified 222 compounds with ≤ 10% cytotoxicity when screened at 12.8 μM that were active against Mtb *in vitro* (Figure 4.2a). Following this assay we next screened the compounds for the ability to inhibit intracellular Mtb growth using a firefly luciferase reporter strain[210]. This reporter strain uses an ATP dependent luciferase that requires the addition of an exogenous luciferin to generate luminescence. This system can be used as a measure for cell death, as ATP is rapidly hydrolyzed following cell death[210]. Of the 222 compounds that had ≤ 10% cytotoxicity, 213 were able to inhibit intracellular Mtb growth $\underline{\geq}$ 25% relative to DMSO and RIF controls when screened at 12.8 μM (Figure 4.2a). These 213 compounds had selective indexes ranging from 1 to > 800 (Table A.4.1)

Following cytotoxicity and intracellular inhibition assays, we performed a chemical structure cluster analysis using DataWarrior software of the 222 compounds that made our assay cutoffs (Figure 4.2b)[259]. The cluster analysis identified compounds with similar structures that clustered tightly together (Figure 4.2b). Manual review of these tight clusters identified INH and thiacetazone (TAC) scaffolds as two of the most prominent scaffolds. To identify compounds with these core structures we performed a scaffold search for the core structures of INH and TAC (Figure 4.2c and 4.2d). This search identified 47 INH and 35 TAC analogs in the 222 compound cut-off hits. INH and TAC are inhibitors of the FAS-II pathway targeting InhA and HadAB

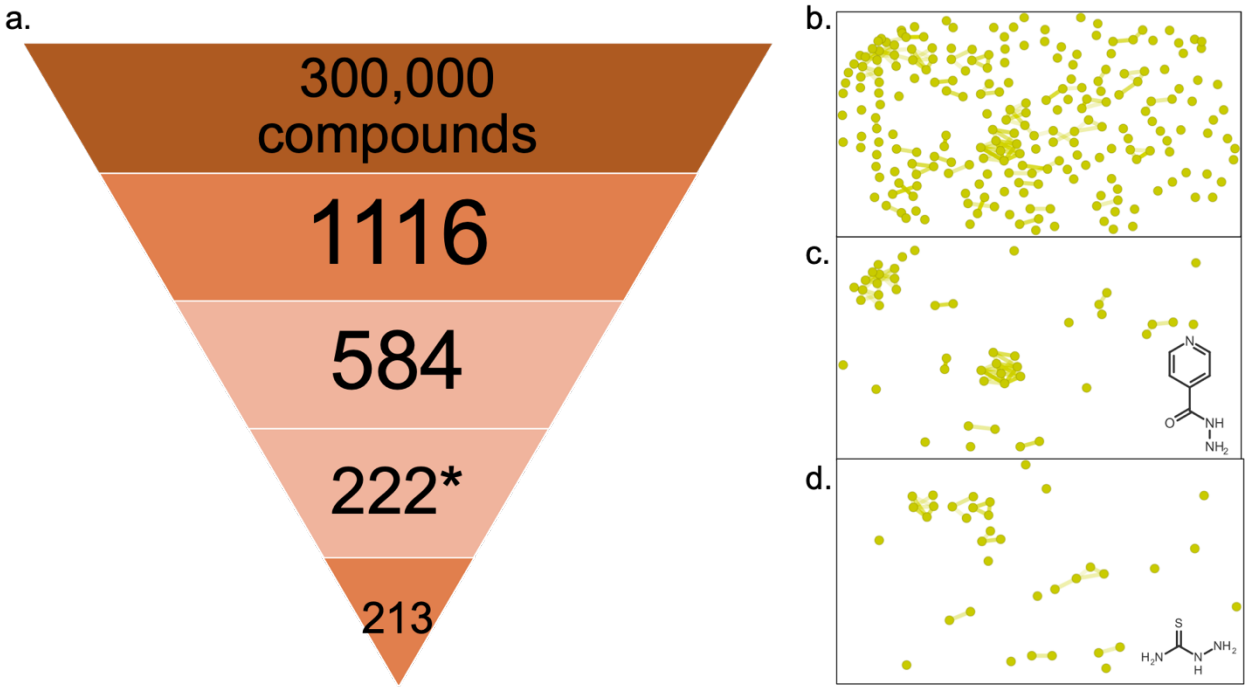

Figure 4.2. Secondary screening assays identify *in vitro* and intracellular Mtb growth inhibitors with low cytotoxicity. The 584 compounds that had ≥ 50% in vitro Mtb growth inhibition at 12.8 μM identified in Figure 4.1a, were screened for cytotoxicity and intracellular Mtb growth inhibition. Compounds were then screened for cytotoxicity against primary bone marrow derived macrophages and measured for luminescence relative to 0.13 μM compound and triton x-100 treated controls. Compounds confirmed for low cytotoxicity had ≤ 10% cytotoxicity. Compounds were then screened for potential to inhibit Mtb growth inside of infected macrophages. Compounds were confirmed for activity if they could inhibit Mtb growth ≥ 25% relative to RIF and 0.13 μM controls. The final 213 compounds were characterized as having ≥ 50% in vitro growth inhibition, ≤ 10% cytotoxicity, and ≥ 25% intracellular Mtb growth inhibition at 12.8 μM. b-d) Chemical similarity charts of the 213 compounds identified that made screening cut offs (a). Compounds were clustered in DataWarrior and clustered by SkelSpheres[259]. Lines connect structurally similar compounds. b) Chemical similarity chart of all 213 compounds identified in the screening assays. c) Scaffold search results for compounds containing INH as part of their structure. d) Scaffold search results for compounds containing part of the TAC scaffold as part of their structure. c and d) Chemical structures used in the scaffold search are illustrated in the bottom right corner of c and d.

respectively[89,115,260]. FAS-II and other mycolic acid biosynthesis pathways are often hit in whole cell screens[261] as these metabolic pathways are required for synthesis of the essential mycomembrane.

Of note, due to an unexplained technical issue, we observed cell death in roughly one third of the macrophages tested that was solely based on the position on one edge of the plate.

These compounds were not included in the 222 compounds that made our ≤ 10% cytotoxicity cut off and their cytotoxicity is to be determined.

A Targeted *mmpL3* Mutant Screen Identifies More than 100 MmpL3 Inhibitor Candidates

Using standard secondary screening assays, we identified a number of compounds that inhibited Mtb growth both *in vitro* and in infected macrophages with low cytotoxicity. However, these hits were heavily biased towards mycolic acid biosynthesis inhibitors including INH and TAC (Figure 4.2b-d). Similar chemical scaffolds were included in the 163 compounds from the ICCB library that were prioritized for further study by our lab (unpublished data)[25].

We previously described the identification of thirteen MmpL3 inhibitors that were included in the 163-compound library[25]. MmpL3 is a mycolic acid flippase[48] and a prioritized target for Mtb drug development due to its essential nature[72]. MmpL3 inhibitors have been identified from a number of HTS including ones that utilized similar secondary screening assays to the ones reported here[20,23,25,26,31,36]. We hypothesized that the 1116 cherry picks from the MLSMR library included MmpL3 inhibitors. However, MmpL3 inhibitors include a large number of structurally unique compounds (Figure A.4.1), making screening for MmpL3 inhibitors using a chemical scaffold search difficult. Further, using such a structure search method would remove novel MmpL3 inhibitors with unique scaffolds. To overcome this, we utilized a whole cell targeted mutant phenotypic screen which directly compared the inhibitory effects of compounds against WT Mtb and an *mmpL3* mixed mutant pool[25]. The twenty-four *mmpL3* mutants, encoding non-synonymous mutations (Table A.4.1), are resistant to MmpL3 inhibitors but not against non-MmpL3 inhibitors rendering the assay largely insensitive to inhibitors of other metabolic pathways[25]. Using the same methods as the ones used for the WT (*hspX*-GFP) screen, we screened the 1116 compounds against the *mmpL3* mutant pool. For our initial analysis, we compared the growth inhibition of the *mmpL3* mutant pool to WT (*hspX-GFP*) Mtb at 12.8 μM using similar cutoffs to the ones previously

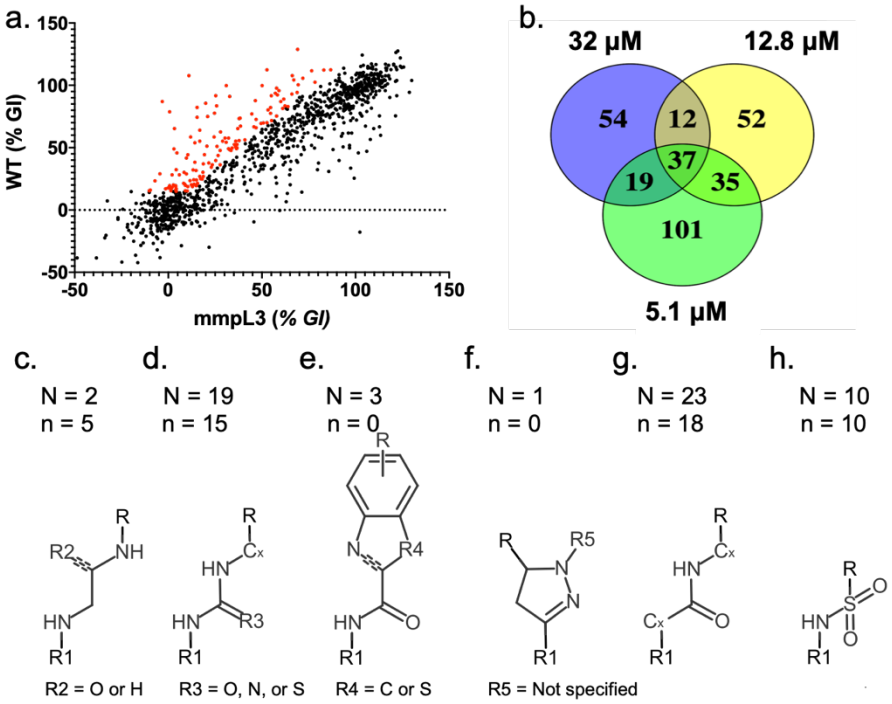

Figure 4.3. A targeted phenotypic mutant screen identifies MmpL3 inhibitor candidates. a) Scatter plot of compounds screened against the WT Mtb (Figure 4.1a) counter screened against a mmpL3 mix mutant population at 12.8 µM. Data points highlighted in red had ≥ 15% growth inhibition (% GI) in the WT background and ≥ 1.3 fold-lower activity in the mmpL3 mutant background. b) Overlap of compounds hit in the mmpL3 screen tested at three concentrations 5.1 µM, 12.8 µM, and 32 µM. The same cut-offs were applied as described in a. c – h) Common core chemical scaffolds identified in the overlap screen (b). Chemical scaffolds include diamine/acetamide (c), urea/thiourea/guanidine (d), indole/thiazole (e), pyrazole (f), amide (g), and sulfonamide (h) based compounds. N – represents the number compounds for each scaffold identified in the overlap screen (b), n – represents the number of compounds for each scaffold identified at 12.8 µM only (a). c-h) R indicates undisclosed lipophilic groups. R1 indicates nondisclosed hydrophobic groups. Cx represents nondisclosed chain lengths. c) R2 represents either a hydrogen (single bond) or a carbonyl group (double bond) depending on if the compound is a diamine or an acetamide. d) R3 represents either a O, S, or N depending on if the compound is a urea, thiourea, or a guanidine. e) R4 represents either a C or a S depending on the exact structure of the compound. R5 indicates an unspecified chemical group.

described[25]. This first look identified 136 compounds that inhibited Mtb growth > 15% in the WT background but 1.3 fold lower in the *mmpL3* mutant mix (Figure 4.3a). The large number of hits in this *mmpL3* screen included known Mtb drugs that inhibit pathways other than MmpL3 and were likely false positives. This was predicted as the original screen of the 163 compounds initially identified thirty-two compounds including nineteen false positives when screened at a single (20 µM) concentration[25]. To reduce the number of false positives, we applied the same 15% and 1.3 fold reduced activity cutoffs to compounds screened at 5.1 µM and 32 µM and selected

compounds that made our minimum cutoffs at $\geq$ 2 concentrations (Figure 4.3b). This resulted in 103 compounds as prioritized MmpL3 inhibitor hits (33% of the total 310 combined hits) and review of the compound structures supports that the number of false positives was greatly reduced. This indicated that the remaining compounds may be true MmpL3 inhibitors; however, the possibility of false positives still remain and follow-up studies using fresh powders will need to be conducted.

MmpL3 Inhibitor Candidates Share Common Core Structures

MmpL3 inhibitors have very diverse structures, however many have shared core structures. These include diamines/acetamides, ureas/guanidines, pyroles/pyrazoles, indole/imidazole/thiazole, amides, and compounds that do not share a common core structure (Figure A.4.1). These core structures are typically flanked by a lipophilic group (i.e. substituted benzene) and a hydrophobic group (*i.e.* adamantyl or cyclohexyl) (Figure A.4.1). To further characterize the new putative MmpL3 inhibitors, we examined these characteristics by manually reviewing each of the 103 putative MmpL3 inhibitors. This resulted in 68 compounds identified as higher confidence hits (66% of 103 hits). These compounds could be separated into those with similarity to previously described chemical scaffolds based on their core chemical groups (Figure A.4.1, Table A.4.2). The first group included two diamines / acetamides similar to previously described SQ109[34] and E11[31] (Figure 4.3c). The second group included nineteen urea / guanidine-based compounds similar to AU1235[29] and CCI7967[36], as well as novel thioureas (Figure 4.3d). The third chemical class included three indole/thiazole-based inhibitors similar to NITD-304[27], CRS400226[157], and HC2184[25]. The fourth class identified included a single pyrazole-based inhibitor similar to Rimonabant[52] (Figure 4.3e). This was surprising as we previously demonstrated that our *mmpL3* mutant pool was equally sensitive to Rimonabant compared to WT control[25]. One possible explanation for this may be due to the extremely low activity Rimonabant demonstrated against Mtb in our assay (EC_{50} = ~50 μM)[25,52]. This concentration was near the

upper limit of the concentration range tested in our previous study (80 μM) which may have obscured a resistance phenotype[25]. Alternatively, specific structural differences between Rimonabant and the compound identified here may also explain why this pyrazole was identified in this screen. To determine if we missed any additional pyrole/pyrazole based MmpL3 inhibitors, we performed an *in silico* search for compounds that were structurally similar to previously described inhibitors of this chemical class including BM212[30], Rimonabant[52], and THPP[24,35] (Figure A.4.2a-c). However, this did not identify any compounds with high structure similarity to the reference compounds suggesting our screen did not miss any additional pyrole/pyrazole-based inhibitors. The fifth class of compounds included twenty-one amide-based compounds similar to HC2091[22] (Figure 4.3f). Finally, we also identified a novel class of putative MmpL3 inhibitors that included a sulfonamide core (Figure 4.3g). This core structure has not been previously described in the literature; however, these compounds did share features typically observed in a MmpL3 inhibitors (Figure A.4.1). In addition to these major classes of compounds we also identified compounds with scaffolds similar to previously described MmpL3 inhibitors including DA-5[34], Spiro[35], HC2032 and HC2134[25] (Table A.4.2).

Based on the similarity of the proposed MmpL3 inhibitors identified in the screen to ones previously described in the literature, as well as the repeated identification of novel sulfonamides, we believe that the 103 compounds identified in this screen are largely composed of MmpL3 inhibitors. However, we do note that four compounds that made all of our cuts offs had high similarity to the HadAB inhibitor TAC (Table A.4.2)[115]. Additionally, thirty-five compounds identified in this list of hits did not share structure similarity with known MmpL3 inhibitors. It may be possible that additional false positives are among these compounds (Table A.4.2) or these are new classes of MmpL3 inhibitors. Therefore, additional conformation assays will be required to determine if these compounds target MmpL3.

Discussion:

We previously conducted a HTS to identify inhibitors of the DosRST regulatory pathway involved in the adaptation of Mtb into a metabolically quiescent state. Here we report on secondary screening results that identified previously described DosRST inhibitors and potentially several other potential new DosRST inhibitors. Follow-up studies with fresh powders will need to be conducted to confirm the activity of these compounds. In the same HTS we also identified > 1000 compounds that inhibited Mtb growth in a DosRST independent manner. Using standard secondary assays, we confirmed the *in vitro* inhibition of Mtb for > 500 compounds, of which nearly half (213) were able to inhibit Mtb growth in infected macrophages without inducing high levels of cytotoxicity against mammalian cells. Included in these growth inhibitors were structural analogs of known Mtb drugs with a metabolic bias towards FAS-II inhibition. We also identified compounds with structures similar to previously described MmpL3 inhibitors. Using a targeted mutant screen, we identified > 100 compounds with lower activity in *mmpL3* mutant pool compared to WT Mtb that is resistant to MmpL3 inhibitors. These compounds included previously described and novel chemical classes of MmpL3 inhibitors including sulfonamide-based compounds. Iterative application of this phenotypic screening system using other Mtb resistant mutants may further identify inhibitors of other metabolic pathways.

The DosRST two component system helps Mtb to sense and adapt to several stresses including hypoxia and nitric oxide[256-258,262]. These environmental stresses trigger Mtb to alters its metabolism and reroute electron flow away from respiration into lipid synthesis[262]. During these states Mtb accumulates lipids such as triacyl glycerol (TAG)[171]. Inhibition of DosRST results in reduced TAG accumulation during the adaptation to states of quiescence[207,255]. Further, disruption of DosRST signaling results in decreased viability when cultured in hypoxic environments[207,255]. Future studies will seek to determine if treatment of Mtb with the novel inhibitors identified here results in these two phenotypes. Further, the inhibition of DosRST signaling can be occur through at several signaling targets including DosS/T heme, sensor kinase function and DNA binding of

DosR to promotor regions[207,255]. The new analogs of HC106 likely function through a similar mechanism of targeting DosS/T heme. GFP quenching assays, followed by specific MOA studies will need to be conducted to determine if HC107 series is a true DosRST inhibitor.

MmpL3 inhibitors consist of structurally diverse series of compounds and novel structures are regularly reported. This makes it difficult to identify MmpL3 inhibitors through *in silico* screening methods. Here we utilized a phenotypic *mmpL3* mutant screen to identify inhibitors of the common target MmpL3. Using this screening method and focusing on compounds with characteristics of previously described MmpL3 inhibitors, we identified sixty-eight compounds that likely target MmpL3; however, additional studies will be required to validate this mechanism of action. MmpL3 is a mycolic acid flippase and the sole transporter of the essential lipid trehalose monomycolate (TMM). Mycobacteria treated with MmpL3 inhibitors accumulate TMM and have reduced levels of trehalose dimycolate (TDM) which is formed from TMM in the mycomembrane[29]. Several studies have looked for relative abundance of these lipids in treated vs untreated cells and serves as a good benchmark for MmpL3 inhibition[22,25,29,31,34,154,176]. However, this method can be confounded by inhibitors that collapse the proton motive force (PMF) which powers MmpL3[49,117]. To this end, a fluorescent probe displacement assay was recently developed that is insensitive to PMF uncoupling[49]. This method along with lipid profiling could be used to further validate MmpL3 as the target of inhibitors identified in this screen.

Of the 213 compounds identified using standard prioritization assays, only seventeen were identified in the MmpL3 screen. Of the remaining 196 compounds, eighty-two strongly resembled INH and TAC leaving 114 compounds as candidates for confirmation and follow up MOA studies. These 114 compounds included additional scaffolds of known antibiotics including seven fluroquinolones, seven cephalosporins, four tetracyclines, and clofazimine. The remaining ninety-five compounds did not have chemical scaffolds of known antibiotics, indicating that they were potentially novel Mtb growth inhibitors. Included in these ninety-five compounds, were four classes of compounds (descriptors not disclosed). Each class of compound had 3-4 similarly

structured core chemical classes and clustered together in the compound clustering analysis. The similarity of the compounds within each class indicates that these classes are true hits and supports follow up studies to identify the MOA. The remaining compounds included unique structures and should also be considered for MOA studies.

The approach used here identified a large number of compounds that inhibit Mtb growth in both MmpL3-dependent and independent manners. The cytotoxicity profiles of many of the MmpL3 inhibitors were above our designated cut off of ≤ 10% when treated at 12.8 μM. Using such cut offs would have limited the number of MmpL3 inhibitors in lead compound follow up studies to only eighteen of the 103 compounds identified. By screening for MmpL3 inhibitors at this secondary screening step, in parallel to traditional steps, we increased the number of possible MmpL3 inhibitors > 5-fold. While the cytotoxicity data suggests there may be limits to their therapeutic potential, studying these additional inhibitors may broaden our understanding of protein-inhibitor interactions. Further, utilization of this mutant screening approach with other resistant mutant strains may result in similar insights into inhibitors of other metabolic pathways. Future experiments can include parallel studies lead compounds identified using traditional pipeline assays and targeted mutant screens for the advancement of Mtb drug development.

Methods:

Bacterial Strains and Media Conditions

Bacterial strains were cultured in T150 standing flasks containing 100 mL of 7H9 OADC and supplemented with glycerol and tween-80 buffered to pH 7.0 with 100 mM MOPS. Cultures were incubated at 37°C with 5.0% CO_2.

WT *in vitro* activity and DosRST Reporter Inhibition Screening

The methods used for screening are as previously reported[207,255]. Briefly, cherry-pick hits from the NIH MLSMR library were diluted 2.5-fold for 8 concentration points ranging from 80 – 0.13 µM. Mtb CDC1551 *hspX*'::GFP reporter strain was cultured to mid-log phase (OD_{600} ~0.6) in 7H9 medium. Cells were aliquoted into 384-well plates at an initial inoculum of OD_{600} = 0.05 and treated with 0.5 µL of each compound along with DMSO and rifampicin controls. Plates were placed into resealable bags with a wet paper towel and incubated for six days at 37°C with 5% CO_2. Plates were then read on a Perkin Elmer plate reader for both OD_{600} and GFP fluorescence. The percent growth inhibition and percent fluorescence inhibition were both calculated relative to controls.

Cytotoxicity

Primary bone marrow macrophages were obtained and cultured as previously described[211]. Plates were seeded with macrophages in 384-well opaque plates. Macrophages were treated via dose response as described for Mtb. Macrophages were then incubated at 37°C and 5% CO_2 in vented resealable bags with a wet paper towel. Following six days of treatment, cell viability was assessed using the cell titer glow assay (Promega) and percent cytotoxicity was calculated relative to DMSO and 4% triton x-100 controls.

Intracellular Mtb Growth Inhibition

Primary bone marrow derived macrophages were obtained and plated into 384-well opaque plates as previously described[211]. Twenty-four hours after plating, macrophages were infected with a Mtb CDC1551 strain expressing fire fly luciferase at an MOI of 1[211]. Macrophages were infected for 1 hour at 37°C prior to treatment. Following treatment infected macrophage plates were incubated at 37°C and 5% CO_2 in vented resealable bags with a wet paper towel. Following six days of treatment, infected macrophages were assessed for intracellular Mtb growth using the bright glow luciferin assay (Promega). Luminescence was measured on a Perkin Elmer plate reader. Due to an edge effect, DMSO treated cells could not be used a negative-controls, and percent intracellular growth was instead measured relative to rifampicin and the average bacterial growth of Mtb treated with the lowest concentrations tested as the negative control.

MmpL3 Inhibitor Screen

MmpL3 inhibitors were screened using previously described methods[25]. Briefly, pooled culture of twenty-four unique *mmpL3* mutants encoding nonsynonymous resistance mutations were cultured to mid-log phase in 7H9 medium. Cultures were aliquoted at a starting cell density of 0.05 OD_{600} in 384 well plates and treated as described above for WT Mtb. The mixed *mmpL3* mutant plates were incubated in resealable bags with a wet paper towel and incubated for six days at 37°C with 5% CO_2. Plates were then read on a Perkin Elmer plate reader for both OD_{600}. The percent growth inhibition to rifampicin and DMSO controls.

Compound Clustering in DataWarrior

SDF files for each compound were provided by the NIH. Compounds were analyzed for structure similarity using the SkelSpheres descriptor calculated in DataWarrior using default settings.

CHAPTER 5: A Genetic Screen for *Mycobacterium smegmatis* Mutants Tolerant to Killing by Sodium Citrate Defines a Role for Magnesium Import and Osmotic Stress in Cell Death

The following authors contributed to the development of this project. John T. Williams, Jacob Baker, Huiqing Zheng, Shelby J. Dechow, Jared Fallon, Haleigh N. Gilliland, Andrew Olive, and Robert B. Abramovitch.

The following individuals contributed to the work in this paper: Mtb viability experiments were performed by JB and JTW. Msm viability assays were performed by JB and JTW. *M. abscessus* viability assay was carried out by HNG and AO. Cell lysis assays were performed by JTW. RNAseq was performed by JTW. Cation supplementation was performed by SJD. Transposon mutagenesis was performed by JB. Complementation experiments were performed by HZ and SJD. Mag-Fura2 (AM) fluorophore assay was performed by JTW. Osmotic protection assays were performed by JTW and JF.

Abstract:

Mycobacteria can colonize environments where the availability of metal ions is limited. Biological or inorganic chelators play an important role in limiting metal availability and we developed a model to examine *M. smegmatis* survival in the presence of the chelator sodium citrate. We observed that instead of restricting *M. smegmatis* growth, concentrated sodium citrate killed *M. smegmatis.* RNA-seq analysis during sodium citrate treatment revealed transcriptional signatures of metal starvation and osmotic stress. A forward genetic transposon screen was conducted to examine why sodium citrate was lethal, and several sodium citrate tolerant mutants were isolated. Based on the identity of three mutants, *mgtE*, *treZ*, and *fadD6,* we propose a dual stress model, where chelation of metals from the cell envelope and osmotic stress drive killing by sodium citrate. This sodium citrate tolerance screen identified several other genes with no known function and this model will serve as a basis to define their function.

Introduction:

In order to maintain cell viability, bacteria must maintain cation homeostasis. Metal cations play crucial roles in every major biological process including protein structure and function, DNA/RNA polymerization[263], and cell envelope stability[264-271]. To this end, bacteria include a variety of metal import and export systems to maintain stable cytoplasmic cation concentrations. The most abundant divalent cation present in bacteria is Mg^{2+} which plays a major role in cell envelope stability[264-271] and it is estimated > 30% of Mg^{2+} is stored in the cell wall of *E. coli*[267]. In both Gram positive and Gram negative bacteria, Mg^{2+} serves as one of the major counter ions to offset negative charges of cell envelope components such as (wall) teichoic acids ((W)TA)[269-271], lipopolysaccharides (LPS)[265-267] and peptidoglycan[270,271]. Mycobacteria contain neither (W)TA nor LPS, but do contain peptidoglycan[268] and phospho-lipids such as phosphatidylinositol mannosides (PIMs) which contain negatively charged phosphate residues[272]. However, the Mg^{2+} content of the mycobacteria cell envelope is not well characterized and methods for measuring cation concentrations in live bacterial cells still remain elusive.

In addition to metal homeostasis, bacteria must also maintain osmotic homeostasis to maintain cell shape and integrity. In conditions with high environmental osmolytes, such as sodium, bacteria will respond using two possible strategies. The first involves the import of environmental salts to counter osmotic pressures[273]. The second strategy is to accumulate non-ionic compatible solutes, such as ectoine or betaine, in the cytoplasm[273,274]. Mycobacteria use the latter of the two strategies and either synthesize ectoine[275] or import host derived betaine into the cytoplasm to offset osmotic pressures[276]. Ectoine biosynthesis in the environmental model mycobacterium species *M. smegmatis* (Msm) allows for adaptation to high saline environments[275]. However, the genes required for this (*ectA*-*ectC*, *thpD*) are not conserved in all mycobacteria. The pathogenic species *M. tuberculosis* (Mtb), does not encode genes for the ectoine biosynthesis[43], and relies on the import of host derived betaine/glycine through the ABC transporter ProXVWZ[276] to adapt to host induced osmotic pressure[277]. This import system is regulated by the Ser/Thr

kinase PknD and the anti-anti-sigma factor OprA (*Rv0516c*) which responds to high saline[278]. Mycobacteria lacking these osmotic stress adaptation pathways are reduced for growth[275,276,278] and pathogenicity[276,278] in high saline and intracellular infection models.

We previously reported on the metabolic adaptation of Mtb to acidic pH in minimal medium supplemented with different carbon sources. In these studies, Mtb enters into a state of non-replicating persistence when cultured in acidic medium supplemented with carbon sources such as glycerol but could grow in the presence of carbon sources that feed into the anaplerotic node[222,279]. To further study this system, we attempted to recapitulate this phenotype in the rapidly growing mycobacterium model organism Msm. However, early attempts at recreating this phenotype indicated that Msm was less sensitive to acidic (pH 5.7) environments than Mtb. Therefore, we lowered the pH further using sodium citrate (100 mM) buffered medium. However, this induced a lethal phenotype in Msm that was more pronounced at neutral pH (pH 7.0) conditions and dependent on carbon supplementation. Transcriptional profiling indicated that Msm was responding to chelation and osmotic stress in sodium citrate medium. However, the relative contributions of these or other stresses to killing of Msm was unknown. Given a strong phenotype for selection, we performed a forward genetic transposon mutagenesis screen for mutants that tolerate killing by sodium citrate. The screen identified sodium citrate tolerant mutants through disruption of *mgtE*, *fadD6, treZ*, and several other seemingly unrelated genes. A cell permeable Mg^{2+}/Ca^{2+} fluorophore indicated that cell viability rescue following cation supplementation was not due to cation import into the cytoplasm, suggesting that citrate chelated cell envelope cations. Additionally, compatible solute supplementation led to cell viability rescue. Based on these observations, we propose a dual stress model in which sodium citrate results in chelation of magnesium and calcium from the cell envelope and osmotic stress, which together cause cell lysis and death. This dual stress model will serve as the basis to define the function of other mutants in genes that promote citrate tolerance but have no known function.

Results:

Concentrated Citrate Kills *M. smegmatis*

Previous studies into the metabolic adaptation of Mtb to acidic environments found that *M. tuberculosis* (Mtb) enters into a state of quiescence when cultured in minimal medium (MMAT) buffered to pH 5.7 and provided specific sole carbon sources[222,279]. This phenotype is genetically regulated and is dependent on both pH and carbon source availability[222,279]. When cultured in MMAT at neutral pH (7.0) Mtb can grow on carbon sources such as glucose and glycerol (Figure A.5.1a)[222,279]. However, at acidic pH, Mtb will slow its metabolism and enter into a state of non-replicating quiescence (Figure A.5.1b)[279]. This process can be reversed through supplementation with "permissive" carbon sources such as acetate or pyruvate[279]. However, the slow doubling time of Mtb acts as a limiting factor for studying this phenotype. To overcome this limitation, we sought to recapitulate this phenotype in the rapidly growing mycobacterium species Msm. However, we found no significant difference in growth of Msm cultured in minimal medium buffered to neutral (100 mM MOPS, pH 7.0) or acidic pH (100 mM MES, pH 5.7) (Figure 5.1). This finding is consistent with the prior findings[279,280], where Msm is more tolerant to acidic pH than Mtb[280280] and we hypothesized Msm may require a more acidic environment to induce growth arrest. To achieve this, we buffered minimal medium with 100 mM sodium citrate (**SC**) in a pH range from pH 7.0 to pH 5.0. Counter to our hypothesis, in this medium, we observed that the growth of Msm was dramatically reduced when the pH approached neutral rather than acidic pH (Figure A.5.1c). Further investigation indicated that SC medium led to decreased viability of Msm at both pH 5.7 and 7.0, but was more pronounced at pH 7.0 (Figure 5.1). This phenotype was not observed in SC medium lacking a carbon source (*i.e.* glycerol), suggesting active replication was required (Figure A.5.1d). This phenotype was not observed in Mtb, where viability was not affected by sodium citrate at either neutral or acidic pH (Figure A.5.1a and A.5.1b). In contrast to Msm, Mtb growth was slightly reduced at neutral pH when supplemented with glycerol, and fully prevented when supplemented with glucose

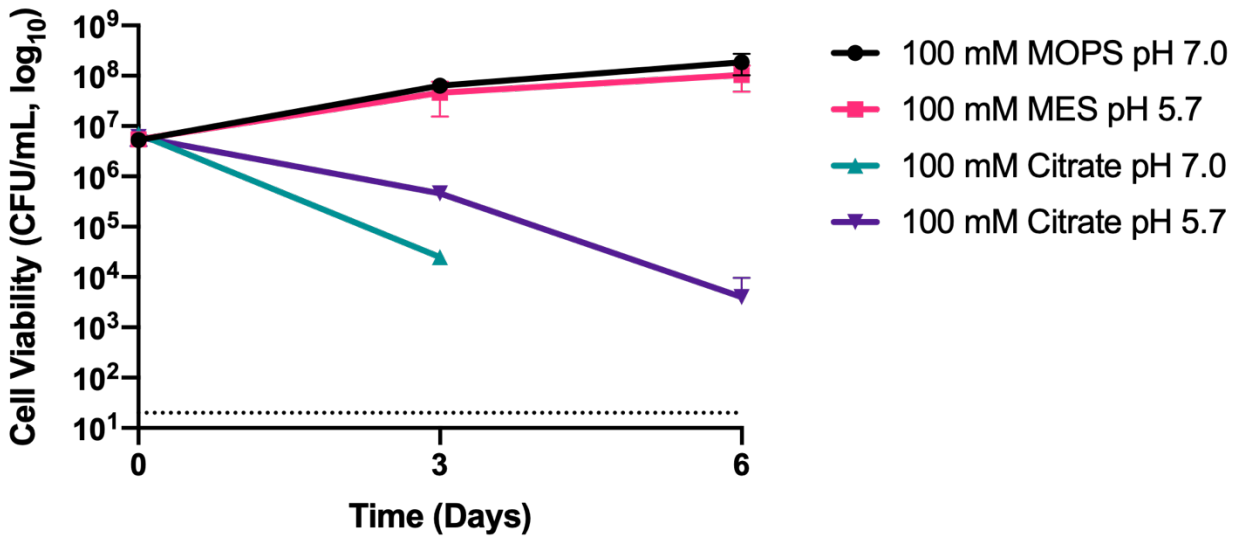

Figure 5.1. Sodium citrate kills *M. smegmatis*. *M. smegmatis* was cultured in MMAT minimal medium supplemented with 10 mM glycerol and buffered with 100 mM MOPS (pH 7.0), MES (pH 5.7), or sodium citrate (pH 5.7 or 7.0) and enumerated for CFU/mL on LB agar. For *M. smegmatis* cultured in 100 mM sodium citrate (pH 7.0) no colonies were isolated from day six samples. The figure represents results typical of these experiments. Experiments were conducted in triplicate and repeated at least twice. The dotted line indicates the limit of detection (20 CFU/mL).

(Figure A.5.1a). We also tested this phenotype in the related rapidly growing mycobacterial species *M. abscessus*, which appeared to be completely insensitive to SC medium compared to MOPS medium (Figure A.5.1e). We found this species-specific phenotype interesting and decided to investigate it believing that it could shed light on the physiology of the model organism *M. smegmatis*.

Citrate Induces Cell Lysis in Msm

Citrate is a carbon source for many bacteria and acts as an intermediate of the TCA cycle. However, several studies have indicated that Msm does not import citrate in conditions similar to the ones reported here[281,282], suggesting that citrate was inducing stress on the cell envelope. A previous study by Nagaoka and colleagues demonstrated that sodium citrate induced cell swelling and burst in *Streptococcus pneumoniae*[283]. Consistent with these observations, we observed a decrease in the opacity of the bacteria grown in SC cultures during the cell viability assays

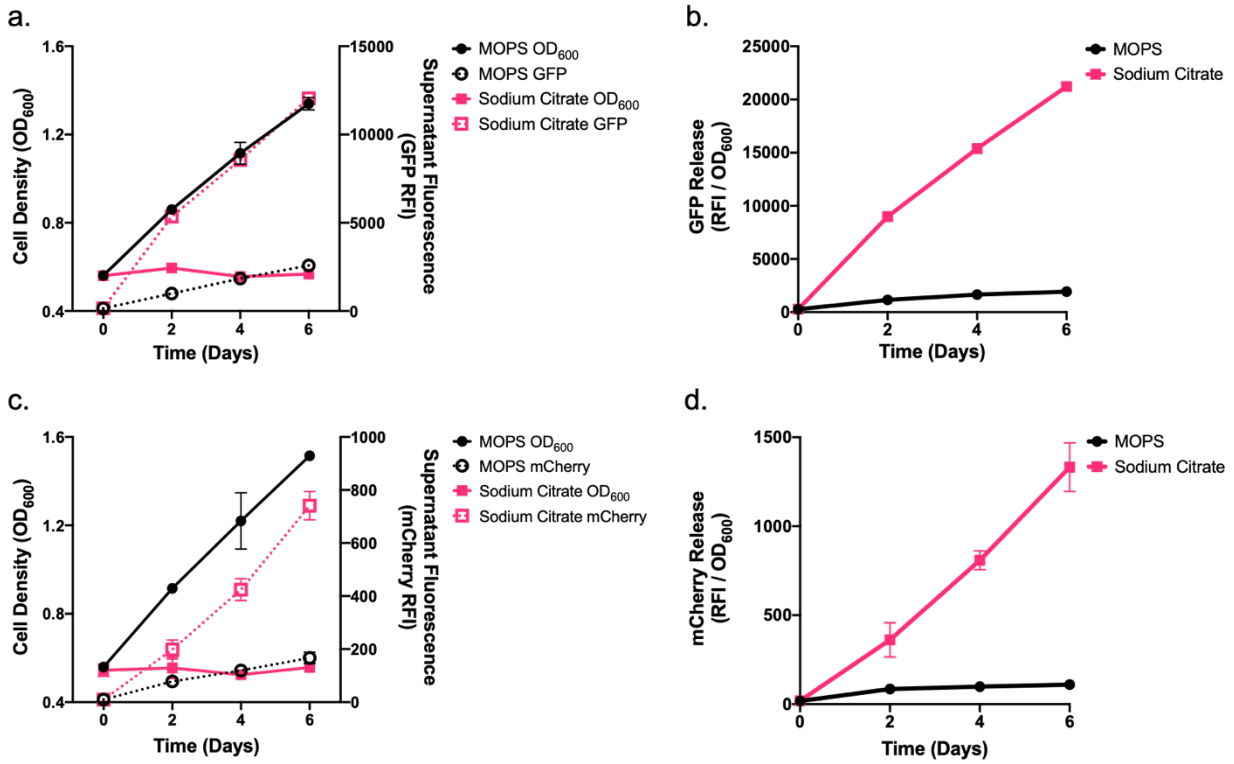

Figure 5.2. Sodium citrate induces *M. smegmatis* cell lysis. *M. smegmatis* strains expressing either GFP of mCherry were cultured in MOPS or sodium citrate buffered medium supplemented with 10 mM glycerol. a and c) At indicated time points 1 mL samples were taken and measured for OD_{600} (solid lines). a and c) Culture filtrates were then measured for fluorescence (GFP (Ex 488 nm / Em 515 nm) or mCherry (Ex 587 nm / Em 610 nm)) (dotted lines). b and d) Relative RFI/OD_{600} measurements were made for each time point. The experiment was conducted in biological duplicate and fluorescent samples were measured in technical triplicate per sample. Data points indicate the mean of each sample. Statistics comparing the ratio of RFI/OD between MOPS and sodium citrate buffered samples were calculated using a two-way ANOVA. Starting on day two, cell lysis measurements were statistically different between MOPS and sodium citrate cultures ($p < 0.0001$) in both assays.

described above indicating that cell lysis may have been occurring. To test for cell lysis, we used a combined optical density (OD_{600}) and fluorescent protein release assay based on work by Sharma and colleagues[284]. For this assay, we cultured Msm expressing either GFP or mCherry in SC or MOPS medium. We hypothesized that cultures undergoing cell lysis would release fluorescent protein into the supernatant[284]. Consistent with this hypothesis, the fluorescence of culture filtrates from SC cultured bacteria increased over time (Figure 5.2a and 5.2c). This increase in fluorescence was in the absence of bacterial growth as the OD_{600} of Msm did not significantly change during the experiment (Figure 5.2a and 5.2c). By comparison, the OD_{600} of

MOPS cultured Msm increased dramatically over time but the filtrate fluorescence only increased marginally (Figure 5.2a and 5.2c) and was likely due to spontaneous cell lysis during cell replication. The differences in the amount of cell lysis was highlighted by the filtrate florescence to cell density ratio (RFI / OD_{600}) in SC compared to the MOPS culture (Figure 5.2b and 5.2d) which were significantly different ($p < 0.0001$) by day two post inoculation. The results of this assay support that SC induces cell envelope stress resulting in cell lysis.

Citrate Induces Chelation and Osmotic Stress

Based on the results of the cell viability and lysis assays, we understood that citrate induced cell death through cell lysis and was dependent on a carbon source; however, the specific mechanisms driving killing remained unclear. To gain a better understanding of what stress Msm sensed and was responding to, we used RNAseq-based transcriptional profiling of Msm cultured in either MOPS or SC buffered minimal medium. To ensure that transcriptional profiles were not obscured by genes associated with cell death, we isolated RNA samples at an early time point (3 hours). RNA was then sequenced by Illumina based high throughput sequencing and analyzed using the SPARTA software package[285]. The resulting transcriptional profiles (Figure 5.3a and 5.3b, Table A.5.1) identified 72 and 54 genes up- or down-regulated in the citrate profile compared to MOPS control (> 2 fold, $q < 0.05$, Figure 5.3a and 5.3b, Table A.5.1). In addition to genes involved in various metabolic pathways, we identified the signature profile of iron starvation including the siderophores exochelin[286-288] and mycobactin[288-292] and their biosynthesis and transport[288,293,294] (*MSEMG_0014*, *MSMEG_0018-MSMEG_0022*, *MSMEG_2130-MSMEG_2131*, *MSMEG_2511, MSMEG_4509-MSMEG4516, MSMEG_4524,* and *MSEG_4383*) (Figure 5.3a and 5.3b). We also identified genes required for the type VII ESX-3 secretion system (*MSMEG_0615-MSMEG_0626*) as upregulated > 2 fold (Figure 3a and 3b). ESX-3 is required for siderophore import[295-297] and is involved in iron and zinc homeostasis[298,299]. In addition to siderophore based iron acquisition, mycobacteria can also import free iron through the IrtAB

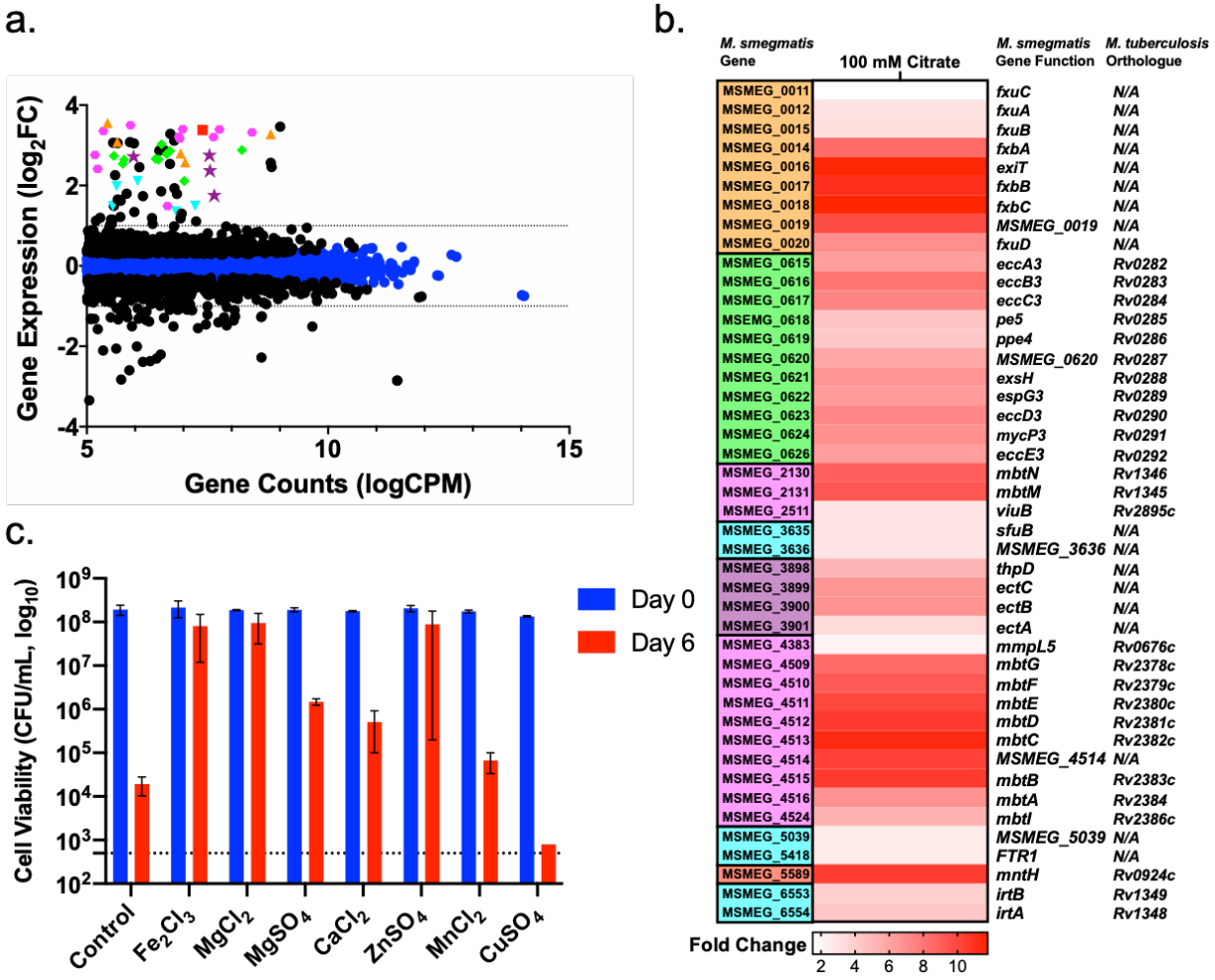

Figure 5.3. Sodium citrate induces chelation and osmotic stress. a) RNAseq scatter plot of genes upregulated in *M. smegmatis* cultured citrate buffered medium relative to MOPS buffered controls. ● indicate significantly differentiated expressed genes ($q < 0.05$). The dotted lines indicate $\log_2$ fold changes of 1 or -1. Genes in specific metabolic pathways are highlighted and include exochelin biosynthesis (orange square), mycobactin biosynthesis (pink hexagon), ESX-3 secretion system (green diamonds), iron interacting genes (blue inverted triangles), ectoine biosynthesis (purple stars), and manganese transport (red square). b) Heat map of genes differentially expressed in RNAseq scatter plot. Genes are color coordinated with scatter plot. Gene function annotations are included as well as M. *tuberculosis* predicted homology. c) Cell viability of *M. smegmatis* cultured in sodium citrate medium supplemented with 100 µM of Fe_2Cl_3, $MgCl_2$, $MgSO_4$, $CaCl_2$, $ZnSO_4$, $MnCl_2$, or $CuSO_4$. Error bars indicate the s.d. of the mean.

transporter[300-302]. Genes for these transporters as well as other iron interacting proteins[288,289,300,301] were also upregulated in our RNAseq profile (*MSMEG_3635, MSMEG_3636, MSMEG_5039, MSMEG_5418, MSMEG_6553,* and *MSMEG_6554*) (Figure 5.3a and 5.3b). We also identified upregulation of *MSMEG_5589* and *MSMEG2607-MSEG-2608* which are predicted to encode manganese and cobalt transporters, respectively (Figure 5.3a and 5.3b)[43]. These results indicated

that sodium citrate was starving the bacteria of metal cations. Citrate can be used as a metal chelator[303] and is often used in food production for the purpose of preventing microbial growth. The profiles generated here support a model in which citrate was starving the bacteria of essential metal cations.

To test the hypothesis that citrate was acting as a metal chelator, we supplemented citrate buffered medium with 100 μM of Fe_2Cl_3, $MgCl_2$, $MgSO_4$, $CaCl_2$, $ZnSO_4$, $MnCl_2$, or $CuSO_4$. Consistent with our hypothesis, supplementation with cations Fe, Mg, Ca, Zn, and Mn led to viability rescue or decreased killing in citrate buffered medium (Figure 5.3c). These results were independent of the counter anion (Cl^- or SO_4^{2-}) present (Figure 5.3c). Supplementation with copper did not lead to cell viability rescue and instead enhanced killing likely due to the bactericidal effects Cu through reactive oxygen species production[304]. The results of this assay support a model where Msm is starved of metal ions.

In addition to metal starvation genes, we also identified genes involved in osmotic stress as upregulated > 2-fold (Figure 5.3a and 5.3b). Included in this list of genes was the osmotic stress regulatory gene *oprA* (*MSMEG_0586*) which is upregulated in Mtb in response to high salinity[278]. We also identified genes involved in the biosynthesis of the compatible solute ectoine *ectA-C* and *thpD* (*MSMEG_3898 – MSMEG_3901*) (Figure 5.3a and 5.3b)[275]. Additionally, we saw an increase in the expression of the sodium/proline importer *putP* (*MSMEG_5303*) which is involved in osmotic stress adaptation in *Staphylococcus aureus*[305]. We believe these genes were in response to the high sodium included as the counter ion to citrate used in our buffering system. This was consistent with a previous study that observed both *oprA* and ectoine biosynthesis genes are upregulated in high sodium[275,278].

The results of the transcriptional profiling suggested that SC medium induced both chelation and osmotic stress in Msm. However, these results did not fully explain the bactericidal and cell lysis effects observed. Mycobacteria can survive in the absence of exogenous cations in

Table 5.1. Sodium citrate tolerant transposon mutants identified in a forward genetic screen

***MSMEG* Gene**	**Gene Name**	**Mtb Homolog**	***M. leprae* Homolog**	**Insertion (nt)**	**Gene Function**
MSMEG_5086	*fadD6*	*Rv1206*	*ML1062*	219, 1718	Very-long-chain acyl-CoA synthetase
MSMEG_6269	*mgtE*	*Rv0362*	pseudo	824, 900	Magnesium transporter
MSMEG_6193	*bagA*	*Rv3679*	*ML2305*	747, 751	ATP-binding protein
MSMEG_6195	*bagB*	*Rv3680*	*ML2306*	314, 397, 715	ATP-binding protein
MSMEG_0973	*MSMEG_0973*	*Rv0528*	*ML2410c*	32, 721	Conserved membrane protein
MSMEG_2788	*MSMEG_2788*	*Rv2670c*	*ML1341*	310, 418, 980	ATP/GTP-binding integral membrane protein
MSMEG_3184	*treZ*	*Rv1562c*	pseudo	670, 675	Malto-oligosyltrehalose trehalohydrolase

nt – nucleotide, pseudo – predicted nonfunctional gene, Mtb – *M. tuberculosis*

culturing condition like phosphate buffer saline (PBS) (Figure A.5.2). Additionally, deletion of ectoine biosynthesis genes in Msm leads to decreased growth but not cell death in high saline solutions[275]. Therefore, we sought to investigate this phenotype further to gain a better understanding of why SC medium induced cell death.

A Forward Genetic Screen Identifies Citrate Tolerant Msm Mutants

The results thus far suggested that SC induces a combination of chelation and osmotic stress, but the relative contribution of these stresses in killing was unknown. In order to gain further insights, we performed a forward genetic screen to identify mutants with resistance to killing by sodium citrate. Using the φMycoMarT7 phage transposon mutagenesis approach[306], we performed a forward genetic screen by culturing an ~30,000 transposon mutant library in SC medium for eight days. Following incubation, surviving cells were plated on solid nutrient rich medium. After an outgrowth period of 4-5 days, individual colonies were picked and cultured in fresh medium. Transposon insertion sites were then identified, including multiple independent insertions in genes of known and unknown function, and several singleton mutants (Table A.5.2 and Table 5.1). Mutants with multiple independent insertions included genes of seemingly unrelated pathways including *fadD6* (*MSMEG_5086, facl6*) involved in very-long-chain fatty acid

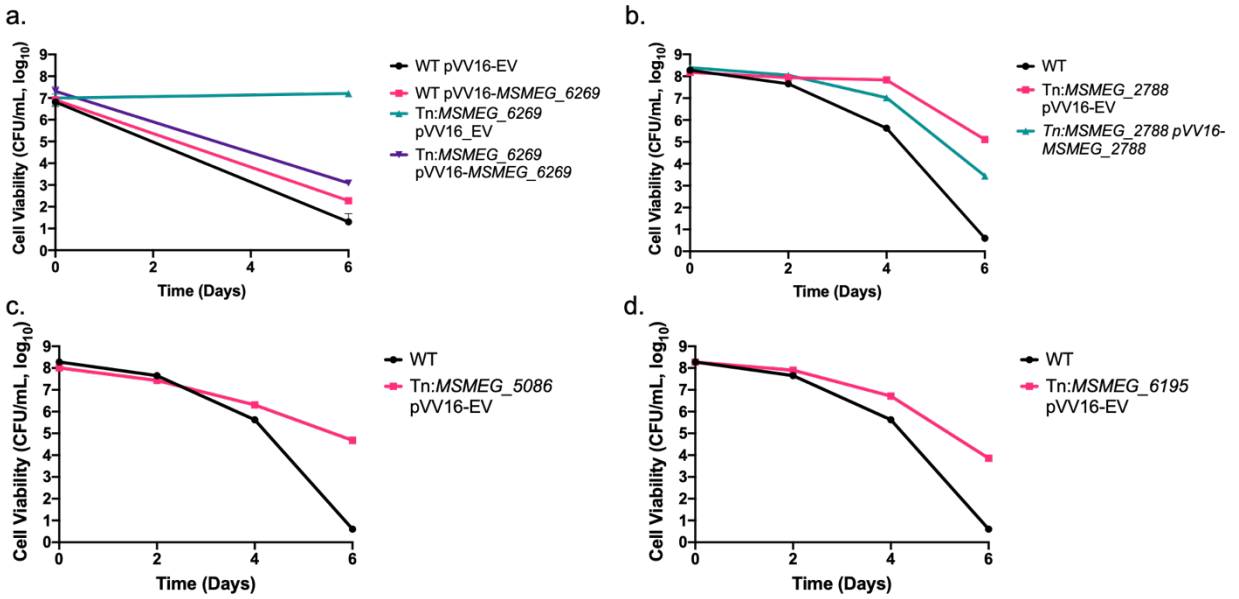

Figure 5.4. *M. smegmatis* transposon mutants are sodium citrate tolerant and complementable. a-d) WT and *MSMEG_6269* (a, *mgtE*), *MSMEG_2788* (b), *MSMEG_5086* (c), and *MSMEG_6195* (d) transposon mutant cell viability in MMAT minimal medium buffered with 100 mM sodium citrate (pH 7.0) and supplemented with 10 mM glycerol. a and b) Cell viability of complemented strains in MMAT minimal medium buffered with 100 mM sodium citrate (pH 7.0) and supplemented with 10 mM glycerol. Error bars indicate the s.d. from the mean.

synthesis and exogenous lipid acquisition[307,308]. Disruption of the magnesium importer *mgtE* (*MSMEG_6269*) was also found to confer SC tolerance. This seemed counterintuitive as Mg^{2+} supplementation led to cell viability rescue (Figure 5.3c). We also identified independent insertions in two genes within a single operon encoding *MSMEG_6193* and *MSMEG_6195* predicted to encode homologs of *bagAB* (*Rv3679* and *Rv3680*) from Mtb[309,310]. Recently *bagAB* were implicated in protecting Mtb from toxicity induced by glycerol metabolism and nitric oxide[310] a finding that was interesting as glycerol was included as our sole carbon source during the genetic screen. We also identified *MSMEG_2788* a gene of unknown function, as well as *MSMEG_0973* a predicted homolog to *Rv0528* of Mtb. Finally, we identified two insertions in *MSMEG_3184* encoding *treZ* involved in trehalose biosynthesis. In confirmation assays enumerating CFUs over time following incubation in SC medium, mutants in *mgtE,* MSMEG_2788, MSMEG_5086 and MSMEG_6195, we exhibited >3 logs higher viability than the parental wild type (WT) Msm (Figure 5.4a-d). We have successfully generated complementation

strains for two of the mutants (*mgtE* and MSMEG_2788), and observed complementation for these genes. (Figure 5.4a and 5.4d). Overall, the screen identified several genes with multiple independent insertions, two of which we have complemented, suggesting that disruption of these genes drives the observed phenotype rather than an unidentified background mutation. Of note, none of the genes identified were differentially regulated in the RNAseq data (Table A.5.1, Figure 5.3a and 5.3b, Table A.5.2, Table 5.1). Several of these genes are also conserved in *M. leprae*, an obligate intracellular species that has undergone extreme genomic reduction[43]. Conservation of the genes identified in *M. leprae* suggests that these genes are involved in intracellular survival. The interpretation of these screening results was not initially clear as gene disruption was not biased to any particular metabolic pathway. To better understand the results of the genetic screen we focused on genes that were best understood from the literature, namely *mgtE*, *fadD6,* and *treZ*.

Citrate Chelates Mg^{2+} and Ca^{2+} from the Cell Environment

MgtE is a magnesium specific importer[311] and one of two Mg^{2+} transporters in mycobacteria along with CorA[312]. Disruption of this gene providing tolerance seemed counter to a chelation stress model where Mg^{2+} supplementation leads to cell viability rescue (Figure 5.3c). However, several studies have indicated that the cell envelope of *E. coli* and *B. subtilis* serve as Mg^{2+} reservoirs and that Mg^{2+}, along with Ca^{2+}, stabilize the bacterial cell wall[264-271]. One model suggests that divalent cations are stored in the cell walls of bacteria bringing them closer to metal transporters in the cytoplasmic membrane[267,270,313]. Little is known about the metal contents of the mycobacterium cell wall; however, mycobacteria do have a peptidoglycan layer[314] which, in *B. subtilis*, serves as a reservoir for metal cations[270,271]. The disruption of *mgtE* suggested that Mg^{2+} supplementation may lead to cell viability rescue by stabilizing the cell envelope rather than

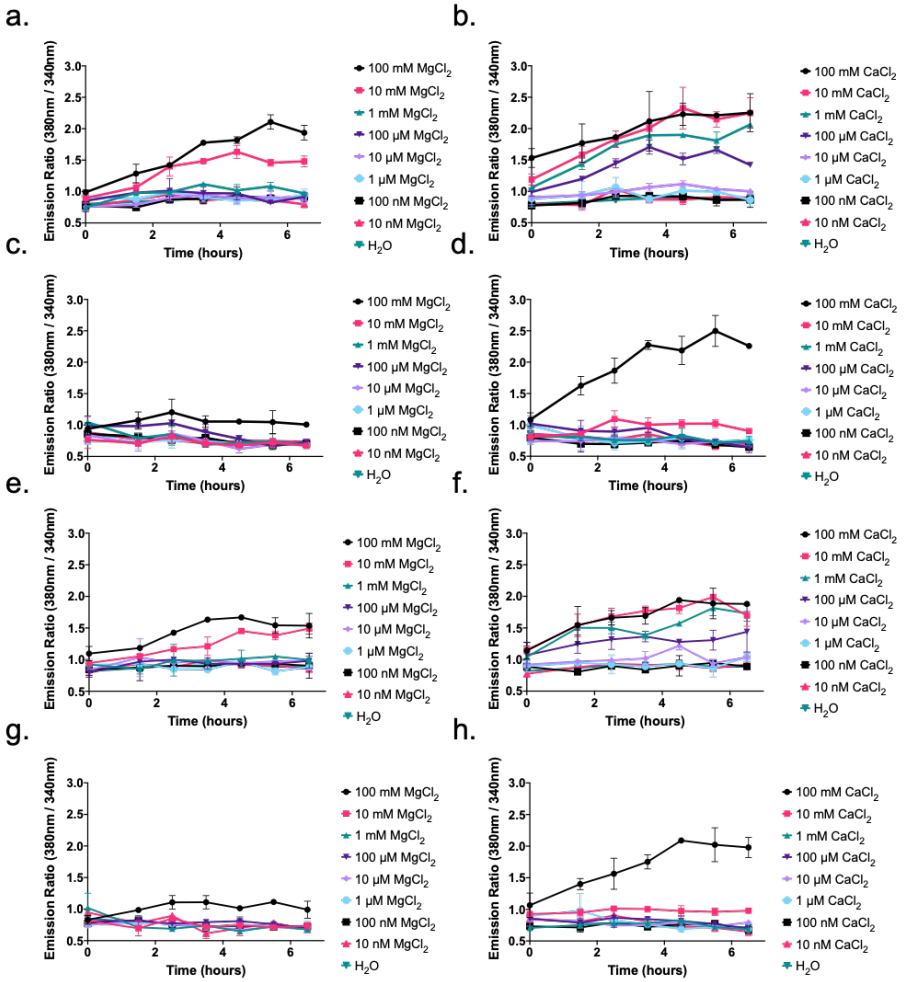

Figure 5.5. Sodium citrate prevents cation import in *M. smegmatis*. a-h) WT *M. smegmatis* (a-d) or a Tn:*mgtE* mutant (e-h) were labeled with the cell permeable Mag-Fura2 (AM) Mg^{2+}/Ca^{2+} fluorophore and cultured in MOPS buffered (a, b, e, and f) or sodium citrate buffered (c, d, g, and h) minimal medium. Cultures were supplemented with 100 mM to 10 nM concentrations of either Mg^{2+} (a, c, e, and g) or Ca^{2+} (b, d, f, and h). The ratio represents the RFI of cells measured at Mg^{2+} bound Mag-Fura2 (High Mg^{2+}, Ex: 380 nm/ Em: 510 nm) relative to free Mag-Fura2 (Low Mg^{2+}, Ex: 340 nm/ Em: 510 nm). The experiments were performed in biological duplicate and repeated at least twice. Error bars indicate the s.d. of the mean.

through Mg^{2+} import. This model is consistent with the inability of *M. smegmatis* to import citrate arguing against chelation of cytoplasmic metals.

Currently, it is challenging to measure cell envelope metal ion concentrations in live cells. As an alternative method to test the hypothesis that citrate is acting at the cell envelope, we labeled the Msm cytoplasm with the cell permeable magnesium fluorophore Mag-Fura2 (AM)[315]. We hypothesized that if citrate was acting on the cell envelope then supplemented cations will

not be imported into the cell. We cultured Mag-Fura2 labeled cells in MOPS or SC buffered medium with or without Mg^{2+} supplementation (100 mM to 10 nM). In addition to Mg^{2+}, MagFura-2 can also detect Ca^{2+} ions[316]. Since Ca^{2+} supplementation also rescued Msm cell viability (Figure 5.3c), we also supplemented Mag-Fura2 loaded cells with Ca^{2+} (100 mM to 10 nM). Following Mg^{2+} and Ca^{2+} supplementation in MOPS cultured cells we observed a dramatic increase in the emission ratio (Ex380nm / Ex340nm) in a dose dependent manner (Figure 5.5a and 5.5b). However, no increase in signal was observed for 100 μM or lower Mg^{2+} which rescued Msm in SC medium. These results indicate that the bacteria are actively importing these cations even at these early time points. By contrast, cells cultured in SC medium did not actively import either Mg^{2+} or Ca^{2+} except at the highest concentrations (100 mM) (Figure 5.5c and 5.5d). This included 100 μM Ca^{2+} which was able to rescue cell viability (Figure 5.3c). Further, SC medium did not result in a decrease in the emission ratio (Figure 5.5c and 5.5d) suggesting that citrate was not chelating Mg^{2+} or Ca^{2+} from the cytosol consistent with the inability of exogenous citrate to enter the cell[281,282]. To determine if the *mgtE* mutant had increased cation import due to an unidentified compensatory system, we also labeled the cytoplasm of the *mgtE* mutant with the Mag-Fura2 fluorophore and tested for cation import via dose response as we did for WT (Figure 5.5e-h), The results of the assay mirrored those observed in the WT suggesting that sodium citrate tolerance in the *mgtE* mutant is not due to enhanced ion import. However, we did note a higher emission ratio following 100 mM Mg^{2+} supplementation in WT (peak 2.1 at 5.5 hours) compared to the *mgtE* (1.5 at 5.5 hours) (Figure A.5.3). This suggested that the *mgtE* mutant was impaired for Mg^{2+} import compared to WT. These data are consistent with our hypothesis that citrate is not acting on the cytoplasm and rather may function to chelate cell envelope cations which is predicted to weaken the cell envelope. These results also suggest that the *mgtE* mutant is tolerant of cell envelope chelation due to decreased cation import from the cell envelope.

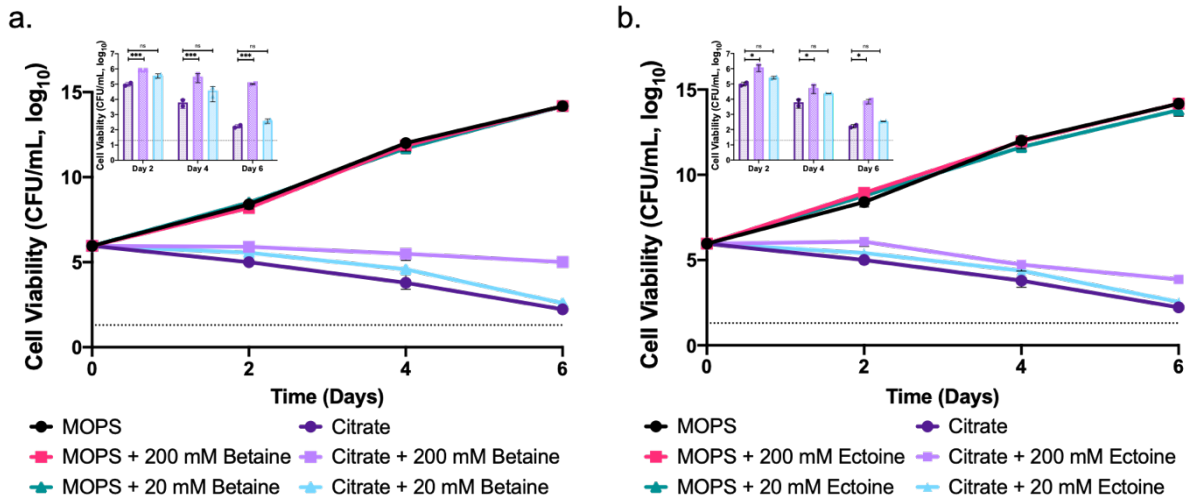

Figure 5.6. Osmolyte supplementation decreases *M. smegmatis* killing in sodium citrate. a and b) *M. smegmatis* was cultured in MOPS or sodium citrate buffered minimal medium supplemented with 20 mM or 200 mM betaine (a) or ectoine (b). Insets demonstrate relative CFU/mL of sodium citrate cultures with or without osmoprotectant supplementation. Samples were compared using a Two-way ANOVA with Fisher's LSD test. Error bars indicate the s.d. of the mean and dotted lines indicate the limit of detection (20 CFU/mL).

Compatible Solute Supplementation Rescues Msm from Citrate Stress

In additional to *mgtE*, disruption of *treZ* and *fadD6* also conferred SC tolerance (Table 5.1). *treZ* is part of a two gene pathway along with *treY* that metabolizes maltodextrin to form the disaccharide trehalose in a unidirectional enzymatic reaction[317]. TreYZ form one of three trehalose metabolic pathways in *M. smegmatis* along with TreS[318,319] and OtsAB[319,320]. A previous study demonstrated that *treYZ* were the most upregulated in Msm as it entered dormancy resulting in cytosolic trehalose accumulation[321]. However, the results of the genetic screen suggested that a decrease in trehalose protected Msm from SC medium. *fadD6* is one of several fatty acyl-CoA ligase (FACL) genes found in mycobacteria[43]. In Mtb, FadD6 is involved in incorporating fatty acids into fatty acid esters such as triacylglycerol (TAG)[307,308] which are stored as cytosolic lipid droplets during dormancy[322]. As both *treZ* and *fadD6* are involved in substrate accumulation following environmental stress, we hypothesized that there was a cytosolic component to the sodium citrate phenotype.

The RNAseq data suggested that Msm was adapting to osmotic stress likely due to the high osmolyte (sodium and citrate) concentration in the SC medium (Figure 5.3a and 5.3b). In the case of both lipid droplet and trehalose accumulation, mycobacteria undergo cell swelling[321,323] which would presumably add additional stress to cells undergoing osmotic and cell envelope stress. Tolerance in the mutants may be driven by lower osmolytes in the cytoplasm of the mutants. To test the hypothesis that Msm was experiencing osmotic stress as part of killing by citrate, we supplemented both MOPS and SC cultures with 200 mM and 20 mM concentrations of the osmolytes betaine and ectoine (Figure 5.6a and 5.6b). Supplementation with both betaine, and to a lesser extent, ectoine at 200 mM, but not 20 mM, resulted in decreased killing of Msm in in SC medium (Figure 5.6a and 5.6b insets). This reduction in killing was not due to decreases in growth as betaine and ectoine did not impact the growth of Msm in MOPS medium (Figure 5.6a and 5.6b). These data, along with the observed cell lysis, support a model in which cell death in SC medium is enhanced through osmotic stress.

Discussion:

In an attempt to recapitulate pH induced persistence in Mtb cultured in minimal medium, we discovered a lethal SC phenotype in the model organism Msm. Transcriptional profiling using RNAseq indicated that SC induced cation chelation in Msm. Supporting this hypothesis, cation supplementation led to cell viability rescue. We also identified genes involved in osmotic stress adaptation, likely in response to the sodium ions in solution. However, Msm can survive in both cation depleted medium as well as high osmotic environments. In order to better understand this phenotype, we performed a forward genetic transposon mutagenesis screen in Msm. We identified citrate tolerant mutants with multiple independent transposon insertions in genes of seemingly unrelated metabolic pathways including *mgtE*, *fadD6,* and *treZ*. Using these mutants, we developed a model in which citrate chelates cell envelope cations to weaken the cell wall while inducing osmotic stress. The combination of these stresses then results in the killing of Msm by cell lysis and relief by either a strengthened cell wall or less osmotic stress promotes tolerance to cell lysis (Figure 5.7a). In this model, WT *mgtE* import Mg^{2+}, and in the presence of SC chelating activity, there is less available Mg^{2+}, so it is stripped from the cell envelope. *mgtE* mutation leads to SC tolerance through increased Mg^{2+} accumulation in cell envelope resulting in increased cell envelope stability in the presence of citrate chelation (Figure 5.7b). This model also proposes that Msm undergoes a stage of cell swelling due to trehalose and lipid droplet accumulation which further weakens the cell envelope. However, this osmotic stress is mitigated in the *treZ* and *fadD6* mutants, as they would not accumulate these solutes in the cytoplasm (Figure 5.7c and 5.7d). This model promises to serve as a starting point for additional investigation of the physiological roles of other genes identified in the transposon mutagenesis screen, several of which have no known function.

Cell death in SC is dependent on bacterial replication as media lacking a carbon source such as glycerol did not have the same bactericidal effects. This suggests that growth is required for the killing phenotype, possibly due to peptidoglycan remodeling, and cell wall weakening

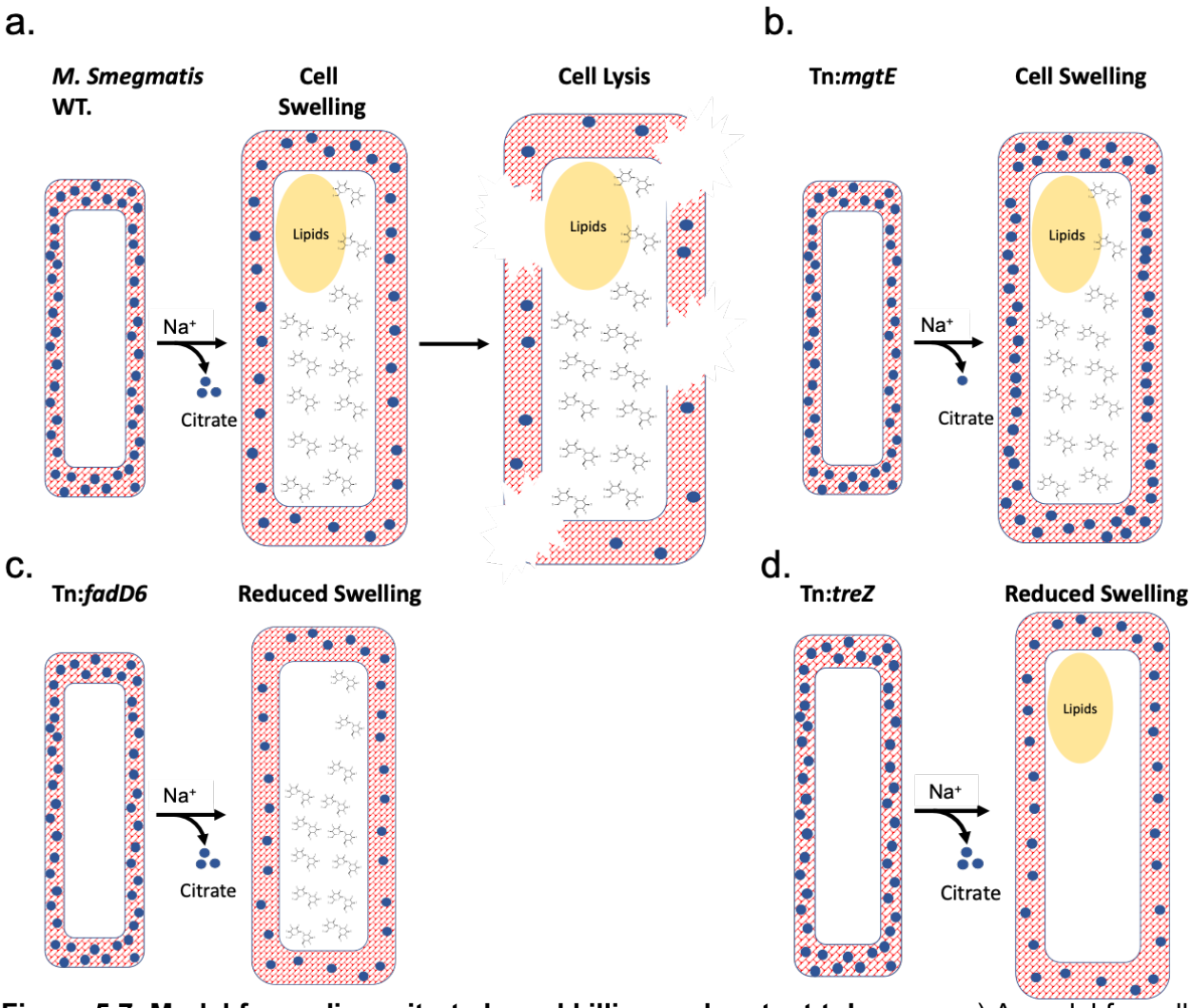

Figure 5.7. Model for sodium citrate based killing and mutant tolerance. a) A model for cell lysis of *M. smegmatis* cultured in sodium citrate medium. In this dual stress model, citrate chelates cell envelope cations (blue spheres) and *M. smegmatis* undergoes a stage of cell swelling induced by high environmental osmolytes as well as trehalose and lipid droplet accumulation. These two stresses result in cell lysis. b) The *mgtE* mutant possesses sodium citrate tolerance due to increased cell envelope stabilizing cations allowing the *mgtE* mutant to tolerate cell swelling induced by high environmental sodium. c and d) The *fadD6* and *treZ* mutants have decreased lipid droplet (c) and trehalose (d) accumulation resulting in reduced cell swelling and lower cell death.

associated with cell division. Consistent with this model, our transposon screen, which used glycerol as its sole carbon source, identified insertions in *MSMEG_6193* and *MSMEG_6195* which are homologous to Mtb *bagAB* (*Rv3679* and *Rv3680*)[309,310]. Recently BagAB were implicated in glycerol and nitric oxide detoxification[310]. Glycerol metabolism results in methylglyoxyl accumulation which can be toxic to mycobacteria[310,324]. These toxic effects result

in decreased growth rate which would normally render Msm strains deficient in detoxification at a selective disadvantage compared to WT strains. However, our studies suggest that higher growth rate is selected against in SC medium and may explain why genes involved in detoxification were identified in our screen. Further supporting this model, we identified insertion mutants in genes involved in central carbon metabolism (*MSMEG_2613* malate:quinone-oxidoreductase (*mqo*)) and electron transport chain biogenesis (*MSMEG_0973* predicted ResB cytochrome c biogenesis like protein (PFAM)). Using this method parallel carbon source screens can be developed to screen for genes required for specific metabolic pathways.

Citrate is a useful tool for studying chelation stress in Msm as exogenous citrate is not taken into the cell[281,282]. The chelation effects of citrate are dependent on the protonation state (pKa) of citrate[303]. At lower pH levels, citrate becomes more protonated and the binding affinity for metals decreases[303]. This would explain why we saw differences in the killing effect of Msm cultured in SC medium at pH 7.0 compared to pH 5.7 when citrate is in the -3 vs -2 charge states respectively. This effect was not due to growth differences, as Msm grew to similar levels at both pH 7.0 and pH 5.7 in MOPS and MES buffered medium. Cation supplementation rescued Msm cell viability at concentrations as low as 100 μM in SC medium. However, this was not due to cytoplasmic uptake as SC prevented Mg^{2+} and Ca^{2+} import at these concentrations, suggesting cation rescue may be due to cell envelope stabilization or saturating the chelation of citrate molecules. Consistent with these observations, a study reported by Sutterlin and colleagues demonstrated that Ca^{2+} supplementation could rescue a lethal LPS accumulation phenotype in *E. coli* through outer membrane stabilization[325]. Future studies could seek to further characterize where these cations are accumulating and what role they play in mycobacterial cell envelope stability. Of note, the lethal phenotype we observed in Msm was not observed in Mtb or *M. abscessus*. These differences in outcome are likely growth rate independent, as the rapidly growing *M. abscessus*, which has a growth rate comparable to Msm, was completely insensitive to the killing effects of SC medium. This suggests that the differences between species was due

to other phenotypic differences, possibly the structures of the cell envelopes. A previous study highlighted the structural differences in the peptidoglycan between Msm, Mtb and *M. leprae*[314]. Peptidoglycan is one of the major reservoirs for cell wall cations in *B. subtilis*[270,271]. Whether the differences in peptidoglycan between mycobacterial species plays a role in the SC phenotypic outcome is unclear, nor is it clear if the differences in peptidoglycan play a role in cation sequestration and further studies will be needed to address this hypothesis.

Methods:

Bacterial Strains and Growth Conditions

Bacterial strains were cultured in the following conditions unless otherwise described. *M. smegmatis* MC2-155 was cultured in LB medium with 0.05% tween-80 shaking at 120 RPM at 37°C in T25 or T75 flasks. *M. tuberculosis* Erdman was cultured in 10 mL of 7H9 supplemented with 10% v/v OADC with 0.05% tween-80 in T25 standing flasks. *M. abscessus* was cultured in LB with 0.05% tween-80 shaking at 200 RPM at 37°C.

MMAT minimal medium was made as previously described[326] 1 g/L KH_2PO_4, 2.5 g/L Na_2PO_4, 0.5 g/L $(NH_4)_2SO_4$, 0.15 g/L asparagine, 10 mg/L $MgSO_4$, 50 mg/L ferric ammonium citrate, 0.1 mg/L $ZnSO_4$, 0.5 mg/L $CaCl_2$, and 0.05% Tyloxapol. MMAT medium was buffered with 100 mM MOPS (pH 7.0), MES (pH 5.7), sodium citrate (pH 5.0 – 7.0) or citric acid (pH 7.0). MMAT was supplemented with 10 mM glucose or 10 mM glycerol as carbon sources.

Growth Curves

Msm was grown to exponential growth (0.6 – 1.0) in LB with 0.05% tween-80 at 37°C in T25 standing flasks. Samples were pelleted and resuspended in MMAT medium buffered to pH 7.0 with 100 mM sodium citrate and supplemented with 10 mM glycerol at a starting OD_{600} of 0.05. AT indicated time points, 1 mL samples were taken and measured for cell growth (OD_{600}). The limit of detection for this assay was 0.05.

Bacteria Viability Assays

Bacteria were grown in nutrient rich medium in conditions described above to an OD_{600} of 0.6 – 1.0. Bacteria were pelleted and washed twice in phosphate buffer saline (PBS, pH 7.4) with 0.05% tyloxapol (PBS-T). Washed cells were resuspended in 10 mL of MMAT minimal medium starting at OD_{600} of 0.05 for *M. smegmatis* and *M. abscessus* or 0.1 for *M. tuberculosis*. At indicated time points, cultures were mixed by pipetting and serial diluted in PBS-T. 50 µL samples

were plated on LB agar plates for *M. smegmatis* and *M. abscessus* or 7H10 AODC (with 100 µg/mL cycloheximide) agar and incubated at 37°C 3-4 days for *M. smegmatis* and *M. abscessus* or 3-4 weeks for *M. tuberculosis*.

Bacterial Lysis Assay

Prior to the assay, *M. smegmatis* was transformed with pSMT1 plasmids expressing either Envy1-GFP or mCherry mycobacterium codon-optimized fluorescent protein genes[327]. *M. smegmatis* strains were cultured in MMAT minimal medium as described above buffered to pH 7.0 with either 100 mM MOPS or 100 mM sodium citrate and supplemented with 10 mM glycerol at a starting OD_{600} of ~0.6. At designated time points, 1 mL samples were taken and the optical density was measured. The 1 mL samples were then gently pelleted at 1000 RPM and supernatants were removed and re-centrifuged to remove cells. Supernatants were then filtered using 0.20 µm filter, and culture filtrates were placed into clear bottom black wall 384-well plates. The RFI was measured using a Perkin Elmer plate reader for Envy1-GFP (Ex 488 nm / Em 515 nm) or mCherry (Ex 580 nm / Em 610 nm). Either MOPS or sodium citrate buffered cell free medium was used for background subtraction. The assays were performed in biological duplicate and fluorescent readings were performed in technical triplicate for each sample. To ensure contaminating bacteria were not present in culture filtrates, following fluorescent readings, filtrates were plated onto LB agar plates and incubated for at least five days at 37°C. No bacteria were detected for any of the samples reported.

Cell lysis is reported as a ratio of two A.U. measures (RFI / OD_{600}) and therefore unitless. Statistics comparing the ratio of RFI/OD between MOPS and sodium citrate buffered samples were calculated using a two-way ANOVA.

Transcriptional Profiling using RNAseq

M. smegmatis was cultured starting in 30 mL of MMAT medium supplemented with 10 mM glycerol buffered to pH 7.0 with 100 mM MOPS to pre-adapt cells. *M. smegmatis* was cultured to an OD_{600} of ~0.6 before being washed twice in MOPS buffered MMAT medium twice and then split into 10 mL cultures of MMAT medium supplemented with 10 mM glycerol buffered to pH 7.0 with either 100 mM MOPS or sodium citrate in T25 flasks. Cultures were incubated for 3 hours standing at 37°C before RNA was extracted and sequenced as previously described[279]. RNAseq data was analyzed using the SPARTA software package[285].

Cation Supplementation

M. smegmatis cells were cultured in sodium citrate buffered MMAT as described above. Sodium citrate cultures were supplemented with 100 µM of Fe_2Cl_3, $MgCl_2$, $MgSO_4$, $CaCl_2$, $ZnSO_4$, $MnCl_2$, or $CuSO_4$. At indicated time points, 50 µL samples were serial diluted and plated on LB agar plates and incubated as described above.

Transposon Mutagenesis

Transposon mutagenesis was performed as previously described[328]. Briefly, φMycoMarT7 phage were harvested from *E. coli* and used to transfect *M. smegmatis* cells resulting in a ~30,000 mutant library selected for using 20 µg/mL kanamycin. Mutants were collected and the library was stored at -80°C. On the day of the experiment, the libraries were inoculated into 100 mL of MMAT medium buffered with 100 mM sodium citrate and supplemented with 10 mM glycerol in a T150 standing flask and cultured for eight days at 37°C. Following incubation, cells were pelleted, washed in PBS-T and plated on 7H10 OADC agar plates with kanamycin and incubated at 37°C. Colonies were picked and grown up in liquid medium with kanamycin. Transposon insertions were sequenced using inverse PCR[329]. Sequences were mapped to the *M. smegmatis* genome to identify insertion sites.

MagFura2-(AM) Assay

Msm cells were labeled with the Mag-Fura2 (AM) fluorophore using a previously described protocol[315] with some modifications. WT or the Tn:*mgtE M. smegmatis* strains were cultured to exponential growth (OD 0.6-1.0) in LB with 0.05% tween-80. Approximately 6 x 10^9 cells (OD_{600} of 0.6 = 1 x 10^8 cells/mL) were harvested from overnight cultures and washed twice in 6 mL of 10 mM HEPES (pH 7.4) with 0.9% saline (HEPES-saline) and resuspended in 1 mL of HEPES-saline. 50 µg of MagFura2-AM was dissolved into 32.4 µL of DMSO and 16 µL were added to the 1 mL cell suspension along with 20 µM Pluronic F-127. Cells were incubated for three hours shaking at 37°C shaking at 120 RPM. Cells were then pelleted, washed twice with 6 mL of PBS-T. Washed cells were resuspended in 6 mL 0.9% saline with 0.05% tyloxapol and incubated at 37°C shaking at 120 RPM for an additional 30 minutes to allow for complete hydrolysis of AM ester. Cells were then pelleted and washed twice in PBS-T and resuspended to 3 x 10^8 cells/mL in MMAT buffered with 100 mM MOPS or sodium citrate and supplemented with 10 mM glycerol. Cells were aliquoted into 384- well plates and Mg^{2+}or Ca^{2+} was added to each well at the concentrations described in the text. Plates were read using a Perkin Elmer plate reader. Excitation and emission were as previously described[315] (High Mg^{2+}, Ex 380 nm / Em 510 nm) or (Low Mg^{2+}, Ex 340 nm / Em 510 nm). The ratios were represented as the emission ratio (3380nm/340nm). Experiments were conducted in biological duplicate and repeated at least twice.

Osmoprotectant Supplementation Assay

M. smegmatis was cultured as described for the cell viability assay. However, after washing the cells, the cells were resuspended in MMAT buffered with MOPS or sodium citrate and supplemented with 200 or 20 mM of betaine or ectoine and 10 mM glycerol. The assay was conducted in biological duplicate and repeated twice with similar results. Comparison between groups was carried out using a two-way ANOVA by Fishers LSD test.

CHAPTER 6: Concluding Chapter

Summary:

Chapter 1 is a review of what is known about the physiological function and consequences of inhibiting the essential mycolic acid flippase MmpL3. MmpL3 has been the focus of several studies on its role in mycomembrane biogenesis driven by the continued identification of MmpL3 inhibitors. These studies have demonstrated that MmpL3 forms a complex in the mycobacterial divisome prominently demonstrated through protein-protein interactions[55,56] and co-localization of MmpL3 to the dividing pole[137]. Further, MmpL3 is regulated in a way that links it to lipid biogenesis[57,58,144]. Protein crystals and co-crystals have demonstrated that the periplasmic loop domains of MmpL3 directly bind trehalose monomycolate (TMM) and phosphatidylethanolamine (PE) [51,52] supporting a direct role in lipid transport[48]. From these functional and physiological studies, we understand that MmpL3 inhibitors directly bind to MmpL3[52,54] resulting in cell wall stress and weakening. Currently, no FDA approved drug targets MmpL3 leaving MmpL3 an unutilized but sought-after target for Mtb and NTM therapy. However, the continued identification and development of novel screening platforms, like the one described in Chapter 2, as well as the clinical success of the MmpL3 inhibitor SQ109 supports that a MmpL3 targeting drug may eventually be deployed for TB treatment.

Chapter 2 identified four compounds that killed mycobacteria *in vitro*. Leveraging this strong selective pressure, I selected resistant mutants to identify the cellular target of these bactericidal compounds. This resulted in the isolation and sequencing of *mmpL3* mutants resistant to the four compounds tested. These compounds resulted in TMM accumulation in treated Mtb supporting that these compounds targeted the essential mycolic acid flippase. To expedite the identification of MmpL3 inhibitors in a small library of 163 compounds, I created a screening platform that utilized the *mmpL3* mutants isolated in our lab[22,25]. The results of this screening system identified twelve MmpL3 inhibitors from our compound library, as well as the SQ109 control, that induced TMM accumulation in treated cells. I also performed a cross resistance study of the thirteen compound and the twenty-four *mmpL3* mutant strains. Follow up

studies demonstrated that differential cross resistance profiles were due to unique protein-inhibitor interactions and the proximity of the mutation substitutions to essential residues for protein function[25].

From the compounds identified in Chapter 2, and in collaboration with Dr. Edmund Ellsworth's lab, we conducted a structure-activity-relationship (SAR) study, described in Chapter 3, to optimize lead compounds for the treatment of Mtb *in vivo*. From this study we identified MSU-43085 as a potent inhibitor of Mtb and NTM growth both *in vitro* and in intracellular infection models. Proof-of-concept studies demonstrated that MSU-43085 was tolerable, orally bioavailable, and present in murine lungs. Further MSU-43085 was able to inhibit Mtb growth during an acute mouse infection. However, MSU-43085 failed to inhibit Mtb survival in a chronic infection, possibly due to limitations in bioavailability and drug clearance. Future studies will seek to address these limitations through formulation optimization and PK profiling.

In Chapter 4, I screened hits from a HTS using standard prioritization assays for Mtb including confirming *in vitro* activity, as well as testing for cytotoxicity and intracellular growth inhibition. The results of these assays identified 213 compounds that met our assay cut-offs. The 163-compound library described in Chapter 2 was the result of similar secondary screening assays for compounds identified from a separate HTS. MmpL3 is possibly the most common target identified from HTSs, and the 163-compounds from the ICCB library included twelve MmpL3 inhibitors. Based on this trend, I screened the >1000 hit compounds from the MLSMR library using the targeted *mmpL3* mutant screen created in Chapter 2 to identify additional MmpL3 inhibitors. This resulted in the identification of new analogs of previously identified MmpL3 inhibitor scaffolds, as well as putative, novel sulfonamide based MmpL3 inhibitors. The purpose for doing this was to identify MmpL3 inhibitors prior to prioritizing a list of compounds for future studies. From this screen, identified MmpL3 inhibitors can be fast tracked for lead optimization studies as described in Chapter 3. Alternatively, hit compounds from the 213 compounds that were not identified as MmpL3 inhibitors can proceed in parallel for MOA studies, such as isolation of

resistant mutants or transcriptional profiling studies. In addition to screening for both non-specific growth and MmpL3 inhibitors, I simultaneously cross screened the compounds for DosRST inhibitors using an *hspX*-GFP reporter strain. The results of this screen identified analogs of previously described DosRST inhibitors as well as a potentially novel series of diamine-based inhibitors. However, hits from both the MmpL3 screen and the *hspX* screen still need to be verified using phenotypic and biochemical assays described in the literature[29,49,207,255].

In Chapter 5 I investigated a lethal sodium citrate phenotype in Msm discovered by other scientists in our lab. Through characterization studies I discovered that sodium citrate induced dual chelation and osmotic stress leading to cell lysis. Based on the selective effects of sodium citrate we conducted a transposon mutagenesis screen in Msm and identified genes in unrelated metabolic pathways that conferred tolerance following gene disruption. Based on the identification of an *mgtE* mutant and measuring intracellular Mg^{2+}, I demonstrated that sodium citrate likely chelates metal cations from the cell envelope of Msm. This suggests that the cell envelope for mycobacteria acts as a reservoir for metal ions. Through osmoprotectant experiments I demonstrated that sodium citrate induces osmotic stress. Based on this, I hypothesized that the *fadD6* and *treZ* mutants are tolerant of citrate due to reduced cell swelling; however, additional experiments are needed to test this hypothesis. Many of these genes are conserved in Mtb; however, their role in Mtb physiology and during infection are not understood. Center to this study was understanding how sodium citrate killed Msm, with the goal of generating a model that can be used to study the function of other genes identified in the transposon screen. Future directions will seek to characterize other genes identified in the screen in Msm and translate those functions to Mtb. Without the fundamental understanding of the selective pressure sodium citrate induces in Msm, such guided experiments would not be possible.

Additional Studies for Screened Compounds

Drug resistance in Mtb continues to be a public health threat that if not addressed could result in the return to pre-antibiotic infection and death rates. The central focus of the first four chapters of my research was the identification and characterization of Mtb growth inhibitors. The intent was to identify lead compounds for pre-clinical development against drug resistant Mtb.

Addressing the Therapeutic Limitations of MmpL3

While the central focus of the first four chapters of my dissertation were on drug development, they leaned near exclusively on the identification and characterization of MmpL3 inhibitors. The focus of these studies was to identify a lead compound for optimization and *in vivo* efficacy studies. The results of Chapter 3 identified MSU-43085 as a potent analog of HC2099 (identified in Chapter 2) with *in vivo* efficacy in an acute infection. While this compound did failed to inhibit Mtb in a chronic mouse infection model, this was likely due to the PK properties and limitations of the formulation. Snapshot PK studies showed MSU-43085 accumulated at 8X the EC_{50} in lungs 4 hours post treatment, therefore, we hypothesize that the time above the effective concentration may not be sufficient for killing Mtb in the chronic infection model. Studies to be conducted in the near future will characterize the PK properties of MSU-43085 including clearance, C_{Max}, lung accumulation and formulation optimization. However, in the event of successful PK optimizations, several fundamental therapeutic questions must be addressed for this series of MmpL3 inhibitors. For one, mycobacteria infected patients must take a combination of drugs in order to successfully treat the infection. Failure to incorporate more than one antibiotic has historically led to infection relapse and the evolution of resistance in subsequent infections. *In vitro* studies have demonstrated that MmpL3 inhibitors act synergistically in combination with Mtb drugs such as RIF, INH, CFZ, and BDQ[25,246,330]. I demonstrated that parental HC2099, as well as all other MmpL3 identified in Chapter 2, act synergistically in combination with RIF[25]. However, RIF resistance in Mtb is increasing and 206,000 cases were reported in 2020[1]

potentially limiting future combinations of MmpL3 inhibitors with RIF. Therefore, additional combinations need to be identified for the treatment of MDR-/XDR-TB. In 2019 the FDA approved a new combination of Bedaquiline, Linezolid, and Pretomanid for the treatment of highly drug resistant Mtb[331]. Incorporation of an MmpL3 inhibitor with one of these drugs may further benefit patient outcomes. However, to date pairwise-drug combinations have been the primary focus of such studies and they have focused primarily on *in vitro* cultures in actively replicating conditions[25,246,330]. These studies are limited in scope and do not address potential drug-drug interactions that occur in the host. For example, studies of SQ109 in combination with other drugs in mice have demonstrated a large increase in bacterial clearance[204]. However, due to host metabolic degradation of SQ109, this has not translated to the clinic[163-165]. Further, SQ109 uncouples the PMF and inhibits menaquinone biosynthesis as secondary and tertiary MOA[117,189]. These additional effects potentially obscure the drug combination effects from targeting MmpL3 alone. To identify such outcomes, I would seek to carryout large multi-conditional combination studies like the ones recently reporter by Larkins-Ford and colleagues[332] (Preprint). This study identified drug combinations that correlated with *in vivo* outcomes of C3HeB/FeJ mice which form complex granulomas more reflective of the infected human lung than the mouse model used in Chapter 3[333].

MmpL3 is essential for growth and viability of Mtb in replicating conditions[64]. However, like other genes involved in cell wall biosynthesis, MmpL3 is not essential during states of non-replicating persistence[64]. During infection, Mtb encounters several host-induced stresses that induce non-replicating persistence, including hypoxia[333]. In conditions of hypoxia, MmpL3 inhibitors, that do not uncouple the PMF, such as HC2091 do not lead to significant loss in viability in Mtb[22]. This phenotype potentially limits the therapeutic potential of inhibitors that target MmpL3 as their sole MOA[64]. Due to this fact, we did not test MSU-43085 for the ability to kill Mtb in states of non-replicating persistence as parental HC2099 and structurally similar MmpL3 inhibitors do not uncouple the PMF[22,25,117]. This therapeutic limitation is not true for all MmpL3 inhibitors and

can be overcome by compounds such as SQ109 which uncouples the PMF and kills non-replicating Mtb[117]. However, this limitation for the HC2099 series of MmpL3 inhibitors should be addressed when considering combinations with an MmpL3 inhibitor. One possible way to address this limitation is to incorporate MmpL3 inhibitors with other TB drugs that do kill non-replicating Mtb such as rifampicin[334], bedaquiline[334], clofazimine[334], pretomanid[335], and linezolid[336]. However, such combinations simply account for the limitation of targeting MmpL3, but do not directly overcome the therapeutic limitations of MmpL3. As an alternative approach, combination of MmpL3 inhibitors with anti-virulence factors that prevent Mtb from entering into states of non-replicating persistence could also overcome this therapeutic limitation. In Chapter 4, I describe the identification of DosRST inhibitors including artemisinin and HC106 analogs. In previous studies, artemisinin and HC106 were shown to reduce the number of Mtb cells from entering into states of non-replication in a hypoxic environment[207,255]. In these studies, artemisinin and HC106 sensitized hypoxic Mtb cultures to INH which also has lower efficacy against non-replicating Mtb[207,255]. Combining MmpL3 inhibitors with such anti-virulence factors could potentially overcome the therapeutic limits of targeting MmpL3 by preventing Mtb form fully adapting to environments like hypoxia.

Mechanism of Action Studies for Non-MmpL3 Inhibitors

Understanding how a compound inhibits bacterial growth is not essential for clinical approval. For example, pyrazinamide has been clinically approved for Mtb therapy since the 1970s and the MOA is still not fully understood. However, understanding the MOA of an inhibitor and the identification of the target can greatly improve drug development. In Chapter 4, I described the identification of compounds that inhibited Mtb growth both *in vitro* and in inside of infected macrophages in a manner that was likely independent of MmpL3. These compounds included scaffolds of known Mtb drugs such as thiacetazone and INH. However, many compounds identified did not have recognizable chemical scaffolds similar to known antibiotics. These

compounds are classified as novel inhibitors of Mtb with an unknown MOA. To address this several possible methods are available to understand what kind of stress the compounds induce in Mtb. Isolating and sequencing resistant mutants, as described in Chapter 2, is one possible method for identifying a target. However, this method is not always successful, (*e.g.* SQ109[34]) and can sometimes select for resistance through off target mutations such as unregulated efflux (e.g. *mmpR5*[239]). An alternative approach would be to understand what stress Mtb is attempting to adapt to through transcriptional profiling, as described in Chapter 5. While this method may not directly identify the target, it can lead to a general understanding of the metabolic stress induced by an inhibitor. TNseq is another possible method to identify metabolic pathways that are sensitized when disrupted in bacteria treated with an inhibitor. Like transcriptional profiling this method is limited to identifying a particular stress rather than the exact target. However, Jinich and colleagues recently published on a new database that allows for comparing TnSeq profiles that have been generated in the literature[337] (Preprint). Comparing new profiles to ones previously generated may allow for rapid understanding of what stresses Mtb is facing following inhibitor treatment. From stress profiles generated by either transcriptional profiling or TNseq, models can be developed to identify the MOA of novel inhibitors. Jointly, these methods can vastly improve our understanding of how a compound inhibits Mtb and future directions should seek to understand these to move these compounds forward for drug development.

As an alternative approach I have also isolated resistant mutants to several other compounds (data not shown) that include analogs of HadAB inhibitors, as well as FolC inhibitor p-amino salicylic acid. We also isolated a transposon disrupted *katG* mutant from a screen performed in our lab. KatG is a catalase/peroxidase and the activating enzyme for the InhA prodrug INH. KatG deficient strains are resistant to INH and sensitized to reactive oxygen species[338]. Using these other mutants, I will screen the 213 compounds as well as the other 1000+ compounds from the library described in Chapter 4, to identify compounds that act on these

metabolic pathways. Similar to the identified MmpL3 inhibitors these compounds could be fast tracked into lead compound optimization studies like the one described in Chapter 3.

Additional Studies for the Citrate Project

Investigation of the Citrate Based Physiology

The model proposed in Chapter 5 predicts that citrate chelates metal cations from the cell envelope of Msm. However, the evidence supporting this model was indirect as direct measurement of cation concentrations in the cell envelope of live bacteria are currently unavailable. Additionally, we do not know where the cations are being stored in the cell envelope. I hypothesized in Chapter 5 that the peptidoglycan was a likely candidate as this is one of the cation reservoirs in *B. subtilis*[270,271]. However, Msm also contains various phospholipids, (*e.g.* acPIM2[196]) which contain negatively charged phosphate moieties that must be neutralized through positive cations. Such lipids may acts as additional reservoirs for cations in the cell envelope of mycobacteria. Future studies may seek to characterize cation interactions using methods previously described in the literature (*i.e.* ICP-MS) with mycobacterial cell envelope fractions such as peptidoglycan and phospholipids. Such studies could investigate whether or not citrate can chelate interacting cations from these cell fractions for the purpose of expanding on the proposed model.

Mg^{2+} supplementation in mycobacterial cultures has been used for several studies including growth of mycobacteria in acidified media[280]. When cultured in acidic medium Mtb reroutes its metabolism and remodels its cell wall lipids[279]. Piddington and colleagues demonstrated that Mg^{2+} supplementation was required for growth of Mtb in mildly acidic conditions[280]. The authors speculated that this phenotype could be driven by either internal Mg^{2+} homeostasis or through stabilizing the membrane but did not conduct experiments to distinguish between the two[280]. The results of the study described in Chapter 5 suggest that this phenotype

should be readdressed with greater focus on distinguishing between these two possibilities and to expand on the roles of Mg^{2+} homeostasis in Mtb.

Application of Citrate Stress for Metabolic Screens

In Chapter 5 I described a lethal sodium citrate phenotype in Msm. This phenotype was specific to replicating Msm that was provided as a carbon source. In this chapter we identified *MSMEG_6193* and *MSMEG_6195* (*bagAB*[309]) mutants that were tolerant of sodium citrate. In Mtb, these genes are involved in detoxifying methyl glyoxal that is formed as a metabolic byproduct of glycerol metabolism[310]. In the discussion of Chapter 5, I speculated that disruption of *bagAB* in Msm led to methyl glyoxal accumulation which poisoned Msm metabolism resulting in a reduced growth rate and citrate tolerance. A simple way to test this hypothesis would be to substitute glycerol for an alternative carbon source (*e.g.* glucose) that does not result in methylglyoxal accumulation. This model predicts that citrate would select for mutations in the metabolic pathway of the carbon source provided resulting in lowered growth rate and citrate tolerance. Based on this prediction, metabolic mutant screens could be designed to identify genes required for the metabolism of specific carbon sources. However, a single screen would likely identify a large number of genes not tied to the metabolic pathway such as *mgtE*. To overcome this limitation, parallel screens would need to be performed to identify genes unique to specific carbon metabolism pathways. This parallel screening system would also select carbon source independent citrate tolerant mutants, such as *mgtE*, that would allow for further investigation of citrate induced stress. Such genes would be identified in the overlap of genes identified in the parallel studies. Further, this screening platform has the advantage of identifying genes involved in metabolic detoxification, such as *bagAB*, that may be missed in other metabolic screens that select for growth vs no growth.

Concluding Remarks:

In conclusion, my dissertation used chemical and genetic approaches to investigate stressors that destabilize the cell envelope of mycobacteria resulting in cell death. The applications of this work exceed my time here in this lab, but I look forward to seeing the fruits of the seeds I helped plant.

APPENDICES

APPENDIX A:

Supplemental Tables

Table A.2.1. Sequencing results of resistant mutants

Compound	Strain	SNP Location (nt)	Quality Score	Gene	Nucleotide Change	AA Change
HC2060	1A / 2C	245506	5308 / 4597	*mmpL3*	GTG --> **A**TG	V643M
	3B	245501	4710	*mmpL3*	TTC --> TT**G**	F644L
	4A	245733	3840	*mmpL3*	CTG --> C**C**G	L567P
	5B	245501	4807	*mmpL3*	TTC --> TT**A**	F644N*
	6C	245349	4795	*mmpL3*	ATG --> A**C**G	M695T*
HC2149	1A	245487	5798	*mmpL3*	ATG --> A**C**G	M649T*
	3A / 4A / 8C / 17A / 19A	247313	5895 / 6057 / 5228 / 4998 / 5725	*mmpL3*	CAG --> CA**T**	Q40H*
	11C / 12A	246316	5127 / 6751	*mmpL3*	CGG --> **T**GG	R373W*
	15A	246501	3836	*mmpL3*	ACC --> A**T**C	T311I*
	16A	246537	3854	*mmpL3*	CTG --> C**A**G	L299Q*
HC2169	1B / 6A / 17A	245662	7164 / 6152 / 6805	*mmpL3*	TCG --> **A**CG	S591T*
	14A	246579	4739	*mmpL3*	GTG --> G**G**G	V285G*
	13A	246675	4585	*mmpL3*	GGG --> G**A**G	G253E
	7A / 9A	246678	6076 / 4312	*mmpL3*	TAC --> T**G**C	Y252C*
	16A	246702	5280	*mmpL3*	ATC --> A**C**C	I244T*
HC2184	1B	245355	5122	*mmpL3*	GAC --> G**G**C	L693P*
	2A	246675	6093	*mmpL3*	CCC --> C**T**C	G253E
	6B	245661	5719	*mmpL3*	TCG --> T**A**G	S591I
	8A	246678	5654	*mmpL3*	ATG --> A**C**G	I585S*
	9C	247313	5824	*mmpL3*	GTC --> GT**G**	Q40H*
	12B	245338	5281	*mmpL3*	GAC --> **T**AC	L699M
	13B	245448	5121	*mmpL3*	CGC --> C**T**C	A662E*
	20A	246714	3800	*mmpL3*	CAC--> C**G**C	V240A*

* - Novel substitutions not previously identified in Mtb

Table A.2.2. Genetic background of Mtb strains used in screen

Compound Background	Mtb Strain Background	Strain	SNP Location	Quality Score	Gene	Nucleotide Change	Amino Acid Substitution	Clade
HC2060	Erdman	1A	245506	5308	*mmpL3*	GTG --> ATG	V643M	I
	Erdman	3B	245501	4710	*mmpL3*	TTC --> TTG	F644L	I
	Erdman	4A	245733	3840	*mmpL3*	CTG --> CCG	L567P	I
	Erdman	5B	245501	4807	*mmpL3*	TTC --> TTA	F644N	I
	Erdman	6C	245349	4795	*mmpL3*	ATG --> ACG	M695T	II
HC2091	CDC 1551	3A	245488	3441	*mmpL3*	ATG --> CTG	M649L	I
	CDC 1551	5A	245424	2685	*mmpL3*	ACC --> AAC	T670L	II
	CDC 1551	23A	245335	2615	*mmpL3*	GCC --> ACC	A700T	II
HC2149	Erdman	1A	245487	5798	*mmpL3*	ATG --> ACG	M649T	II
	Erdman	3A	247313	5895	*mmpL3*	CAG --> CAT	Q40H	II
	Erdman	11C	246316	5127	*mmpL3*	CGG --> TGG	R373W	II
	Erdman	15A	246501	3836	*mmpL3*	ACC --> ATC	T311I	II
	Erdman	16A	246537	3854	*mmpL3*	CTG --> CAG	L299Q	II
HC2169	Erdman	1B	245662	7164	*mmpL3*	TCG --> ACG	S591T	I
	Erdman	14A	246579	4739	*mmpL3*	GTG --> GGG	V285G	I
	Erdman	13A	246675	4585	*mmpL3*	GGG --> GAG	G253E	I
	Erdman	7A	246678	6076	*mmpL3*	TAC --> TGC	Y252C	I
	Erdman	16A	246702	5280	*mmpL3*	ATC --> ACC	I244T	II

Table A.2.2 (cont'd)

HC2184	Erdman	1B	245355	5122	*mmpL3*	GAC --> GGC	L693P	I
	Erdman	6B	245661	5719	*mmpL3*	TCG --> TAG	S591I	I
	Erdman	8A	246678	5654	*mmpL3*	ATG --> ACG	I585S	I
	Erdman	12B	245338	5281	*mmpL3*	GAC --> TAC	L699M	II
	Erdman	13B	245448	5121	*mmpL3*	CGC --> CTC	A662E	II
	Erdman	20A	246714	3800	*mmpL3*	CAC--> CGC	V240A	II

Table A.2.3. EC_{50} values of control compounds

Treatment	WT EC_{50}	Mix Mutant EC_{50}	95% Confidence Interval
INH	0.15	0.18	n.s.
HC2051	3.2	4.5	n.s.
CFZ	4.4	3.8	n.s.
BDQ	0.03	0.06	n.s.
RIF	0.009	<0.009	N.D.
PAS	0.05	0.02	n.s.

n.s. – Not significant
N.D. – Not determined

Table A.2.4. AUC values from cross resistance profiling

	HC2032	HC2060	HC2091	HC2099	HC2134	HC2138	HC2149	HC2169	HC2178	HC2183	HC2184	C215	SQ109
Q40H^{E}	42.98	68.03	84.3	101.8	63.23	37.49	44.07	42.17	92.35	96.53	63.86	131.7	143
V240A^{E}	102.2	82.81	73.08	89.43	68.44	15.86	77.88	94.26	108.7	107.7	68.1	26.77	143.3
I244T^{E}	110.9	69.62	60.8	67.29	86.09	65.59	58.91	52.76	97.73	96.78	73.2	33.41	132.8
T252C^{E}	149.4	48.76	27.29	55.58	35.23	14.64	23.38	35.96	87.77	60.9	58.37	18.72	181.4
G253E^{E}	18.23	60.32	18.2	44.63	11.15	7.195	10.61	29.13	54.42	57.9	32.29	15.03	146
V285G^{E}	31.87	40.62	39.38	48.43	29.35	34.77	34.81	41.29	78.09	57.41	59.12	33.96	117.1
L299Q^{E}	95.93	85.39	72.67	90.14	59.81	37.88	21.73	55.48	91.53	93.22	73.78	40.02	157.2
T311I^{E}	94.83	84.38	101.8	115.7	106.2	68.61	23.31	54.41	114.1	123.6	96.01	127.8	167.8
R373W^{E}	62.68	78.36	70.65	79.96	53.12	85.28	37.85	35.57	105.8	91.78	100.1	62.15	157.2
L567P^{E}	43.81	40.82	40.23	52.93	35.96	69.17	120.2	157.9	80.5	61.52	69.83	137.5	157.3
I585S^{E}	165.1	47.59	26.81	40.55	31.87	53.06	23.38	19.76	90.54	34.68	35.16	31.11	201.3
S591I^{E}	28.78	21.79	76.97	38.94	18.47	18.89	12.86	22.95	35.47	55.81	28.15	11.45	110.7

Table A.2.4 (cont'd)

S591T[E]	31.85	39.27	66.47	65.59	68.16	43.98	24.29	28.08	80.44	90.53	50.04	32.04	144.8
V643M[E]	33.28	40.88	28.28	41.06	36.34	48.63	38.99	98.7	56.54	46.87	54.33	88.44	117.9
F644L[E]	34.12	21.31	25.91	48.32	130.9	123.7	93.34	58.46	51.75	38.31	65.11	48.58	132.2
F644N[E]	25.76	27.24	38.88	53.13	123.5	101.5	95.12	54.82	54.16	54.71	82.96	14.76	117.6
M649L[C]	22.92	82.01	38.01	68.54	73.58	72.83	47.07	28.83	96.72	41.98	62.24	55.8	175.5
M649T[E]	43.61	72.15	47.2	66.99	84	82.72	17.65	23.53	105.5	97.45	67.32	50.67	171.8
A662E[E]	100.1	101.7	51.92	83.82	132.1	129.6	69.05	44.16	134.3	110.9	70.83	37.18	183.2
T670L[C]	75.25	75.14	21.15	52.09	109.1	118.3	56.69	71.4	151.6	64.69	59.74	88.44	174.2
L693P[E]	88.03	73.82	86.89	88.84	96.19	107.3	83.23	39.29	93.76	111.5	63.13	71.82	169.4
M695T[E]	79.44	55.82	89.55	103.1	92.69	45.96	61.88	79.04	60.96	103.9	68.95	92.96	139.8
L699M[E]	55.85	69.13	57.75	89.07	90.94	42.28	60.88	69.08	90.47	90.9	66	51.01	134.2
A700T[C]	69.86	79.3	43.85	78.75	90.92	132.3	59.37	45.64	106.9	99.82	83.75	61.3	151.5
WT-CDC1551	136.2	93.86	114	129.8	159	150.7	96.38	151.5	148.2	154.7	123	97.66	193.8
Average WT - Erdman	115.96	74.87	101.18	115.1	142.74	140.3	89.33	141.14	130.32	138.96	94.88	69.12	171.88

E or C indicates the WT background that the AUC was compared to.
E – Erdman and C – CDC1551

Table A.3.1. *in vitro* activity of HC2099 analogs against *M. tuberculosis*

Compound Name	Structure	Molecular Weight (g/mol)	EC_{50} (μM)	Hillslope	EC_{90} (μM)
HC2099	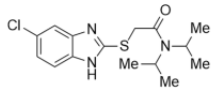	325.1	5.1	2.4	12.8
HC2183	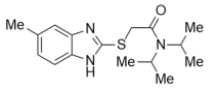	305.16	7.3	2.8	16.0
MSU-42765	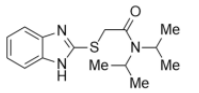	291.14	> 80	24	N.D.
MSU-42766	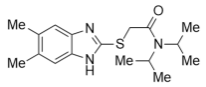	319.17	1.3	1.2	8.2
MSU-42767	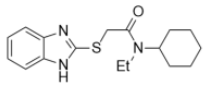	317.16	Inactive	Inactive	Inactive
MSU-42768	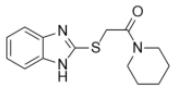	275.11	Inactive	Inactive	Inactive
MSU-42769	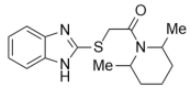	303.14	Inactive	Inactive	Inactive
MSU-42770	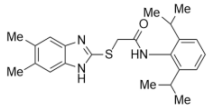	397.22	Inactive	Inactive	Inactive
MSU-42771	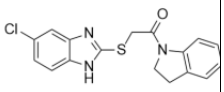	343.05	Inactive	Inactive	Inactive
MSU-42772	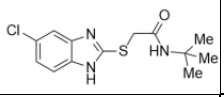	297.07	> 80	N.D.	N.D.
MSU-42773	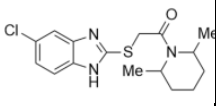	337.87	24.3	0.9	N.D.
MSU-42774	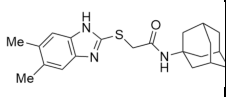	369.19	Inactive	Inactive	Inactive
MSU-42828	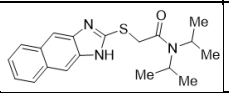	341.15	14.3	3.2	28.6

Table A.3.1 (cont'd)

MSU-42829	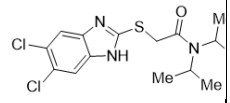	359.06	1.9	3.6	3.5
MSU-42830	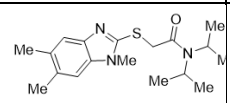	333.19	Inactive	Inactive	Inactive
MSU-42831	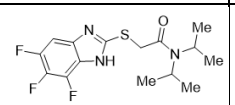	345.11	1.4	3.2	2.8
MSU-42885	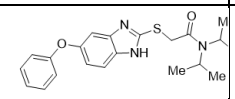	383	2.4	4.8	3.6
MSU-42886	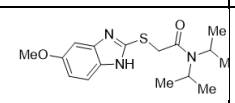	321	51.4	1.4	N.D.
MSU-42887	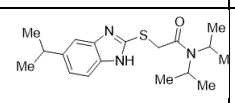	333.5	4.9	2.6	11.5
MSU-43065	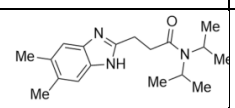	301.43	0.46	4.4	0.77
MSU-43066	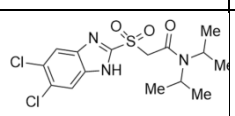	392.30	Inactive	Inactive	Inactive
MSU-43085	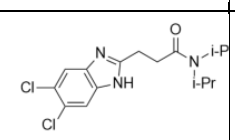	342.26	0.12	2.9	0.25
MSU-43086	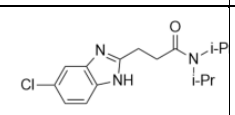	307.82	0.63	3.8	1.1
MSU-43125	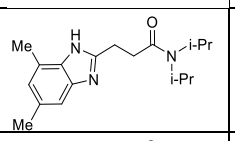	301.43	0.95	3.0	2.0
MSU-43126	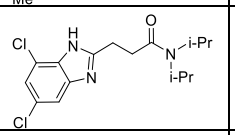	342.26	0.37	3.3	0.73
MSU-43127	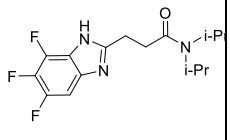	327.35	0.38	3.9	0.66

Table A.3.1 (cont'd)

MSU-43128	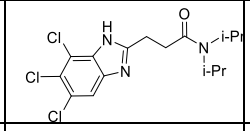	376.71	0.17	3.0	0.35
MSU-43129	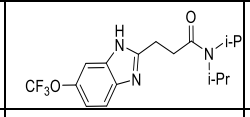	357.38	0.36	5.4	0.55
MSU-43130	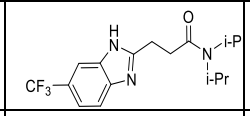	341.38	0.43	5.2	0.66
MSU-43131	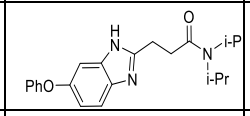	365.48	1.1	4.6	1.8
MSU-43132	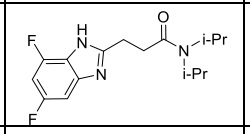	309.36	1.0	3.5	1.9
MSU-43133	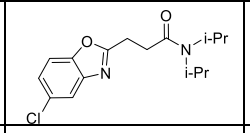	308.81	22.7	2.6	52.1
MSU-43134	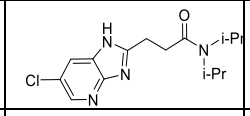	308.81	6.1	4.3	10.3
MSU-43165	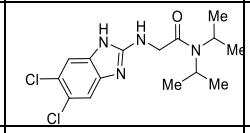	342.1	0.38	4.4	0.63
MSU-43166	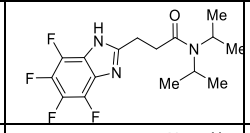	345.15	0.42	5.8	0.61
MSU-43167	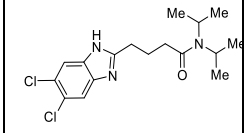	355.12	4.7	2.1	13.4
MSU-43170	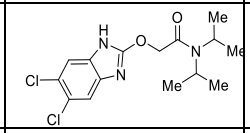	343.09	0.12	2.7	0.26
MSU-43171	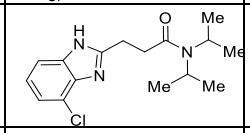	307.15	1.7	3.9	3.0
MSU-43172	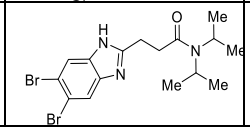	439.0	0.11	2.8	0.24

Table A.3.1 (Cont'd)

MSU-43173	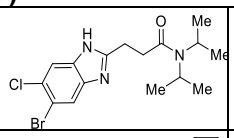	385.0	0.29	2.3	0.77
MSU-43288	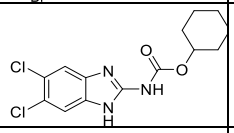	328.19	Inactive	Inactive	Inactive
MSU-43325	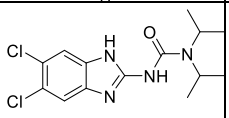	329.22	Inactive	Inactive	Inactive
MSU-43388	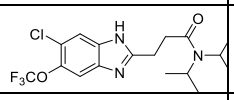	391.81	0.88	3.7	1.6
MSU-43389	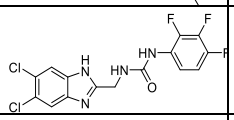	389.15	Inactive	Inactive	Inactive
MSU-43390	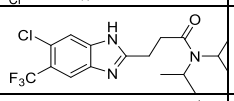	375.82	0.43	5.0	0.66
MSU-43391	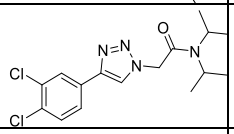	355.23	Inactive	Inactive	Inactive
MSU-43414	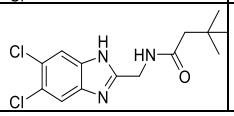	314.21	> 40	1.1	N.D.

N.D. – Not determined.

Table A.3.2. Activity of select HC2099 analogs against intracellular *M. tuberculosis*

Compound Name	*ex vivo* EC_{50} (μM)	Hillslope	*ex vivo* EC_{90} (μM)	BMMΦ CC_{50} (μM)	S.I. (CC_{50} / EC_{50})
MSU-42766	0.41	2.5	0.97	> 80	> 195.6
MSU-42829	0.24	5.1	0.62	79.6	332.7
MSU-42831	0.85	14.3	0.99	75.7	89.0
MSU-42885	1.8	12.7	2.1	72.5	40.7
MSU-42887	1.7	4.6	2.8	> 80	> 47
MSU-43065	0.29	17.8	0.33	> 80	> 274.3
MSU-43085	0.13	1.8	0.46	> 80	> 595.7
MSU-43086	0.33	21.3	0.37	> 80	> 238.8
MSU-43125	0.72	16.6	0.83	> 80	> 110.4
MSU-43126	0.37	13.1	0.43	> 80	> 218.8
MSU-43127	0.39	2.0	1.2	> 80	> 202.9
MSU-43128	0.32	14.2	0.38	> 80	> 248.7
MSU-43129	0.73	19.5	0.82	> 80	> 109.5
MSU-43130	0.80	30	0.86	> 80	> 100.4
MSU-43131	1.5	6.9	2.1	> 80	> 53.7
MSU-43132	0.77	17.9	0.88	> 80	> 103.4
MSU-43165	0.13	16.5	0.15	> 80	> 596.6
MSU-43166	0.6	6.2	0.86	> 80	> 132.2
MSU-43170	0.035	1.6	0.14	> 80	> 2285
MSU-43171	0.95	1.2	6.0	> 80	> 83.8
MSU-43172	0.13	70.7	0.14	> 80	> 608.8
MSU-43173	0.25	4.7	0.39	> 80	> 324.7
MSU-43176	1.2	197	1.2	40	34.3
MSU-43185	1.5	3.3	2.83	> 80	> 54.9
MSU-43187	0.12	18.3	0.14	> 80	> 644.6

BMMΦ – Priamry bone marrow derived macrophages, CC_{50} – Cytoxicity of compounds against , S.I. – Selective index

Table A.3.3. Cytotoxicity of select HC2099 analogs against additional cell lines

Compound Name	THP-1 Cytotoxicity (IC_{50} µg/mL)	HepG2 Cytotoxicity (IC_{50} µg/mL)	HeLa Cytotoxicity (IC_{50} µg/mL)
MSU- 42766	39.6	> 128	> 128
MSU- 43065	69.51	> 128	> 128
MSU- 43085	> 128	> 128	> 128
Mitomycin C	3.094	23	10.54

Table A.3.4. *M. tuberculosis mmpL3* mutants used in pooled mutant cross resistance study

Compound Background	Mtb Strain Background	Strain	SNP Location	Quality Score	Gene	Nucleotide Change	Amino Acid Substitution
HC2060	Erdman	1A	245506	5308	*mmpL3*	GTG --> ATG	V643M
	Erdman	3B	245501	4710	*mmpL3*	TTC --> TTG	F644L
	Erdman	4A	245733	3840	*mmpL3*	CTG --> CCG	L567P
	Erdman	5B	245501	4807	*mmpL3*	TTC --> TTA	F644N
	Erdman	6C	245349	4795	*mmpL3*	ATG --> ACG	M695T
HC2091	CDC 1551	3A	245488	3441	*mmpL3*	ATG --> CTG	M649L
	CDC 1551	5A	245424	2685	*mmpL3*	ACC --> AAC	T670L
	CDC 1551	23A	245335	2615	*mmpL3*	GCC --> ACC	A700T
HC2149	Erdman	1A	245487	5798	*mmpL3*	ATG --> ACG	M649T
	Erdman	3A	247313	5895	*mmpL3*	CAG --> CAT	Q40H
	Erdman	11C	246316	5127	*mmpL3*	CGG --> TGG	R373W
	Erdman	15A	246501	3836	*mmpL3*	ACC --> ATC	T311I
	Erdman	16A	246537	3854	*mmpL3*	CTG --> CAG	L299Q
HC2169	Erdman	1B	245662	7164	*mmpL3*	TCG --> ACG	S591T
	Erdman	14A	246579	4739	*mmpL3*	GTG --> GGG	V285G
	Erdman	13A	246675	4585	*mmpL3*	GGG --> GAG	G253E
	Erdman	7A	246678	6076	*mmpL3*	TAC --> TGC	Y252C
	Erdman	16A	246702	5280	*mmpL3*	ATC --> ACC	I244T

Table A.3.4 (cont'd)

HC2184	Erdman	1B	245355	5122	*mmpL3*	GAC --> G**G**C	L693P
	Erdman	6B	245661	5719	*mmpL3*	TCG --> T**A**G	S591I
	Erdman	8A	246678	5654	*mmpL3*	ATG --> A**C**G	I585S
	Erdman	12B	245338	5281	*mmpL3*	GAC --> **T**AC	L699M
	Erdman	13B	245448	5121	*mmpL3*	CGC --> C**T**C	A662E
	Erdman	20A	246714	3800	*mmpL3*	CAC--> C**G**C	V240A

Mtb – *M. tuberculosis*, SNP – single nucleotide polymorphism

Table A.3.5. Cross resistance of active HC2099 analogs against a mixed *mmpL3* mutant pool

Compound Name	WT AUC	Mixed *mmpL3* AUC	Fold Resistance (WT / *mmpL3*)
HC2183	101.7	34.08	2.92
MSU-42766	169.9	73.44	2.35
MSU-42773	92.87	51.49	1.81
MSU-42828	173	85.64	2.04
MSU-42829	148.9	70.47	2.12
MSU-42831	145.9	88.11	1.66
MSU-42885	131.9	69.67	1.89
MSU-42887	111.1	60.37	1.96
MSU-43065	204.8	133.1	1.54
MSU-43085	231.7	165.2	1.41
MSU-43086	179.5	87.47	2.04
MSU-43125	174.3	96.53	1.82
MSU-43126	196.4	115.8	1.69
MSU-43127	192.2	100.2	1.92
MSU-43128	219.6	169.6	1.30
MSU-43129	194.6	103.4	1.89
MSU-43130	186.4	117.7	1.59
MSU-43131	173.2	98.95	1.75
MSU-43132	176.4	95.11	1.85
MSU-43133	42.59	21.8	1.96
MSU-43134	94.13	26.8	3.57
MSU-43165	214.5	147.2	1.45
MSU-43166	205.9	101.7	2.04
MSU-43167	119.7	48.05	2.5
MSU-43170	247.5	160.3	1.54
MSU-43171	151.2	56.81	2.63
MSU-43172	240.6	179.8	1.33
MSU-43173	237.8	166.9	1.43
MSU-43175	61.7	26.37	2.38
MSU-43185	157.2	61.43	2.56
MSU-43187	231.3	170.6	1.35
MSU-43247	162.7	107.1	1.52
MSU-43248	120.1	47.85	2.51
MSU-43552	109.3	58.05	1.88
MSU-43554	169.9	109.3	1.55
MSU-43557	288.9	226.4	1.28

AUC – area under the curve

Table A.3.6. Cross resistance of select active HC2099 analogs against an *mmpR5* efflux mutant

Compound Name	WT EC_{50} (μM)	*mmpR5* EC_{50} (μM)
MSU-42766	1.3	1.8
MSU-42773	13.9	15.7
MSU-42828	2.0	2.1
MSU-42829	2.8	5.4
MSU-42831	1.9	2.3
MSU-42885	3.0	7.2
MSU-42887	6.1	7.4
MSU-43065	0.54	0.39

Table A.3.7. Early pharmacokinetic properties of prioritized HC2099 analogs

Compound Name	cLogP	Kinetic solubility at pH 7.4 (μM)	Kinetic solubility at pH 2.0 (μM)	Microsome Stability (%)
HC2099	3.7	178	> 300	71
HC2183	3.6	> 200	> 300	25
MSU-43085	3.5	> 75	> 300	102
MSU-43128	4.0	N.T.	> 300	87
MSU-43165	3.3	> 150	> 300	106
MSU-43170	3.2	> 50	> 300	95
MSU-43187	N.T.	N.T.	N.T.	61

% - % of compound remaining after 30 minutes of incubation with mouse microsomes, N.T. – not tested

Table A.3.8. COA of HC2099 analogs

Compound Name	Source and Data package
MSU-42765	^{1}H NMR (500 MHz, Chloroform-*d*) δ 7.47 (dd, *J* = 6.1, 3.1 Hz, 2H), 7.17 (dd, *J* = 6.0, 3.2 Hz, 2H), 3.60 (s, 2H), 3.34 (p, *J* = 6.5 Hz, 2H), 1.34 (d, *J* = 6.5 Hz, 11H). APCI [M+H] calc'd = 292.1478, observed = 292.1485
MSU-42766	^{1}H NMR (500 MHz, DMSO-d_6) δ 12.23 (s, 1H), 7.24 (s, 1H), 7.11 (s, 1H), 4.35 (s, 2H), 4.06 (p, *J* = 6.6 Hz, 1H), 3.52 – 3.45 (m, 1H), 2.25 (d, *J* = 6.7 Hz, 6H), 2.07 (s, 2H), 1.27 (d, *J* = 6.7 Hz, 6H), 1.17 (d, *J* = 6.6 Hz, 6H). APCI HRMS [M+H] calc'd = 320.1791, found 320.1790 m.p = 172 ^{o}C
MSU-42767	^{1}H NMR (500 MHz, Chloroform-*d*) δ 9.64 (s, 2H), 7.48 (dd, *J* = 6.0, 3.2 Hz, 2H), 7.17 (dd, *J* = 6.0, 3.1 Hz, 2H), 3.67 (s, 2H), 2.98 (q, *J* = 7.2 Hz, 2H), 2.86 (tt, *J* = 11.7, 3.9 Hz, 1H), 2.05 (dd, *J* = 12.4, 3.8 Hz, 2H), 1.74 (dt, *J* = 13.3, 3.5 Hz, 2H), 1.60 (dt, *J* = 13.0, 3.3 Hz, 1H), 1.42 (dd, *J* = 12.3, 3.5 Hz, 1H), 1.37 (dd, *J* = 12.4, 3.6 Hz, 1H), 1.29 (t, *J* = 7.2 Hz, 3H), 1.19 (qt, *J* = 12.9, 3.2 Hz, 2H), 1.08 (ddt, *J* = 16.2, 12.7, 6.2 Hz, 1H). APCI HRMS [M-H] calc'd = 316.1489, found 316.1436
MSU-42768	^{1}H NMR (500 MHz, Chloroform-*d*) δ 7.54 (t, *J* = 4.9 Hz, 1H), 7.24 – 7.16 (m, 1H), 3.98 (s, 1H), 3.68 – 3.62 (m, 1H), 3.51 (t, *J* = 5.1 Hz, 1H), 1.73 – 1.65 (m, 2H), 1.64 – 1.57 (m, 1H). APCI [M+H] calc'd = 276.1165, observed = 276.1169
MSU-42769	^{1}H NMR (500 MHz, Chloroform-*d*) δ 7.48 (t, *J* = 4.7 Hz, 1H), 7.21 – 7.14 (m, 1H), 3.64 (s, 1H), 3.00 (q, *J* = 6.5 Hz, 1H), 1.87 – 1.77 (m, 1H), 1.80 – 1.73 (m, 1H), 1.61 – 1.52 (m, 1H), 1.55 – 1.39 (m, 1H), 1.34 (d, *J* = 6.3 Hz, 4H). APCI [M+H] calc'd = 304.1478, observed = 304.1505
MSU-42770	^{1}H NMR (500 MHz, DMSO-d_6) δ 12.38 (s, 1H), 9.68 (s, 1H), 7.25 (s, 1H), 7.20 (t, *J* = 7.7 Hz, 1H), 7.14 (s, 1H), 7.08 (d, *J* = 7.7 Hz, 2H), 4.18 (s, 2H), 3.02 (hept, *J* = 6.9 Hz, 2H), 2.26 (d, *J* = 6.1 Hz, 6H), 0.98 (s, 11H). APCI [M+H] calc'd = 396.2104, observed = 396.2117
MSU-42771	^{1}H NMR (500 MHz, DMSO-d_6) δ 8.05 – 7.87 (m, 1H), 7.81 – 7.50 (m, 1H), 7.34 – 7.10 (m, 3H), 7.09 – 6.96 (m, 1H), 5.32 (d, *J* = 9.0 Hz, 1H), 4.61 – 4.48 (m, 1H), 4.37 (t, *J* = 8.4 Hz, 1H), 4.33 – 4.22 (m, 1H), 3.27 (t, *J* = 8.4 Hz, 1H), 3.24 – 3.14 (m, 1H), 2.93 – 2.69 (m, 1H). APCI [M+H] calc'd = 344.0618, observed = 344.0619
MSU-42772	^{1}H NMR (500 MHz, Chloroform-*d*) δ 11.49 (s, 1H), 7.77 (s, 1H), 7.51 (s, 1H), 7.41 (d, *J* = 8.5 Hz, 1H), 7.18 (dd, *J* = 8.5, 2.0 Hz, 1H), 3.71 (s, 2H), 1.36 (s, 9H). APCI [M+H] calc'd = 298.0775, observed = 298.0782

Table A.3.8 (cont'd)

MSU-42773	^{1}H NMR (500 MHz, DMSO-d_6) δ 12.71 (s, 1H), 7.59 – 7.29 (m, 2H), 7.11 (d, *J* = 8.4 Hz, 1H), 4.71 – 4.43 (m, 2H), 4.39 – 4.12 (m, 2H), 1.85 – 1.39 (m, 6H), 1.37 – 0.99 (m, 5H). APCI [M+H] calc'd = 338.1088, observed = 338.1091
MSU-42774	^{1}H NMR (500 MHz, DMSO-d_6) δ 12.33 (s, 1H), 7.99 (s, 1H), 7.22 (s, 1H), 7.14 (s, 1H), 3.87 (s, 2H), 2.25 (s, 6H), 1.97 (dd, *J* = 5.8, 3.1 Hz, 3H), 1.87 (d, *J* = 2.9 Hz, 6H), 1.58 (s, 5H). APCI [M+H] calc'd = 370.1947, observed = 370.1955
MSU-42828	^{1}H NMR (500 MHz, DMSO-d_6) δ 12.57 (s, 1H), 7.97 (s, 1H), 7.93 (d, *J* = 8.7 Hz, 2H), 7.80 (s, 1H), 7.34 (ddt, *J* = 7.7, 5.5, 3.3 Hz, 2H), 4.52 (s, 2H), 4.12 (p, *J* = 6.6 Hz, 1H), 3.55 – 3.48 (m, 1H), 1.29 (d, *J* = 6.7 Hz, 7H), 1.22 (d, *J* = 6.6 Hz, 6H). APCI [M+H] calc'd = 342.1634 observed = 342.1649
MSU-42829	^{1}H NMR (500 MHz, DMSO-d_6) δ 12.87 (s, 1H), 7.74 (s, 1H), 7.63 (s, 1H), 4.45 (s, 2H), 4.10 – 4.00 (m, 1H), 3.55 – 3.48 (m, 1H), 1.31 – 1.24 (m, 8H), 1.20 (d, *J* = 6.6 Hz, 7H). APCI [M+H] calc'd = 360.0698 observed = 360.0712
MSU-42830	^{1}H NMR (500 MHz, Chloroform-*d*) δ 7.43 (s, 1H), 7.03 (s, 1H), 4.50 (s, 2H), 4.19 (p, *J* = 6.7 Hz, 1H), 3.69 (s, 3H), 3.52 – 3.45 (m, 1H), 2.37 (d, *J* = 11.7 Hz, 6H), 1.42 (d, *J* = 6.8 Hz, 6H), 1.25 (d, *J* = 6.7 Hz, 7H). APCI [M+H] calc'd = 334.1947 observed = 334.1972
MSU-42831	^{1}H NMR (500 MHz, DMSO-d_6) δ 13.22 (d, *J* = 153.4 Hz, 1H), 7.69 – 7.24 (m, 1H), 4.60 – 4.34 (m, 2H), 4.15 – 3.86 (m, 1H), 3.61 – 3.40 (m, 1H), 1.58 – 0.91 (m, 11H). ^{19}F NMR (470 MHz, DMSO-d_6) δ -141.53 – -145.48 (m, 1F), -151.39 – -153.64 (m, 1F), -168.86 – -172.22 (m, 1F). APCI [M+H] calc'd = 346.1195 observed = 346.1209
MSU-42885	^{1}H NMR (500 MHz, DMSO-d_6) δ 12.56 (d, *J* = 42.3 Hz, 1H), 7.57 – 7.25 (m, 3H), 7.18 – 6.80 (m, 4H), 4.41 (d, *J* = 6.3 Hz, 2H), 4.14 – 3.99 (m, 1H), 3.59 – 3.44 (m, 1H), 1.29 (d, *J* = 6.7 Hz, 6H), 1.19 (dd, *J* = 6.1, 2.0 Hz, 6H). APCI [M+H] calc'd = 384.1740 observed = 384.1750
MSU-42886	^{1}H NMR (500 MHz, DMSO-d_6) δ 12.36 (s, 1H), 7.45 – 6.62 (m, 3H), 4.45 – 4.29 (m, 2H), 4.15 – 3.95 (m, 1H), 3.74 (s, 3H), 3.49 (t, *J* = 6.9 Hz, 1H), 1.28 (d, *J* = 6.7 Hz, 6H), 1.18 (d, *J* = 6.5 Hz, 6H). APCI [M+H] calc'd = 322.1583 observed = 322.1529
MSU-42887	^{1}H NMR (500 MHz, DMSO-d_6) δ 12.38 (s, 1H), 7.48 – 6.88 (m, 4H), 4.39 (d, *J* = 3.1 Hz, 2H), 4.06 (tt, *J* = 15.2, 7.0 Hz, 1H), 3.50 (s, 1H), 2.96 (hept, *J* = 7.0 Hz, 1H), 1.43 – 1.10 (m, 16H). APCI [M+H] calc'd = 334.1947 observed = 334.2001

Table A.3.8 (cont'd)

MSU-43066	^{1}H NMR (500 MHz, DMSO-d_6) δ 7.67 (s, 2H), 4.52 (s, 2H), 4.17 (p, *J* = 6.6 Hz, 1H), 3.45 (dd, *J* = 11.9, 5.2 Hz, 1H), 1.27 (d, *J* = 6.7 Hz, 6H), 1.16 – 1.08 (m, 6H). APCI [M-H] calc'd = 390.0451 observed = 390.0444
MSU-43065	^{1}H NMR (500 MHz, DMSO-d_6) δ 11.88 (s, 1H), 7.20 (s, 2H), 4.11 – 3.95 (m, 1H), 3.46 (s, 1H), 2.94 (dd, *J* = 9.0, 6.3 Hz, 2H), 2.78 (dd, *J* = 9.0, 6.3 Hz, 2H), 2.26 (s, 6H), 1.27 (d, *J* = 6.7 Hz, 6H), 1.18 – 1.10 (m, 6H). APCI [M+H] calc'd = 302.2226 observed = 302.2274 m.p. = 182 °C
MSU-43085	^{1}H NMR (500 MHz, DMSO-d_6) δ 12.49 (s, 1H), 7.72 (s, 2H), 4.04 (hept, *J* = 6.8 Hz, 1H), 3.50 (s, 1H), 3.00 (dd, *J* = 8.5, 6.4 Hz, 2H), 2.82 (dd, *J* = 8.5, 6.4 Hz, 2H), 1.25 (d, *J* = 6.7 Hz, 6H), 1.13 (d, *J* = 6.6 Hz, 6H). APCI [M+H] calc'd = 342.1134 observed = 342.1168
MSU-43086	^{1}H NMR (500 MHz, DMSO-d_6) δ 12.56 – 12.25 (m, 1H), 7.63 – 7.37 (m, 2H), 7.11 (ddd, *J* = 12.9, 8.4, 2.0 Hz, 1H), 4.02 (tt, *J* = 11.1, 6.9 Hz, 1H), 3.45 (br s, 1H), 2.98 (dd, *J* = 8.7, 6.4 Hz, 2H), 2.80 (dd, *J* = 8.7, 6.4 Hz, 2H), 1.25 (d, *J* = 6.7 Hz, 6H), 1.12 (d, *J* = 6.6 Hz, 6H). APCI [M+H] calc'd = 308.1524 observed = 308.1550
MSU-43125	^{1}H NMR (500 MHz, DMSO-d_6) δ 11.92 (d, *J* = 26.3 Hz, 1H), 7.00 (s, 1H), 6.71 (s, 1H), 4.05 (p, *J* = 6.6 Hz, 1H), 3.46 (br s, 1H), 2.95 (dd, *J* = 9.0, 6.3 Hz, 2H), 2.78 (t, *J* = 7.6 Hz, 2H), 2.40 (s, 3H), 2.32 (s, 3H), 1.31 – 1.20 (m, 6H), 1.13 (d, *J* = 6.6 Hz, 6H). APCI [M+H] calc'd = 302.2226 observed = 302.2258
MSU-43126	^{1}H NMR (500 MHz, DMSO-d_6) δ 12.72 (d, *J* = 95.0 Hz, 1H), 7.67 – 7.40 (m, 1H), 7.37 – 7.16 (m, 1H), 4.05 (tt, *J* = 13.4, 6.0 Hz, 1H), 3.45 (s, 1H), 3.00 (dd, *J* = 8.3, 6.5 Hz, 2H), 2.82 (q, *J* = 7.4 Hz, 2H), 1.24 (d, *J* = 6.7 Hz, 6H), 1.13 (d, *J* = 6.6 Hz, 6H). APCI [M+H] calc'd = 342.1134 observed = 342.1145
MSU-43127	^{1}H NMR (500 MHz, DMSO-d_6) δ 12.75 (s, 1H), 7.40 (ddd, *J* = 10.3, 6.1, 1.7 Hz, 1H), 4.04 (p, *J* = 6.7 Hz, 1H), 3.46 (br s, 1H), 2.98 (dd, *J* = 8.5, 6.4 Hz, 2H), 2.81 (dd, *J* = 8.6, 6.4 Hz, 2H), 1.24 (d, *J* = 6.7 Hz, 6H), 1.13 (d, *J* = 6.6 Hz, 6H). ^{19}F NMR (470 MHz, DMSO-d_6) δ -143.32, -152.23, -171.93. APCI [M+H] calc'd = 328.1631 observed = 328.1642
MSU-43128	^{1}H NMR (500 MHz, DMSO-d_6) δ 12.83 (s, 1H), 7.75 (s, 1H), 4.05 (dq, *J* = 20.3, 7.1, 6.2 Hz, 1H), 3.45 (s, 1H), 3.02 (t, *J* = 7.4 Hz, 2H), 2.82 (t, *J* = 7.4 Hz, 2H), 1.24 (d, *J* = 6.8 Hz, 6H), 1.13 (d, *J* = 6.6 Hz, 6H). APCI [M+H] calc'd = 376.0744 observed = 376.0759

Table A.3.8 (cont'd)

MSU-43129	^{1}H NMR (500 MHz, DMSO-d_6) δ 12.42 (d, *J* = 17.2 Hz, 1H), 7.68 – 7.33 (m, 2H), 7.26 – 6.98 (m, 1H), 4.04 (p, *J* = 6.7 Hz, 1H), 3.39 (s, 1H), 3.00 (dd, *J* = 8.7, 6.4 Hz, 2H), 2.82 (t, *J* = 7.6 Hz, 2H), 1.26 (d, *J* = 6.7 Hz, 6H), 1.13 (d, *J* = 6.6 Hz, 6H). ^{19}F NMR (470 MHz, DMSO-d_6) δ -57.06 (d, *J* = 21.7 Hz). APCI [M+H] calc'd = 358.1736 observed = 358.1758
MSU-43130	^{1}H NMR (500 MHz, DMSO-d_6) δ 12.69 (d, *J* = 94.9 Hz, 1H), 7.97 – 7.55 (m, 2H), 7.54 – 7.33 (m, 1H), 4.13 – 3.96 (m, 1H), 3.44 (s, 1H), 3.02 (d, *J* = 8.9 Hz, 2H), 2.84 (t, *J* = 7.5 Hz, 2H), 1.25 (d, *J* = 6.7 Hz, 6H), 1.13 (d, *J* = 6.7 Hz, 6H). ^{19}F NMR (470 MHz, DMSO-d_6) δ -58.63 (d, *J* = 25.6 Hz). APCI [M+H] calc'd = 342.1787 observed = 342.1816
MSU-43131	^{1}H NMR (500 MHz, Chloroform-*d*) δ 7.57 – 7.44 (m, 1H), 7.37 – 7.25 (m, 3H), 7.20 (d, *J* = 5.5 Hz, 1H), 7.05 (dt, *J* = 7.3, 1.2 Hz, 1H), 7.03 – 6.91 (m, 3H), 4.02 (p, *J* = 6.7 Hz, 1H), 3.51 (s, 1H), 3.35 – 3.20 (m, 2H), 2.92 – 2.78 (m, 2H), 1.43 (d, *J* = 6.8 Hz, 6H), 1.19 (d, *J* = 6.6 Hz, 6H). APCI [M+H] calc'd = 366.2176 observed = 366.2187
MSU-43132	^{1}H NMR (500 MHz, DMSO-d_6) δ 12.69 (m, 1H), 7.26 – 6.80 (m, 2H), 4.14 – 3.97 (m, 1H), 3.45 (br s, 1H), 2.97 (t, *J* = 7.4 Hz, 2H), 2.81 (q, *J* = 7.9, 7.3 Hz, 2H), 1.25 (d, *J* = 6.7 Hz, 6H), 1.13 (d, *J* = 6.6 Hz, 6H). ^{19}F NMR (470 MHz, DMSO-d_6) δ -118.43 (d, *J* = 9.9 Hz), -118.81 (t, *J* = 9.1 Hz), -120.52 (t, *J* = 9.9 Hz), -125.86 (d, *J* = 11.5 Hz), -126.18 (d, *J* = 10.6 Hz), -127.97 (d, *J* = 10.7 Hz). APCI [M+H] calc'd = 310.1725 observed = 310.1743
MSU-43133	^{1}H NMR (500 MHz, DMSO-d_6) δ 7.76 (d, *J* = 2.1 Hz, 1H), 7.69 (d, *J* = 8.6 Hz, 1H), 7.37 (dd, *J* = 8.6, 2.1 Hz, 1H), 4.05 (p, *J* = 6.7 Hz, 1H), 3.55 (s, 1H), 3.10 (t, *J* = 7.1 Hz, 2H), 2.87 (t, *J* = 7.1 Hz, 2H), 1.23 (d, *J* = 6.7 Hz, 6H), 1.15 (d, *J* = 6.6 Hz, 6H). APCI [M+H] calc'd = 309.1364 observed = 309.1382
MSU-43134	^{1}H NMR (500 MHz, DMSO-d_6) δ 13.12 – 12.51 (m, 1H), 8.22 (s, 1H), 8.00 (d, *J* = 23.9 Hz, 1H), 4.04 (hept, *J* = 6.3 Hz, 1H), 3.45 (s, 1H), 3.01 (t, *J* = 7.4 Hz, 2H), 2.84 (dd, *J* = 8.5, 6.4 Hz, 2H), 1.24 (d, *J* = 6.7 Hz, 6H), 1.13 (d, *J* = 6.6 Hz, 6H). APCI [M+H] calc'd = 309.1476 observed = 309.1494
MSU-43165	^{1}H NMR (500 MHz, DMSO-d_6) δ 10.86 (s, 1H), 7.32 (d, *J* = 36.8 Hz, 2H), 6.85 (s, 1H), 4.11 (s, 2H), 3.91 (s, 1H), 3.50 (s, 1H), 1.30 (d, *J* = 6.7 Hz, 6H), 1.16 (d, *J* = 6.6 Hz, 6H). ESI (+) calc'd for [M+Na] = 365.0911, found = 365.0917.

Table A.3.8 (cont'd)

MSU-43166	^{1}H NMR (500 MHz, DMSO-d_6) δ 13.41 (s, 1H), 4.04 (p, *J* = 6.8 Hz, 1H), 3.45 (s, 1H), 3.00 (t, *J* = 7.4 Hz, 2H), 2.83 (t, *J* = 7.4 Hz, 2H), 1.24 (d, *J* = 6.7 Hz, 6H), 1.14 (d, *J* = 6.6 Hz, 6H). ^{19}F NMR (470 MHz, DMSO-d_6) δ -156.49 (d, *J* = 408.5 Hz), -168.34 (d, *J* = 886.4 Hz). HRMS ESI (+) calc'd for [M+Na] = 368.1361, found = 368.1344.
MSU-43167	^{1}H NMR (500 MHz, DMSO-d_6) δ 12.53 (s, 1H), 7.77 (s, 1H), 7.66 (s, 1H), 3.94 (p, *J* = 6.7 Hz, 1H), 3.46 (br s, 1H), 2.83 (t, *J* = 7.5 Hz, 2H), 2.33 (t, *J* = 7.4 Hz, 2H), 1.95 (p, *J* = 7.5 Hz, 2H), 1.26 (d, *J* = 6.7 Hz, 6H), 1.08 (d, *J* = 6.6 Hz, 6H). HRMS ESI (+) calc'd for [M+H] = 356.1292, found = 356.1303.
MSU-43171	^{1}H NMR (500 MHz, DMSO-d_6) δ 12.52 (d, *J* = 48.0 Hz, 1H), 7.54 – 7.31 (m, 1H), 7.23 – 7.01 (m, 2H), 4.04 (ddd, *J* = 18.3, 12.4, 6.9 Hz, 1H), 3.46 (br s, 1H), 3.01 (dd, *J* = 8.7, 6.4 Hz, 2H), 2.82 (dd, *J* = 8.6, 6.4 Hz, 2H), 1.26 (d, *J* = 6.7 Hz, 6H), 1.14 (d, *J* = 6.6 Hz, 6H). HRMS ESI (+) calc'd for [M+H] = 308.1525, found = 308.1546.
MSU-43172	^{1}H NMR (500 MHz, DMSO-d_6) δ 12.47 (s, 1H), 7.85 (s, 2H), 4.03 (p, *J* = 6.7 Hz, 1H), 3.45 (s, 1H), 2.99 (dd, *J* = 8.5, 6.4 Hz, 2H), 2.81 (dd, *J* = 8.5, 6.5 Hz, 2H), 1.25 (d, *J* = 6.7 Hz, 6H), 1.13 (d, *J* = 6.6 Hz, 6H). HRMS ESI (+) calc'd for [M+H] = 430.0125, found = 430.0125.
MSU-43173	^{1}H NMR (500 MHz, DMSO-d_6) δ 12.48 (s, 1H), 7.78 (dd, *J* = 57.7, 32.5 Hz, 2H), 4.03 (dd, *J* = 13.5, 7.0 Hz, 1H), 3.46 (br s, 1H), 2.98 (t, *J* = 7.3 Hz, 2H), 2.80 (t, *J* = 7.4 Hz, 2H), 1.24 (d, *J* = 6.7 Hz, 6H), 1.12 (d, *J* = 6.6 Hz, 6H). HRMS ESI (+) calc'd for [M+H] = 386.0631, found = 386.0627.
MSU-43175	1H NMR (500 MHz, DMSO-d6) δ 12.58 (d, J = 90.6 Hz, 1H), 7.84 – 7.63 (m, 2H), 3.41 (q, J = 5.5 Hz, 4H), 3.02 (t, J = 7.3 Hz, 2H), 2.86 (q, J = 8.2, 7.3 Hz, 2H), 1.56 (q, J = 5.8 Hz, 2H), 1.52 – 1.44 (m, 2H), 1.38 (dd, J = 10.9, 5.7 Hz, 2H). HRMS ESI (+) calc'd for [M+H] = 326.0823, found = 326.0822.
MSU-43176	1H NMR (500 MHz, DMSO-d6) δ 12.49 (s, 1H), 7.72 (d, J = 12.0 Hz, 2H), 4.54 (s, 1H), 4.15 (s, 1H), 3.11 – 2.86 (m, 3H), 3.37 (1H, s), 2.76 (dd, J = 15.9, 8.1 Hz, 1H), 1.74 (qd, J = 12.9, 11.4, 5.4 Hz, 1H), 1.61 – 1.34 (m, 5H), 1.29 – 1.14 (m, 3H), 1.06 (d, J = 7.1 Hz, 3H). HRMS ESI (+) calc'd for [M+H] = 354.1136, found = 354.1140.
MSU-43177	1H NMR (500 MHz, DMSO-d6) δ 12.49 (s, 1H), 7.76 (s, 1H), 7.68 (s, 1H), 3.44 (dd, J = 12.7, 7.7 Hz, 4H), 3.02 (t, J = 7.2 Hz, 2H), 2.86 (t, J = 7.2 Hz, 2H), 2.27 (t, J = 5.0 Hz, 2H), 2.20 (t, J = 5.2 Hz, 2H), 2.15 (s, 3H). HRMS ESI (+) calc'd for [M+H] = 341.0932, found = 341.0928.

Table A.3.8 (cont'd)

MSU-43186	1H NMR (500 MHz, DMSO-d6) δ 12.49 (s, 1H), 7.71 (d, J = 32.6 Hz, 2H), 3.45 (t, J = 6.1 Hz, 2H), 3.41 – 3.37 (m, 2H), 3.03 (t, J = 7.2 Hz, 2H), 2.85 (t, J = 7.3 Hz, 2H), 1.67 (p, J = 5.9 Hz, 2H), 1.58 – 1.52 (m, 2H), 1.52 – 1.40 (m, 4H). ESI (+) calc'd for [M+H] = 340.0979, found = 340.0977.
MSU-43187	^{1}H NMR (500 MHz, DMSO-d_6) δ 13.10 (s, 1H), 7.91 (s, 1H), 7.81 (s, 1H), 7.51 (d, *J* = 15.5 Hz, 1H), 7.27 (d, *J* = 15.5 Hz, 1H), 4.17 (s, 1H), 3.74 (s, 1H), 1.31 (d, *J* = 6.6 Hz, 6H), 1.23 (d, *J* = 6.8 Hz, 6H). ESI (+) calc'd for [M+H] = 340.0979, found = 340.1025.
MSU-43185	^{1}H NMR (500 MHz, DMSO-d_6) δ 12.48 (s, 1H), 7.71 (d, *J* = 20.2 Hz, 2H), 3.13 (d, *J* = 7.6 Hz, 2H), 3.08 (d, *J* = 7.5 Hz, 2H), 3.04 (t, *J* = 7.2 Hz, 2H), 2.85 (t, *J* = 7.2 Hz, 2H), 1.89 (tp, *J* = 13.7, 6.8 Hz, 2H), 0.86 (d, *J* = 6.6 Hz, 6H), 0.74 (d, *J* = 6.6 Hz, 6H). HRMS ESI (+) calc'd for [M+H] = 370.1449, found = 370.1471.
MSU-43249	1H NMR (500 MHz, DMSO-d6) δ 11.96 (s, 1H), 7.56 – 7.41 (m, 2H), 7.11 (dt, J = 6.0, 3.6 Hz, 2H), 6.59 (t, J = 5.4 Hz, 1H), 4.39 (d, J = 5.4 Hz, 2H), 3.74 (p, J = 6.9 Hz, 2H), 1.18 (d, J = 6.7 Hz, 12H). HRMS ESI (+) calc'd for [M+H] = 275.1868, found = 275.1881.
MSU-43248	1H NMR (500 MHz, DMSO-d6) δ 12.23 (s, 1H), 7.78 (s, 1H), 7.71 (s, 1H), 6.66 (t, J = 5.4 Hz, 1H), 4.38 (d, J = 5.5 Hz, 2H), 3.73 (p, J = 5.7 Hz, 2H), 1.18 (d, J = 6.7 Hz, 12H). HRMS ESI (+) calc'd for [M+H] = 343.1088, found = 343.1109.
MSU-43247	1H NMR (500 MHz, DMSO-d6) δ 10.87 (s, 1H), 7.24 (s, 1H), 7.00 (s, 1H), 3.09 (t, J = 6.4 Hz, 2H), 1.75 – 1.63 (m, 4H), 1.63 – 1.48 (m, 2H), 1.23 – 1.06 (m, 4H), 0.96 – 0.84 (m, 2H). HRMS ESI (+) calc'd for [M+H] = 298.0874, 298.0874.
MSU-43170	1H NMR (500 MHz, DMSO-d6) δ 12.37 (s, 1H), 7.71 – 7.38 (m, 2H), 5.14 (s, 2H), 3.83 (p, J = 6.7 Hz, 1H), 3.50 (dt, J = 13.9, 4.8 Hz, 1H), 1.23 (dd, J = 39.5, 6.6 Hz, 12H). HRMS ESI (+) calc'd for [M+H] = 344.0928, 344.0941.
MSU-43246	1H NMR (500 MHz, DMSO-d6) δ 13.58 (s, 1H), 7.94 (d, J = 190.5 Hz, 2H), 3.03 (d, J = 6.9 Hz, 2H), 1.94 (ddt, J = 18.2, 10.8, 3.2 Hz, 1H), 1.63 (dtd, J = 24.9, 14.4, 7.4 Hz, 5H), 1.28 – 1.07 (m, 3H), 1.01 (qd, J = 13.8, 13.1, 3.8 Hz, 2H). HRMS ESI (+) calc'd for [M+H] = 311.0714, found = 311.0717.

Table A.3.8 (cont'd)

MSU-43245	1H NMR (500 MHz, DMSO-d6) δ 8.43 – 8.04 (m, 2H), 8.00 – 7.89 (m, 1H), 5.46 (d, J = 16.7 Hz, 2H), 3.23 (t, J = 7.3 Hz, 2H), 3.11 (dd, J = 12.9, 7.5 Hz, 2H), 2.09 – 1.98 (m, 1H), 1.93 (tt, J = 13.6, 6.0 Hz, 1H), 0.95 (t, J = 6.1 Hz, 6H), 0.80 (t, J = 6.2 Hz, 6H). HRMS ESI (+) calc'd for [M+H] = 356.1292, found = 356.1304.
MSU-43285	1H NMR (500 MHz, DMSO-d6) δ 13.22 (s, 1H), 7.97 – 7.72 (m, 2H), 3.18 (d, J = 7.5 Hz, 4H), 2.14 – 1.94 (m, 2H), 0.94 (d, J = 6.6 Hz, 6H), 0.83 (d, J = 6.5 Hz, 6H). HRMS ESI (+) [M+H] calc'd = 374.0855, found = 374.0856
MSU-43286	1H NMR (500 MHz, DMSO-d6) δ 7.40 (s, 1H), 7.06 (s, 1H), 6.93 (s, 2H), 3.38 (br s, 2H), 2.96 (dd, J = 13.7, 7.8 Hz, 2H), 1.97 (s, 2H), 0.82 (s, 12H). HRMS ESI (+) [M+H] calc'd = 357.1243, found = 357.1265
MSU-43287	1H NMR (500 MHz, Chloroform-d) δ 7.46 (s, 1H), 7.12 (s, 1H), 5.65 – 5.47 (m, 2H), 3.75 (s, 2H), 3.32 (ddd, J = 13.3, 8.4, 4.3 Hz, 2H), 2.00 – 1.48 (m, 12H). HRMS ESI (+) [M+H] calc'd = 327.0774, found = 327.0790
MSU-43288	1H NMR (500 MHz, DMSO-d6) δ 8.00 – 7.10 (m, 4H), 5.01 (s, 1H), 2.14 – 1.10 (m, 10H). HRMS ESI (+) [M+H] calc'd = 328.0614, found = 328.0623
MSU-43325	1H NMR (500 MHz, DMSO-d6) δ 7.37 (s, 1H), 7.10 (s, 1H), 6.87 (s, 2H), 3.61 (s, 2H), 1.29 (s, 12H). HRMS ESI (+) calc'd for [M+H] = 329.0932, found = 329.0947
MSU-43388	1H NMR (500 MHz, DMSO-d6) δ 12.58 (s, 1H), 7.83 – 7.55 (m, 2H), 4.03 (p, J = 6.4 Hz, 1H), 3.47 (d, J = 17.4 Hz, 1H), 3.00 (t, J = 7.4 Hz, 2H), 2.81 (dd, J = 8.4, 6.5 Hz, 2H), 1.24 (d, J = 6.7 Hz, 6H), 1.12 (d, J = 6.6 Hz, 6H). 19F NMR (470 MHz, DMSO-d6) δ -57.34 (d, J = 24.5 Hz). HRMS ESI (+) Calc'd for [M+Na] = 414.1172, found = 414.1182.
MSU-43389	1H NMR (500 MHz, DMSO-d6) δ 12.59 (s, 1H), 8.82 (d, J = 2.0 Hz, 1H), 7.85 (dd, J = 19.5, 11.5 Hz, 2H), 7.71 (s, 1H), 7.33 – 7.15 (m, 2H), 4.53 (d, J = 5.6 Hz, 2H). 19F NMR (470 MHz, DMSO-d6) δ -144.58 – -144.89 (m), -149.78, -161.35 – -161.71 (m). HRMS ESI (+) Calc'd for [M+Na] = 411.0004, found = 411.0014.

Table A.3.8 (cont'd)

MSU-43390	1H NMR (500 MHz, DMSO-d6) δ 12.75 (d, J = 12.4 Hz, 1H), 8.00 – 7.69 (m, 2H), 4.03 (p, J = 6.7 Hz, 1H), 3.45 (s, 1H), 3.03 (q, J = 7.2 Hz, 2H), 2.83 (t, J = 7.4 Hz, 2H), 1.24 (d, J = 6.7 Hz, 6H), 1.13 (d, J = 6.6 Hz, 6H). 19F NMR (470 MHz, DMSO-d6) δ -59.04, -59.20 (d, J = 4.0 Hz), -59.62 (d, J = 3.7 Hz). HRMS ESI (+) Calc'd for [M+Na] = 398.1223, found = 398.1245.
MSU-43391	1H NMR (500 MHz, Chloroform-d) δ 8.01 (s, 1H), 7.97 (d, J = 2.1 Hz, 1H), 7.68 (dd, J = 8.4, 2.1 Hz, 1H), 7.48 (d, J = 8.4 Hz, 1H), 5.24 (s, 2H), 4.00 (p, J = 6.7 Hz, 1H), 3.57 (s, 1H), 1.40 (d, J = 6.8 Hz, 6H), 1.29 (d, J = 6.7 Hz, 6H). HRMS ESI (+) Calc'd for [M+Na] = 377.0912, found = 377.0938.
MSU-43414	1H NMR (500 MHz, DMSO-d6) δ 12.46 (s, 1H), 8.43 (t, J = 5.4 Hz, 1H), 7.75 (s, 2H), 4.43 (d, J = 5.7 Hz, 2H), 2.04 (s, 2H), 0.94 (s, 9H). HRMS ESI (+) Calc'd for [M+H] = 314.0823, found = 314.0824.

Table A.4.1. Half maximal effective concentrations of compounds that made screen cutoffs

Compound Name	Intracellular EC_{50} (μM)	Cytotox (CC_{50}, μM)	S.I. (Approx)
3-A15	< 0.1	> 32	320.0
3-B12	< 0.1	> 80	800.0
3-B16	4.915	> 80	16.3
3-C09	< 0.1	> 80	800.0
3-C19	4.283	> 80	18.7
3-D09	< 0.1	> 32	320.0
3-D17	0.907	> 80	88.2
3-E14	< 0.1	> 80	800.0
3-E21	< 0.1	> 80	800.0
3-F14	1.766	> 80	45.3
3-F17	1.927	> 80	41.5
3-F18	< 0.1	> 80	800.0
3-F21	< 0.1	> 80	800.0
3-G10	< 0.3	> 80	266.7
3-G16	< 0.1	> 80	800.0
3-G17	< 0.32	> 80	250.0
3-H10	< 0.1	> 80	800.0
3-H12	< 0.1	> 80	800.0
3-H14	< 0.1	> 80	800.0
3-H17	< 0.1	> 80	800.0
3-H22	< 0.3	> 80	266.7
3-I11	1.84	> 80	43.5
3-I12	< 0.1	> 80	800.0
3-I13	< 0.1	> 80	800.0
3-I15	< 0.1	> 80	800.0
3-I18	4.59	> 80	17.4
3-I19	< 0.1	> 80	800.0
3-I21	10.78	> 80	7.4
3-I23	< 0.1	> 80	800.0
3-J10	1.814	> 32	17.6
3-J11	1.906	> 80	42.0
3-J15	< 0.1	> 80	800.0
3-J19	< 0.1	> 80	800.0
3-J20	0.856	> 80	93.5
3-L11	1.607	> 80	49.8
3-L17	< 0.1	> 80	800.0
3-L20	0.7517	> 80	106.4
3-L22	9.59	> 80	8.3
3-M09	< 0.1	> 80	800.0
3-M11	< 0.1	> 80	800.0
3-N13	< 0.1	> 80	800.0
3-N20	< 0.1	> 80	800.0
3-N22	< 0.3	> 80	266.7
3-N24	< 0.1	> 80	800.0

Table A.4.1 (cont'd)

3-O11	< 0.1	> 80	800.0
3-O14	< 0.1	> 80	800.0
3-O18	< 0.1	> 80	800.0
3-O24	< 0.1	> 80	800.0
3-P24	1.997	> 80	40.1
4-A15	< 0.1	> 80	800.0
4-A16	0.341	> 32	93.8
4-A19	0.6465	> 80	123.7
4-A20	3.621	29.41	8.1
4-B08	< 0.3	> 32	106.7
4-B12	12.95	> 80	6.2
4-B13	< 0.1	> 80	800.0
4-B14	0.3127	> 80	255.8
4-B16	< 0.1	> 80	800.0
4-B18	< 0.1	> 80	800.0
4-B20	< 0.1	> 80	800.0
4-B21	0.3099	>12.8	42.6
4-B22	< 0.1	37.6	376
4-C08	< 0.1	> 32	320.0
4-C09	1.00106	> 80	79.9
4-C11	0.1028	> 32	311.3
4-C12	1.801	> 12.8	7.1
4-C14	< 0.1	> 80	800.0
4-C18	12.29	> 80	6.5
4-C20	< 0.1	> 80	800.0
4-C22	< 0.1	> 80	800.0
4-D13	< 0.1	> 80	800.0
4-D16	< 0.1	> 80	800.0
4-D20	< 0.1	> 80	800.0
4-D22	< 0.3	> 80	266.7
4-D24	0.1179	> 32	271.4
4-E10	0.6134	> 12.8	20.9
4-E13	< 0.8	> 80	100.0
4-E16	0.3301	> 80	242.4
4-E18	16.51	> 80	4.8
4-E20	0.1174	> 80	681.4
4-F10	< 0.8	> 80	100.0
4-F22	< 0.3	30.36	101.2
4-F23	< 0.1	> 80	800.0
4-G10	0.2993	> 80	267.3
4-G11	<0.8	> 32	40
4-G12	< 0.1	> 80	800.0
4-G14	< 0.1	> 80	800.0
4-G17	< 0.1	> 80	800.0
4-G18	< 0.1	> 80	800.0
4-G22	< 0.1	> 80	800.0
4-G24	1.79	> 80	44.7
4-H10	< 0.1	> 80	800.0

Table A.4.1 (cont'd)

4-H19	< 0.3	> 80	266.7
4-H20	< 0.1	> 80	800.0
4-H21	< 0.3	> 32	106.7
4-H22	< 0.1	> 80	800.0
4-I11	< 0.1	> 80	800.0
4-I13	< 0.3	> 80	266.7
4-I15	< 0.1	> 80	800.0
4-I16	0.3464	> 80	230.9
4-I17	< 0.1	> 80	800.0
4-I18	0.2526	> 80	316.7
4-I21	0.4378	> 80	182.7
4-I22	< 0.1	> 80	800.0
4-J11	< 0.1	> 80	800.0
4-J18	< 12.8	> 80	6.3
4-J20	< 0.1	> 80	800.0
4-J24	< 0.1	> 80	800.0
4-K12	< 0.1	> 80	800.0
4-K14	< 80	> 80	1.0
4-K20	< 0.1	> 80	800.0
4-K24	< 0.1	> 80	800.0
4-L12	< 0.1	> 80	800.0
4-L14	< 0.1	> 80	800.0
4-L23	< 0.1	> 80	800.0
4-L24	< 0.1	> 80	800.0
4-M12	< 0.1	> 80	800.0
4-M13	< 0.1	> 80	800.0
4-M14	< 0.1	> 80	800.0
4-M22	0.3113	> 32	102.8
4-N12	0.8469	> 12.8	15.1
4-N13	< 0.1	> 80	800.0
4-N16	< 0.3	> 80	266.7
4-N17	< 0.8	> 80	100.0
4-N19	0.6651	> 80	120.3
4-N24	< 0.1	> 80	800.0
4-O12	12.3	> 80	6.5
4-O13	< 0.1	> 80	800.0
4-O14	< 0.8	30.31	37.9
4-O18	0.2027	> 80	394.7
4-O19	< 0.3	48.11	160.4
4-O20	< 0.1	> 80	800.0
4-O23	< 0.8	> 80	100.0
4-P22	< 0.1	> 80	800.0
4-P23	0.3119	> 80	256.5
5-A19	< 0.3	> 80	266.7
5-A21	2.825	> 80	28.3
5-A24	4.719	> 32	6.8
5-B10	< 0.1	79.74	797.4
5-B12	0.9304	> 80	86.0

Table A.4.1 (cont'd)

5-B14	11.83	> 80	6.8
5-B24	0.9913	32.1	32.4
5-C08	< 5	> 80	16.0
5-C14	< 2.1	> 80	38.1
5-C16	< 0.1	> 80	800.0
5-C17	4.028	> 32	7.9
5-C18	1.93	> 80	41.5
5-C20	5.243	> 80	15.3
5-C23	< 0.1	> 80	800.0
5-D15	0.3455	> 80	231.5
5-D16	5.03	> 80	15.9
5-D17	1.968	> 80	40.7
5-D21	10.75	> 80	7.4
5-E09	< 0.1	> 80	800.0
5-E10	1.164	> 80	68.7
5-E12	< 0.1	> 80	800.0
5-E14	0.9085	> 80	88.1
5-E15	< 0.1	> 80	800.0
5-E18	0.5297	> 80	151.0
5-E22	< 0.1	> 80	800.0
5-E23	1.507	> 80	53.1
5-E24	< 0.1	> 80	800.0
5-F10	< 0.1	> 80	800.0
5-F11	< 0.1	> 80	800.0
5-F13	< 0.3	> 80	266.7
5-F14	< 0.1	> 80	800.0
5-F16	4.491	> 80	17.8
5-F17	< 0.1	> 80	800.0
5-F19	0.7002	> 80	114.3
5-F20	4.298	> 80	18.6
5-G10	< 0.1	> 80	800.0
5-G13	4.299	> 80	18.6
5-G17	< 0.1	> 80	800.0
5-G18	0.6496	> 80	123.2
5-G20	10.61	> 80	7.5
5-H10	4.2	> 80	19.0
5-H11	1.484	> 80	53.9
5-H12	12.15	> 80	6.6
5-H13	0.6811	> 80	117.5
5-H14	0.2219	> 80	360.5
5-H19	< 0.8	> 80	100.0
5-H20	47.63	> 80	1.7
5-H21	6.406	> 80	12.5
5-H23	< 0.1	> 80	800.0
5-I13	4.443	> 80	18.0
5-I14	0.7557	> 80	105.9
5-I17	0.6837	> 80	117.0
5-I19	< 0.8	> 80	100.0

Table A.4.1 (cont'd)

5-I22	1.961	> 80	40.8
5-I24	5.17	> 80	15.5
5-J10	140.8	40.49	0.3
5-J11	4.542	> 80	17.6
5-J14	< 0.1	> 80	800.0
5-J17	10.94	> 80	7.3
5-K10	1.836	> 32	17.4
5-K12	< 0.1	> 80	800.0
5-K14	0.2299	> 80	348.0
5-K15	0.7991	> 80	100.1
5-K16	< 0.1	> 80	800.0
5-K17	< 0.1	> 80	800.0
5-K20	< 0.1	> 80	800.0
5-K23	< 0.1	> 80	800.0
5-L16	< 0.1	> 80	800.0
5-L21	< 0.8	> 80	100.0
5-L23	< 0.1	> 80	800.0
5-M12	1.846	> 80	43.3
5-M21	< 0.1	> 80	800.0
5-M22	4.176	> 80	19.2
5-M23	< 0.1	> 80	800.0
5-N22	< 0.1	> 80	800.0
5-O14	0.8547	> 80	93.6
5-O24	5.801	> 80	13.8
5-P24	2.787	83.04	29.8

S.I. – selective index (EC_{50}/CC_{50}), Approx – approximate values not accounting for > or < values

Table A.4.2. *M. tuberculosis mmpL3* mutants used in pooled mutant cross resistance study

Compound Background	Mtb Strain Background	Strain	SNP Location	Quality Score	Gene	Nucleotide Change	Amino Acid Substitution
HC2060	Erdman	1A	245506	5308	*mmpL3*	GTG --> **A**TG	V643M
	Erdman	3B	245501	4710	*mmpL3*	TTC --> TT**G**	F644L
	Erdman	4A	245733	3840	*mmpL3*	CTG --> C**C**G	L567P
	Erdman	5B	245501	4807	*mmpL3*	TTC --> TT**A**	F644N
	Erdman	6C	245349	4795	*mmpL3*	ATG --> A**C**G	M695T
HC2091	CDC 1551	3A	245488	3441	*mmpL3*	ATG --> **C**TG	M649L
	CDC 1551	5A	245424	2685	*mmpL3*	ACC --> A**A**C	T670L
	CDC 1551	23A	245335	2615	*mmpL3*	GCC --> **A**CC	A700T
HC2149	Erdman	1A	245487	5798	*mmpL3*	ATG --> A**C**G	M649T
	Erdman	3A	247313	5895	*mmpL3*	CAG --> CA**T**	Q40H
	Erdman	11C	246316	5127	*mmpL3*	CGG --> **T**GG	R373W
	Erdman	15A	246501	3836	*mmpL3*	ACC --> A**T**C	T311I
	Erdman	16A	246537	3854	*mmpL3*	CTG --> C**A**G	L299Q
HC2169	Erdman	1B	245662	7164	*mmpL3*	TCG --> **A**CG	S591T
	Erdman	14A	246579	4739	*mmpL3*	GTG --> G**G**G	V285G
	Erdman	13A	246675	4585	*mmpL3*	GGG --> G**A**G	G253E
	Erdman	7A	246678	6076	*mmpL3*	TAC --> T**G**C	Y252C
	Erdman	16A	246702	5280	*mmpL3*	ATC --> A**C**C	I244T
HC2184	Erdman	1B	245355	5122	*mmpL3*	GAC --> G**G**C	L693P
	Erdman	6B	245661	5719	*mmpL3*	TCG --> T**A**G	S591I
	Erdman	8A	246678	5654	*mmpL3*	ATG --> A**C**G	I585S
	Erdman	12B	245338	5281	*mmpL3*	GAC --> **T**AC	L699M
	Erdman	13B	245448	5121	*mmpL3*	CGC --> C**T**C	A662E
	Erdman	20A	246714	3800	*mmpL3*	CAC--> C**G**C	V240A

Mtb – *M. tuberculosis*, SNP – single nucleotide polymorphism

Table A.4.3. Results of *mmpL3* mutant screen

Compound Name	*mmpL3* Fold Resistance			Follow the Three MmpL3 Descriptors (Yes / No)	MmpL3 Inhibitor Chemical Class	% GI at 12.8 µM	% Tox at 12.8 µM	*ex vivo* % GI at 12.8 µM
	5.1 µM	12.8 µM	32 µM					
5-A15	1.5	0.5	4.1	Yes	Amide	6.0	N.D.	2.8
4-G15	3.1	0.8	24.3	Yes	Amide	5.0	-50.3	100.2
5-O13	1.6	1.3	5.1	Yes	Amide	19.5	N.D.	100.0
5-P15	1.9	3.6	16.5	Yes	Amide	30.2	94.9	94.7
4-L13	7.3	0.3	2.5	Yes	Amide	3.7	-11.7	97.5
4-B19	2.3	16.3	3.2	Yes	Amide	49.0	11.1	85.2
4-K12	5.3	1.9	1.4	Yes	Amide	87.7	-13.6	99.4
4-G04	1.7	1.4	1.2	Yes	Amide	87.0	99.9	99.8
3-K23	18.9	1.5	0.8	Yes	Amide	15.3	24.1	95.5
3-O06	2.9	1.5	1.3	Yes	Amide	52.5	N.D.	44.0
4-N15	0.0	2.1	5.8	Yes	Amide	19.7	13.0	96.8
5-G15	1.9	4.3	5.7	Yes	Amide	10.7	N.D.	97.7
5-N16	1.7	3.1	2.6	Yes	Amide	14.1	41.0	96.5
5-P17	3.5	7.4	9.2	Yes	Amide	20.1	N.D.	94.3
6-H05	352.5	2.8	4.2	Yes	Amide	91.1	N.D.	88.3
5-N19	1.4	1.0	2.2	Yes	Amide	32.9	38.6	46.6
5-L17	8.9	1.7	3.4	Yes	Amide	14.1	N.D.	97.8
5-P13	1.8	3.0	3.2	Yes	Amide	28.9	N.D.	99.4
4-I17	3.6	3.1	3.6	Yes	Amide	77.7	N.D.	98.0
4-P24	1.6	1.4	1.9	Yes	Amide	25.0	N.D.	96.6
3-E22	1.5	1.5	1.0	Yes	Amide	34.3	-6.5	95.8
3-N18	2.5	4.9	0.9	Yes	Amide	58.6	N.D.	-5.7
5-G05	0.6	11.0	1.6	Yes	Amide	15.4	N.D.	72.8
4-H21	2.9	1.7	1.1	Yes	Benzithiazole	77.0	8.8	96.8
4-L10	1.8	2.1	1.1	Yes	Benzithiazole	31.7	26.9	98.2
5-P05	1.7	1.4	2.5	Yes	DA-5-like	100.4	N.D.	85.5
5-I18	1.7	0.4	9.7	Yes	Diamine	3.9	-52.9	93.1
4-O23	1.1	1.4	51.6	Yes	Diamine	112.3	-20.6	99.5
4-A20	1.7	1.5	0.9	Yes	Guanidine	80.3	-25.7	97.0
3-I06	3.0	1.4	1.2	Yes	Guanidine	93.0	99.6	98.0
4-P04	4.2	3.6	1.0	Yes	HC2032-like	75.0	99.9	68.9
5-K12	1.2	1.5	1.3	Yes	HC2134-like	66.7	N.D.	88.9
4-O08	1.7	0.9	1.5	Yes	ICA	16.3	N.D.	94.7
5-P22	4.4	1.8	35.8	No	N/A	24.2	N.D.	57.5
5-P07	0.9	1.5	1.5	No	N/A	18.8	99.8	84.2
3-M10	3.2	1.7	1.0	No	N/A	91.7	57.5	60.0
5-P20	1.6	19.8	1.0	No	N/A	65.3	84.7	97.8
4-H04	1.7	1.3	0.7	No	N/A	71.7	99.9	58.2
5-A03	1.4	1.3	1.1	No	N/A	112.5	95.3	90.2
4-I20	2.0	1.0	1.6	No	N/A	23.0	7.0	77.3
5-H16	9.2	0.7	13.1	No	N/A	7.3	0.3	-792.5
4-E14	1.7	1.5	0.8	No	N/A	48.3	75.8	83.8
4-L22	2.3	3.6	2.4	No	N/A	15.0	N.D.	67.1

Table A.4.3 (cont'd)

5-G08	0.8	10.0	1.9	No	N/A	45.8	96.5	94.3
5-F17	1.7	1.4	1.0	No	N/A	52.5	-17.4	100.0
5-N10	4.2	4.3	1.4	No	N/A	41.7	69.7	-153.5
3-O15	0.1	2.2	1.5	No	N/A	62.6	-51.9	-120.1
5-P23	3.6	1.5	1.4	No	N/A	49.1	N.D.	95.3
4-A17	1.4	7.7	1.8	No	N/A	32.3	6.8	81.4
5-B07	1.4	1.5	1.4	No	N/A	15.4	N.D.	-115.2
5-A06	0.9	1.4	1.4	No	N/A	69.4	79.1	-94.6
4-F18	10.9	0.1	3.3	No	N/A	1.0	-34.2	85.3
5-K13	2.5	5.0	3.1	No	N/A	19.5	7.0	39.3
4-N07	2.8	0.4	11.6	No	N/A	0.3	99.3	63.1
6-A03	1.7	1.5	1.4	No	N/A	111.7	98.5	43.9
5-K24	1.1	1.5	1.4	No	N/A	55.2	18.9	75.1
5-P21	1.9	0.5	3.5	No	N/A	1.9	87.7	23.8
5-N07	2.3	3.3	2.9	No	N/A	55.2	99.1	83.3
4-N09	2.1	0.9	1.4	No	N/A	54.3	84.5	99.1
3-D18	18.3	0.6	1.8	No	N/A	4.5	16.6	96.0
3-B24	2.0	2.4	2.2	No	N/A	32.2	4.2	-60.3
5-A10	2.3	27.9	2.7	No	N/A	19.5	N.D.	38.0
3-O10	1.7	1.3	0.9	No	N/A	102.5	72.1	97.7
5-O14	1.5	2.4	0.5	No	N/A	58.6	N.D.	99.3
4-L16	4.1	0.1	2.3	Yes	Novel	1.0	7.7	98.8
5-H12	1.6	2.1	1.1	Yes	Novel	112.5	-57.9	74.7
4-P11	3.1	177.0	2.7	Yes	Novel	17.7	71.1	42.8
3-O23	2.7	0.7	1.5	Yes	Novel	20.7	-6.8	-31.7
4-L15	0.1	4.3	1.4	Yes	Novel	44.3	-23.8	98.3
4-J13	4.2	35.4	2.3	Yes	Novel	17.7	-64.8	92.2
4-K11	60.6	1.4	0.9	Yes	Pyrazole	56.3	54.1	15.2
5-L04	1.7	4.3	1.3	Yes	Spiro-like	85.6	99.9	99.9
4-E18	2.7	2.0	1.3	Yes	Sulfonamide	51.0	-26.5	35.0
4-A10	2.0	1.8	1.4	Yes	Sulfonamide	54.3	48.3	65.1
5-O19	6.7	4.8	2.3	Yes	Sulfonamide	18.8	64.9	73.7
4-O05	2.1	1.6	1.1	Yes	Sulfonamide	43.7	100.0	62.2
4-J08	4.0	1.6	1.1	Yes	Sulfonamide	39.7	N.D.	63.6
5-A09	2.2	3.8	2.7	Yes	Sulfonamide	53.9	93.9	44.3
4-H17	4.3	6.4	0.9	Yes	Sulfonamide	29.0	-44.0	80.4
5-H05	2.8	1.9	1.5	Yes	Sulfonamide	55.2	N.D.	-52.0
5-L07	1.9	1.7	1.9	Yes	Sulfonamide	47.8	99.4	53.7
4-B10	2.8	1.9	1.2	Yes	Sulfonamide	57.7	47.0	57.9
3-N13	3.9	1.8	0.7	No	TAC-like	65.3	N.D.	97.4
4-N19	1.5	1.6	1.0	No	TAC-like	104.3	-3.3	71.4
4-A13	1.4	1.5	1.1	No	TAC-like	55.7	-45.1	96.9
5-N11	4.5	1.6	1.1	No	TAC-like	26.9	49.8	80.1
5-P16	14.4	4.8	3.6	Yes	Thiourea	28.2	95.0	92.1
5-C21	1.5	2.3	1.3	Yes	Thiourea	44.4	N.D.	97.2
5-M12	1.9	9.8	2.8	Yes	Thiourea	107.8	9.1	84.2
3-A06	18.5	3.2	2.2	Yes	Thiourea	99.8	N.D.	96.9
5-K23	2.3	1.7	1.0	Yes	Thiourea	67.3	-72.1	92.8

Table A.4.3 (cont'd)

3-A05	2.1	1.6	1.9	Yes	Thiourea	24.1	92.5	92.4
6-L05	2.6	1.2	1.7	Yes	Urea	85.4	100.3	82.3
4-A04	3.2	4.8	1.2	Yes	Urea	74.3	39.7	95.4
4-K19	2.1	1.9	1.4	Yes	Urea	73.7	N.D.	95.3
4-F24	4.0	2.7	3.2	Yes	Urea	38.3	-1.8	71.1
5-B05	2.6	1.6	3.3	Yes	Urea	93.6	70.2	38.5
5-B24	1.5	1.6	1.1	Yes	Urea	107.8	-25.9	52.8
5-I17	1.7	1.7	1.6	Yes	Urea	97.7	-18.7	91.4
4-A23	1.7	5.3	30.1	Yes	Urea	82.3	N.D.	92.2
5-J13	2.7	112.6	1.2	Yes	Urea	78.8	24.0	98.0
5-M17	3.2	3.2	2.7	Yes	Urea	83.5	N.D.	92.7
4-O19	2.3	3.6	1.7	Yes	Urea	91.7	0.4	98.6

ICA – indolecarboxamides, TAC – thiacetazone, % Tox – cytotoxicity, % GI – percent growth inhibition, N.D. – not determined

APPENDIX B:

Supplemental Figures

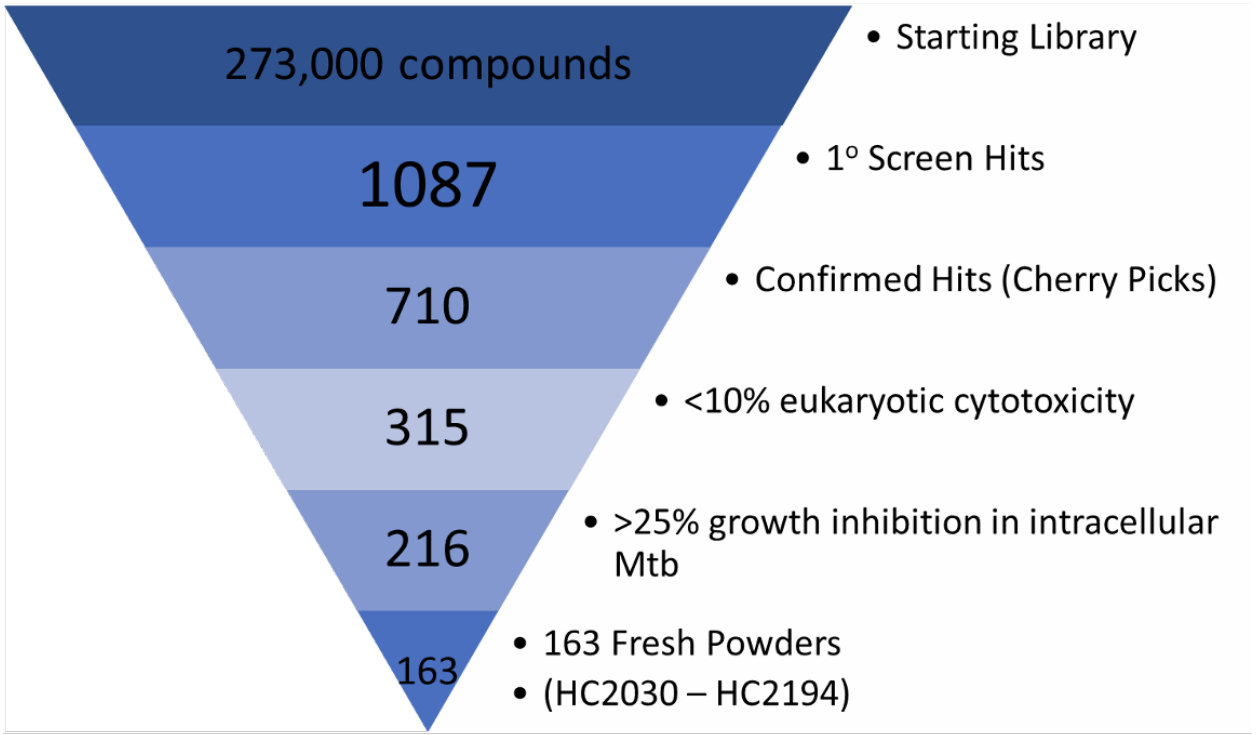

Figure A.2.1. Prioritization funnel of growth inhibitors from a high throughput screen. A high throughput screen of 273,000 compounds identified 1087 compounds that inhibit Mtb growth independent of the targeted two component regulators at 10 μM. These compounds were further tested as being able to inhibit Mtb growth (confirmed hits), have low eukaryotic cytotoxicity (<10%), able to inhibit intracellular Mtb growth (>25%) resulting in 216 compounds that meet the minimum requirements. Of the 216 compounds 163 commercially available compounds were purchased as fresh powders.

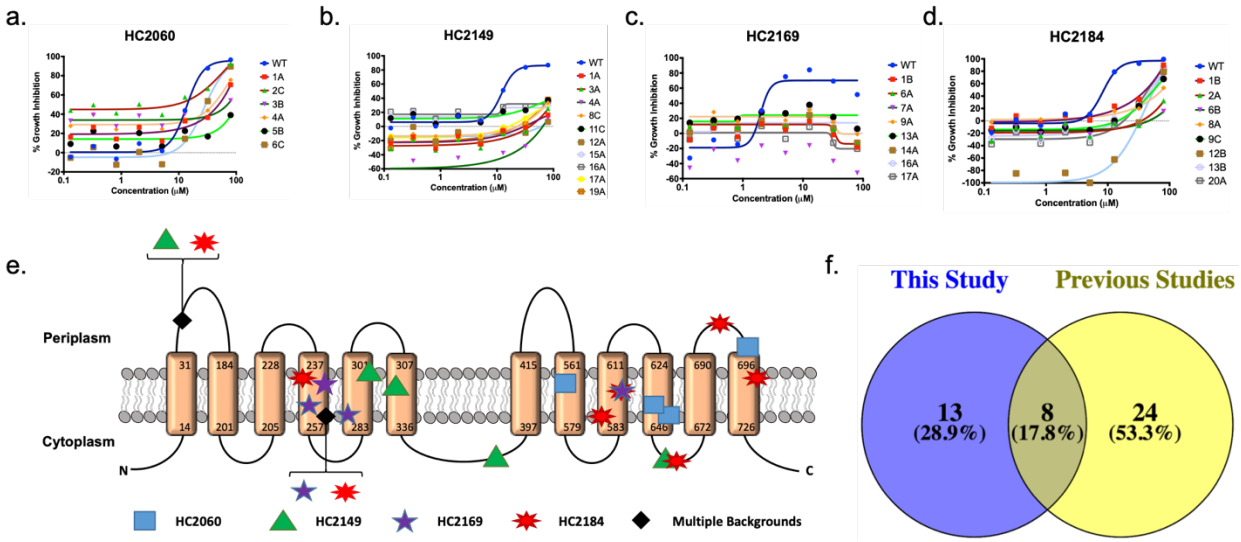

Figure A.2.2. Resistant mutants to four novel inhibitors map to *mmpL3*. a-d) Dose response curves of resistance mutant to four novel Mtb growth inhibitors. Curves are based on 2.5 dilutions of inhibitors ranging from 80 to 0.13μM. Experiments were conducted in triplicate and the error bars indicated the standard deviation of the mean. e) Transmembrane domain map shows diversity of substitutions conferred by mutations in *mmpL3*. Transmembrane domain map is based on Phyre2 analysis of H37Rv MmpL3 protein sequence. f) Venn Diagram identifies novel MmpL3 substitutions identified in this study. A total of 21 MmpL3 amino acid substitutions were identified in this study, including 14 novel substitutions and 7 previously identified substitutions (see TABLE A.2.1 for list of substitutions).

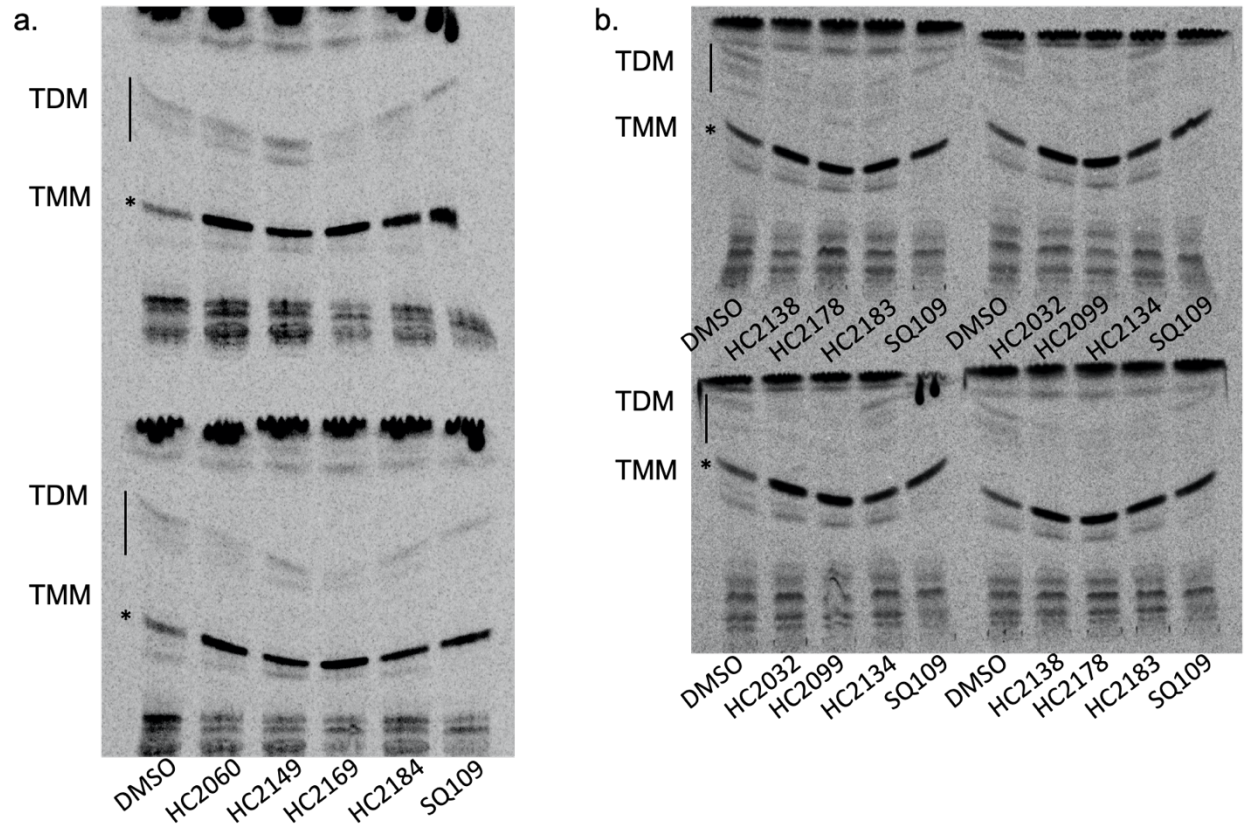

Figure A.2.3. TLCs show TMM/TDM modulation. a-c) Mtb cells were grown in the presence of 8μCi of 14C-acetate for twenty-four hours and treated with 20μM of a) the four prioritized inhibitors (HC2060, HC2149, HC2169 or HC2184) or b and c) the six inhibitors identified from the targeted mutant phenotypic screen (HC2032, HC2099, HC2134, HC2138, HC2178, HC2183). Lipids were isolated from whole cell extracts and analyzed by TLC. In each experiment samples of cells were also treated with either 20μM of SQ109 or DMSO.

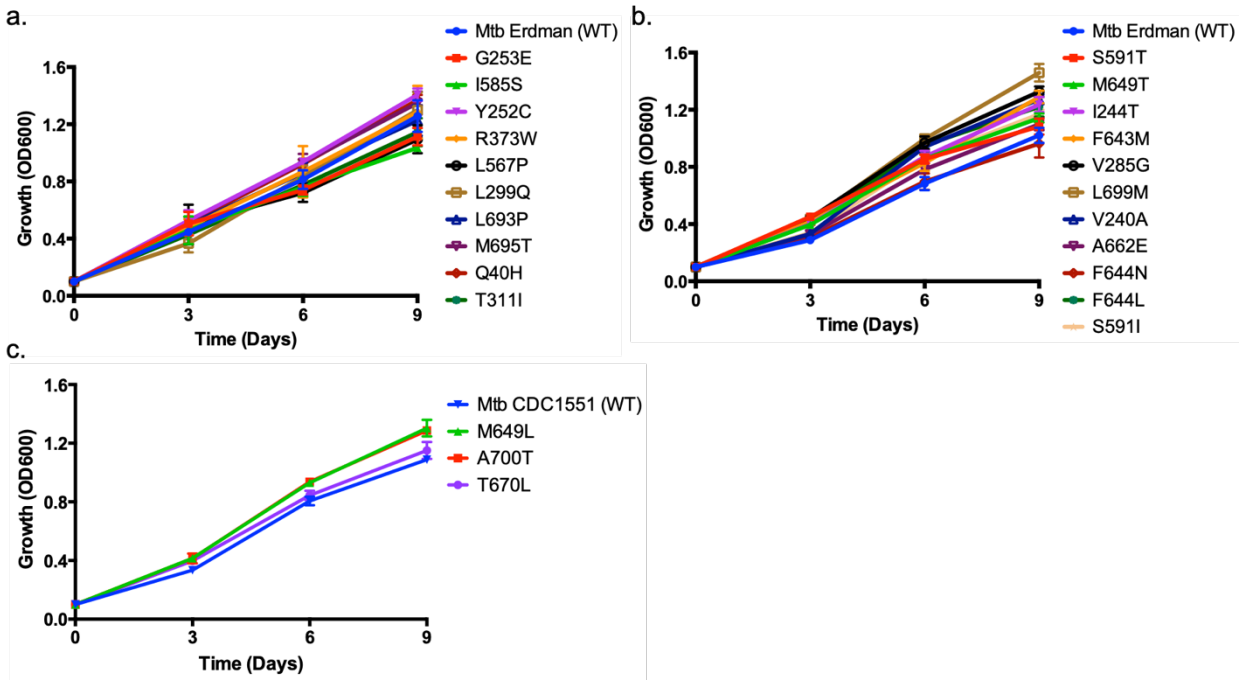

Figure A.2.4. Growth curves of mutants used in targeted mutant phenotypic screen. a - c) Growth of curves of WT Mtb and mmpL3 mutant strains. Mtb strains were grown in 8 mL of 7H9 OADC + .05% Tween-80 in T25 standing flasks at 37°C + 5% CO2. 0Do600 samples were taken every three days. a and b) Show the growth curves for Erdman background strains. c) Shows the growth curves for CDC1551 strains. Figures show the average of three biological replicates ± SD.

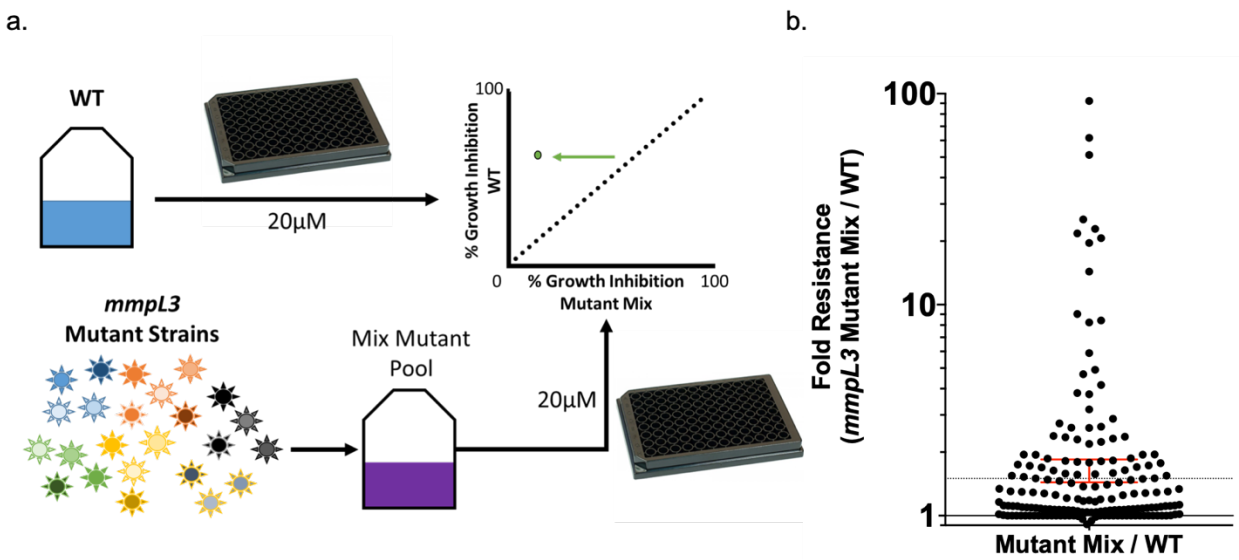

Figure A.2.5. Illustrated outline of targeted mutant phenotypic screen. a) Growth inhibition of a pooled culture of twenty-four unique mmpL3 mutant strains of Mtb (multicolored suns) is directly compared with WT Mtb strains. Samples of either pooled mmpL3 mutant strains or WT Mtb are aliquoted into separate 96 well plates and treated with 163 prioritized Mtb growth inhibitors, as well as BDQ, CFZ, INH, PAS, SQ109 and H2O2. Growth inhibition (%) is calculated as the growth inhibition relative to the DMSO and RIF controls. b) Beehive plot of relative fold decrease in activity of compounds in the mixed mmpL3 mutant background compared to WT treated cells. Dotted line indicates a 1.5-fold resistance in the mmpL3 mixed mutant background relative to the WT. Error bars (red) indicate the 95% confidence interval of the geometric mean.

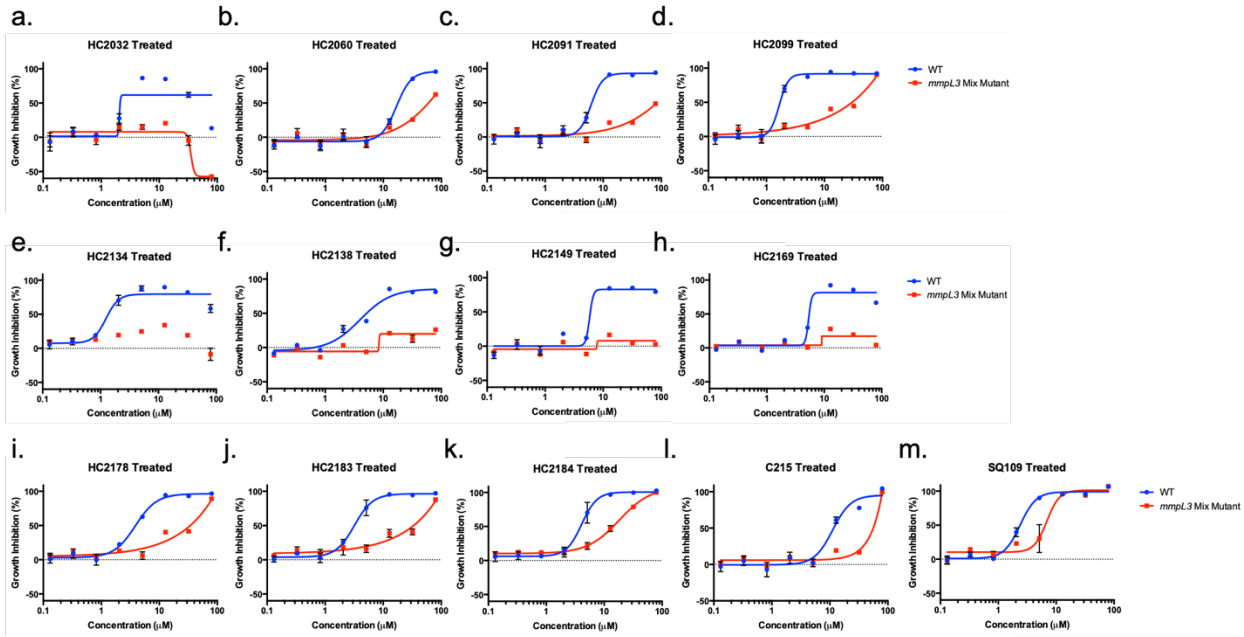

Figure A.2.6. 13 Dose response curves of thirteen proposed MmpL3 inhibitors on pooled *mmpL3* mutant strains. a-m) Dose response curves of thirteen Mtb growth inhibitors confirmed to have reduced activity in the pooled mmpL3 mutant background (red) compared to WT Mtb (blue). Samples were treated with a series of (2.5 fold dilutions) of each inhibitor ranging form 80μM to 0.13μM. Growth inhibition (%) is calculated as the growth inhibition relative to the DMSO and RIF controls. Experiments were conducted in triplicate and error bars indicate the standard deviation from the mean.

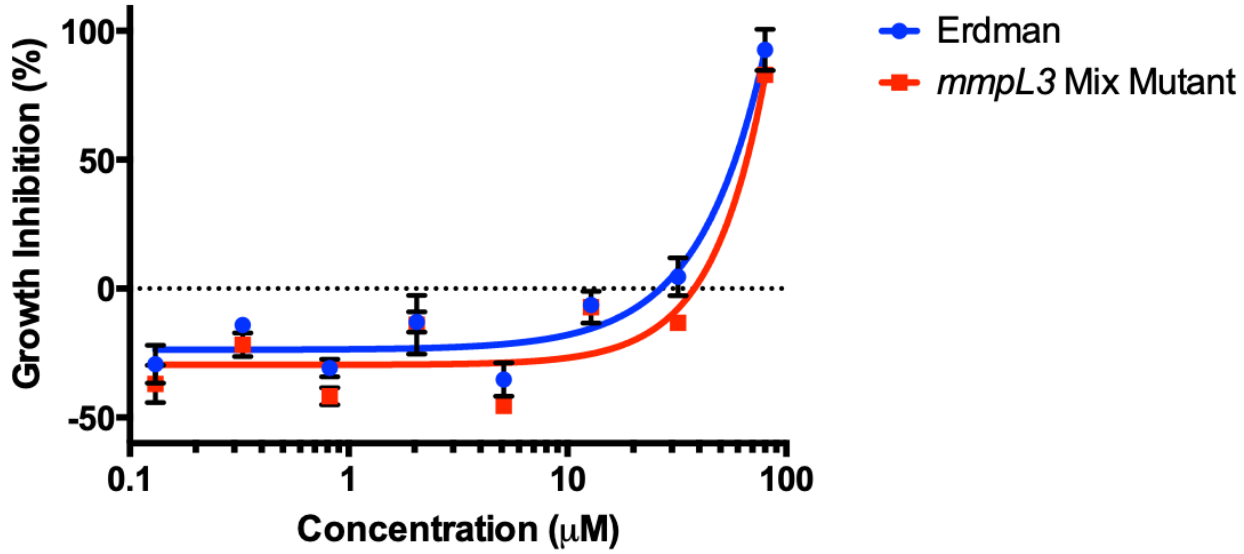

Figure A.2.7. Dose response curves for Rimonabant. Dose response curves of thirteen Mtb growth inhibitors confirmed to have reduced activity in the pooled mmpL3 mutant background (red) compared to WT Mtb (blue). Samples were treated with a series of (2.5 fold dilutions) of each inhibitor ranging from 80μM to 0.13μM. Growth inhibition (%) is calculated as the growth inhibition relative to the DMSO and RIF controls.

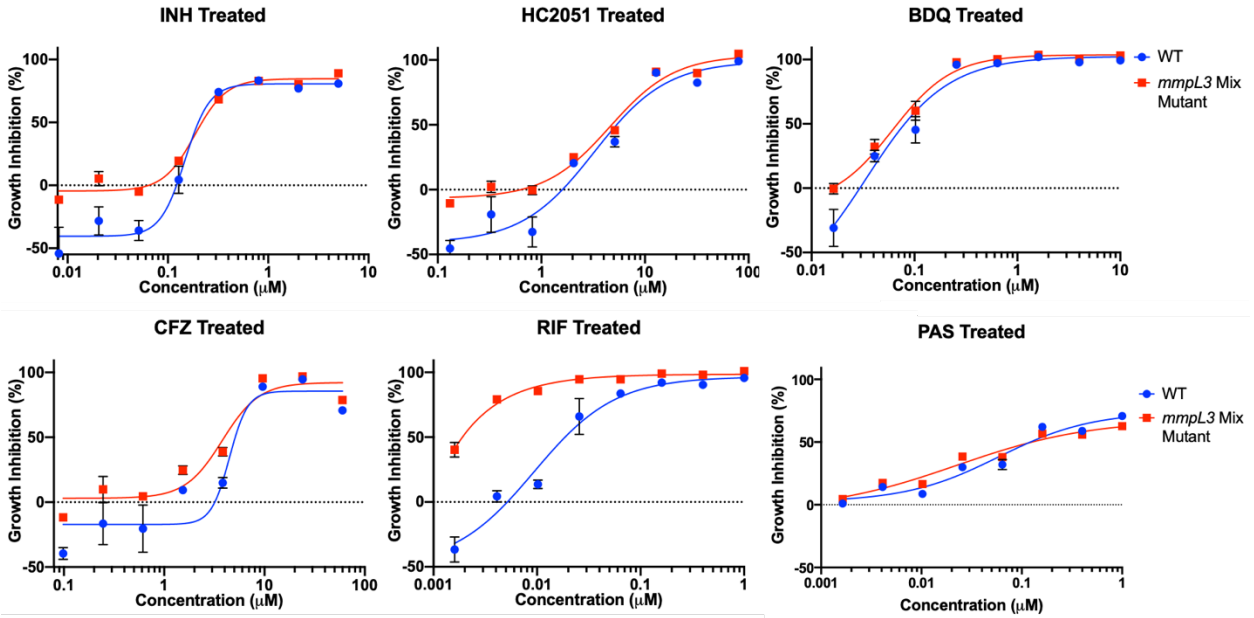

Figure A.2.8. Impact of Non-MmpL3 inhibitors on pooled *mmpL3* mutant strains. Dose response curves of thirteen Mtb growth inhibitors confirmed to have reduced activity in the pooled mmpL3 mutant background (red) compared to WT Mtb (blue). Samples were treated with a series of (2.5 fold dilutions) of each inhibitor ranging form 80μM to 0.13μM. Growth inhibition (%) is calculated as the growth inhibition relative to the DMSO and RIF controls. Samples were run in triplicate and error bars indicate the standard deviation from the mean.

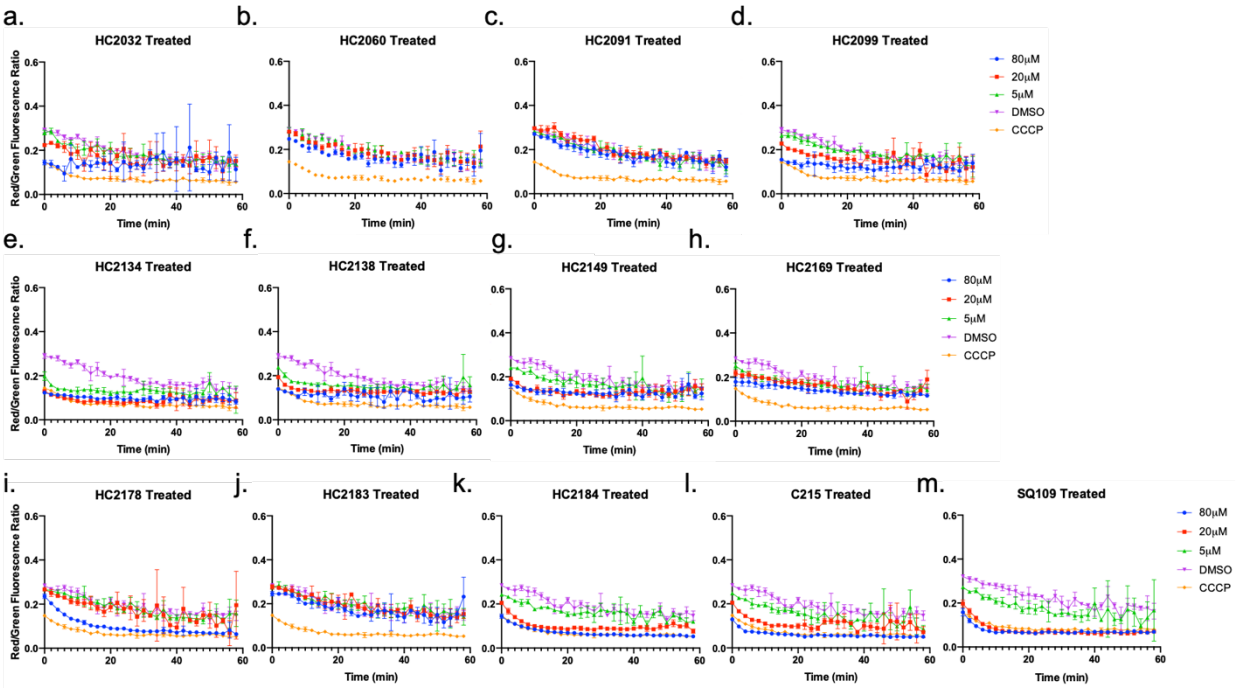

Figure A.2.9. Capacity of inhibitors to disrupt membrane potential. a-m) Mtb cells labeled with DiOC2 and treated with 80μM (blue circle), 20μM (red square) or 5μM (green triangle) of each of the thirteen MmpL3 inhibitors for one hour. As controls DMSO (negative, purple inverted triangles) and CCCP (positive, orange diamonds) treatments were also included. Experiments were carried out using the DiOC2 membrane potential assay kit. The experiment was repeated twice with similar results. Data points are the geometric mean of three technical repeats. Error bars indicate the geometric standard deviation of three technical replicates. The experiment was repeated with similar results.

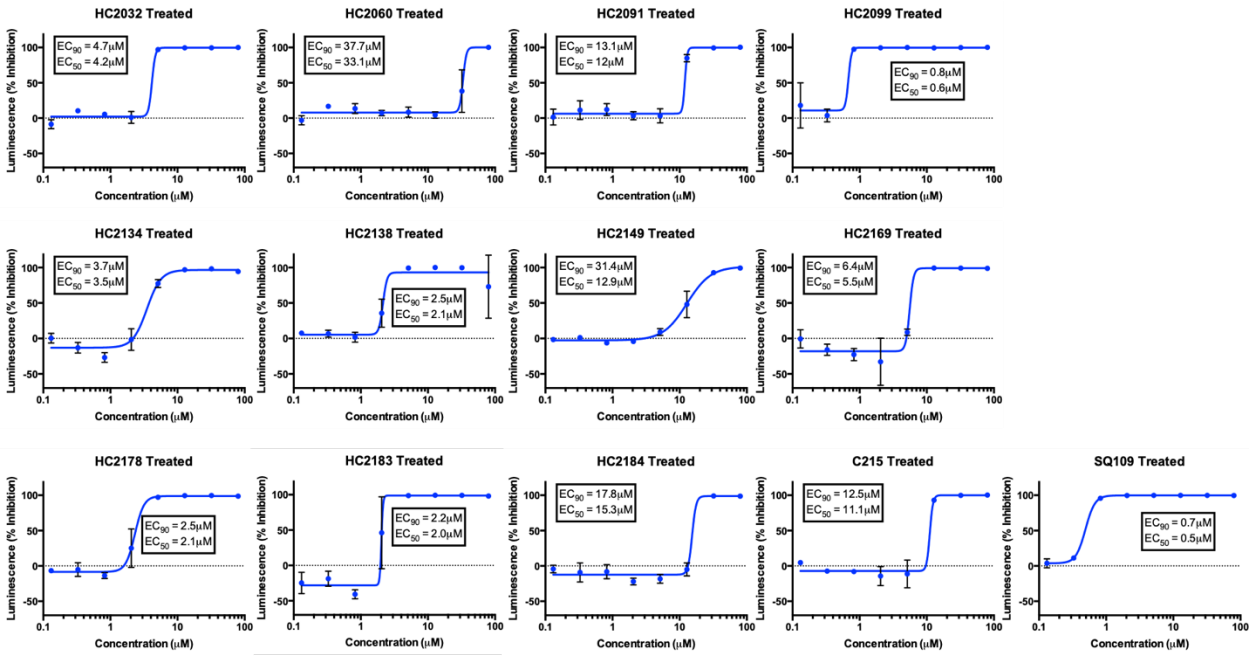

Figure A.2.10. Bactericidal activity of MmpL3 inhibitors. Mtb CDC1551 luc reporter strains were treated with a series of dilutions (2.5-fold) from 80 to 0.13μM of each of the thirteen MmpL3 inhibitors for six days in vitro. Cells were then tested for luciferase expression using the Bright-Glo Luciferase assay kit. Growth inhibition (%) is the normalized luciferase activity relative to the DMSO – positive and RIF – negative controls. Experiments were conducted in triplicate and the error bars indicated the standard deviation of the mean.

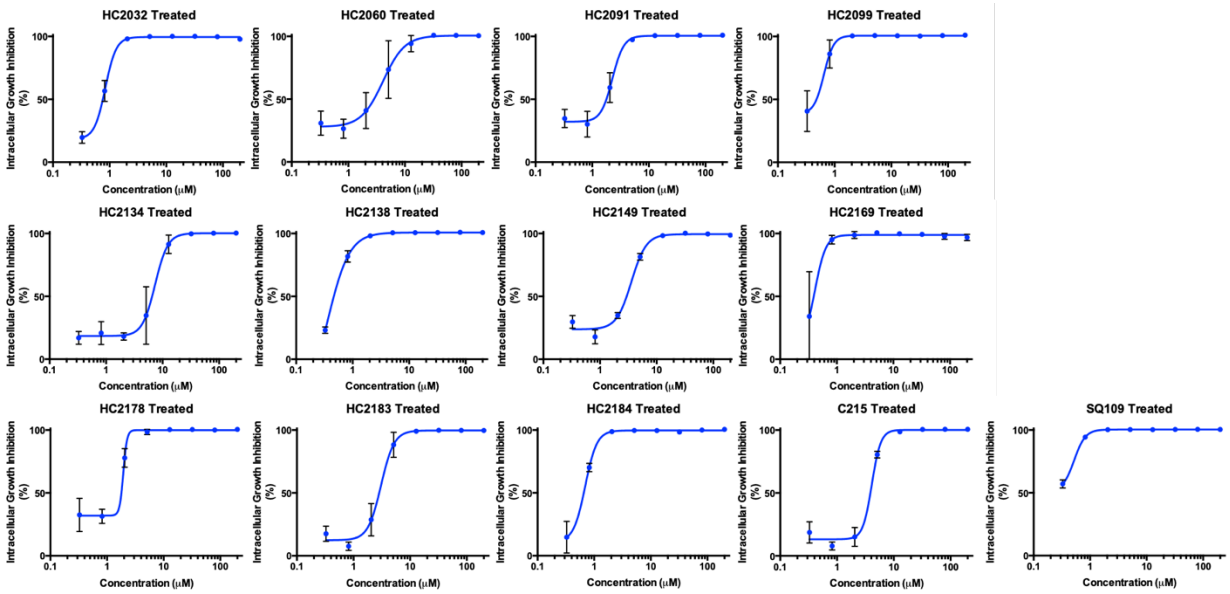

Figure A.2.11. Impact of MmpL3 inhibitors on intracellular growth. Primary bone marrow macrophages were infected with Mtb CDC1551 luc reporter strains. Infected macrophages were treated with a series of dilutions (2.5-fold) from 200 to 0.3μM of each of the thirteen MmpL3 inhibitors for six days in vitro. Cells were then tested for luciferase expression using the Bright-Glo Luciferase assay kit. Growth inhibition (%) is the normalized luciferase activity relative to the DMSO – positive and RIF – negative controls. Experiments were conducted in triplicate and the error bars indicated the standard deviation of the mean.

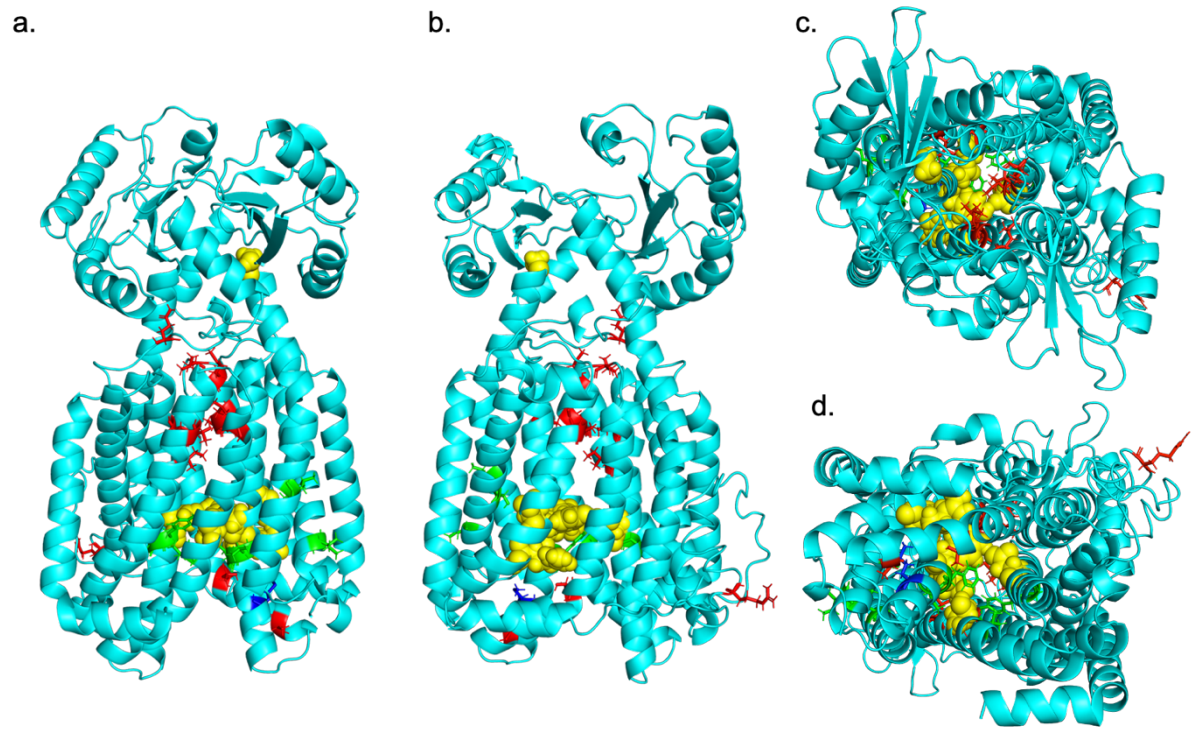

Figure A.2.12. Clade substitutions differ in proximity to essential residues. a-d) Front, back, top, and bottom (respectively) views of an I-TASSER predicted structure of Mtb MmpL3 based on MmpL3 structure of Msm (PDB: 6AJH). Substitutions conferred by mutations in mmpL3. Substitutions are colored based on clade from cross resistance profiling, Clade I substitutions (green), Clade II substitutions (red), or M649 (blue) which fell into both clades depending on substitution. Yellow spheres indicate the seven essential residues (D251, S288, G543, D640, Y641, D710, and R715) for MmpL3 activity identified by Bellardinelli and colleagues. The model shows a truncated version (732/944aa) of the MmpL3 protein lacking the C-terminal tail.

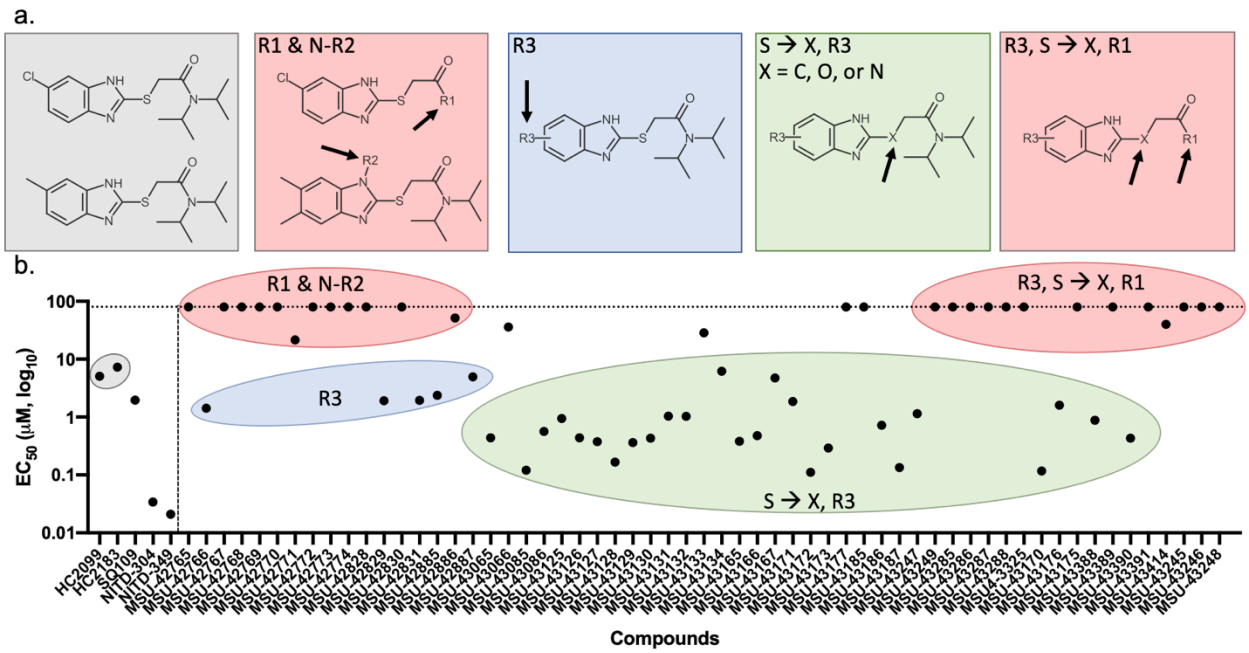

Figure A.3.1. General trend for the gain of activity for HC2099 analogs. a) Illustration for the general approach taken to study the activity of HC2099 series analogs. R1-R4 substitutions are described in the text. R3 substitutions are illustrated to indicate any substitution(s) of the benzene ring. X indicates a hetero atom (C - carbon, N - nitrogen, or O - oxygen) substitution for the sulfur (S) atom in parental HC2099. The structures for parental HC2099 and HC2183 are highlight in grey. b) A scatter plot of the EC50 for each HC2099 analog as well as lead competitors SQ109, NITD-304, and NITD-349. Colored circles are meant to show general trends in the data and are matched to the colors used in Figure S1a. Data points outside of the circles may fall into one of the general groups. Specific EC50s and other activity data for each compound are listed in Table A.5.1.

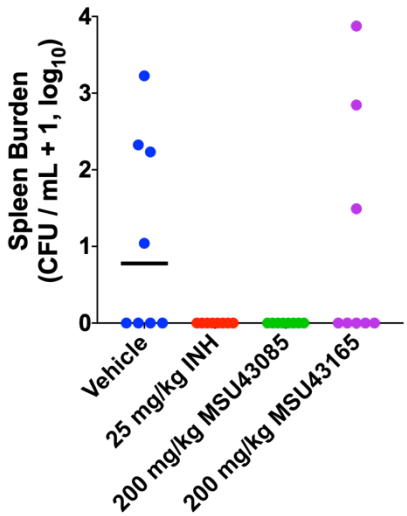

Figure A.3.2. Spleen burden of Mtb acute infection. Spleen bacterial burden of C57Bl6 micefollow an acute (two week) infection with Mtb Erdman and treated with vehicle (corn oil), INH (25 mg/kg), MSU-43085 (200 mg/kg) or MSU-43165 (200 mg/kg). No detectable colonies were isolated from most vehicle control mice. Solid black line indicates the median burden. Due to inconsistency of infection, statistical tests were not performed.

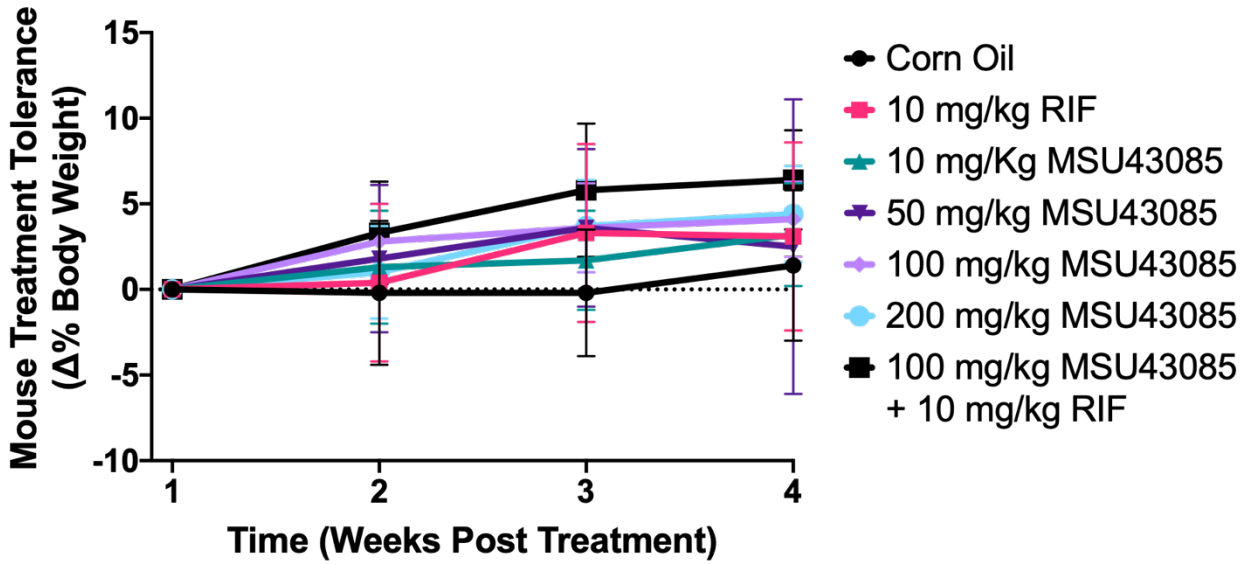

Figure A.3.3. MSU-43085 is tolerable in mice at high doses. Line graph of changes in mouse body weights (Δ%) relative to start of treatment (Week 1). Week 4 corresponds to the 4th week of treatment.

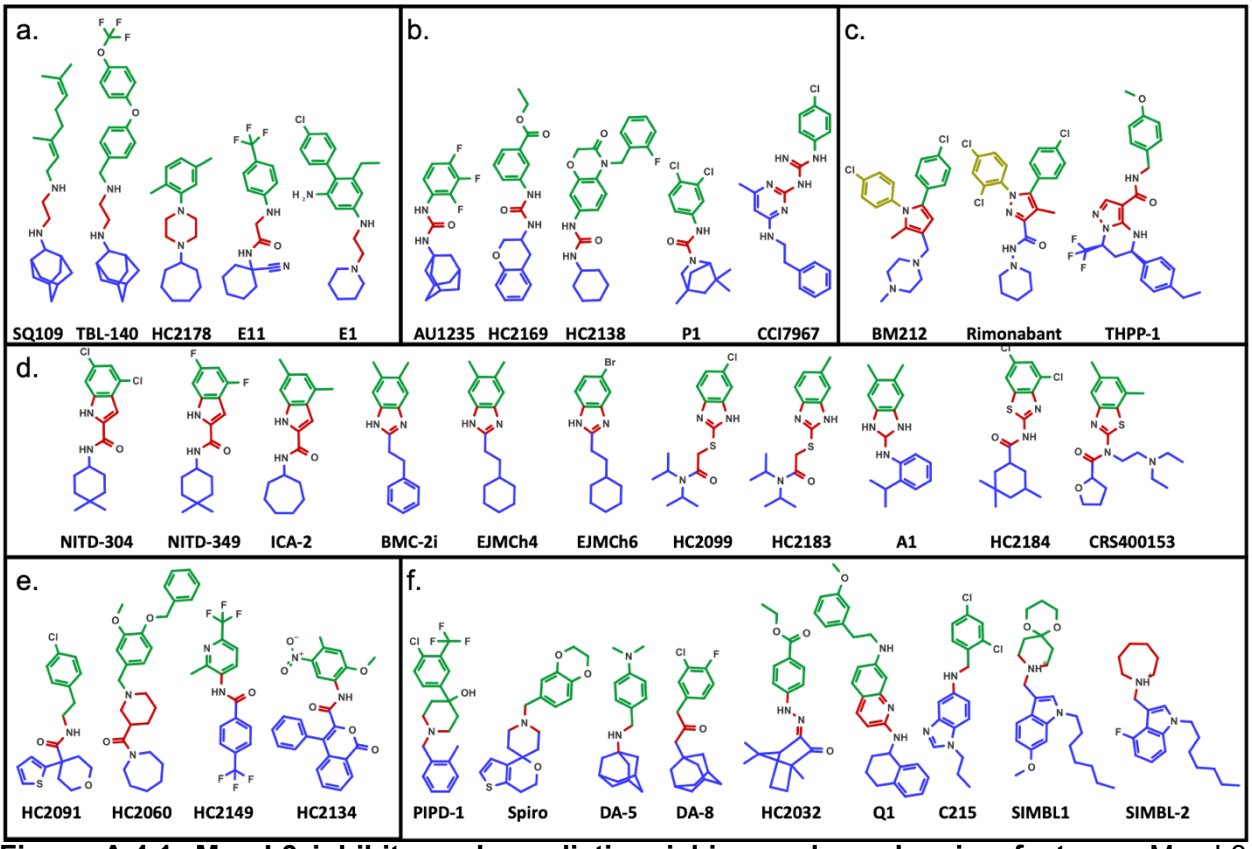

Figure A.4.1. MmpL3 inhibitors share distinguishing and overlapping features. MmpL3 inhibitors fall into five distinct classes of inhibitors based on shared Central core chemical groups including diamines / acetamides (a), ureas / guanidines (b), pyrole / pyrazoles (c), indoles / imidazoles / thiazoles (d), amides (e), and a sixth class of unshared core chemical groups (f). Colored circles indicate shared chemical groups found between all MmpL3 inhibitors including the Northern lipophilic groups (Green), the Central electrophilic / basic core group (Red), and the Southern hydrophobic group (Blue). Noted exception are the additional North Western chemical groups (Yellow) found in BM212 and Rimonabant. North, Central, and South chemical nomenclature is based on work done by Guardia and colleagues[158].

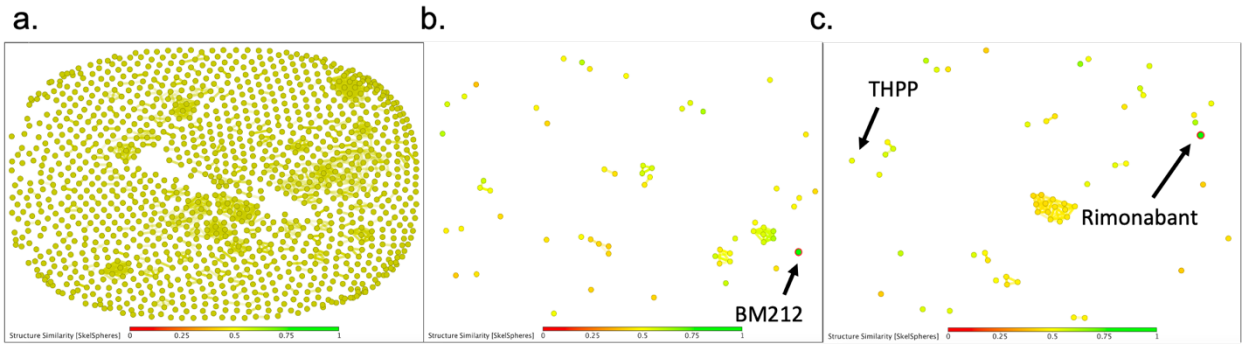

Figure A.4.2. An *in silico* scaffold search does not identify additional pyrole/pyrazole based inhibitors. A structure similarity plot of the > 1000 compound library generated in DataWarrior[259]. Similarity is based calculations using SkelSpheres using default settings. Similarity is ranged from low (0, red) to high (1, green). b-c) Results of a chemical scaffold search for the identification of compounds with either a pyrole (b) or pyrazole groups (c). The search indicates that there are not additional pyrole/pyrazole-based inhibitors similar to known MmpL3 inhibitors.

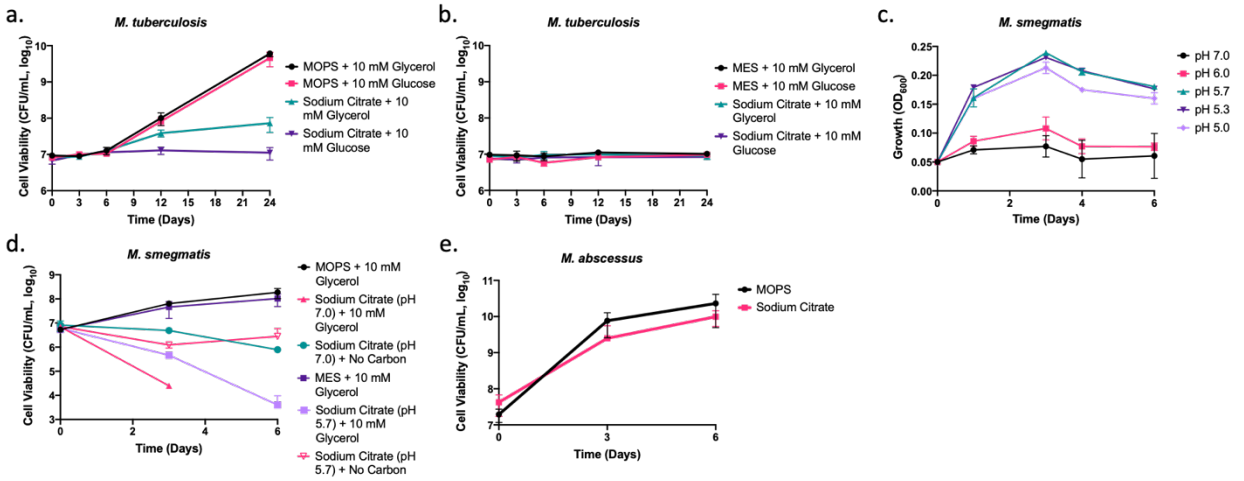

Figure A.5.1. Sodium citrate differentially effects the cell viability and growth of mycobacteria. a and b) *M. tuberculosis* cultured in MMAT minimal medium buffered with 100 mM MOPS (pH 7.0) (a), MES (pH 5.7) (b), or sodium citrate (pH 7.0 or pH 5.7) (a and b respectively) supplemented with 10 mM glucose or glycerol. c) Growth (OD600) of *M. smegmatis* cultured in MMAT minimal medium buffered with 100 mM sodium citrate to pH 7.0, 6.5, 5.7, 5.3, or 5.0. Minimal medium was supplemented with 10 mM glycerol. d) Cell viability of *M. smegmatis* cultured in minimal medium buffered with 100 mM MOPS (pH 7.0), MES (pH 5.7), or sodium citrate (pH 7.0 or 5.7). Sodium citrate buffered cultures were supplemented with or without 10 mM glycerol. e) Cell viability of *M. abscessus* cultured in MMAT minimal medium buffered to pH 7.0 with 100 mM MOPS or sodium citrate and supplemented with 10 mM glycerol. Error bars indicate the s.d, of the mean.

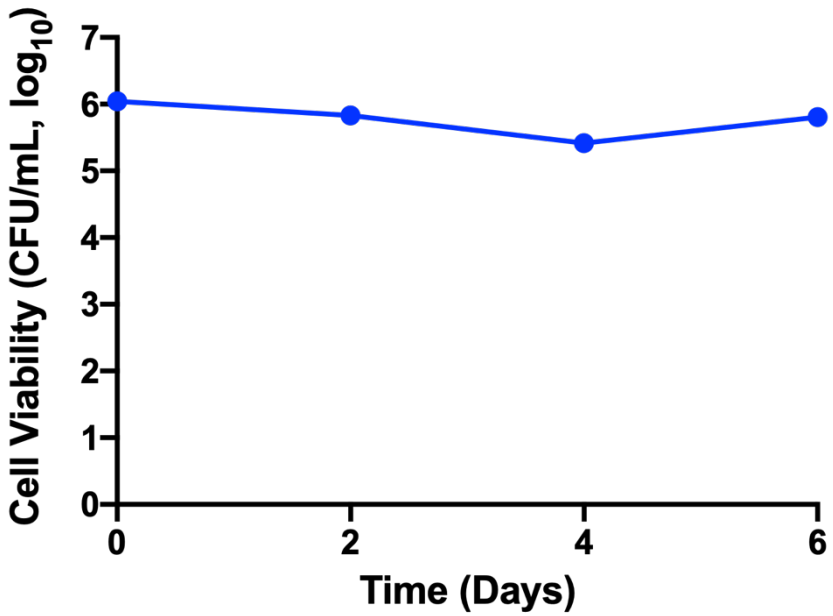

Figure A.5.2. *M. smegmatis* is viable in the absence of environmental cations. *M. smegmatis* was cultured in phosphate buffered saline (pH 7.4) with 0.05% tween-80 and supplemented with 10 mM glycerol.

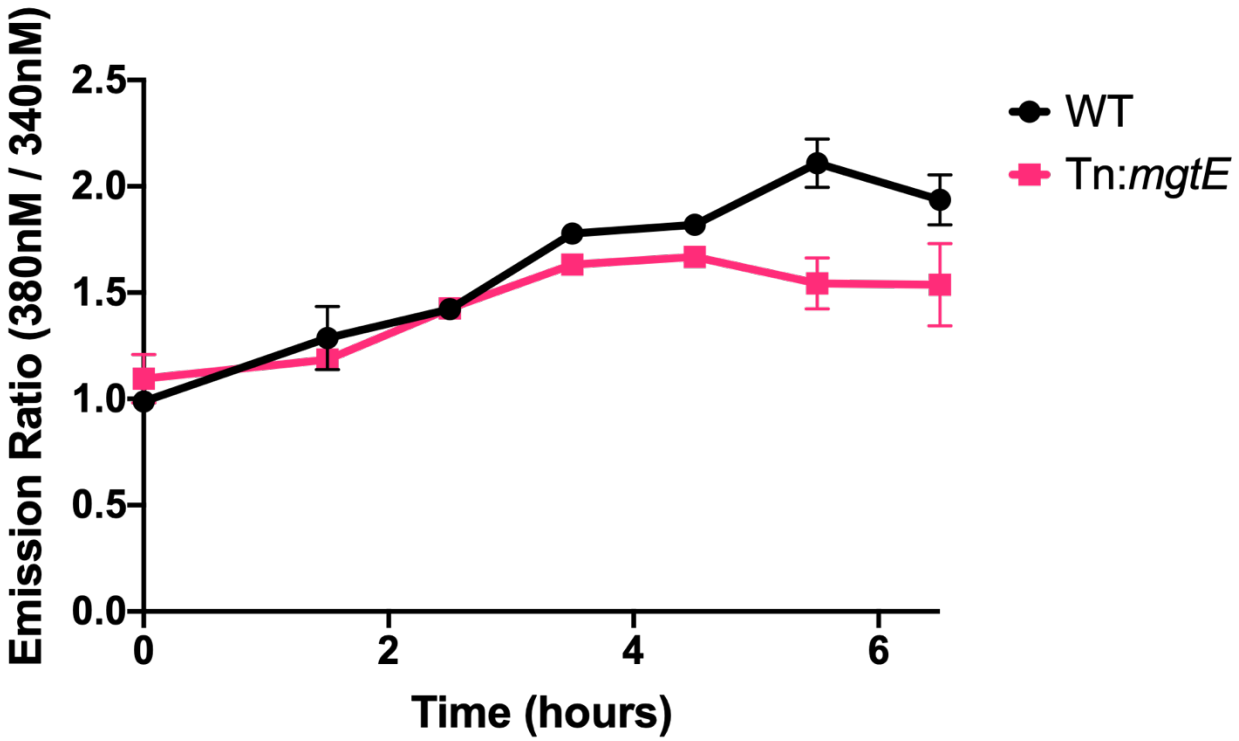

Figure A.5.3. An *mgtE* mutant has decreased Mg^{2+} import relative to WT Msm. WT *M. smegmatis* or a Tn:*mgtE* mutant were labeled with the cell permeable Mag-Fura2 (AM) Mg^{2+}/Ca^{2+} fluorophore and cultured in MOPS or sodium citrate buffered minimal medium pH 7.0. Cultures were supplemented with 100 mM Mg^{2+}. The ratio represents the RFI of cells measured at Mg^{2+} bound Mag-Fura2 (High Mg^{2+}, Ex: 380 nm/ Em: 510 nm) relative to free Mag-Fura2 (Low Mg^{2+}, Ex: 340 nm/ Em: 510 nm). The experiments were performed in biological duplicate and repeated at least twice. Error bars indicate the s.d. of the mean.

APPENDIX C:

Supplemental Methods

Methods A.2.1 *M. abscessus*

Bacterial strains and culture media

For screens and hit confirmation, *Mycobacterium abscessus* Bamboo was used. *M. abscessus* Bamboo was isolated from the sputum of a patient with amyotrophic lateral sclerosis and bronchiectasis and was provided by Wei Chang Huang, Taichung Veterans General Hospital, Taichung, Taiwan. *M. abscessus* Bamboo whole genome sequencing showed that the strains belongs to *M. abscessus* subsp. *abscessus* and harbors an inactive clarithromycin-sensitive erm C28 sequevar (GenBank accession no. MVDX00000000). *M. abscessus* Bamboo cultures were grown in standard mycobacterium medium, Middlebrook 7H9 broth (BD Difco) supplemented with 0.5% albumin, 0.2% glucose, 0.085% sodium chloride, 0.0003% catalase, 0.2% glycerol, and 0.05% Tween 80. Solid cultures were grown on Middlebrook 7H10 agar (BD Difco) supplemented with 0.5% albumin, 0.2% glucose, 0.085% sodium chloride, 0.5% glycerol, 0.0003% catalase, and 0.006% oleic acid.

Single-point growth inhibition screening assay

The compound library was screened in microtiter plates as previously described with minor modifications. Briefly, the screen was carried out in 96-well flat-bottom Corning Costar plates at a single-point concentration of 20 μM with a starting inoculum of an optical density at 600 nm (OD_{600}) of 0.05 (107 CFU/ml) in a final volume of 200 μl. The culture for the starting inoculum was diluted from a pre-culture at mid-log phase (OD_{600}, 0.4 to 0.6). The plates were sealed using a Breathe-Easy sealing membrane (SigmaAldrich), put in an airtight container with moist tissue, and incubated for 3 days at 37°C on an orbital shaker at 110 rpm. Each plate had a medium-only control and a drug-free control, as well as positive control, clarithromycin at 20 μM. After 3 days of incubation, the cultures in the wells were manually resuspended before the OD_{600} was read in a TECAN Infinite Pro 200 plate reader. Compounds were scored according to their growth inhibition of the treated culture compared to the untreated culture (DMSO-treated). The experiment was conducted in duplicate.

Methods A.3.1

HC2099 analogs synthesis Scheme

The following synthesis schemes were used by Dr. Ellsworth's lab to produce the compounds tested in this study.

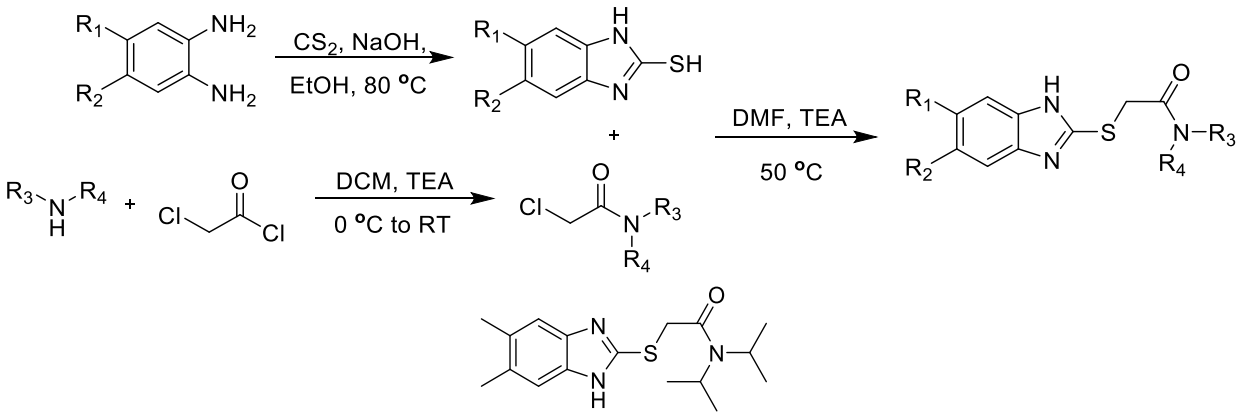

2-chloro-N,N-bis(propan-2-yl)acetamide. The title compound was prepared by the following method (Chen, T. C.; Yu, D. S.; Fu, Y. C.; Lee, C. C.; Chen, C. L.; Huang, F. C.; Hsieh, H. H.; Lin, J. J.; Huang, H. S., *Eur. J. Med. Chem*, **2013**, *69*, 278). A 100 mL 24/40 round bottom flask (argon atmosphere) was charged with dichloromethane (20.0 mL) and chloroacetyl chloride (1.12 g, 10.0 mmol) and cooled to 0 °C. Diisopropylamine (2.52 g, 25.0 mmol), dissolved in dichloromethane (10.0 mL), was added (0 °C) to the rapidly stirring solution, in a dropwise fashion. resulting in a precipitate. The mixture was stirred for 30 minutes at 0 °C, then treated with 30.0 mL of a 1.00 N aqueous hydrochloric acid solution. The biphasic reaction mixture was stirred for 5 minutes at 0 °C, then transferred to a separatory funnel and partitioned. The aqueous layer was washed with 15.0 mL dichloromethane and combined with the organic layer. The organic mixture was washed with brine, dried over sodium sulfate, filtered, and concentrated *in vacuo* to yield an oil, which was filtered through a plug of silica (100 % dichloromethane). The filtrate was concentrated *in vacuo* to yield the pure product as a clear, colorless oil (1.51 g, 85 % yield). ^{1}H NMR (500 MHz, $CDCl_3$) δ 4.01 (s, 2H), 3.95 (p, *J* = 6.7 Hz, 1H), 3.43 (dd, *J* = 13.1, 6.9 Hz, 1H), 1.39 (d, *J* = 6.8 Hz, 6H), 1.24 (d, *J* = 6.7 Hz, 6H).

5,6-dimethyl-1H-1,3-benzodiazole-2-thiol. A 100 mL 24/40 round bottom flask was charged with ethanol (20.0 mL), carbon disulfide (1.67 g, 22.0 mol) and solid sodium hydroxide (0.880 g, 22.0 mmoles). 4,5-dimethylbenzene-1,2-diamine (2.58 g, 19.0 mmol) was added, followed by 3.00 mL water. The reaction mixture (argon atmosphere) was heated to reflux for 3 hours and a precipitate formed. The reaction mixture was cooled to room temperature, filtered, and washed with ethanol. The filtrate was diluted with 20.0 mL water, heated to 70 ºC with stirring, and treated with 10.0 mL of a 1:1 acetic acid and water mixture, resulting in the formation of a precipitate. The mixture was cooled to 0 ºC for 3 hours, filtered, and dried *in vacuo* for 20 hours to yield a solid (2.50 g, 74 %, prepared according to the method described by Peddibhotla, S.; Shi, R.; Kahn, P.; Smith, L. H.; Mangravita-Novo, A.; Vicchiarelli, M.; Su, Y.; Okolotowica, K. J.; Cashman, J. R.; Reed, J. C.; Roth, G. P.; *J. Med. Chem.*, **2010**, *53*, 4793.). ^{1}H NMR (500 MHz, $CDCl_3$) δ 7.47 (dd, *J* = 6.0, 3.2 Hz, 1H), 7.17 (dd, *J* = 6.0, 3.1 Hz, 1H), 3.61 (s, 1H), 3.33 (h, *J* = 6.5 Hz, 1H), 1.34 (d, *J* = 6.5 Hz, 6H).

2-[(5,6-dimethyl-1H-1,3-benzodiazol-2-yl)sulfanyl]-N,N-bis(propan-2-yl)acetamide. A 50.0 mL round bottom flask was charged with 2-chloro-N,N-bis(propan-2-yl)acetamide (0.354 g, 2.00 mmol), dry dimethylformamide (2.00 mL), and 5,6-dimethyl-1H-1,3-benzodiazole-2-thiol (1.00 mmol, 0.178 g). The reaction mixture was stirred, under an argon atmosphere, and treated with triethylamine (0.252 g, 2.50 mmol). After 18 hours, the mixture was poured into water (50.0 mL), and the resulting solid filtered, washed with water and hexanes, then dried *in vacuo* to provide 2-[(5,6-dimethyl-1H-1,3-benzodiazol-2-yl)sulfanyl]-N,N-bis(propan-2-yl)acetamide (0.161 g, 50 %). ^{1}H NMR (500 MHz, DMSO-d_6) δ 12.23 (s, 1H), 7.24 (s, 1H), 7.11 (s, 1H), 4.35 (s, 2H), 4.06 (p, *J* = 6.6 Hz, 1H), 3.52 – 3.45 (m, 1H), 2.25 (d, *J* = 6.7 Hz, 6H), 2.07 (s, 2H), 1.27 (d, *J* = 6.7 Hz, 6H), 1.17 (d, *J* = 6.6 Hz, 6H). APCI HRMS [M+H] calc'd = 320.1791, found 320.1790. m.p = 172 ^{o}C.

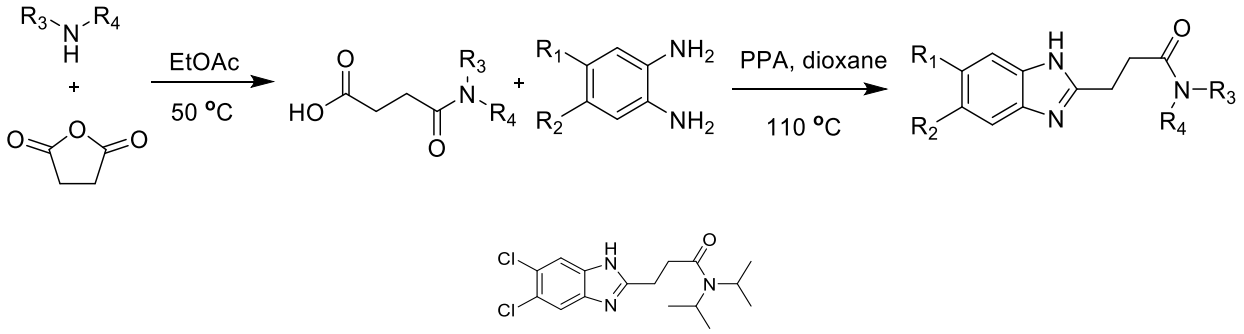

3-[bis(propan-2-yl)carbamoyl]propanoic acid. A 100 mL 24/40 round bottom flask was charged with succinic anhydride (2.00 g, 19.0 mmol) and ethyl acetate (20.0 mL) and treated dropwise with diisopropylamine (3.08 mL, 22.0 mmol). The mixture was heated to reflux for 23 hours, then concentrated *in vacuo* to yield the product as an oil (3.8 g, 100 %). ^{1}H NMR (500 MHz, DMSO-d_6) δ 4.00 (dq, *J* = 13.2, 6.9 Hz, 1H), 3.18 (p, *J* = 6.4 Hz, 1H), 2.45 (dd, *J* = 7.2, 6.1 Hz, 2H), 2.37 – 2.30 (m, 2H), 1.24 (d, *J* = 6.7 Hz, 4H), 1.17 – 1.08 (m, 8H).

3-(5,6-dichloro-1H-1,3-benzodiazol-2-yl)-N,N-bis(propan-2-yl)propenamide. A 100 mL 24/40 round bottom flask was charged with 4,5-dichlorobenzene-1,2-diamine (0.299 g, 2.20 mmol) and anhydrous 1,4-dioxane (6.00 mL). 3-[bis(propan-2-yl)carbamoyl]propanoic acid (0.482 g, 2.40 mmol) was added, followed by polyphosphoric acid (1.63 g, 16.0 mmol). The reaction vessel was heated to 105 °C and stirred under an argon atmosphere for 20 hours. The reaction was quenched by adding water (30.0 mL) and sodium carbonate (12.3 g, 117 mmol). The reaction mixture was partitioned with ethyl acetate and concentrated *in vacuo*. The crude material was purified by Reverse-phase Medium Pressure Liquid Chromatography (50 g C18 column, methanol in 25.0 mmolar ammonium formate). The resulting formate salt was then partitioned between ethyl acetate and a saturated sodium bicarbonate solution, the organic layer washed with brine, dried over sodium sulfate, filtered, and concentrated *in vacuo* to yield pure product as a powder (0.151 g, 22%). ^{1}H NMR (500 MHz, DMSO-d_6) δ 11.88 (s, 1H), 7.20 (s, 2H), 4.11 – 3.95 (m, 1H), 3.46 (s, 1H), 2.94 (dd, *J* = 9.0, 6.3 Hz, 2H), 2.78 (dd, *J* = 9.0, 6.3

Hz, 2H), 2.26 (s, 6H), 1.27 (d, *J* = 6.7 Hz, 6H), 1.18 – 1.10 (m, 6H). APCI [M+H] calc'd = 302.2226 observed = 302.2274. m.p. = 182 °C.

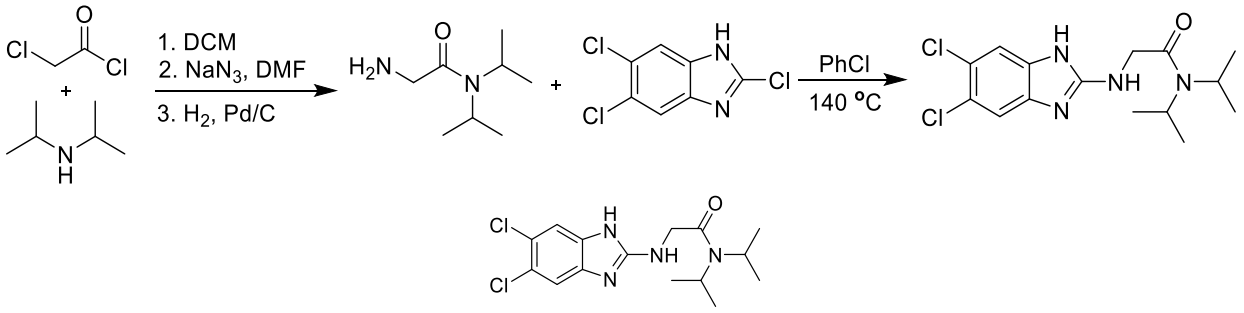

2-amino-N,N-bis(propan-2-yl)acetamide. 2-chloro-N,N-bis(propan-2-yl)acetamide (1.77 g, 10.0 mmol) was prepared according to the method described in Example 2, dissolved in dimethylformamide (20.0 mL), combined with sodium azide (1.95 g, 30.0 mmol), and heated to 50 °C under argon for 19 hours. The reaction mixture was cooled to room temperature, partitioned between ethyl acetate and water, washed with brine, 1.00 N aqueous hydrochloric acid, brine, dried over sodium sulfate, filtered and concentrated to yield the product as an oil (1.82 yield, 99 %). 1H NMR (500 MHz, Chloroform-d) δ 3.87 (s, 2H), 3.72 (h, J = 6.7 Hz, 1H), 3.53 (s, 1H), 1.41 (d, J = 6.8 Hz, 6H), 1.28 – 1.18 (m, 6H). Spectra match that reported for this compound in *Eur. J. Med. Chem.*, **2013**, *69*, 338.

This material was dissolved in ethanol (30.0 mL), stirred with 10 % palladium on carbon (0.304 g, 2.85 mmol). The reaction vessel was sealed and hydrogenated using a balloon filled with hydrogen for 14 hours. The reaction was filtered through Celite (washing with ethanol) and concentrated *in vacuo* to yield the product as an oil (1.50 g, 95 %). ^{1}H NMR (500 MHz, Chloroform-d) δ 3.79 (dt, J = 13.4, 6.7 Hz, 1H), 3.42 (d, J = 18.0 Hz, 1H), 3.36 (s, 2H), 1.36 (d, J = 6.8 Hz, 6H), 1.15 (d, J = 6.6 Hz, 6H). Spectra match that reported in Monaghan, Sandra Marina; Mantell, Simon John, WO2000023457.

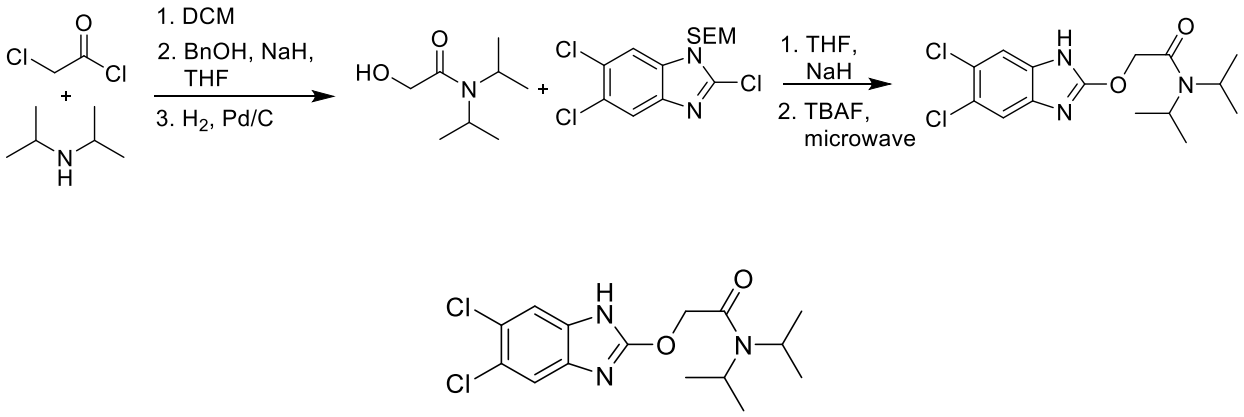

2-hydroxy-N,N-bis(propan-2-yl)acetamide. 2-chloro-N,N-bis(propan-2-yl)acetamide (2.27 g, 12.7 mmol) was dissolved in tetrahydrofuran (40.0 mL) and benzyl alcohol (1.62 g, 15.0 mmol). The reaction mixture was cooled to 0 ºC under argon and sodium hydride was added (0.537 g, 16.0 mmol). The reaction mixture was heated to 50 ºC for 19 hours, at which time it was quenched with a solution of saturated aqueous ammonium chloride (20.0 mL) and partitioned with ethyl acetate. The aqueous layer was extracted with ethyl acetate, the organic layers were combined, washed with brine, dried over sodium sulfate, filtered, and concentrated *in vacuo* to yield the crude product as an oil. The product was purified by silica gel chromatography (1:4 ethyl acetate in hexanes) to yield the pure product as an oil (2.89 g, 91 %, Miyatake, Tsuneo; Tanaka, Shigeyuki; Shimada, Atsuo, JP49011412 B.). ^{1}H NMR (500 MHz, Chloroform-d) δ 7.41 – 7.24 (m, 5H), 4.60 (s, 2H), 4.10 (s, 2H), 4.03 – 3.92 (m, 1H), 3.48 – 3.35 (m, 1H), 1.42 (d, J = 6.8 Hz, 6H), 1.17 (dd, J = 11.0, 6.4 Hz, 6H). This material was dissolved in ethanol (30.0 mL) and stirred with 10 % palladium on carbon (0.442 g, 4.15 mmol) under a hydrogen atmosphere applied with a balloon for 20 hours. The reaction mixture was filtered through celite (washing with ethanol) and concentrated *in vacuo* to yield the product as a white solid (1.59 g, 91 %, Scardovi, N.; Casalini, A.; Peri, F.; Righi, P., *Org. Lett.*, **2002**, *4*, 965.). 1H NMR (500 MHz, Chloroform-d) δ 4.07 (d, J = 4.2 Hz, 2H), 3.60 (dt, J = 13.3, 6.6 Hz, 2H), 3.48 (p, J = 6.7 Hz, 1H), 1.41 (d, J = 6.7 Hz, 6H), 1.19 (d, J = 6.5 Hz, 6H).

2,5,6-trichloro-1-{[2-(trimethylsilyl)ethoxy]methyl}-1H-1,3-benzodiazole. This material was prepared according to the general method described in Duane Burnett, Wen-Lian Wu, Thavalakulamgara Sasikumar, William Greenlee, Mary Caplen, Tao Guo, Rachael Hunter, US20050054628. A 100 mL 24/40 roundbottom flask was charged with 2,5,6-trichloro-1H-1,3-benzodiazole (0.424 g, 1.90 mmol) and dimethylformamide (10.0 mL). Under an argon atmosphere, sodium hydride was added (0.100, g, 3.0 mmol), and once gas evolution was complete, 2-(chloromethoxy)ethyl trimethylsilane (0.416 g, 2.50 mmol) was added via syringe. The mixture was stirred for 19 hours at which time water was added (20.0 mL). The mixture was extracted with ethyl acetate, the organic layer washed with brine, dried over sodium sulfate, decanted and concentrated *in vacuo* to yield the crude product which was purified by silica gel chromatography (3:7 ethyl acetate/hexanes) to yield the product (0.510 g, 76 %). ^{1}H NMR (500 MHz, DMSO-d_6) δ 8.12 (s, 1H), 7.95 (s, 1H), 5.64 (s, 2H), 3.54 (t, J = 7.9 Hz, 2H), 0.81 (t, J = 7.9 Hz, 2H), -0.12 (s, 9H).

2-[(5,6-dichloro-1-{[2-(trimethylsilyl)ethoxy]methyl}-1H-1,3-benzodiazol-2-yl)oxy]-N,N-bis(propan-2-yl)acetamide. A 50 mL 24/40 round bottom flask was charged with 2-hydroxy-N,N-bis(propan-2-yl)acetamide (0.318 g, 2.00 mmol) and tetrahydrofuran (5.00 ml). The mixture was cooled to 0 ºC, under an argon atmosphere, and sodium hydride added (0.100 g, 3.00 mmol). Once gas evolution stopped, 2,5,6-trichloro-1-{[2-(trimethylsilyl)ethoxy]methyl}-1H-1,3-benzodiazole (0.476 g, 1.30 mmol) was added as a solution in tetrahydrofuran (5.00 mL). The reaction was warmed to room temperature and stirred for 19 hours, at which time an aqueous solution of saturated ammonium chloride (20.0 mL) was added. The reaction was extracted with ethyl acetate and the organic layer washed with brine, dried over sodium sulfate, decanted, and concentrated *in vacuo* to yield the crude product. This material was purified by silica gel chromatography (1:1 ethyl acetate/hexanes) to yield the final product as a white solid (0.510 g,

83 %). 1H NMR (500 MHz, DMSO-d6) δ 7.75 (s, 1H), 7.64 (s, 1H), 5.44 (s, 2H), 5.22 (s, 2H), 3.83 (p, J = 6.6 Hz, 1H), 3.64 – 3.56 (m, 2H), 3.48 (tt, J = 13.4, 7.3 Hz, 1H), 1.24 (d, J = 6.7 Hz, 6H), 1.17 (d, J = 6.4 Hz, 6H), 0.88 – 0.78 (m, 2H), -0.09 (s, 9H).

2-[(5,6-dichloro-1H-1,3-benzodiazol-2-yl)oxy]-N,N-bis(propan-2-yl)acetamide. 2-[(5,6-dichloro-1-{[2-(trimethylsilyl)ethoxy]methyl}-1H-1,3-benzodiazol-2-yl)oxy]-N,N-bis(propan-2-yl)acetamide was dissolved in tetrahydrofuran (10.0 mL) under an argon atmosphere and tetrabutylammonium fluoride was added as a 1.00 M solution in tetrahydrofuran (10.0 mL), followed by 0.050 mL of water. The reaction mixture was heated to 50 ºC for 70 hours at which time it was concentrated *in vacuo*. The crude material was purified by Reverse-phase Medium Pressure Liquid Chromatography (50 g C18 column, methanol in 25.0 mmolar ammonium formate). The product was partitioned between ethyl acetate and saturated sodium bicarbonate. The organic layer was then washed with brine, dried over sodium sulfate, filtered, and concentrated *in vacuo*. The product was additionally purified by silica gel chromatography (15:85 methanol/dichloromethane) to yield an oil. This material was recrystallized from dichloromethane/hexanes to yield the product as white needles (0.092 g, 26 %). ^{1}H NMR (500 MHz, DMSO-d_6) δ 12.37 (s, 1H), 7.71 – 7.38 (m, 2H), 5.14 (s, 2H), 3.83 (p, *J* = 6.7 Hz, 1H), 3.50 (dt, *J* = 13.9, 4.8 Hz, 1H), 1.23 (dd, *J* = 39.5, 6.6 Hz, 12H). HRMS ESI (+) calc'd for [M+H] = 344.0928, 344.0941.

REFERENCES

REFERENCES

1 WHO. Global Tuberculosis Report. (2020).

2 Ding, P., Li, X., Jia, Z. & Lu, Z. Multidrug-resistant tuberculosis (MDR-TB) disease burden in China: a systematic review and spatio-temporal analysis. *BMC Infect Dis* **17**, 57, doi:10.1186/s12879-016-2151-5 (2017).

3 Shen, Y. *et al.* In Vitro Susceptibility of Mycobacterium abscessus and Mycobacterium fortuitum Isolates to 30 Antibiotics. *Biomed Res Int* **2018**, 4902941, doi:10.1155/2018/4902941 (2018).

4 Pang, H., Jiang, Y. & Wan, K. Drug Susceptibility of 33 Reference Strains of Slowly Growing Mycobacteria to 19 Antimicrobial Agents. *Biomed Res Int* **2017**, 1584658, doi:10.1155/2017/1584658 (2017).

5 Wu, M. L., Aziz, D. B., Dartois, V. & Dick, T. NTM drug discovery: status, gaps and the way forward. *Drug Discov Today* **23**, 1502-1519, doi:10.1016/j.drudis.2018.04.001 (2018).

6 Abrahams, K. A. *et al.* Identification of novel imidazo[1,2-a]pyridine inhibitors targeting M. tuberculosis QcrB. *PLoS One* **7**, e52951, doi:10.1371/journal.pone.0052951 (2012).

7 Cleghorn, L. A. T. *et al.* Identification of Morpholino Thiophenes as Novel Mycobacterium tuberculosis Inhibitors, Targeting QcrB. *J Med Chem* **61**, 6592-6608, doi:10.1021/acs.jmedchem.8b00172 (2018).

8 Foo, C. S. *et al.* Arylvinylpiperazine Amides, a New Class of Potent Inhibitors Targeting QcrB of Mycobacterium tuberculosis. *mBio* **9**, doi:10.1128/mBio.01276-18 (2018).

9 Harrison, G. A. *et al.* Identification of 4-Amino-Thieno[2,3-d]Pyrimidines as QcrB Inhibitors in Mycobacterium tuberculosis. *mSphere* **4**, doi:10.1128/mSphere.00606-19 (2019).

10 Lupien, A. *et al.* New 2-Ethylthio-4-methylaminoquinazoline derivatives inhibiting two subunits of cytochrome bc1 in Mycobacterium tuberculosis. *PLoS Pathog* **16**, e1008270, doi:10.1371/journal.ppat.1008270 (2020).

11 Moraski, G. C. *et al.* Arrival of Imidazo[2,1-b]thiazole-5-carboxamides: Potent Anti-tuberculosis Agents That Target QcrB. *ACS Infect Dis* **2**, 393-398, doi:10.1021/acsinfecdis.5b00154 (2016).

12 Phummarin, N. *et al.* SAR and identification of 2-(quinolin-4-yloxy)acetamides as Mycobacterium tuberculosis cytochrome bc1 inhibitors. *Medchemcomm* **7**, 2122-2127, doi:10.1039/c6md00236f (2016).

13 Rybniker, J. *et al.* Lansoprazole is an antituberculous prodrug targeting cytochrome bc1. *Nat Commun* **6**, 7659, doi:10.1038/ncomms8659 (2015).

14 Subtil, F. T. *et al.* Activity of 2-(quinolin-4-yloxy)acetamides in Mycobacterium tuberculosis clinical isolates and identification of their molecular target by whole-genome sequencing. *Int J Antimicrob Agents* **51**, 378-384, doi:10.1016/j.ijantimicag.2017.08.023 (2018).

15 Christophe, T. *et al.* High content screening identifies decaprenyl-phosphoribose 2' epimerase as a target for intracellular antimycobacterial inhibitors. *PLoS Pathog* **5**, e1000645, doi:10.1371/journal.ppat.1000645 (2009).

16 Grover, S. *et al.* Benzothiazinones mediate killing of Corynebacterineae by blocking decaprenyl phosphate recycling involved in cell wall biosynthesis. *J Biol Chem* **289**, 6177-6187, doi:10.1074/jbc.M113.522623 (2014).

17 Makarov, V. *et al.* Benzothiazinones kill Mycobacterium tuberculosis by blocking arabinan synthesis. *Science* **324**, 801-804, doi:10.1126/science.1171583 (2009).

18 Neres, J. *et al.* 2-Carboxyquinoxalines kill mycobacterium tuberculosis through noncovalent inhibition of DprE1. *ACS Chem Biol* **10**, 705-714, doi:10.1021/cb5007163 (2015).

19 Panda, M. *et al.* Discovery of pyrazolopyridones as a novel class of noncovalent DprE1 inhibitor with potent anti-mycobacterial activity. *J Med Chem* **57**, 4761-4771, doi:10.1021/jm5002937 (2014).

20 Stanley, S. A. *et al.* Identification of novel inhibitors of M. tuberculosis growth using whole cell based high-throughput screening. *ACS Chem Biol* **7**, 1377-1384, doi:10.1021/cb300151m (2012).

21 Korycka-Machala, M. *et al.* 1H-Benzo[d]Imidazole Derivatives Affect MmpL3 in Mycobacterium tuberculosis. *Antimicrob Agents Chemother* **63**, doi:10.1128/AAC.00441-19 (2019).

22 Zheng, H., Williams, J. T., Coulson, G. B., Haiderer, E. R. & Abramovitch, R. B. HC2091 Kills Mycobacterium tuberculosis by Targeting the MmpL3 Mycolic Acid Transporter. *Antimicrob Agents Chemother* **62**, doi:10.1128/AAC.02459-17 (2018).

23 Zampieri, M. *et al.* High-throughput metabolomic analysis predicts mode of action of uncharacterized antimicrobial compounds. *Sci Transl Med* **10**, doi:10.1126/scitranslmed.aal3973 (2018).

24 Ioerger, T. R. *et al.* Identification of new drug targets and resistance mechanisms in Mycobacterium tuberculosis. *PLoS One* **8**, e75245, doi:10.1371/journal.pone.0075245 (2013).

25 Williams, J. T. *et al.* Identification of New MmpL3 Inhibitors by Untargeted and Targeted Mutant Screens Defines MmpL3 Domains with Differential Resistance. *Antimicrob Agents Chemother* **63**, doi:10.1128/AAC.00547-19 (2019).

26 Dal Molin, M. *et al.* Identification of novel scaffolds targeting Mycobacterium tuberculosis. *J Mol Med (Berl)* **97**, 1601-1613, doi:10.1007/s00109-019-01840-7 (2019).

27 Rao, S. P. *et al.* Indolcarboxamide is a preclinical candidate for treating multidrug-resistant tuberculosis. *Sci Transl Med* **5**, 214ra168, doi:10.1126/scitranslmed.3007355 (2013).

28 Lun, S. *et al.* Indoleamides are active against drug-resistant Mycobacterium tuberculosis. *Nat Commun* **4**, 2907, doi:10.1038/ncomms3907 (2013).

29 Grzegorzewicz, A. E. *et al.* Inhibition of mycolic acid transport across the Mycobacterium tuberculosis plasma membrane. *Nat Chem Biol* **8**, 334-341, doi:10.1038/nchembio.794 (2012).

30 La Rosa, V. *et al.* MmpL3 is the cellular target of the antitubercular pyrrole derivative BM212. *Antimicrob Agents Chemother* **56**, 324-331, doi:10.1128/AAC.05270-11 (2012).

31 Shetty, A. *et al.* Novel Acetamide Indirectly Targets Mycobacterial Transporter MmpL3 by Proton Motive Force Disruption. *Front Microbiol* **9**, 2960, doi:10.3389/fmicb.2018.02960 (2018).

32 Dupont, C. *et al.* A piperidinol-containing molecule is active against Mycobacterium tuberculosis by inhibiting the mycolic acid flippase activity of MmpL3. *J Biol Chem* **294**, 17512-17523, doi:10.1074/jbc.RA119.010135 (2019).

33 Li, M. *et al.* Potency Increase of Spiroketal Analogs of Membrane Inserting Indolyl Mannich Base Antimycobacterials Is Due to Acquisition of MmpL3 Inhibition. *ACS Infect Dis* **6**, 1882-1893, doi:10.1021/acsinfecdis.0c00121 (2020).

34 Tahlan, K. *et al.* SQ109 targets MmpL3, a membrane transporter of trehalose monomycolate involved in mycolic acid donation to the cell wall core of Mycobacterium tuberculosis. *Antimicrob Agents Chemother* **56**, 1797-1809, doi:10.1128/AAC.05708-11 (2012).

35 Remuinan, M. J. *et al.* Tetrahydropyrazolo[1,5-a]pyrimidine-3-carboxamide and N-benzyl-6',7'-dihydrospiro[piperidine-4,4'-thieno[3,2-c]pyran] analogues with bactericidal efficacy against Mycobacterium tuberculosis targeting MmpL3. *PLoS One* **8**, e60933, doi:10.1371/journal.pone.0060933 (2013).

36 Grover, S. *et al.* Two-Way Regulation of MmpL3 Expression Identifies and Validates Inhibitors of MmpL3 Function in Mycobacterium tuberculosis. *ACS Infect Dis* **7**, 141-152, doi:10.1021/acsinfecdis.0c00675 (2021).

37 Tantry, S. J. *et al.* Whole cell screen based identification of spiropiperidines with potent antitubercular properties. *Bioorg Med Chem Lett* **25**, 3234-3245, doi:10.1016/j.bmcl.2015.05.087 (2015).

38 Lee, B. S. & Pethe, K. Therapeutic potential of promiscuous targets in Mycobacterium tuberculosis. *Curr Opin Pharmacol* **42**, 22-26, doi:10.1016/j.coph.2018.06.006 (2018).

39 Sorayah, R. *et al.* Naturally-Occurring Polymorphisms in QcrB Are Responsible for Resistance to Telacebec in Mycobacterium abscessus. *ACS Infect Dis* **5**, 2055-2060, doi:10.1021/acsinfecdis.9b00322 (2019).

40 Incandela, M. L. *et al.* DprE1, a new taxonomic marker in mycobacteria. *FEMS Microbiol Lett* **348**, 66-73, doi:10.1111/1574-6968.12246 (2013).

41 Shi, J. *et al.* In Vitro Activity of PBTZ169 against Multiple Mycobacterium Species. *Antimicrob Agents Chemother* **62**, doi:10.1128/AAC.01314-18 (2018).

42 Li, W. *et al.* MmpL3 as a Target for the Treatment of Drug-Resistant Nontuberculous Mycobacterial Infections. *Front Microbiol* **9**, 1547, doi:10.3389/fmicb.2018.01547 (2018).

43 Cole, S. T. *et al.* Deciphering the biology of Mycobacterium tuberculosis from the complete genome sequence. *Nature* **393**, 537-544, doi:10.1038/31159 (1998).

44 Chim, N. *et al.* The Structure and Interactions of Periplasmic Domains of Crucial MmpL Membrane Proteins from Mycobacterium tuberculosis. *Chem Biol* **22**, 1098-1107, doi:10.1016/j.chembiol.2015.07.013 (2015).

45 Belardinelli, J. M. *et al.* Structure-Function Profile of MmpL3, the Essential Mycolic Acid Transporter from Mycobacterium tuberculosis. *ACS Infect Dis* **2**, 702-713, doi:10.1021/acsinfecdis.6b00095 (2016).

46 Bernut, A. *et al.* Insights into the smooth-to-rough transitioning in Mycobacterium bolletii unravels a functional Tyr residue conserved in all mycobacterial MmpL family members. *Mol Microbiol* **99**, 866-883, doi:10.1111/mmi.13283 (2016).

47 Viljoen, A. *et al.* The diverse family of MmpL transporters in mycobacteria: from regulation to antimicrobial developments. *Mol Microbiol* **104**, 889-904, doi:10.1111/mmi.13675 (2017).

48 Xu, Z., Meshcheryakov, V. A., Poce, G. & Chng, S. S. MmpL3 is the flippase for mycolic acids in mycobacteria. *Proc Natl Acad Sci U S A* **114**, 7993-7998, doi:10.1073/pnas.1700062114 (2017).

49 Li, W. *et al.* Direct Inhibition of MmpL3 by Novel Antitubercular Compounds. *ACS Infect Dis* **5**, 1001-1012, doi:10.1021/acsinfecdis.9b00048 (2019).

50 Melly, G. & Purdy, G. E. MmpL Proteins in Physiology and Pathogenesis of M. tuberculosis. *Microorganisms* **7**, doi:10.3390/microorganisms7030070 (2019).

51 Su, C. C. *et al.* MmpL3 is a lipid transporter that binds trehalose monomycolate and phosphatidylethanolamine. *Proc Natl Acad Sci U S A* **116**, 11241-11246, doi:10.1073/pnas.1901346116 (2019).

52 Zhang, B. *et al.* Crystal Structures of Membrane Transporter MmpL3, an Anti-TB Drug Target. *Cell* **176**, 636-648 e613, doi:10.1016/j.cell.2019.01.003 (2019).

53 Nikaido, H. Structure and mechanism of RND-type multidrug efflux pumps. *Adv Enzymol Relat Areas Mol Biol* **77**, 1-60, doi:10.1002/9780470920541.ch1 (2011).

54 Yang, X. *et al.* Structural Basis for the Inhibition of Mycobacterial MmpL3 by NITD-349 and SPIRO. *J Mol Biol* **432**, 4426-4434, doi:10.1016/j.jmb.2020.05.019 (2020).

55 Belardinelli, J. M. *et al.* The MmpL3 interactome reveals a complex crosstalk between cell envelope biosynthesis and cell elongation and division in mycobacteria. *Sci Rep* **9**, 10728, doi:10.1038/s41598-019-47159-8 (2019).

56 Fay, A. *et al.* Two Accessory Proteins Govern MmpL3 Mycolic Acid Transport in Mycobacteria. *mBio* **10**, doi:10.1128/mBio.00850-19 (2019).

57 Le, N. H. *et al.* The protein kinase PknB negatively regulates biosynthesis and trafficking of mycolic acids in mycobacteria. *J Lipid Res* **61**, 1180-1191, doi:10.1194/jlr.RA120000747 (2020).

58 Zeng, J. *et al.* Protein kinases PknA and PknB independently and coordinately regulate essential Mycobacterium tuberculosis physiologies and antimicrobial susceptibility. *PLoS Pathog* **16**, e1008452, doi:10.1371/journal.ppat.1008452 (2020).

59 Owens, C. P. *et al.* The Mycobacterium tuberculosis secreted protein Rv0203 transfers heme to membrane proteins MmpL3 and MmpL11. *J Biol Chem* **288**, 21714-21728, doi:10.1074/jbc.M113.453076 (2013).

60 Sassetti, C. M., Boyd, D. H. & Rubin, E. J. Genes required for mycobacterial growth defined by high density mutagenesis. *Mol Microbiol* **48**, 77-84, doi:10.1046/j.1365-2958.2003.03425.x (2003).

61 Sassetti, C. M. & Rubin, E. J. Genetic requirements for mycobacterial survival during infection. *Proc Natl Acad Sci U S A* **100**, 12989-12994, doi:10.1073/pnas.2134250100 (2003).

62 Griffin, J. E. *et al.* High-resolution phenotypic profiling defines genes essential for mycobacterial growth and cholesterol catabolism. *PLoS Pathog* **7**, e1002251, doi:10.1371/journal.ppat.1002251 (2011).

63 Varela, C. *et al.* MmpL genes are associated with mycolic acid metabolism in mycobacteria and corynebacteria. *Chem Biol* **19**, 498-506, doi:10.1016/j.chembiol.2012.03.006 (2012).

64 Li, W. *et al.* Therapeutic Potential of the Mycobacterium tuberculosis Mycolic Acid Transporter, MmpL3. *Antimicrob Agents Chemother* **60**, 5198-5207, doi:10.1128/AAC.00826-16 (2016).

65 Degiacomi, G. *et al.* Essentiality of mmpL3 and impact of its silencing on Mycobacterium tuberculosis gene expression. *Sci Rep* **7**, 43495, doi:10.1038/srep43495 (2017).

66 DeJesus, M. A. *et al.* Comprehensive Essentiality Analysis of the Mycobacterium tuberculosis Genome via Saturating Transposon Mutagenesis. *mBio* **8**, doi:10.1128/mBio.02133-16 (2017).

67 Xiong, L. B. *et al.* Improving the production of 22-hydroxy-23,24-bisnorchol-4-ene-3-one from sterols in Mycobacterium neoaurum by increasing cell permeability and modifying multiple genes. *Microb Cell Fact* **16**, 89, doi:10.1186/s12934-017-0705-x (2017).

68 Bannantine, J. P., Zinniel, D. K. & Barletta, R. G. Transposon Mutagenesis in Mycobacterium avium Subspecies Paratuberculosis. *Methods Mol Biol* **2016**, 117-125, doi:10.1007/978-1-4939-9570-7_11 (2019).

69 McNeil, M. B. & Cook, G. M. Utilization of CRISPR Interference To Validate MmpL3 as a Drug Target in Mycobacterium tuberculosis. *Antimicrob Agents Chemother* **63**, doi:10.1128/AAC.00629-19 (2019).

70 Mendum, T. A. *et al.* Transposon libraries identify novel Mycobacterium bovis BCG genes involved in the dynamic interactions required for BCG to persist during in vivo passage in cattle. *BMC Genomics* **20**, 431, doi:10.1186/s12864-019-5791-1 (2019).

71 Rego, E. H., Audette, R. E. & Rubin, E. J. Deletion of a mycobacterial divisome factor collapses single-cell phenotypic heterogeneity. *Nature* **546**, 153-157, doi:10.1038/nature22361 (2017).

72 Domenech, P., Reed, M. B. & Barry, C. E., 3rd. Contribution of the Mycobacterium tuberculosis MmpL protein family to virulence and drug resistance. *Infect Immun* **73**, 3492-3501, doi:10.1128/IAI.73.6.3492-3501.2005 (2005).

73 Bloch, K. Control mechanisms for fatty acid synthesis in Mycobacterium smegmatis. *Adv Enzymol Relat Areas Mol Biol* **45**, 1-84, doi:10.1002/9780470122907.ch1 (1977).

74 Kikuchi, S., Rainwater, D. L. & Kolattukudy, P. E. Purification and characterization of an unusually large fatty acid synthase from Mycobacterium tuberculosis var. bovis BCG. *Arch Biochem Biophys* **295**, 318-326, doi:10.1016/0003-9861(92)90524-z (1992).

75 Portevin, D. *et al.* The acyl-AMP ligase FadD32 and AccD4-containing acyl-CoA carboxylase are required for the synthesis of mycolic acids and essential for mycobacterial growth: identification of the carboxylation product and determination of the acyl-CoA carboxylase components. *J Biol Chem* **280**, 8862-8874, doi:10.1074/jbc.M408578200 (2005).

76 Brown, A. K. *et al.* Probing the mechanism of the Mycobacterium tuberculosis beta-ketoacyl-acyl carrier protein synthase III mtFabH: factors influencing catalysis and substrate specificity. *J Biol Chem* **280**, 32539-32547, doi:10.1074/jbc.M413216200 (2005).

77 Choi, K. H., Kremer, L., Besra, G. S. & Rock, C. O. Identification and substrate specificity of beta -ketoacyl (acyl carrier protein) synthase III (mtFabH) from Mycobacterium tuberculosis. *J Biol Chem* **275**, 28201-28207, doi:10.1074/jbc.M003241200 (2000).

78 Scarsdale, J. N., Kazanina, G., He, X., Reynolds, K. A. & Wright, H. T. Crystal structure of the Mycobacterium tuberculosis beta-ketoacyl-acyl carrier protein synthase III. *J Biol Chem* **276**, 20516-20522, doi:10.1074/jbc.M010762200 (2001).

79 Ghadbane, H., Brown, A. K., Kremer, L., Besra, G. S. & Futterer, K. Structure of Mycobacterium tuberculosis mtFabD, a malonyl-CoA:acyl carrier protein transacylase (MCAT). *Acta Crystallogr Sect F Struct Biol Cryst Commun* **63**, 831-835, doi:10.1107/S1744309107042455 (2007).

80 Gurvitz, A. Physiological function of mycobacterial mtFabD, an essential malonyl-CoA:AcpM transacylase of type 2 fatty acid synthase FASII, in yeast mct1Delta cells. *Comp Funct Genomics*, 836172, doi:10.1155/2009/836172 (2009).

81 Kremer, L. *et al.* Biochemical characterization of acyl carrier protein (AcpM) and malonyl-CoA:AcpM transacylase (mtFabD), two major components of Mycobacterium tuberculosis fatty acid synthase II. *J Biol Chem* **276**, 27967-27974, doi:10.1074/jbc.M103687200 (2001).

82 Banerjee, A., Sugantino, M., Sacchettini, J. C. & Jacobs, W. R., Jr. The mabA gene from the inhA operon of Mycobacterium tuberculosis encodes a 3-ketoacyl reductase that fails to confer isoniazid resistance. *Microbiology (Reading)* **144 (Pt 10)**, 2697-2704, doi:10.1099/00221287-144-10-2697 (1998).

83 Cohen-Gonsaud, M. *et al.* Crystal structure of MabA from Mycobacterium tuberculosis, a reductase involved in long-chain fatty acid biosynthesis. *J Mol Biol* **320**, 249-261, doi:10.1016/S0022-2836(02)00463-1 (2002).

84 Cohen-Gonsaud, M., Ducasse-Cabanot, S., Quemard, A. & Labesse, G. Ligand-induced fit in mycobacterial MabA: the sequence-specific C-terminus locks the conformational change. *Proteins* **60**, 392-400, doi:10.1002/prot.20494 (2005).

85 Marrakchi, H. *et al.* MabA (FabG1), a Mycobacterium tuberculosis protein involved in the long-chain fatty acid elongation system FAS-II. *Microbiology (Reading)* **148**, 951-960, doi:10.1099/00221287-148-4-951 (2002).

86 Cantaloube, S., Veyron-Churlet, R., Haddache, N., Daffe, M. & Zerbib, D. The Mycobacterium tuberculosis FAS-II dehydratases and methyltransferases define the specificity of the mycolic acid elongation complexes. *PLoS One* **6**, e29564, doi:10.1371/journal.pone.0029564 (2011).

87 Sacco, E. *et al.* The missing piece of the type II fatty acid synthase system from Mycobacterium tuberculosis. *Proc Natl Acad Sci U S A* **104**, 14628-14633, doi:10.1073/pnas.0704132104 (2007).

88 Dessen, A., Quemard, A., Blanchard, J. S., Jacobs, W. R., Jr. & Sacchettini, J. C. Crystal structure and function of the isoniazid target of Mycobacterium tuberculosis. *Science* **267**, 1638-1641, doi:10.1126/science.7886450 (1995).

89 Quemard, A. *et al.* Enzymatic characterization of the target for isoniazid in Mycobacterium tuberculosis. *Biochemistry* **34**, 8235-8241, doi:10.1021/bi00026a004 (1995).

90 Vilcheze, C. *et al.* Inactivation of the inhA-encoded fatty acid synthase II (FASII) enoyl-acyl carrier protein reductase induces accumulation of the FASI end products and cell lysis of Mycobacterium smegmatis. *J Bacteriol* **182**, 4059-4067, doi:10.1128/jb.182.14.4059-4067.2000 (2000).

91 Kremer, L. *et al.* Mycolic acid biosynthesis and enzymic characterization of the beta-ketoacyl-ACP synthase A-condensing enzyme from Mycobacterium tuberculosis. *Biochem J* **364**, 423-430, doi:10.1042/BJ20011628 (2002).

92 Schaeffer, M. L. *et al.* Purification and biochemical characterization of the Mycobacterium tuberculosis beta-ketoacyl-acyl carrier protein synthases KasA and KasB. *J Biol Chem* **276**, 47029-47037, doi:10.1074/jbc.M108903200 (2001).

93 Veyron-Churlet, R. *et al.* The biosynthesis of mycolic acids in Mycobacterium tuberculosis relies on multiple specialized elongation complexes interconnected by specific protein-protein interactions. *J Mol Biol* **353**, 847-858, doi:10.1016/j.jmb.2005.09.016 (2005).

94 Veyron-Churlet, R., Guerrini, O., Mourey, L., Daffe, M. & Zerbib, D. Protein-protein interactions within the Fatty Acid Synthase-II system of Mycobacterium tuberculosis are essential for mycobacterial viability. *Mol Microbiol* **54**, 1161-1172, doi:10.1111/j.1365-2958.2004.04334.x (2004).

95 Dubnau, E. *et al.* Oxygenated mycolic acids are necessary for virulence of Mycobacterium tuberculosis in mice. *Mol Microbiol* **36**, 630-637, doi:10.1046/j.1365-2958.2000.01882.x (2000).

96 George, K. M., Yuan, Y., Sherman, D. R. & Barry, C. E., 3rd. The biosynthesis of cyclopropanated mycolic acids in Mycobacterium tuberculosis. Identification and functional analysis of CMAS-2. *J Biol Chem* **270**, 27292-27298, doi:10.1074/jbc.270.45.27292 (1995).

97 Glickman, M. S. The mmaA2 gene of Mycobacterium tuberculosis encodes the distal cyclopropane synthase of the alpha-mycolic acid. *J Biol Chem* **278**, 7844-7849, doi:10.1074/jbc.M212458200 (2003).

98 Glickman, M. S., Cahill, S. M. & Jacobs, W. R., Jr. The Mycobacterium tuberculosis cmaA2 gene encodes a mycolic acid trans-cyclopropane synthetase. *J Biol Chem* **276**, 2228-2233, doi:10.1074/jbc.C000652200 (2001).

99 Glickman, M. S., Cox, J. S. & Jacobs, W. R., Jr. A novel mycolic acid cyclopropane synthetase is required for cording, persistence, and virulence of Mycobacterium tuberculosis. *Mol Cell* **5**, 717-727, doi:10.1016/s1097-2765(00)80250-6 (2000).

100 Huang, C. C., Smith, C. V., Glickman, M. S., Jacobs, W. R., Jr. & Sacchettini, J. C. Crystal structures of mycolic acid cyclopropane synthases from Mycobacterium tuberculosis. *J Biol Chem* **277**, 11559-11569, doi:10.1074/jbc.M111698200 (2002).

101 Yuan, Y., Crane, D. C., Musser, J. M., Sreevatsan, S. & Barry, C. E., 3rd. MMAS-1, the branch point between cis- and trans-cyclopropane-containing oxygenated mycolates in Mycobacterium tuberculosis. *J Biol Chem* **272**, 10041-10049, doi:10.1074/jbc.272.15.10041 (1997).

102 Yuan, Y., Lee, R. E., Besra, G. S., Belisle, J. T. & Barry, C. E., 3rd. Identification of a gene involved in the biosynthesis of cyclopropanated mycolic acids in Mycobacterium tuberculosis. *Proc Natl Acad Sci U S A* **92**, 6630-6634, doi:10.1073/pnas.92.14.6630 (1995).

103 Gavalda, S. *et al.* The Pks13/FadD32 crosstalk for the biosynthesis of mycolic acids in Mycobacterium tuberculosis. *J Biol Chem* **284**, 19255-19264, doi:10.1074/jbc.M109.006940 (2009).

104 Kuhn, M. L. *et al.* Structure of the Essential Mtb FadD32 Enzyme: A Promising Drug Target for Treating Tuberculosis. *ACS Infect Dis* **2**, 579-591, doi:10.1021/acsinfecdis.6b00082 (2016).

105 Li, W., Gu, S., Fleming, J. & Bi, L. Crystal structure of FadD32, an enzyme essential for mycolic acid biosynthesis in mycobacteria. *Sci Rep* **5**, 15493, doi:10.1038/srep15493 (2015).

106 Portevin, D. *et al.* A polyketide synthase catalyzes the last condensation step of mycolic acid biosynthesis in mycobacteria and related organisms. *Proc Natl Acad Sci U S A* **101**, 314-319, doi:10.1073/pnas.0305439101 (2004).

107 Gavalda, S. *et al.* The polyketide synthase Pks13 catalyzes a novel mechanism of lipid transfer in mycobacteria. *Chem Biol* **21**, 1660-1669, doi:10.1016/j.chembiol.2014.10.011 (2014).

108 Lea-Smith, D. J. *et al.* The reductase that catalyzes mycolic motif synthesis is required for efficient attachment of mycolic acids to arabinogalactan. *J Biol Chem* **282**, 11000-11008, doi:10.1074/jbc.M608686200 (2007).

109 Barry, C. E., 3rd *et al.* Mycolic acids: structure, biosynthesis and physiological functions. *Prog Lipid Res* **37**, 143-179, doi:10.1016/s0163-7827(98)00008-3 (1998).

110 Daffé, M., Lanéelle, M. A., Asselineau, C., Lévy-Frébault, V. & David, H. Intérêt taxonomiquedes acides gras des mycobactéries: Proposition d'une méthode d'analyse. *Annales de l'Institut Pasteur Microbiologie* **134**, 241-256, doi:10.1016/S0769-2609(83)80037-4 (1983).

111 Papaioannou, N., Cheon, H. S., Lian, Y. & Kishi, Y. Product-regulation mechanisms for fatty acid biosynthesis catalyzed by Mycobacterium smegmatis FAS I. *Chembiochem* **8**, 1775-1780, doi:10.1002/cbic.200700380 (2007).

112 Zimhony, O., Vilcheze, C. & Jacobs, W. R., Jr. Characterization of Mycobacterium smegmatis expressing the Mycobacterium tuberculosis fatty acid synthase I (fas1) gene. *J Bacteriol* **186**, 4051-4055, doi:10.1128/JB.186.13.4051-4055.2004 (2004).

113 Hok, T. T. A Comparative Study of the Susceptibility to Ethionamide, Thiosemicarbazone, and Isoniazid of Tubercle Bacilli from Patients Never Treated with Ethionamide or Thiosemicarbazone. *Am Rev Respir Dis* **90**, 468-469, doi:10.1164/arrd.1964.90.3.468 (1964).

114 Wang, F. *et al.* Mechanism of thioamide drug action against tuberculosis and leprosy. *J Exp Med* **204**, 73-78, doi:10.1084/jem.20062100 (2007).

115 Grzegorzewicz, A. E. *et al.* A common mechanism of inhibition of the Mycobacterium tuberculosis mycolic acid biosynthetic pathway by isoxyl and thiacetazone. *J Biol Chem* **287**, 38434-38441, doi:10.1074/jbc.M112.400994 (2012).

116 Yamaryo-Botte, Y. *et al.* Acetylation of trehalose mycolates is required for efficient MmpL-mediated membrane transport in Corynebacterineae. *ACS Chem Biol* **10**, 734-746, doi:10.1021/cb5007689 (2015).

117 Li, W. *et al.* Novel insights into the mechanism of inhibition of MmpL3, a target of multiple pharmacophores in Mycobacterium tuberculosis. *Antimicrob Agents Chemother* **58**, 6413-6423, doi:10.1128/AAC.03229-14 (2014).

118 Kavunja, H. W. *et al.* Photoactivatable Glycolipid Probes for Identifying Mycolate-Protein Interactions in Live Mycobacteria. *J Am Chem Soc* **142**, 7725-7731, doi:10.1021/jacs.0c01065 (2020).

119 Armitige, L. Y., Jagannath, C., Wanger, A. R. & Norris, S. J. Disruption of the genes encoding antigen 85A and antigen 85B of Mycobacterium tuberculosis H37Rv: effect on growth in culture and in macrophages. *Infect Immun* **68**, 767-778, doi:10.1128/iai.68.2.767-778.2000 (2000).

120 Backus, K. M. *et al.* The three Mycobacterium tuberculosis antigen 85 isoforms have unique substrates and activities determined by non-active site regions. *J Biol Chem* **289**, 25041-25053, doi:10.1074/jbc.M114.581579 (2014).

121 Belisle, J. T. *et al.* Role of the major antigen of Mycobacterium tuberculosis in cell wall biogenesis. *Science* **276**, 1420-1422, doi:10.1126/science.276.5317.1420 (1997).

122 Jackson, M. *et al.* Inactivation of the antigen 85C gene profoundly affects the mycolate content and alters the permeability of the Mycobacterium tuberculosis cell envelope. *Mol Microbiol* **31**, 1573-1587, doi:10.1046/j.1365-2958.1999.01310.x (1999).

123 Puech, V. *et al.* Evidence for a partial redundancy of the fibronectin-binding proteins for the transfer of mycoloyl residues onto the cell wall arabinogalactan termini of Mycobacterium tuberculosis. *Mol Microbiol* **44**, 1109-1122, doi:10.1046/j.1365-2958.2002.02953.x (2002).

124 Bloch, H., Sorkin, E. & Erlenmeyer, H. A toxic lipid component of the tubercle bacillus (cord factor). I. Isolation from petroleum ether extracts of young bacterial cultures. *Am Rev Tuberc* **67**, 629-643, doi:10.1164/art.1953.67.5.629 (1953).

125 Julian, E. *et al.* Microscopic cords, a virulence-related characteristic of Mycobacterium tuberculosis, are also present in nonpathogenic mycobacteria. *J Bacteriol* **192**, 1751-1760, doi:10.1128/JB.01485-09 (2010).

126 Rath, P. *et al.* Cord factor (trehalose 6,6'-dimycolate) forms fully stable and non-permeable lipid bilayers required for a functional outer membrane. *Biochim Biophys Acta* **1828**, 2173-2181, doi:10.1016/j.bbamem.2013.04.021 (2013).

127 Ojha, A. K., Trivelli, X., Guerardel, Y., Kremer, L. & Hatfull, G. F. Enzymatic hydrolysis of trehalose dimycolate releases free mycolic acids during mycobacterial growth in biofilms. *J Biol Chem* **285**, 17380-17389, doi:10.1074/jbc.M110.112813 (2010).

128 Bekierkunst, A. Acute granulomatous response produced in mice by trehalose-6,6-dimycolate. *J Bacteriol* **96**, 958-961, doi:10.1128/JB.96.4.958-961.1968 (1968).

129 Bekierkunst, A. *et al.* Granuloma formation induced in mice by chemically defined mycobacterial fractions. *J Bacteriol* **100**, 95-102, doi:10.1128/JB.100.1.95-102.1969 (1969).

130 Saito, R., Tanaka, A., Sugiyama, K., Azuma, I. & Yamamura, Y. Adjuvant effect of cord factor, a mycobacterial lipid. *Infect Immun* **13**, 776-781, doi:10.1128/IAI.13.3.776-781.1976 (1976).

131 Miyake, Y. *et al.* C-type lectin MCL is an FcRgamma-coupled receptor that mediates the adjuvanticity of mycobacterial cord factor. *Immunity* **38**, 1050-1062, doi:10.1016/j.immuni.2013.03.010 (2013).

132 Ishikawa, E. *et al.* Direct recognition of the mycobacterial glycolipid, trehalose dimycolate, by C-type lectin Mincle. *J Exp Med* **206**, 2879-2888, doi:10.1084/jem.20091750 (2009).

133 Lang, R. Recognition of the mycobacterial cord factor by Mincle: relevance for granuloma formation and resistance to tuberculosis. *Front Immunol* **4**, 5, doi:10.3389/fimmu.2013.00005 (2013).

134 Sakamoto, K. *et al.* Mycobacterial trehalose dimycolate reprograms macrophage global gene expression and activates matrix metalloproteinases. *Infect Immun* **81**, 764-776, doi:10.1128/IAI.00906-12 (2013).

135 Aldridge, B. B. *et al.* Asymmetry and aging of mycobacterial cells lead to variable growth and antibiotic susceptibility. *Science* **335**, 100-104, doi:10.1126/science.1216166 (2012).

136 Murphy, K. C. *et al.* ORBIT: a New Paradigm for Genetic Engineering of Mycobacterial Chromosomes. *mBio* **9**, doi:10.1128/mBio.01467-18 (2018).

137 Carel, C. *et al.* Mycobacterium tuberculosis proteins involved in mycolic acid synthesis and transport localize dynamically to the old growing pole and septum. *PLoS One* **9**, e97148, doi:10.1371/journal.pone.0097148 (2014).

138 Xu, W. X. *et al.* The Wag31 protein interacts with AccA3 and coordinates cell wall lipid permeability and lipophilic drug resistance in Mycobacterium smegmatis. *Biochem Biophys Res Commun* **448**, 255-260, doi:10.1016/j.bbrc.2014.04.116 (2014).

139 Jani, C. *et al.* Regulation of polar peptidoglycan biosynthesis by Wag31 phosphorylation in mycobacteria. *BMC Microbiol* **10**, 327, doi:10.1186/1471-2180-10-327 (2010).

140 Kang, C. M., Nyayapathy, S., Lee, J. Y., Suh, J. W. & Husson, R. N. Wag31, a homologue of the cell division protein DivIVA, regulates growth, morphology and polar cell wall synthesis in mycobacteria. *Microbiology (Reading)* **154**, 725-735, doi:10.1099/mic.0.2007/014076-0 (2008).

141 Fu, J., Zong, G., Zhang, P., Gu, Y. & Cao, G. Deletion of the beta-Propeller Protein Gene Rv1057 Reduces ESAT-6 Secretion and Intracellular Growth of Mycobacterium tuberculosis. *Curr Microbiol* **75**, 401-409, doi:10.1007/s00284-017-1394-8 (2018).

142 Pacheco, S. A., Hsu, F. F., Powers, K. M. & Purdy, G. E. MmpL11 protein transports mycolic acid-containing lipids to the mycobacterial cell wall and contributes to biofilm formation in Mycobacterium smegmatis. *J Biol Chem* **288**, 24213-24222, doi:10.1074/jbc.M113.473371 (2013).

143 Lun, S. *et al.* Advancing the Therapeutic Potential of Indoleamides for Tuberculosis. *Antimicrob Agents Chemother* **63**, doi:10.1128/AAC.00343-19 (2019).

144 Delmar, J. A. *et al.* Structural Basis for the Regulation of the MmpL Transporters of Mycobacterium tuberculosis. *J Biol Chem* **290**, 28559-28574, doi:10.1074/jbc.M115.683797 (2015).

145 Galagan, J. E. *et al.* The Mycobacterium tuberculosis regulatory network and hypoxia. *Nature* **499**, 178-183, doi:10.1038/nature12337 (2013).

146 Boshoff, H. I. *et al.* The transcriptional responses of Mycobacterium tuberculosis to inhibitors of metabolism: novel insights into drug mechanisms of action. *J Biol Chem* **279**, 40174-40184, doi:10.1074/jbc.M406796200 (2004).

147 Carette, X. *et al.* Multisystem Analysis of Mycobacterium tuberculosis Reveals Kinase-Dependent Remodeling of the Pathogen-Environment Interface. *mBio* **9**, doi:10.1128/mBio.02333-17 (2018).

148 Gee, C. L. *et al.* A phosphorylated pseudokinase complex controls cell wall synthesis in mycobacteria. *Sci Signal* **5**, ra7, doi:10.1126/scisignal.2002525 (2012).

149 Mir, M. *et al.* The extracytoplasmic domain of the Mycobacterium tuberculosis Ser/Thr kinase PknB binds specific muropeptides and is required for PknB localization. *PLoS Pathog* **7**, e1002182, doi:10.1371/journal.ppat.1002182 (2011).

150 Prisic, S. *et al.* Extensive phosphorylation with overlapping specificity by Mycobacterium tuberculosis serine/threonine protein kinases. *Proc Natl Acad Sci U S A* **107**, 7521-7526, doi:10.1073/pnas.0913482107 (2010).

151 Lamichhane, G., Tyagi, S. & Bishai, W. R. Designer arrays for defined mutant analysis to detect genes essential for survival of Mycobacterium tuberculosis in mouse lungs. *Infect Immun* **73**, 2533-2540, doi:10.1128/IAI.73.4.2533-2540.2005 (2005).

152 Dupont, C. *et al.* A new piperidinol derivative targeting mycolic acid transport in Mycobacterium abscessus. *Mol Microbiol* **101**, 515-529, doi:10.1111/mmi.13406 (2016).

153 Foss, M. H. *et al.* Diphenylether-Modified 1,2-Diamines with Improved Drug Properties for Development against Mycobacterium tuberculosis. *ACS Infect Dis* **2**, 500-508, doi:10.1021/acsinfecdis.6b00052 (2016).

154 Kozikowski, A. P. *et al.* Targeting Mycolic Acid Transport by Indole-2-carboxamides for the Treatment of Mycobacterium abscessus Infections. *J Med Chem* **60**, 5876-5888, doi:10.1021/acs.jmedchem.7b00582 (2017).

155 Poce, G. *et al.* Improved BM212 MmpL3 inhibitor analogue shows efficacy in acute murine model of tuberculosis infection. *PLoS One* **8**, e56980, doi:10.1371/journal.pone.0056980 (2013).

156 Raynaud, C. *et al.* Active Benzimidazole Derivatives Targeting the MmpL3 Transporter in Mycobacterium abscessus. *ACS Infect Dis* **6**, 324-337, doi:10.1021/acsinfecdis.9b00389 (2020).

157 De Groote, M. A. *et al.* Optimization and Lead Selection of Benzothiazole Amide Analogs Toward a Novel Antimycobacterial Agent. *Front Microbiol* **9**, 2231, doi:10.3389/fmicb.2018.02231 (2018).

158 Guardia, A. *et al.* Easy-To-Synthesize Spirocyclic Compounds Possess Remarkable in Vivo Activity against Mycobacterium tuberculosis. *J Med Chem* **61**, 11327-11340, doi:10.1021/acs.jmedchem.8b01533 (2018).

159 Pandya, A. N. *et al.* Indole-2-Carboxamides Are Active against Mycobacterium abscessus in a Mouse Model of Acute Infection. *Antimicrob Agents Chemother* **63**, doi:10.1128/AAC.02245-18 (2019).

160 Poce, G. *et al.* Novel Pyrazole-Containing Compounds Active against Mycobacterium tuberculosis. *ACS Med Chem Lett* **10**, 1423-1429, doi:10.1021/acsmedchemlett.9b00204 (2019).

161 Protopopova, M. *et al.* Identification of a new antitubercular drug candidate, SQ109, from a combinatorial library of 1,2-ethylenediamines. *J Antimicrob Chemother* **56**, 968-974, doi:10.1093/jac/dki319 (2005).

162 Stec, J. *et al.* Indole-2-carboxamide-based MmpL3 Inhibitors Show Exceptional Antitubercular Activity in an Animal Model of Tuberculosis Infection. *J Med Chem* **59**, 6232-6247, doi:10.1021/acs.jmedchem.6b00415 (2016).

163 Boeree, M. J. *et al.* High-dose rifampicin, moxifloxacin, and SQ109 for treating tuberculosis: a multi-arm, multi-stage randomised controlled trial. *Lancet Infect Dis* **17**, 33-49, doi:10.1016/S1473-3099(16)30274-2 (2016).

164 Heinrich, N. *et al.* Early phase evaluation of SQ109 alone and in combination with rifampicin in pulmonary TB patients. *J Antimicrob Chemother* **70**, 1558-1566, doi:10.1093/jac/dku553 (2015).

165 Borisov S.E. *et al.* Efficiency and Safety of Chemotherapy Regimen with SQ109 in Those Suffering from Multiple Drug Resistance Tuberculoisis. *Tuberculosis and Lung Disease* **96(3)**, 6-18, doi:https://doi.org/10.21292/2075-1230-2018-96-3-6-18 (2018).

166 Jia, L., Coward, L., Gorman, G. S., Noker, P. E. & Tomaszewski, J. E. Pharmacoproteomic effects of isoniazid, ethambutol, and N-geranyl-N'-(2-adamantyl)ethane-1,2-diamine (SQ109) on Mycobacterium tuberculosis H37Rv. *J Pharmacol Exp Ther* **315**, 905-911, doi:10.1124/jpet.105.087817 (2005).

167 Jia, L. *et al.* Pharmacodynamics and pharmacokinetics of SQ109, a new diamine-based antitubercular drug. *Br J Pharmacol* **144**, 80-87, doi:10.1038/sj.bjp.0705984 (2005).

168 Wayne, L. G. & Sohaskey, C. D. Nonreplicating persistence of mycobacterium tuberculosis. *Annu Rev Microbiol* **55**, 139-163, doi:10.1146/annurev.micro.55.1.139 (2001).

169 McCune, R. M., Jr. & Tompsett, R. Fate of Mycobacterium tuberculosis in mouse tissues as determined by the microbial enumeration technique. I. The persistence of drug-

susceptible tubercle bacilli in the tissues despite prolonged antimicrobial therapy. *J Exp Med* **104**, 737-762, doi:10.1084/jem.104.5.737 (1956).

170 Karakousis, P. C., Williams, E. P. & Bishai, W. R. Altered expression of isoniazid-regulated genes in drug-treated dormant Mycobacterium tuberculosis. *J Antimicrob Chemother* **61**, 323-331, doi:10.1093/jac/dkm485 (2008).

171 Deb, C. *et al.* A novel in vitro multiple-stress dormancy model for Mycobacterium tuberculosis generates a lipid-loaded, drug-tolerant, dormant pathogen. *PLoS One* **4**, e6077, doi:10.1371/journal.pone.0006077 (2009).

172 Liu, Y. *et al.* Immune activation of the host cell induces drug tolerance in Mycobacterium tuberculosis both in vitro and in vivo. *J Exp Med* **213**, 809-825, doi:10.1084/jem.20151248 (2016).

173 Robitzek, E. H., Selikoff, I. J. & Ornstein, G. G. Chemotherapy of human tuberculosis with hydrazine derivatives of isonicotinic acid; preliminary report of representative cases. *Q Bull Sea View Hosp* **13**, 27-51 (1952).

174 Koul, A. *et al.* Diarylquinolines are bactericidal for dormant mycobacteria as a result of disturbed ATP homeostasis. *J Biol Chem* **283**, 25273-25280, doi:10.1074/jbc.M803899200 (2008).

175 Iacobino, A., Piccaro, G., Giannoni, F., Mustazzolu, A. & Fattorini, L. Mycobacterium tuberculosis Is Selectively Killed by Rifampin and Rifapentine in Hypoxia at Neutral pH. *Antimicrob Agents Chemother* **61**, doi:10.1128/AAC.02296-16 (2017).

176 McNeil, M. B., Dennison, D. & Parish, T. Mutations in MmpL3 alter membrane potential, hydrophobicity and antibiotic susceptibility in Mycobacterium smegmatis. *Microbiology (Reading)* **163**, 1065-1070, doi:10.1099/mic.0.000498 (2017).

177 McNeil, M. B. *et al.* Multiple Mutations in Mycobacterium tuberculosis MmpL3 Increase Resistance to MmpL3 Inhibitors. *mSphere* **5**, doi:10.1128/mSphere.00985-20 (2020).

178 Alangaden, G. J. *et al.* Mechanism of resistance to amikacin and kanamycin in Mycobacterium tuberculosis. *Antimicrob Agents Chemother* **42**, 1295-1297, doi:10.1128/AAC.42.5.1295 (1998).

179 Andries, K. *et al.* A diarylquinoline drug active on the ATP synthase of Mycobacterium tuberculosis. *Science* **307**, 223-227, doi:10.1126/science.1106753 (2005).

180 Flentie, K. *et al.* Chemical disarming of isoniazid resistance in Mycobacterium tuberculosis. *Proc Natl Acad Sci U S A* **116**, 10510-10517, doi:10.1073/pnas.1818009116 (2019).

181 Ismail, N., Omar, S. V., Ismail, N. A. & Peters, R. P. H. In vitro approaches for generation of Mycobacterium tuberculosis mutants resistant to bedaquiline, clofazimine or linezolid and identification of associated genetic variants. *J Microbiol Methods* **153**, 1-9, doi:10.1016/j.mimet.2018.08.011 (2018).

182 Makobongo, M. O., Einck, L., Peek, R. M., Jr. & Merrell, D. S. In vitro characterization of the anti-bacterial activity of SQ109 against Helicobacter pylori. *PLoS One* **8**, e68917, doi:10.1371/journal.pone.0068917 (2013).

183 Mariam, D. H., Mengistu, Y., Hoffner, S. E. & Andersson, D. I. Effect of rpoB mutations conferring rifampin resistance on fitness of Mycobacterium tuberculosis. *Antimicrob Agents Chemother* **48**, 1289-1294, doi:10.1128/aac.48.4.1289-1294.2004 (2004).

184 Srivastava, S. *et al.* Efflux-pump-derived multiple drug resistance to ethambutol monotherapy in Mycobacterium tuberculosis and the pharmacokinetics and pharmacodynamics of ethambutol. *J Infect Dis* **201**, 1225-1231, doi:10.1086/651377 (2010).

185 Stoffels, K., Mathys, V., Fauville-Dufaux, M., Wintjens, R. & Bifani, P. Systematic analysis of pyrazinamide-resistant spontaneous mutants and clinical isolates of Mycobacterium tuberculosis. *Antimicrob Agents Chemother* **56**, 5186-5193, doi:10.1128/AAC.05385-11 (2012).

186 Sun, J. *et al.* Rifampin resistance and its fitness cost in Riemerella anatipestifer. *BMC Microbiol* **19**, 107, doi:10.1186/s12866-019-1478-7 (2019).

187 Zhang, S. *et al.* Identification of novel mutations associated with clofazimine resistance in Mycobacterium tuberculosis. *J Antimicrob Chemother* **70**, 2507-2510, doi:10.1093/jac/dkv150 (2015).

188 Cox, J. A. *et al.* THPP target assignment reveals EchA6 as an essential fatty acid shuttle in mycobacteria. *Nat Microbiol* **1**, 15006, doi:10.1038/nmicrobiol.2015.6 (2016).

189 Li, K. *et al.* Multitarget drug discovery for tuberculosis and other infectious diseases. *J Med Chem* **57**, 3126-3139, doi:10.1021/jm500131s (2014).

190 North, E. J. *et al.* Design, synthesis and anti-tuberculosis activity of 1-adamantyl-3-heteroaryl ureas with improved in vitro pharmacokinetic properties. *Bioorg Med Chem* **21**, 2587-2599, doi:10.1016/j.bmc.2013.02.028 (2013).

191 Scherman, M. S. *et al.* Screening a library of 1600 adamantyl ureas for anti-Mycobacterium tuberculosis activity in vitro and for better physical chemical properties for bioavailability. *Bioorg Med Chem* **20**, 3255-3262, doi:10.1016/j.bmc.2012.03.058 (2012).

192 Grover, S. *et al.* Two-Way Regulation of MmpL3 Expression Identifies and Validates Inhibitors of MmpL3 Function in Mycobacterium tuberculosis. *ACS Infect Dis*, doi:10.1021/acsinfecdis.0c00675 (2020).

193 Alland, D. *et al.* Identification of differentially expressed mRNA in prokaryotic organisms by customized amplification libraries (DECAL): the effect of isoniazid on gene expression in Mycobacterium tuberculosis. *Proc Natl Acad Sci U S A* **95**, 13227-13232, doi:10.1073/pnas.95.22.13227 (1998).

194 Alland, D., Steyn, A. J., Weisbrod, T., Aldrich, K. & Jacobs, W. R., Jr. Characterization of the Mycobacterium tuberculosis iniBAC promoter, a promoter that responds to cell wall

biosynthesis inhibition. *J Bacteriol* **182**, 1802-1811, doi:10.1128/jb.182.7.1802-1811.2000 (2000).

195 McNeil, M. B., Chettiar, S., Awasthi, D. & Parish, T. Cell wall inhibitors increase the accumulation of rifampicin in Mycobacterium tuberculosis. *Access Microbiol* **1**, e000006, doi:10.1099/acmi.0.000006 (2019).

196 Bansal-Mutalik, R. & Nikaido, H. Mycobacterial outer membrane is a lipid bilayer and the inner membrane is unusually rich in diacyl phosphatidylinositol dimannosides. *Proc Natl Acad Sci U S A* **111**, 4958-4963, doi:10.1073/pnas.1403078111 (2014).

197 He, H., Hovey, R., Kane, J., Singh, V. & Zahrt, T. C. MprAB is a stress-responsive two-component system that directly regulates expression of sigma factors SigB and SigE in Mycobacterium tuberculosis. *J Bacteriol* **188**, 2134-2143, doi:10.1128/JB.188.6.2134-2143.2006 (2006).

198 Pang, X. *et al.* Evidence for complex interactions of stress-associated regulons in an mprAB deletion mutant of Mycobacterium tuberculosis. *Microbiology (Reading)* **153**, 1229-1242, doi:10.1099/mic.0.29281-0 (2007).

199 Smith, T. C., 2nd *et al.* Morphological profiling of tubercle bacilli identifies drug pathways of action. *Proc Natl Acad Sci U S A* **117**, 18744-18753, doi:10.1073/pnas.2002738117 (2020).

200 Lee, Y. V., Wahab, H. A. & Choong, Y. S. Potential inhibitors for isocitrate lyase of Mycobacterium tuberculosis and non-M. tuberculosis: a summary. *Biomed Res Int* **2015**, 895453, doi:10.1155/2015/895453 (2015).

201 Zheng, H., Williams, J. T., Coulson, G. B., Haiderer, E. R. & Abramovitch, R. B. HC2091 Kills Mycobacterium tuberculosis by Targeting the MmpL3 Mycolic Acid Transporter. *Antimicrob Agents Chemother* **62**, e02459-02417, doi:10.1128/AAC.02459-17 (2018).

202 Xu, Z. J., Meshcheryakov, V. A., Poce, G. & Chng, S. S. MmpL3 is the flippase for mycolic acids in mycobacteria. *P Natl Acad Sci USA* **114**, 7993-7998, doi:10.1073/pnas.1700062114 (2017).

203 McNeil, M. B., Dennison, D. & Parish, T. Mutations in MmpL3 alter membrane potential, hydrophobicity and antibiotic susceptibility in Mycobacterium smegmatis. *Microbiology* **163**, 1065-1070, doi:10.1099/mic.0.000498 (2017).

204 Sacksteder, K. A., Protopopova, M., Barry, C. E., 3rd, Andries, K. & Nacy, C. A. Discovery and development of SQ109: a new antitubercular drug with a novel mechanism of action. *Future Microbiol* **7**, 823-837, doi:10.2217/fmb.12.56 (2012).

205 Lee, B. S. & Pethe, K. Therapeutic potential of promiscuous targets in Mycobacterium tuberculosis. *Current Opinion in Pharmacology* **42**, 22-26, doi:10.1016/j.coph.2018.06.006 (2018).

206 Poce, G., Consalvi, S. & Biava, M. MmpL3 Inhibitors: Diverse Chemical Scaffolds Inhibit the Same Target. *Mini Rev Med Chem* **16**, 1274-1283 (2016).

207 Zheng, H. *et al.* Inhibitors of Mycobacterium tuberculosis DosRST signaling and persistence. *Nat Chem Biol* **13**, 218-225, doi:10.1038/nchembio.2259 (2017).

208 Johnson, B. K. *et al.* The Carbonic Anhydrase Inhibitor Ethoxzolamide Inhibits the Mycobacterium tuberculosis PhoPR Regulon and Esx-1 Secretion and Attenuates Virulence. *Antimicrob Agents Chemother* **59**, 4436-4445, doi:10.1128/AAC.00719-15 (2015).

209 Coulson, G. B. *et al.* Targeting Mycobacterium tuberculosis Sensitivity to Thiol Stress at Acidic pH Kills the Bacterium and Potentiates Antibiotics. *Cell chemical biology* **24**, 993-1004 e1004, doi:10.1016/j.chembiol.2017.06.018 (2017).

210 Andreu, N. *et al.* Optimisation of bioluminescent reporters for use with mycobacteria. *PLoS One* **5**, e10777, doi:10.1371/journal.pone.0010777 (2010).

211 Johnson, B. K. & Abramovitch, R. B. Macrophage infection models for Mycobacterium tuberculosis. *Methods Mol Biol* **1285**, 329-341, doi:10.1007/978-1-4939-2450-9_20 (2015).

212 Garcia-Garcia, V., Oldfield, E. & Benaim, G. Inhibition of Leishmania mexicana Growth by the Tuberculosis Drug SQ109. *Antimicrob Agents Chemother* **60**, 6386-6389, doi:10.1128/AAC.00945-16 (2016).

213 Biava, M., Porretta, G. C. & Manetti, F. New derivatives of BM212: A class of antimycobacterial compounds based on the pyrrole ring as a scaffold. *Mini-Rev Med Chem* **7**, 65-78, doi:Doi 10.2174/138955707779317786 (2007).

214 Ballell, L. *et al.* Fueling open-source drug discovery: 177 small-molecule leads against tuberculosis. *ChemMedChem* **8**, 313-321, doi:10.1002/cmdc.201200428 (2013).

215 Colan, S. D. The Why and How of Z Scores. *Journal of the American Society of Echocardiography* **26**, 38-40, doi:10.1016/j.echo.2012.11.005 (2013).

216 Cokol, M., Kuru, N., Bicak, E., Larkins-Ford, J. & Aldridge, B. B. Efficient measurement and factorization of high-order drug interactions in Mycobacterium tuberculosis. *Sci Adv* **3**, e1701881, doi:10.1126/sciadv.1701881 (2017).

217 Li, W. *et al.* Synergistic Interactions of MmpL3 Inhibitors with Antitubercular Compounds In Vitro. *Antimicrob Agents Chemother* **61**, e02399-02316, doi:10.1128/AAC.02399-16 (2017).

218 Chen, P., Gearhart, J., Protopopova, M., Einck, L. & Nacy, C. A. Synergistic interactions of SQ109, a new ethylene diamine, with front-line antitubercular drugs in vitro. *J Antimicrob Chemother* **58**, 332-337, doi:10.1093/jac/dkl227 (2006).

219 Ramesh, R. *et al.* Repurposing of a drug scaffold: Identification of novel sila analogues of rimonabant as potent antitubercular agents. *Eur J Med Chem* **122**, 723-730, doi:10.1016/j.ejmech.2016.07.009 (2016).

220 Bollenbach, T. Antimicrobial interactions: mechanisms and implications for drug discovery and resistance evolution. *Curr Opin Microbiol* **27**, 1-9, doi:10.1016/j.mib.2015.05.008 (2015).

221 Singh, N. & Yeh, P. J. Suppressive drug combinations and their potential to combat antibiotic resistance. *J Antibiot* **70**, 1033-1042, doi:10.1038/ja.2017.102 (2017).

222 Baker, J. J. & Abramovitch, R. B. Genetic and metabolic regulation of Mycobacterium tuberculosis acid growth arrest. *Sci Rep* **8**, 4168, doi:10.1038/s41598-018-22343-4 (2018).

223 McKenna, A. *et al.* The Genome Analysis Toolkit: a MapReduce framework for analyzing next-generation DNA sequencing data. *Genome Res* **20**, 1297-1303, doi:10.1101/gr.107524.110 (2010).

224 Suzuki, R. & Shimodaira, H. Pvclust: an R package for assessing the uncertainty in hierarchical clustering. *Bioinformatics* **22**, 1540-1542, doi:10.1093/bioinformatics/btl117 (2006).

225 Yang, J. & Zhang, Y. I-TASSER server: new development for protein structure and function predictions. *Nucleic Acids Res* **43**, W174-181, doi:10.1093/nar/gkv342 (2015).

226 Kapopoulou, A., Lew, J. M. & Cole, S. T. The MycoBrowser portal: a comprehensive and manually annotated resource for mycobacterial genomes. *Tuberculosis (Edinb)* **91**, 8-13, doi:10.1016/j.tube.2010.09.006 (2011).

227 Schrodinger, L. L. C. (2015).

228 Bevan, C. D. & Lloyd, R. S. A high-throughput screening method for the determination of aqueous drug solubility using laser nephelometry in microtiter plates. *Anal Chem* **72**, 1781-1787, doi:10.1021/ac9912247 (2000).

229 Obach, R. S. Prediction of human clearance of twenty-nine drugs from hepatic microsomal intrinsic clearance data: An examination of in vitro half-life approach and nonspecific binding to microsomes. *Drug Metab Dispos* **27**, 1350-1359 (1999).

230 WHO. Global Tuberculosis Report 2020. (2020).

231 Leung, E. C. *et al.* Transmission of multidrug-resistant and extensively drug-resistant tuberculosis in a metropolitan city. *Eur Respir J* **41**, 901-908, doi:10.1183/09031936.00071212 (2013).

232 Borisov, S. E. *et al.* Efficiency and Safety of Chemotherapy Regimen with SQ109 in Those Suffering from Muliple Drug Resistant Tuberculosis. *Tuberkulez i Bolezni Lëgkih* **96(3)**, 6-18, doi:10.21292/2075-1230-2018-96-3-6-18 (2018).

233 Jia, L. *et al.* Interspecies pharmacokinetics and in vitro metabolism of SQ109. *Br J Pharmacol* **147**, 476-485, doi:10.1038/sj.bjp.0706650 (2006).

234 Gobis, K., Foks, H., Serocki, M., Augustynowicz-Kopec, E. & Napiorkowska, A. Synthesis and evaluation of in vitro antimycobacterial activity of novel 1H-benzo[d]imidazole

derivatives and analogues. *Eur J Med Chem* **89**, 13-20, doi:10.1016/j.ejmech.2014.10.031 (2015).

235 Mitchell, S. C. & Nickson, R. M. Metabolism of Sulfur-Containing Xenobiotics. *Sulfur Reports* **13(2)**, 161-195, doi:10.1080/01961779308048955 (1993).

236 Rohde, K. H., Abramovitch, R. B. & Russell, D. G. Mycobacterium tuberculosis invasion of macrophages: linking bacterial gene expression to environmental cues. *Cell Host Microbe* **2**, 352-364, doi:10.1016/j.chom.2007.09.006 (2007).

237 Lee, R. E. *et al.* Combinatorial lead optimization of [1,2]-diamines based on ethambutol as potential antituberculosis preclinical candidates. *J Comb Chem* **5**, 172-187, doi:10.1021/cc020071p (2003).

238 Radhakrishnan, A. *et al.* Crystal structure of the transcriptional regulator Rv0678 of Mycobacterium tuberculosis. *J Biol Chem* **289**, 16526-16540, doi:10.1074/jbc.M113.538959 (2014).

239 Hartkoorn, R. C., Uplekar, S. & Cole, S. T. Cross-resistance between clofazimine and bedaquiline through upregulation of MmpL5 in Mycobacterium tuberculosis. *Antimicrob Agents Chemother* **58**, 2979-2981, doi:10.1128/AAC.00037-14 (2014).

240 Andries, K. *et al.* Acquired resistance of Mycobacterium tuberculosis to bedaquiline. *PLoS One* **9**, e102135, doi:10.1371/journal.pone.0102135 (2014).

241 Somoskovi, A., Bruderer, V., Homke, R., Bloemberg, G. V. & Bottger, E. C. A mutation associated with clofazimine and bedaquiline cross-resistance in MDR-TB following bedaquiline treatment. *Eur Respir J* **45**, 554-557, doi:10.1183/09031936.00142914 (2015).

242 Villellas, C. *et al.* Unexpected high prevalence of resistance-associated Rv0678 variants in MDR-TB patients without documented prior use of clofazimine or bedaquiline. *J Antimicrob Chemother* **72**, 684-690, doi:10.1093/jac/dkw502 (2017).

243 Li, M., Nyantakyi, S. A., Go, M. L. & Dick, T. Resistance against Membrane-Inserting MmpL3 Inhibitor through Upregulation of MmpL5 in Mycobacterium tuberculosis. *Antimicrob Agents Chemother* **64**, doi:10.1128/AAC.01100-20 (2020).

244 Yang, J. *et al.* Molecular characteristics and in vitro susceptibility to bedaquiline of Mycobacterium tuberculosis isolates circulating in Shaanxi, China. *Int J Infect Dis* **99**, 163-170, doi:10.1016/j.ijid.2020.07.044 (2020).

245 Manjunatha, U. H. *et al.* Identification of a nitroimidazo-oxazine-specific protein involved in PA-824 resistance in Mycobacterium tuberculosis. *Proc Natl Acad Sci U S A* **103**, 431-436, doi:10.1073/pnas.0508392103 (2006).

246 Li, W. *et al.* Synergistic Interactions of MmpL3 Inhibitors with Antitubercular Compounds In Vitro. *Antimicrob Agents Chemother* **61**, doi:10.1128/AAC.02399-16 (2017).

247 Batt, S. M. *et al.* Whole Cell Target Engagement Identifies Novel Inhibitors of Mycobacterium tuberculosis Decaprenylphosphoryl-beta-d-ribose Oxidase. *ACS Infect Dis* **1**, 615-626, doi:10.1021/acsinfecdis.5b00065 (2015).

248 Chatterji, M. *et al.* 1,4-azaindole, a potential drug candidate for treatment of tuberculosis. *Antimicrob Agents Chemother* **58**, 5325-5331, doi:10.1128/AAC.03233-14 (2014).

249 Chikhale, R. *et al.* Development of selective DprE1 inhibitors: Design, synthesis, crystal structure and antitubercular activity of benzothiazolylpyrimidine-5-carboxamides. *Eur J Med Chem* **96**, 30-46, doi:10.1016/j.ejmech.2015.04.011 (2015).

250 Magnet, S. *et al.* Leads for antitubercular compounds from kinase inhibitor library screens. *Tuberculosis (Edinb)* **90**, 354-360, doi:10.1016/j.tube.2010.09.001 (2010).

251 Makarov, V. *et al.* Towards a new combination therapy for tuberculosis with next generation benzothiazinones. *EMBO Mol Med* **6**, 372-383, doi:10.1002/emmm.201303575 (2014).

252 Naik, M. *et al.* 4-aminoquinolone piperidine amides: noncovalent inhibitors of DprE1 with long residence time and potent antimycobacterial activity. *J Med Chem* **57**, 5419-5434, doi:10.1021/jm5005978 (2014).

253 Wang, F. *et al.* Identification of a small molecule with activity against drug-resistant and persistent tuberculosis. *Proc Natl Acad Sci U S A* **110**, E2510-2517, doi:10.1073/pnas.1309171110 (2013).

254 Gupta, R., Netherton, M., Byrd, T. F. & Rohde, K. H. Reporter-Based Assays for High-Throughput Drug Screening against Mycobacterium abscessus. *Front Microbiol* **8**, 2204, doi:10.3389/fmicb.2017.02204 (2017).

255 Zheng, H., Williams, J. T., Aleiwi, B., Ellsworth, E. & Abramovitch, R. B. Inhibiting Mycobacterium tuberculosis DosRST Signaling by Targeting Response Regulator DNA Binding and Sensor Kinase Heme. *ACS Chem Biol* **15**, 52-62, doi:10.1021/acschembio.8b00849 (2020).

256 Lee, J. M. *et al.* O2- and NO-sensing mechanism through the DevSR two-component system in Mycobacterium smegmatis. *J Bacteriol* **190**, 6795-6804, doi:10.1128/JB.00401-08 (2008).

257 Kumar, A. *et al.* Heme oxygenase-1-derived carbon monoxide induces the Mycobacterium tuberculosis dormancy regulon. *J Biol Chem* **283**, 18032-18039, doi:10.1074/jbc.M802274200 (2008).

258 Park, H. D. *et al.* Rv3133c/dosR is a transcription factor that mediates the hypoxic response of Mycobacterium tuberculosis. *Mol Microbiol* **48**, 833-843, doi:10.1046/j.1365-2958.2003.03474.x (2003).

259 Sander, T., Freyss, J., von Korff, M. & Rufener, C. DataWarrior: an open-source program for chemistry aware data visualization and analysis. *J Chem Inf Model* **55**, 460-473, doi:10.1021/ci500588j (2015).

260 Banerjee, A. *et al.* inhA, a gene encoding a target for isoniazid and ethionamide in Mycobacterium tuberculosis. *Science* **263**, 227-230, doi:10.1126/science.8284673 (1994).

261 Abrahams, K. A. & Besra, G. S. Mycobacterial cell wall biosynthesis: a multifaceted antibiotic target. *Parasitology* **145**, 116-133, doi:10.1017/S0031182016002377 (2018).

262 Voskuil, M. I. *et al.* Inhibition of respiration by nitric oxide induces a Mycobacterium tuberculosis dormancy program. *J Exp Med* **198**, 705-713, doi:10.1084/jem.20030205 (2003).

263 Mildvan, A. S. & Loeb, L. A. The role of metal ions in the mechanisms of DNA and RNA polymerases. *CRC Crit Rev Biochem* **6**, 219-244, doi:10.3109/10409237909102564 (1979).

264 Chandrangsu, P., Rensing, C. & Helmann, J. D. Metal homeostasis and resistance in bacteria. *Nat Rev Microbiol* **15**, 338-350, doi:10.1038/nrmicro.2017.15 (2017).

265 Clifton, L. A. *et al.* Effect of divalent cation removal on the structure of gram-negative bacterial outer membrane models. *Langmuir* **31**, 404-412, doi:10.1021/la504407v (2015).

266 Coughlin, R. T., Tonsager, S. & McGroarty, E. J. Quantitation of metal cations bound to membranes and extracted lipopolysaccharide of Escherichia coli. *Biochemistry* **22**, 2002-2007, doi:10.1021/bi00277a041 (1983).

267 Groisman, E. A., Kayser, J. & Soncini, F. C. Regulation of polymyxin resistance and adaptation to low-Mg2+ environments. *J Bacteriol* **179**, 7040-7045, doi:10.1128/jb.179.22.7040-7045.1997 (1997).

268 Maitra, A. *et al.* Cell wall peptidoglycan in Mycobacterium tuberculosis: An Achilles' heel for the TB-causing pathogen. *FEMS Microbiol Rev* **43**, 548-575, doi:10.1093/femsre/fuz016 (2019).

269 Marquis, R. E., Mayzel, K. & Carstensen, E. L. Cation exchange in cell walls of gram-positive bacteria. *Can J Microbiol* **22**, 975-982, doi:10.1139/m76-142 (1976).

270 Thomas, K. J., 3rd & Rice, C. V. Revised model of calcium and magnesium binding to the bacterial cell wall. *Biometals* **27**, 1361-1370, doi:10.1007/s10534-014-9797-5 (2014).

271 Thomas, K. J., 3rd & Rice, C. V. Equilibrium binding behavior of magnesium to wall teichoic acid. *Biochim Biophys Acta* **1848**, 1981-1987, doi:10.1016/j.bbamem.2015.05.003 (2015).

272 Rodrigo-Unzueta, A. *et al.* Molecular Basis of Membrane Association by the Phosphatidylinositol Mannosyltransferase PimA Enzyme from Mycobacteria. *J Biol Chem* **291**, 13955-13963, doi:10.1074/jbc.M116.723676 (2016).

273 Oren, A., Heldal, M., Norland, S. & Galinski, E. A. Intracellular ion and organic solute concentrations of the extremely halophilic bacterium Salinibacter ruber. *Extremophiles* **6**, 491-498, doi:10.1007/s00792-002-0286-3 (2002).

274 Roesser, M. & Muller, V. Osmoadaptation in bacteria and archaea: common principles and differences. *Environ Microbiol* **3**, 743-754, doi:10.1046/j.1462-2920.2001.00252.x (2001).

275 Ofer, N. *et al.* Ectoine biosynthesis in Mycobacterium smegmatis. *Appl Environ Microbiol* **78**, 7483-7486, doi:10.1128/AEM.01318-12 (2012).

276 Price, C. T., Bukka, A., Cynamon, M. & Graham, J. E. Glycine betaine uptake by the ProXVWZ ABC transporter contributes to the ability of Mycobacterium tuberculosis to initiate growth in human macrophages. *J Bacteriol* **190**, 3955-3961, doi:10.1128/JB.01476-07 (2008).

277 Bourque, C. W. Central mechanisms of osmosensation and systemic osmoregulation. *Nat Rev Neurosci* **9**, 519-531, doi:10.1038/nrn2400 (2008).

278 Hatzios, S. K. *et al.* Osmosensory signaling in Mycobacterium tuberculosis mediated by a eukaryotic-like Ser/Thr protein kinase. *Proc Natl Acad Sci U S A* **110**, E5069-5077, doi:10.1073/pnas.1321205110 (2013).

279 Baker, J. J., Johnson, B. K. & Abramovitch, R. B. Slow growth of Mycobacterium tuberculosis at acidic pH is regulated by phoPR and host-associated carbon sources. *Mol Microbiol* **94**, 56-69, doi:10.1111/mmi.12688 (2014).

280 Piddington, D. L., Kashkouli, A. & Buchmeier, N. A. Growth of Mycobacterium tuberculosis in a defined medium is very restricted by acid pH and Mg(2+) levels. *Infect Immun* **68**, 4518-4522, doi:10.1128/iai.68.8.4518-4522.2000 (2000).

281 Jones, C. M. & Niederweis, M. Role of porins in iron uptake by Mycobacterium smegmatis. *J Bacteriol* **192**, 6411-6417, doi:10.1128/JB.00986-10 (2010).

282 Messenger, A. J. & Ratledge, C. Iron transport in Mycobacterium smegmatis: Uptake of iron from ferric citrate. *J Bacteriol* **149**, 131-135, doi:10.1128/JB.149.1.131-135.1982 (1982).

283 Nagaoka, S., Murata, S., Kimura, K., Mori, T. & Hojo, K. Antimicrobial activity of sodium citrate against Streptococcus pneumoniae and several oral bacteria. *Lett Appl Microbiol* **51**, 546-551, doi:10.1111/j.1472-765X.2010.02932.x (2010).

284 Sharma, M., Tyagi, J. L. & Poluri, K. M. Quantifying bacterial cell lysis using GFP based fluorimetric assay. *Int J Biol Macromol* **138**, 881-889, doi:10.1016/j.ijbiomac.2019.07.172 (2019).

285 Johnson, B. K., Scholz, M. B., Teal, T. K. & Abramovitch, R. B. SPARTA: Simple Program for Automated reference-based bacterial RNA-seq Transcriptome Analysis. *BMC Bioinformatics* **17**, 66, doi:10.1186/s12859-016-0923-y (2016).

286 Yu, S., Fiss, E. & Jacobs, W. R., Jr. Analysis of the exochelin locus in Mycobacterium smegmatis: biosynthesis genes have homology with genes of the peptide synthetase family. *J Bacteriol* **180**, 4676-4685, doi:10.1128/JB.180.17.4676-4685.1998 (1998).

287 Zhu, W. *et al.* Exochelin genes in Mycobacterium smegmatis: identification of an ABC transporter and two non-ribosomal peptide synthetase genes. *Mol Microbiol* **29**, 629-639, doi:10.1046/j.1365-2958.1998.00961.x (1998).

288 Zhang, L. *et al.* Comprehensive analysis of iron utilization by Mycobacterium tuberculosis. *PLoS Pathog* **16**, e1008337, doi:10.1371/journal.ppat.1008337 (2020).

289 Dragset, M. S. *et al.* Genome-wide Phenotypic Profiling Identifies and Categorizes Genes Required for Mycobacterial Low Iron Fitness. *Sci Rep* **9**, 11394, doi:10.1038/s41598-019-47905-y (2019).

290 Li, W., He, J., Xie, L., Chen, T. & Xie, J. Comparative genomic insights into the biosynthesis and regulation of mycobacterial siderophores. *Cell Physiol Biochem* **31**, 1-13, doi:10.1159/000343343 (2013).

291 Quadri, L. E., Sello, J., Keating, T. A., Weinreb, P. H. & Walsh, C. T. Identification of a Mycobacterium tuberculosis gene cluster encoding the biosynthetic enzymes for assembly of the virulence-conferring siderophore mycobactin. *Chem Biol* **5**, 631-645, doi:10.1016/s1074-5521(98)90291-5 (1998).

292 Ratledge, C. & Marshall, B. J. Iron transport in Mycobacterium smegmatis: the role of mycobactin. *Biochim Biophys Acta* **279**, 58-74, doi:10.1016/0304-4165(72)90241-3 (1972).

293 Sandhu, P. & Akhter, Y. Siderophore transport by MmpL5-MmpS5 protein complex in Mycobacterium tuberculosis. *J Inorg Biochem* **170**, 75-84, doi:10.1016/j.jinorgbio.2017.02.013 (2017).

294 Wells, R. M. *et al.* Discovery of a siderophore export system essential for virulence of Mycobacterium tuberculosis. *PLoS Pathog* **9**, e1003120, doi:10.1371/journal.ppat.1003120 (2013).

295 Fang, Z., Newton-Foot, M., Sampson, S. L. & Gey van Pittius, N. C. Two promoters in the esx-3 gene cluster of Mycobacterium smegmatis respond inversely to different iron concentrations in vitro. *BMC Res Notes* **10**, 426, doi:10.1186/s13104-017-2752-0 (2017).

296 Siegrist, M. S. *et al.* Mycobacterial Esx-3 is required for mycobactin-mediated iron acquisition. *Proc Natl Acad Sci U S A* **106**, 18792-18797, doi:10.1073/pnas.0900589106 (2009).

297 Tufariello, J. M. *et al.* Separable roles for Mycobacterium tuberculosis ESX-3 effectors in iron acquisition and virulence. *Proc Natl Acad Sci U S A* **113**, E348-357, doi:10.1073/pnas.1523321113 (2016).

298 Serafini, A., Boldrin, F., Palu, G. & Manganelli, R. Characterization of a Mycobacterium tuberculosis ESX-3 conditional mutant: essentiality and rescue by iron and zinc. *J Bacteriol* **191**, 6340-6344, doi:10.1128/JB.00756-09 (2009).

299 Serafini, A., Pisu, D., Palu, G., Rodriguez, G. M. & Manganelli, R. The ESX-3 secretion system is necessary for iron and zinc homeostasis in Mycobacterium tuberculosis. *PLoS One* **8**, e78351, doi:10.1371/journal.pone.0078351 (2013).

300 Arnold, F. M. *et al.* The ABC exporter IrtAB imports and reduces mycobacterial siderophores. *Nature* **580**, 413-417, doi:10.1038/s41586-020-2136-9 (2020).

301 Rodriguez, G. M. & Smith, I. Identification of an ABC transporter required for iron acquisition and virulence in Mycobacterium tuberculosis. *J Bacteriol* **188**, 424-430, doi:10.1128/JB.188.2.424-430.2006 (2006).

302 Ryndak, M. B., Wang, S., Smith, I. & Rodriguez, G. M. The Mycobacterium tuberculosis high-affinity iron importer, IrtA, contains an FAD-binding domain. *J Bacteriol* **192**, 861-869, doi:10.1128/JB.00223-09 (2010).

303 D. Wyrzykowski D., Czupryniak J., Ossowski T. & L., L. C. s. Thermodynamic interactions of the alkaline earth metal ions with citric acid. *J Therm Anal Calorim* **102** (2010).

304 Shi, X. & Darwin, K. H. Copper homeostasis in Mycobacterium tuberculosis. *Metallomics* **7**, 929-934, doi:10.1039/c4mt00305e (2015).

305 Schwan, W. R., Lehmann, L. & McCormick, J. Transcriptional activation of the Staphylococcus aureus putP gene by low-proline-high osmotic conditions and during infection of murine and human tissues. *Infect Immun* **74**, 399-409, doi:10.1128/IAI.74.1.399-409.2006 (2006).

306 Sassetti, C. M., Boyd, D. H. & Rubin, E. J. Comprehensive identification of conditionally essential genes in mycobacteria. *Proc Natl Acad Sci U S A* **98**, 12712-12717, doi:10.1073/pnas.231275498 (2001).

307 Andersson, C. S. *et al.* The Mycobacterium tuberculosis very-long-chain fatty acyl-CoA synthetase: structural basis for housing lipid substrates longer than the enzyme. *Structure* **20**, 1062-1070, doi:10.1016/j.str.2012.03.012 (2012).

308 Daniel, J., Sirakova, T. & Kolattukudy, P. An acyl-CoA synthetase in Mycobacterium tuberculosis involved in triacylglycerol accumulation during dormancy. *PLoS One* **9**, e114877, doi:10.1371/journal.pone.0114877 (2014).

309 Hu, K. *et al.* Characterization of Guided Entry of Tail-Anchored Proteins 3 Homologues in Mycobacterium tuberculosis. *J Bacteriol* **201**, doi:10.1128/JB.00159-19 (2019).

310 Whitaker, M. *et al.* Two interacting ATPases protect Mycobacterium tuberculosis from glycerol and nitric oxide toxicity. *J Bacteriol*, doi:10.1128/JB.00202-20 (2020).

311 Takeda, H. *et al.* Structural basis for ion selectivity revealed by high-resolution crystal structure of Mg2+ channel MgtE. *Nat Commun* **5**, 5374, doi:10.1038/ncomms6374 (2014).

312 Park, Y. *et al.* Inhibition of CorA-Dependent Magnesium Homeostasis Is Cidal in Mycobacterium tuberculosis. *Antimicrob Agents Chemother* **63**, doi:10.1128/AAC.01006-19 (2019).

313 Groisman, E. A. *et al.* Bacterial Mg2+ homeostasis, transport, and virulence. *Annu Rev Genet* **47**, 625-646, doi:10.1146/annurev-genet-051313-051025 (2013).

314 Mahapatra, S., Crick, D. C., McNeil, M. R. & Brennan, P. J. Unique structural features of the peptidoglycan of Mycobacterium leprae. *J Bacteriol* **190**, 655-661, doi:10.1128/JB.00982-07 (2008).

315 Froschauer, E. M., Kolisek, M., Dieterich, F., Schweigel, M. & Schweyen, R. J. Fluorescence measurements of free [Mg2+] by use of mag-fura 2 in Salmonella enterica. *FEMS Microbiol Lett* **237**, 49-55, doi:10.1016/j.femsle.2004.06.013 (2004).

316 Hyrc, K. L., Bownik, J. M. & Goldberg, M. P. Ionic selectivity of low-affinity ratiometric calcium indicators: mag-Fura-2, Fura-2FF and BTC. *Cell Calcium* **27**, 75-86, doi:10.1054/ceca.1999.0092 (2000).

317 De Smet, K. A. L., Weston, A., Brown, I. N., Young, D. B. & Robertson, B. D. Three pathways for trehalose biosynthesis in mycobacteria. *Microbiology (Reading)* **146 (Pt 1)**, 199-208, doi:10.1099/00221287-146-1-199 (2000).

318 Kalscheuer, R. *et al.* Self-poisoning of Mycobacterium tuberculosis by targeting GlgE in an alpha-glucan pathway. *Nat Chem Biol* **6**, 376-384, doi:10.1038/nchembio.340 (2010).

319 Murphy, H. N. *et al.* The OtsAB pathway is essential for trehalose biosynthesis in Mycobacterium tuberculosis. *J Biol Chem* **280**, 14524-14529, doi:10.1074/jbc.M414232200 (2005).

320 Korte, J. *et al.* Trehalose-6-Phosphate-Mediated Toxicity Determines Essentiality of OtsB2 in Mycobacterium tuberculosis In Vitro and in Mice. *PLoS Pathog* **12**, e1006043, doi:10.1371/journal.ppat.1006043 (2016).

321 Shleeva, M. O. *et al.* Free Trehalose Accumulation in Dormant Mycobacterium smegmatis Cells and Its Breakdown in Early Resuscitation Phase. *Front Microbiol* **8**, 524, doi:10.3389/fmicb.2017.00524 (2017).

322 Daniel, J., Maamar, H., Deb, C., Sirakova, T. D. & Kolattukudy, P. E. Mycobacterium tuberculosis uses host triacylglycerol to accumulate lipid droplets and acquires a dormancy-like phenotype in lipid-loaded macrophages. *PLoS Pathog* **7**, e1002093, doi:10.1371/journal.ppat.1002093 (2011).

323 Wayne, L. G. & Hayes, L. G. An in vitro model for sequential study of shiftdown of Mycobacterium tuberculosis through two stages of nonreplicating persistence. *Infect Immun* **64**, 2062-2069, doi:10.1128/IAI.64.6.2062-2069.1996 (1996).

324 Pethe, K. *et al.* A chemical genetic screen in Mycobacterium tuberculosis identifies carbon-source-dependent growth inhibitors devoid of in vivo efficacy. *Nat Commun* **1**, 57, doi:10.1038/ncomms1060 (2010).

325 Sutterlin, H. A. *et al.* Disruption of lipid homeostasis in the Gram-negative cell envelope activates a novel cell death pathway. *Proc Natl Acad Sci U S A* **113**, E1565-1574, doi:10.1073/pnas.1601375113 (2016).

326 Lee, W., VanderVen, B. C., Fahey, R. J. & Russell, D. G. Intracellular Mycobacterium tuberculosis exploits host-derived fatty acids to limit metabolic stress. *J Biol Chem* **288**, 6788-6800, doi:10.1074/jbc.M112.445056 (2013).

327 Carroll, P., Muwanguzi-Karugaba, J., Melief, E., Files, M. & Parish, T. Identification of the translational start site of codon-optimized mCherry in Mycobacterium tuberculosis. *BMC Res Notes* **7**, 366, doi:10.1186/1756-0500-7-366 (2014).

328 Bardarov, S. *et al.* Conditionally replicating mycobacteriophages: a system for transposon delivery to Mycobacterium tuberculosis. *Proc Natl Acad Sci U S A* **94**, 10961-10966, doi:10.1073/pnas.94.20.10961 (1997).

329 Ochman, H., Gerber, A. S. & Hartl, D. L. Genetic applications of an inverse polymerase chain reaction. *Genetics* **120**, 621-623 (1988).

330 Reddy, V. M., Einck, L., Andries, K. & Nacy, C. A. In vitro interactions between new antitubercular drug candidates SQ109 and TMC207. *Antimicrob Agents Chemother* **54**, 2840-2846, doi:10.1128/AAC.01601-09 (2010).

331 Conradie, F. *et al.* Treatment of Highly Drug-Resistant Pulmonary Tuberculosis. *N Engl J Med* **382**, 893-902, doi:10.1056/NEJMoa1901814 (2020).

332 Larkins-Ford, J. *et al.* Systematic measurement of combination drug landscapes to predict in vivo treatment outcomes for tuberculosis. *bioRxiv*, doi:https://doi.org/10.1101/2021.02.03.429579 (2021).

333 Driver, E. R. *et al.* Evaluation of a mouse model of necrotic granuloma formation using C3HeB/FeJ mice for testing of drugs against Mycobacterium tuberculosis. *Antimicrob Agents Chemother* **56**, 3181-3195, doi:10.1128/AAC.00217-12 (2012).

334 Piccaro, G., Poce, G., Biava, M., Giannoni, F. & Fattorini, L. Activity of lipophilic and hydrophilic drugs against dormant and replicating Mycobacterium tuberculosis. *J Antibiot (Tokyo)* **68**, 711-714, doi:10.1038/ja.2015.52 (2015).

335 Singh, R. *et al.* PA-824 kills nonreplicating Mycobacterium tuberculosis by intracellular NO release. *Science* **322**, 1392-1395, doi:10.1126/science.1164571 (2008).

336 Drusano, G. L. *et al.* Linezolid Kills Acid-Phase and Nonreplicative-Persister-Phase Mycobacterium tuberculosis in a Hollow-Fiber Infection Model. *Antimicrob Agents Chemother* **62**, doi:10.1128/AAC.00221-18 (2018).

337 Jinich, A. *et al.* The Mycobacterium tuberculosis transposon sequencing database (MtbTnDB): a large-scale guide to genetic conditional essentiality. *bioRxiv*, doi:https://doi.org/10.1101/2021.03.05.434127 (2021).

338 Bulatovic, V. M. *et al.* Oxidative stress increases susceptibility of Mycobacterium tuberculosis to isoniazid. *Antimicrob Agents Chemother* **46**, 2765-2771, doi:10.1128/aac.46.9.2765-2771.2002 (2002).